

STUDY OF THE REACTIVITY OF ELECTROLYTE SOLVENTS
AND ADDITIVES IN LI-ION CELLS AND DESIGN OF NEW
ELECTROLYTE BLENDS

by

Rémi Petibon

Submitted in partial fulfilment of the requirements
for the degree of Doctor of Philosophy

at

Dalhousie University
Halifax, Nova Scotia
June 2016

© Copyright by Rémi Petibon, 2016

To my wife, my son and my daughter to be,

TABLE OF CONTENTS

LIST OF TABLES	ix
LIST OF FIGURES	xi
ABSTRACT	xxi
LIST OF ABBREVIATIONS USED	xxii
ACKNOWLEDGEMENTS	xxvi
CHAPTER 1. INTRODUCTION	1
1.1 Motivation.....	1
1.2 Li-ion cells	6
1.2.1 General configuration.....	6
1.2.2 Electrolyte systems.....	10
1.2.3 Positive electrode materials	12
1.2.4 Negative electrode materials.....	13
1.2.5 Separators	15
CHAPTER 2. ELECTRODE-ELECTROLYTE INTERPHASE AND ELECTROLYTE ADDITIVES.....	17
2.1 Electrolyte reactivity.....	17
2.2 Solid electrolyte interphase (SEI)	18
2.2.1 Solid electrolyte interphase at the negative electrode in standard electrolyte..	18
2.2.2 Solid electrolyte interphase at the positive electrode in standard electrolyte..	22
2.3 Electrolyte additives.....	24
2.3.1 Electrolyte additives for improved cycle performance	25
2.3.2 Study of electrolyte additives.....	28

CHAPTER 3. EXPERIMENTAL METHODS..... 31

3.1 Cell format and cell chemistry 31

 3.1.1 Cell preparation 33

 3.1.2 Electrolyte chemicals..... 34

3.2 Electrochemical cell testing 34

 3.2.1 Galvanostatic cycling..... 34

 3.2.2 High precision coulometry 34

 3.2.3 Open circuit voltage storage 36

 3.2.4 Electrochemical impedance spectroscopy..... 38

 3.2.5 Electrolyte conductivity measurements 42

3.3 Cell volume change measurements..... 43

3.4 Gas chromatography coupled with mass spectrometry and thermal
conductivity detection..... 43

 3.4.1 Gas chromatography..... 44

 3.4.2 Separation principles..... 45

 3.4.3 Electron impact mass spectrometry..... 47

 3.4.4 Thermal conductivity detection 50

 3.4.5 GC-MS settings for liquid component analysis..... 51

 3.4.6 GC-MS settings for the analysis of gaseous compounds and high vapor
pressure liquid compounds..... 52

 3.4.7 GC-TCD settings for gas components analysis 53

3.5 Error calculation..... 54

**CHAPTER 4. NOVEL METHODS FOR THE EXTRACTION OF LIQUID AND
GASEOUS COMPONENTS FROM LI-ION CELLS AND SUBSEQUENT GC
ANALYSIS 55**

4.1 Gas chromatography experiments for the study of electrolytes and gas
composition in Li-ion cells 55

 4.1.1 GC-MS measurements of the electrolyte..... 55

 4.1.2 GC and GC-MS measurements of the gas composition..... 57

4.2	Method for extracting the liquid components of Li-ion cells	59
4.2.1	Experimental procedure.....	59
4.2.2	Recovery tests.....	61
4.2.3	Proof of concept.....	63
4.3	Extraction method for gaseous and volatile components of Li-ion cells.....	66
4.3.1	Experimental procedure.....	66
4.3.2	Proof of concept.....	68
4.4	Concluding remarks on the extraction procedures.....	71
CHAPTER 5. ANALYSIS AND QUANTIFICATION OF ADDITIVE		
CONSUMPTION AND GAS GENERATION DURING OPERATION OF		
LI-ION CELLS CONTAINING VINYLENE CARBONATE OR PROP-1-ENE-		
1,3-SULTONE		
73		
5.1	Additive consumption and gas production during the first charge of NMC/graphite cells to low voltage containing VC or PES	73
5.1.1	Gas production in NMC/graphite cells charged to 3.5 V.....	74
5.1.2	Additive consumption during the first charge of NMC/graphite cells containing VC or PES.....	81
5.1.3	Prevention of trans-esterification in presence of VC.....	84
5.2	Additive consumption during 4.2 V operation	89
5.2.1	Additive consumption at the negative and positive electrodes.....	89
5.2.2	Correlation between impedance and VC consumption.....	95
5.3	Gas generation in cells cycled to high voltage.....	99
5.4	Concluding remarks	104
CHAPTER 6. CYCLING PERFORMANCE, GAS GENERATION AND		
ADDITIVE CONSUMPTION IN CELLS CONTAINING PHENYL		
CARBONATES.....		
106		
6.1	Electrochemistry and gas volume generation	109
6.2	Additive consumption during formation to 3.5 V.....	110

6.3	Qualitative composition of the gas generated at 3.5 V	113
6.4	High precision coulometry of cells containing MPC, EPC, and EPC + VC ..	115
6.5	Additive consumption after extended storage at 4.2 V and 40°C.....	117
6.6	Storage at 4.2 V and 40°C of cells containing VC, MPC or DPC.....	119
6.7	Symmetric cell construction from pouch cells containing 1% MPC	121
6.8	Storage at 4.3 V and 40°C of cells containing DPC	123
6.9	Performance of NMC(811)/graphite cells containing DPC	125
6.10	Concluding remarks on phenyl carbonates	126
CHAPTER 7. ANALYSIS OF THE FADE MECHANISM OF LCO/SILICON		
ALLOY-GRAPHITE POUCH CELLS		129
7.1	Why studies of Si-containing full cells is important.....	129
7.2	Room temperature cycling of LCO/Si-alloy:graphite pouch cells filled with FEC-containing electrolytes.....	131
7.2.1	Prevention of trans-esterification in presence of FEC	134
7.3	Gas generated during the first charge of LCO/Si-alloy:graphite pouch cells filled with FEC-containing electrolytes	138
7.4	FEC consumption and irreversible capacity during the first cycle of LCO/Si-alloy:graphite pouch cells	139
7.5	Cycling of LCO/Si-alloy:graphite cells at 40°C	142
7.6	Modeling the capacity fade and consumption of FEC in LCO/Si-alloy: graphite cells cycled at 40°C	145
7.7	Concluding remarks on the fade and FEC consumption in LCO/Si- alloy:graphite pouch cells	151
CHAPTER 8. DESIGN OF NEW ELECTROLYTE SYSTEMS		154
8.1	Ester-based electrolytes	154

8.1.1	Formation of NMC/graphite cells filled with ester-based electrolytes.....	157
8.1.2	Reduction mechanism of various esters	159
8.1.3	High precision coulometry measurements of cells filled with ester-based electrolytes.....	161
8.1.4	Long term cycling of cells filled with ester-based electrolytes	163
8.1.5	Low temperature rate performance of cells filled with ester-based electrolytes.....	168
8.1.6	High temperature performance of cells filled with ester-based electrolytes..	170
8.1.7	Other passivating agents allowing the use of esters.....	171
8.1.8	Performance of ester-based electrolyte in cells operated to 4.3 V	173
8.1.9	Concluding remarks on ester-based electrolytes.....	174
8.2	Linear alkyl carbonate-based electrolytes.....	176
8.2.1	Conductivity of linear alkyl carbonate-based electrolytes.....	178
8.2.2	First cycle of NMC(442)/graphite cells with linear alkyl carbonate-based electrolytes.....	180
8.2.3	Open circuit performance of cells filled with linear alkyl carbonate-based electrolyte vs. ester-based electrolyte.....	181
8.2.4	Optimization of the initial VC content in linear alkyl carbonate-based electrolytes.....	182
8.2.5	Comparison between VC, FEC, and EC as passivating agents	188
8.2.6	Long term cycling of NMC(442)/graphite cells filled with EMC:VC-based electrolytes and operated to 4.4 V.....	191
8.2.7	Safety properties of charged NMC(442) and graphite electrodes in EMC-based electrolytes.....	193
8.2.8	Concluding remarks on linear alkyl carbonate-based electrolytes	195
8.3	Concluding remarks on EC-free solvents	196
CHAPTER 9. FUTURE WORK		198
9.1	GC-MS experiments	198
9.1.1	Reactivity of additives with lithium alkoxides	198
9.1.2	Exploring the reactivity of additive blends.....	199
9.1.3	Determination of reduction pathways of atypical solvents.....	199

9.1.4	Evaluation of the solvent consumption in cells operated at high voltage	200
9.2	LC-MS experiments.....	201
9.2.1	Using Reverse-phase chromatography to detect polar molecular by-..... products	201
9.2.2	Using gel permeation chromatography to detect oligomers.....	202
9.3	Linear alkyl carbonate-based electrolyte exploration	203
CHAPTER 10. CONCLUSION.....		205
REFERENCES.....		209
APPENDIX A		233
APPENDIX B		237
APPENDIX C		238
APPENDIX D		243
APPENDIX E		246
APPENDIX F		251
APPENDIX G.....		263

LIST OF TABLES

Table 3.1. Dry pouch cell electrode active material, cell balance, capacity and manufacturer.	31
Table 3.2. Electrode formulations in the four pouch cell types used.	32
Table 4.1. Recovery efficiency results of the extraction of the electrolyte from NMC(111)/graphite pouch cells using the extraction procedure described in Section 4.2.1.	62
Table 4.2. Mass difference of the silicon wafers after depositing a few drops of each phase in the vials shown in Figure 4.2 and then after heating the same sample at 240°C for 15 min..	65
Table 4.3. Expected and measured composition of a drop of electrolyte extracted in a mixture consisting of 10 mL of CH ₂ Cl ₂ and 0.2 mL of H ₂ O and measured by GC-MS.....	66
Table 6.1. Summary of some of the results presented in the patent filed by Nakagawa <i>et al.</i> [226].	108
Table 7.1. Results of the GC-MS analysis of the electrolyte extracted from cells A, B and C shown in Figure 7.1.	133
Table 7.2. Calculated free energies of reactions (1) to (7) shown in Figures 7.2.	135
Table 7.3. Composition of the gas produced during the first cycle between 4.35 V and 3.0 V at C/20 and 40°C of LCO/Si-alloy:graphite pouch cells filled with a 1M LiPF ₆ EC:EMC:FEC (27:63:10) electrolyte..	138
Table 7.4. Parameters obtained from the fitting of the data presented in Figure 7.6a using Equation 7.2.....	147
Table 7.5. Comparison of the time dependence of lithium loss with values available in the literature.....	148
Table 7.6. Parameters obtained from the fitting of the data presented in Figure 7.6b using Equation 7.3..	150
Table 8.1. Physical characteristics of selected organic carbonates and esters..	155
Table 8.2. Gas volume produced in NMC(111)/graphite pouch cells containing a 1M LiPF ₆ + 0.5 M LiFSi MP:VC (95:5) electrolyte stored for 800 h at open circuit and 40°C.....	174

Table A1. Supplier and purity of chemicals used	235
Table A2. Oven temperature program during GC-MS measurements of liquid components of Li-ion cells.	236
Table A3. Oven temperature program during GC-MS measurements of gaseous and liquid components formed during Li-ion cell use.	236
Table A4. Oven temperature program during GC-TCD measurements of gaseous compounds produced during Li-ion cell use.....	236
Table F1. Volume change of 180 mAh NMC(442)/graphite pouch cells during the first charge, cycling or storage at various voltages and temperatures..	261

LIST OF FIGURES

Figure 1.1. Capacity vs. cycle number for Li[Ni _{0.33} Mn _{0.33} Co _{0.33}]O ₂ /graphite 18650 cells with varying VC concentrations cycling at 1C at 30°C.	2
Figure 1.2. Schematic of a Li-ion cell with a graphite negative electrode (right) and Li[M]O ₂ positive electrode where M is a transition metal (left).....	7
Figure 1.3. Galvanostatic charge-discharge curves for a Li[Ni _{0.33} Mn _{0.33} Co _{0.33}]O ₂ positive electrode (a) and a graphite negative electrode (b) cycled vs. Li/Li ⁺ at a current of C/20.....	9
Figure 1.4. Chemical structures of common salts used in the formulation of electrolytes of Li-ion cells.....	11
Figure 1.5. Chemical structure of common solvents used in electrolytes of Li-ion cells.....	12
Figure 2.1. Reduction of EC at the graphite electrode of Li-ion cells.	19
Figure 2.2. Reduction of PC at the graphite electrode of Li-ion cells.	19
Figure 2.3. Reduction of linear dialkyl carbonates at the graphite electrode of Li-ion cells.	20
Figure 2.4. Proposed reaction pathways for the formation of LiF and fluorophosphates at the graphite electrode of Li-ion cells.	20
Figure 2.5. Proposed reaction pathways for the formation of polycarbonate and polyethylene oxide at the graphite electrode of Li-ion cells..	21
Figure 2.6. Example of high molecular weight organophosphate identified by Tahira <i>et al.</i> in LCO/graphite cells cycled at 60°C [123].....	21
Figure 2.7. Reaction pathways proposed by Aurbach <i>et al.</i> [125] for the formation of lithium alkyl carbonates at the positive electrode of Li-ion cells.	22
Figure 2.8. Proposed reaction pathways for the formation of polycarbonates through cationic ring opening polymerization as proposed in Ref [92].	23
Figure 2.9. Chemical structure of some electrolyte additives for improved cycle performance of Li-ion cells.	26

Figure 2.10. Proposed mechanisms of the cationic (left) and radical (right) polymerization of VC.....	27
Figure 3.1. Voltage vs. capacity for a NMC(111)/graphite pouch cell filled with a 1M LiPF ₆ EC:EMC (3:7) + 0.5% methyl phenyl carbonate..	35
Figure 3.2. Typical cell voltage vs. time profile during a smart OCV storage experiment.....	37
Figure 3.3. Schematic of a single active particle (a) along with its simplified circuit model (b) and Nyquist representation of its impedance (c)..	39
Figure 3.4. Equivalent circuit of a full lithium cell derived from reference [180] (a) and Nyquist representation of the impedance of an LCO/graphite cell (b)..	41
Figure 3.5. Simplified schematic of a gas chromatograph.	44
Figure 3.6. Simplified schematic of a mass spectrometer.	47
Figure 3.7. Ionization mechanism in electron ionization modules.	48
Figure 3.8. Simplified schematic of a quadrupole mass analyzer.....	49
Figure 3.9. Simplified schematic of a thermal conductivity detector with a Wheatstone design.....	50
Figure 4.1. Schematic of the electrolyte extraction method used for the analysis of the electrolyte components by GC-MS..	60
Figure 4.2. Picture of a vial containing 40 drops of a 1 M LiPF ₆ EC EMC (3:7) electrolyte in 10.0 mL of CH ₂ Cl ₂ and 1.0 mL of H ₂ O (a) and of a vial containing 40 drops of a 1 M LiPF ₆ EC EMC (3:7) electrolyte in 10.0 mL of CH ₂ Cl ₂ and 3.0 mL of H ₂ O (b)..	63
Figure 4.3. Picture of the gas extraction device designed for the extraction of gaseous and volatile components of Li-ion cells..	67
Figure 4.4. Chromatogram of the gas extracted from a NMC(111)/graphite pouch cell charged to 3.5 V at 40°C.	69
Figure 4.5. Comparison of the gas volume measured ex-situ and gas volume (and composition) measured using the extraction method described in Section 4.3.1 and GC-TCD for NMC(442)/graphite pouch cells vacuum dried at various temperature prior to electrolyte filling..	70

Figure 5.1. Peak area of compounds detected by GC-MS analysis (a) and volume of gases detected by GC-TCD analysis (b) of the gas and GC-MS analysis of the solvents (c) extracted from NMC(111)/graphite pouch cells filled with various electrolytes and charged to 3.5 V at 40°C and C/20..	74
Figure 5.2. Proposed reaction schemes for the reduction of water, HF, EC and linear carbonates based on the results shown in Figure 5.1.	77
Figure 5.3. VC and PES remaining in NMC(111)/graphite pouch cells initially containing 2.2 % VC or 2.2 % PES, charged to different voltage cut-offs during formation, shown alongside the potential vs. capacity curves (a) and shown alongside the differential capacity vs. voltage curves (b).	82
Figure 5.4. Amount of VC (a) and PES (b) consumed as a function of initial additive loading during the first cycle of NMC(111)/graphite pouch cells containing a 1M LiPF ₆ EC:EMC (3:7) base electrolyte, magnitude of the impedance (R_{ct}) after the first charge and partial discharge to 3.8 V of VC-containing cells (c) and PES-containing cells (d) as a function of initial additive loading.	83
Figure 5.5. EMC, DMC, and DEC mole ratio as a function of time after adding lithium methoxide (LiOMe, (a)) or lithium ethoxide (LiOEt, (b)) to EMC.	85
Figure 5.6. EMC, DMC and DEC mole ratio (a, c) and amount of VC left (normalized to the starting content) (b, d) as a function of time after adding lithium methoxide (a,b) or lithium ethoxide (c,d) to EMC + 10% VC mixtures.	87
Figure 5.7. Possible reaction pathways between VC and lithium alkoxides and subsequent VC oligomerization.	88
Figure 5.8. NMC(111)/graphite pouch cell voltage vs. specific capacity of the fourth cycle shown alongside the fitted NMC(111) electrode and graphite electrode potential vs. specific capacity.	89
Figure 5.9. Amount of VC (a) and PES consumed (b), volume of gas produced in cells containing VC (c) and PES (d), and magnitude of the impedance of cells containing VC (e) and PES (f) for NMC(111)/graphite pouch cells held for 250 h and 40°C at either 3.9 V or 4.2 V.	91
Figure 5.10. Magnitude of the impedance (R_{ct}) vs. amount of VC consumed in NMC(111)/graphite pouch cells filled with electrolytes initially containing various VC contents after various cycling and storage protocols.	95
Figure 5.11. Magnitude of the impedance (R_{ct}) (a) and amount of ES consumed (b) vs. amount of VC consumed after the first cycle of NMC(111)/graphite pouch cells filled with electrolytes initially containing various VC, ES and TTSPi contents.	97

Figure 5.12. In-situ volume measurements during the first charge to 4.7 V of NMC(442)/graphite pouch cells filled with electrolytes containing various additive blends.	99
Figure 5.13. Summary of GC-TCD (a) and GC-MS (b) analysis of the gas extracted from NMC(442)/graphite pouch cells containing various additive contents and charged to 4.7 V for the first time.....	101
Figure 5.14. Possible oxidation pathways for EC and EMC.	102
Figure 6.1. Chromatogram of the electrolyte extracted from a commercial 18650 Li-ion cell produced by a major manufacturer.	107
Figure 6.2. Chemical structure of phenyl carbonates studied.	108
Figure 6.3. Differential capacity vs. cell voltage during the first 10 mAh of the first charge (a) and gas volume produced during the first charge to 3.5 V (b) for 220 mAh NMC(111)/graphite pouch cells filled with different electrolyte blends.	109
Figure 6.4. Mass percent (relative to total electrolyte mass) of VC consumed (a); mass percent (relative to total electrolyte mass) of MPC consumed (b) and mass percent of EMC converted into DMC and DEC (c) in 220 mAh NMC(111)/graphite pouch cells filled with control electrolyte, control electrolyte + 1% MPC, control electrolyte + 2% VC + 1% MPC and control electrolyte + 2% VC after the first charge to 3.5 V and 40°C.....	111
Figure 6.5. Relative peak area of the GC chromatogram of the gas extracted from 220 mAh NMC(111)/graphite pouch cells filled with control electrolyte, control electrolyte + 1% MPC and control electrolyte + 1% DPC after being charged to 3.5 V at C/20 and 40°C.....	113
Figure 6.6. Proposed reduction mechanisms of phenyl carbonates and subsequent reactions of the reduction by-products.	114
Figure 6.7. Charge endpoint capacity slippage rate (a) and CIE (b) of NMC(111)/graphite pouch cells containing various electrolytes and cycled between 2.8 – 4.2 V at C/20 and 40°C.....	115
Figure 6.8. Amount of additive left in 220 mAh NMC(111)/graphite pouch cells filled with 1M LiPF ₆ EC:EMC (3:7) base electrolyte with MPC alone or in combination with 2% VC, after two 500 h of OCV storage at 4.2 V and 40°C....	118

Figure 6.9. OCV vs. time of 220 mAh NMC(111)/graphite pouch cells filled with control electrolyte in combination with various additive blends stored at 40°C at 4.2 V (a); impedance spectra after the storage period (c) and gas volume produced during the first charge to 3.5 V and during the 500 h storage period (d)..	120
Figure 6.10. Impedance spectra of negative electrode symmetric cells (a) and positive electrode symmetric cells (b) reconstructed from 220 mAh NMC(111)/graphite pouch cells filled with control electrolyte and control electrolyte + 1% MPC..	122
Figure 6.11. Cell voltage vs. time during a 500 h open circuit voltage storage at 4.3 V and 40°C of 220 mAh NMC(111)/graphite pouch cells filed with a 1M LiPF ₆ EC:EMC (3:7) electrolyte containing 2% diphenyl carbonate or 2% PES + 1% MMDS + 1% TTSPi.	124
Figure 6.12. Discharge capacity (a) vs. cycle number and difference between average charge and discharge voltage (ΔV , b) for 200 mAh NMC811/graphite pouch cells cycled with clamps at C/2.5 at 40°C between 2.8 and 4.3 V.	125
Figure 7.1. Discharge capacity vs. cycle number of 200 mAh LCO/Si-alloy: graphite pouch cells cycled at room temperature (22°C) between 2.75 V and 4.35 V using a current of C/2.	132
Figure 7.2. Proposed reaction pathways between lithium alkoxides and FEC (a) and between lithium alkoxides and EC (b).	134
Figure 7.3. EMC, DMC, and DEC mole ratio (a, c) and amount of FEC left (normalized to the starting content) (b, d) as a function of time after adding lithium methoxide (a,b) or lithium ethoxide (c,d) to EMC + 10% FEC mixtures.	137
Figure 7.4. Cell voltage (left axis) and FEC consumption (right axis) vs. capacity (a) and FEC consumption vs. irreversible capacity (b) during the partial charging of 200 mAh LCO/Si-alloy:graphite pouch cells.	140
Figure 7.5. Discharge capacity vs. cycle number (a), cell polarization vs. cycle number (b), and fitting of the differential voltage vs. capacity curve (c-d) of the 7 th cycle (c), 12 th cycle (d), 52 nd cycle (e) and 112 th cycle (f) of 200 mAh LCO/Si-alloy:graphite pouch cells.	143

Figure 7.6. Experimental and fitted normalized charge capacity (a), experimental and fitted FEC consumption (b) as a function of cycling time at various rates, as well as experimental normalized charge capacity (c) and FEC consumption (d) for cells cycled at C/2 shown alongside the fitted time dependent and cycle number dependent capacity fade and FEC consumption of 200 mAh LCO/Si-alloy:graphite pouch cells.	146
Figure 8.1. Conductivity vs. temperature for various esters containing 1M LiPF ₆	156
Figure 8.2. Cell voltage vs. capacity (a) and differential capacity vs. cell voltage (b) during the first charge of NMC(111)/graphite pouch cells filled with ester-based electrolytes with or without VC.	157
Figure 8.3. Chromatogram (total ion counts) of the gas extracted from NMC(111)/graphite pouch cells containing various ester-based electrolytes and charged to 20 mAh at C/20 and 40°C..	159
Figure 8.4. Proposed reduction pathways for organic esters at the graphite surface and subsequent reactions of the reduction by-products..	160
Figure 8.5. Charge endpoint capacity slippage rate (a) and CIE (b) of NMC(111)/graphite pouch cells containing various electrolytes and cycled between 2.8 – 4.2 V at C/20 and 40°C.....	162
Figure 8.6. Discharge capacity vs. cycle number of 240 mAh NMC(111)/graphite pouch cells filled with 1M LiPF ₆ x% MP + 100-x% VC electrolytes, cycled at C/5 between 2.8 V and 4.2 V at 40°C..	164
Figure 8.7. Impedance spectra (a) and gas volume formed (b) for 240 mAh NMC(111)/graphite pouch cells filled with 1M LiPF ₆ x% MP + 100-x% VC electrolytes, cycled at C/5 between 2.8 V and 4.2 V at 40°C for 1700 h..	165
Figure 8.8. Amount of VC consumed (a), and amount of VC left (b) in 240 mAh NMC(111)/graphite pouch cells filled with electrolytes filled with various MP + VC electrolyte blends after 1700 h of cycling at C/5 between 2.8 V and 4.2 V at 40°C.....	167
Figure 8.9. Differential capacity vs. cell voltage during the first charge to 3.5 V at 40°C and C/20 of 220 mAh NMC(111)/graphite pouch cells filled with various ester:VC blends	168
Figure 8.10. Discharge energy at -14°C at various rates of 240 mAh MC(111)/graphite pouch cells previously cycled at C/2 at 40°C and filled with either 1M LiPF ₆ EC:EMC + 2% VC or 1M LiPF ₆ MP:VC (95:5) electrolytes.....	169
Figure 8.11. Discharge capacity of NMC(111)/graphite pouch cells filled with various electrolyte blends and cycled between 2.8 – 4.2 V at 55°C and C/10. .	170

Figure 8.12. Cell voltage vs. capacity during the first charge at 40°C and C/10 of NMC(111)/graphite pouch cells filled with ester-based electrolytes containing various additives.....	172
Figure 8.13. Potential vs. capacity of a Li[Ni _{0.4} Mn _{0.4} Co _{0.2}]O ₂ cycled at 40°C and C/20 using Li foil as counter and reference electrode.	176
Figure 8.14. Discharge capacity vs. cycle number of 220 mAh NMC(442)/graphite pouch cells cycled at 40°C at a current of C/5 between 2.8 – 4.4 V for the first 50 cycles and then between 2.8 – 4.5 V.....	177
Figure 8.15. Conductivity vs. temperature of 1M LiPF ₆ in pure linear alkyl carbonate solution (a) and in blends of linear alkyl carbonates (b).	179
Figure 8.16. Differential capacity vs. cell voltage during the first charge to 3.5 V at 40°C and C/20 of 180 mAh NMC(442)/graphite pouch cells filled with various EMC-based blends... ..	180
Figure 8.17. Cell voltage vs. time (a) and gas volume produced (b) for NMC(111)/graphite pouch cells filled with various electrolyte blends during a 500 h open circuit voltage storage at 4.3 V and 40°C.. ..	182
Figure 8.18. Amount of VC left (a) and % EMC trans-esterification (b) vs. initial VC content in NMC(442)/graphite pouch cells that underwent one full cycle between 2.8 – 4.4 V at 40°C and filled with 1M LiPF ₆ EMC + x% VC electrolytes.	183
Figure 8.19. Amount of VC left vs. cycling time during the first cycle at 40°C in NMC(442)/graphite pouch cells initially filled with a 1M LiPF ₆ EMC + 1.8% VC electrolyte.	184
Figure 8.20. Reversible capacity loss (a), irreversible capacity loss (b), magnitude of the impedance (R _{ct} , c) and gas volume generated (c) during 500 h 4.4 V smart storage at 40°C for 180 mAh NMC(442)/graphite pouch cells filled with various electrolyte blends.....	186
Figure 8.21. Voltage vs. time during OCV storage at 4.2 V (a-c) and 4.5 V (d-f) and coulombic efficiency during cycling between 2.8 – 4.5 V(g-i) for 180 mAh NMC(442)/graphite pouch cells filled with various electrolyte blends.. ..	189
Figure 8.22. Discharge capacity vs. cycle number (a) and polarization growth (b) during cycling between 2.8 – 4.4 V and 20°C; discharge capacity vs. cycle number (c) and polarization growth (d) during cycling between 2.8 – 4.4 V and 55°C for 180 mAh NMC(442)/graphite pouch cells filled with various electrolyte blends.. ..	192

Figure 8.23. Self heating rate vs. temperature of lithiated graphite powder (a) and delithiated NMC(442) powder (b) recovered from NMC(442)/graphite pouch cells charged to 4.5 V and filled with various electrolyte blends.....	194
Figure A1. Picture of NMC/graphite and LCO/graphite pouch cells used throughout the work presented in this thesis.	233
Figure A2. Voltage vs. capacity of LCO/gr (a), NMC(111)/gr (b), NMC(442)/gr (c) and LCO/Si:gr (d) pouch cells measured at 40°C along with the potential vs. capacity of the negative electrode and positive electrode as fitted by differential voltage analysis.	233
Figure B1. Chromatogram of the electrolyte extracted from a cycled LCO/graphite pouch cell filled with a 1M LiPF ₆ EC:EMC (3:7) + 2% VC electrolyte.....	237
Figure C1. EMC, DMC and DEC mole ratio as a function of time after adding lithium methoxide or lithium ethoxide to an EC:EMC (3:7) solution..	238
Figure C2. Structure and molar mass of the compounds listed as EC-OMe and EC-OEt resulting from the addition-neutralization reaction between VC and LiOMe or LiOEt shown in Equation 5.6.	239
Figure C3. Amount of VC (a) and PES consumed (b), volume of gas produced in cells containing VC (c) and PES (d), and magnitude of the impedance of cells containing VC (e) and PES (f) for NMC(111)/graphite pouch cells held for 250 h and 50°C at either 3.9 V or 4.2 V.....	240
Figure C4. Impedance spectra of negative electrode symmetric cells (a,c,e) and positive electrode symmetric cells (b,d,f) reconstructed from NMC(111)/graphite pouch cells filled with electrolytes containing various amounts of PES after formation, after a 250 h hold at 3.9 V and 40°C or after a 250 h hold at 4.2 V and 40°C..	241
Figure C5. Cell voltage vs. storage time (a) and gas volume production (b) during OCV storage at 4.2 V and 60°C for NMC(111)/graphite pouch cells filled with a 1M LiPF ₆ EC:EMC (3:7) base electrolyte containing 2% VC or 4% VC + 1% ES + 1% TTSPi.	242
Figure D1. Chromatogram of an EMC:MPC (90:10) solution before and after the addition of 1% lithium methoxide.....	243
Figure D2. Discharge capacity (Q _D) (a); charge-end-point capacity (b) and coulombic efficiency (c) of 220 mAh NMC(111)/graphite pouch cells filled with control electrolyte in combination with various additive blends, cycled between 2.8 V and 4.2 V at C/20 and 40 ± 0.1°C.....	244

Figure D3. OCV vs. time (a) of 220 mAh NMC(111)/graphite pouch cells filled with control electrolyte in combination with various additive blends stored at 40°C at 4.2 V and cell impedance after storage (b).....	245
Figure E1. EMC, DMC, and DEC mole ratio (a, c) and amount of FEC left (normalized to the starting content) (b, d) as a function of time after adding lithium methoxide (a,b) or lithium ethoxide (c,d) to EC:EMC + 10% FEC mixtures.....	247
Figure E2. XRD pattern of the solid product of the reaction resulting from the addition of 1% lithium ethoxide to a EMC:FEC (90:10) mixture and a reference pattern for LiF.....	248
Figure E3. Impedance spectra of negative electrode symmetric cells (a) and positive electrode symmetric cells (b) reconstructed from the electrodes of 200 mAh LCO/Si-alloy:graphite pouch cells filled with a 1 M LiPF ₆ EC:EMC:FEC (27:63:10) electrolyte cycled at 40°C between 3.0 V and 4.35V and a current of C/2..	249
Figure E4. Charge and discharge capacity (a) and coulombic efficiency (b) vs. cycle number as well as differential capacity vs. potential of Si-alloy:graphite/Li half cells filled with a 1 M LiPF ₆ EC:EMC:FEC (27:63:10) electrolyte cycled at 40°C with currents corresponding to C/28 and C/10.	250
Figure F1. Cell voltage vs. capacity (a,b) and differential capacity vs. cell voltage (c,d) during the first charge of NMC(111)/graphite pouch cells filled with ester- based electrolytes with or without VC.....	251
Figure F2. Chromatogram (total ion count) of the gas extracted from 220 mAh NMC(111)/graphite pouch cells containing various MB, MA or MP-based (a) and EA or PA-based electrolytes and charged to 20 mAh at C/20 and 40°C.	252
Figure F3. Discharge capacity vs. cycle number of 240 mAh NMC(111)/graphite pouch cells filled with 1M LiPF ₆ x% MP + 100-x% VC or 1M LiPF ₆ x% EA + 100-x% VC electrolytes, cycled at C/5 between 2.8 V and 4.2 V at 40°C....	253
Figure F4. Impedance spectra (a) and gas volume formed (b) for 240 mAh NMC(111)/graphite pouch cells filled with 1M LiPF ₆ x% MP + 100-x% VC or 1M LiPF ₆ x% EA + 100-x% VC electrolytes, cycled at C/5 between 2.8 V and 4.2 V at 40°C for 1700 h.....	254
Figure F5. Discharge capacity of NMC(111)/graphite pouch cells filled with various electrolyte blends and cycled between 2.8 – 4.2 V at 55°C and C/10..	255
Figure F6. Conductivity vs. temperature for MP or MB-based electrolytes with or without LiFSi.	256

Figure F7. Discharge capacity of NMC(111)/graphite pouch cells filled with various electrolyte blends and cycled between 2.8 – 4.2 V at 40°C and C/5. ...257

Figure F8. Structure and common names of the additives tested in Section 7.1.7258

Figure F9. Impedance spectra after the first cycle between 2.8 – 4.2 V at 40°C of 240 mAh NMC(111)/graphite pouch cells filled with various ester-based electrolytes..259

Figure F10. Gas volume produced during the first charge to 3.5 V at 40°C and C/20 of 180 mAh NMC(442)/graphite pouch cells filled with various EMC-based blends.....260

ABSTRACT

While electrolyte additives have a great impact on Li-ion cell lifetime, the ways they work are still poorly understood. In an effort to better understand how additives function, two gas chromatography-based methods were developed. One of the methods allows the neutral and organic components of the electrolyte to be determined, while the other allows the composition of the gas produced during cell use to be determined. These two methods were used in order to determine the concentration-time profiles of some additives as well as the gas produced in Li-ion cells charged to low voltage (*i.e.* 3.5 V) and high voltage (*i.e.* 4.7 V). Some of the measurements allowed the reduction and oxidation pathways of solvents and additives to be determined and other measurements allowed the relationship between impedance and additive consumption to be determined.

Using the information gathered on ethylene carbonate-based electrolytes, new ethylene carbonate-free electrolyte systems were also developed. These consist of ester or linear alkyl carbonate-based electrolytes containing small amounts of passivating agents. Once the passivating agent loading was optimized, cells with ester-based electrolytes presented good capacity retention when cycled up to 40°C and 4.2 V and good low temperature rate capability. Cells with the linear alkyl-based electrolytes on the other hand presented better capacity retention than cells with state of the art ethylene carbonate-based electrolytes when cycled at high voltage (*i.e.* > 4.3 V), even at 55°C.

LIST OF ABBREVIATIONS USED

AFM	Atomic force microscopy
CE	Coulombic efficiency
CI	Chemical ionization
CIE	Coulombic inefficiency
CPE	Constant phase element
DEC	Diethyl carbonate
DEOHC	Diethyl-2,5-dioxahexane carboxylate
DMC	Dimethyl carbonate
DMOHC	Dimethyl-2,5-dioxahexane carboxylate
DPC	Diphenyl carbonate
DTD	Ethylene sulfite
EA	Ethyl acetate
EC	Ethylene carbonate
EI	Electron impact ionization
EIS	Electrochemical impedance spectroscopy
EMC	Ethyl methyl carbonate
EMOHC	Ethylmethyl-2,5-dioxahexane
EP	Ethyl propanoate
EPC	Ethyl phenyl carbonate
ES	Ethylene sulfite
ESI	Electrospray ionization
EV	Electric vehicles
FEC	Fluoro ethylene carbonate
FID	Flame ionization detector
FT-IR	Fourier transform infrared spectroscopy
GC	Gas chromatography
GC-MS	Gas chromatography coupled with mass spectrometry
HPC	High precision coulometry
IRC	First cycle irreversible capacity
LCO	LiCoO_2
LEDC	Lithium ethylene dicarbonate
LFP	LiFePO_4
LiBOB	$\text{LiB}(\text{C}_2\text{O}_4)_2$
LiFSi	Lithium bis(fluorosulfonyl) imide ($\text{LiN}(\text{SO}_2\text{F})_2$)
$\text{Li}[\text{M}]\text{O}_2$	Lithium transition metal dioxide
LiOEt	Lithium ethoxide
LiOMe	Lithium methoxide
LiTFSI	Lithium bis(trifluoromethanesulfonyl) imide ($\text{LiN}(\text{SO}_2\text{CF}_3)_2$)
LMO	$\text{Li}_{1+x}\text{Mn}_{2-x}\text{O}_4$
LNMO	$\text{LiNi}_{0.5}\text{Mn}_{1.5}\text{O}_2$
LTO	$\text{Li}_{4/3}\text{Ti}_{5/4}\text{O}_4$
MA	Methyl acetate

MEC	Methylene ethylene carbonate
MMDS	Methylene methanedisulfonate
MO	Rock-salt structure
MO ₂	Charged surface of a layered positive electrode
MP	Methyl propanoate
MPC	Methyl phenyl carbonate
MPrC	Methyl propyl carbonate
MS	Mass spectrometry
NCA	LiNi _x Co _y Al _{1-x-y} O ₂
NMC	Li(Ni _{1-x-y} Mn _x Co _y)O ₂
NMC(111)	Li[Ni _{0.33} Mn _{0.33} Co _{0.33}]O ₂
NMC(442)	Li[Ni _{0.4} Mn _{0.4} Co _{0.2}]O ₂
NMC(811)	Li[Ni _{0.8} Mn _{0.8} Co _{0.1}]O ₂
NMR	Nuclear magnetic resonance
OCV	Open circuit voltage
PA	Propyl acetate
PBF	Pyridine trifluoroborate
PC	Propylene carbonate
PES	Prop-1-ene-1,3-sultone
PFA	Perfluoroalkoxy polymer
PLS	Propylene sulfate
PPF	Pyridine pentafluorophosphate
PS	1,3-Propanesultone
PTFE	Polytetrafluoroethylene
PVDF	Polyvinylidene fluoride
ROLi	Lithium alkoxide
SEI	Solid electrolyte interphase
SEM	Scanning electron microscopy
TAP	Triallyl phosphate
TCD	Thermal conductivity detector
TMS	1,3,2-dioxathiane-2,2-dioxide
TTSPi	Tris(trimethylsilyl)phosphite
UHPC	Ultra-high precision coulometry
VC	Vinylene carbonate
XPS	X-ray photoelectron spectroscopy
XRD	X-ray diffraction
gr	Graphite
<i>Slvt</i>	Solvent molecule
<i>Slvt</i> ⁺	Product of the oxidation of a solvent molecule
<i>Slvt</i> -O	Product of a pseudo combustion reaction between oxygen released from the charged positive electrode surface
e ⁻	Electron
<i>B</i>	Constant related to the time dependence of the capacity fade of a Li-ion cell

C	Constant related to the cycle number dependence of the capacity fade of a Li-ion cell
D	Constant related to the time dependence of the consumption of FEC in a Li-ion cell
D_0	Capacity of the discharge prior to a 500 h OCV storage period
D_1	Capacity of the 1 st discharge after a 500 h OCV storage period
D_2	Capacity of the 2 nd discharge after a 500 h OCV storage period
F	Tension in a wire
g	Gravitational acceleration
i_s	Compound i in the stationary phase
i_m	Compound i in the mobile phase
$[i]_s$	Concentration of compound i in the stationary phase
$[i]_m$	Concentration of compound i in the mobile phase
I	Current
K_i	Partition coefficient of compound i between the stationary and mobile phase
m	Mass of an object
m_{FEC}	Mass of FEC consumed in a Li-ion cell
M	Molecular compound
M	Transition metal
M^+	Molecular ion resulting from the collision of an electron and a molecular (neutral) compound M
p_i	Partial pressure of component i in a mixture
p_i^*	Partial pressure of the pure component i
Q	Normalized capacity
Q_0	Capacity of a reference cycle
Q_{irrev}	Irreversible capacity loss during storage
Q_{rev}	Reversible capacity loss during storage
Q_{tot}	Total capacity loss during storage
R	Resistive element
R_{ct}	Sum of the diameters of the overlapping semi-circles of the Nyquist representation of the impedance spectrum of a Li-ion cell
t	Time
t_0	Constant correcting the real cycling time of a Li-ion cell in the capacity fade fitting equation
t_m	Retention time of an unretained compound
$t_{r,i}$	Retention time of compound i
$t'_{r,i}$	Corrected retention time of compound i
V	Voltage
V_{cell}	Volume of a Li-ion cell
V_s	Volume of the stationary phase
V_m	Volume of the mobile phase
W	Warburg-type element
x_i	Molar fraction of the component i
X	Constant related to the cycle number dependence of the consumption of FEC in a Li-ion cell

X^+	Ionic product resulting from the fragmentation of a molecular ion
Y	Neutral product resulting from the fragmentation of a molecular ion
z	Charge of an ion
Z	Impedance
φ	Phase
ρ	Density of water
ω	Frequency

ACKNOWLEDGEMENTS

I would like to thank the *Natural Sciences and Engineering Research Council* (NSERC) and the Walter C. Sumner memorial fellowship, for their financial support, along with 3M for the partial funding of this work.

I am very grateful to a great number of people for their help and support throughout these past years. Special thanks go to my supervisor Jeff Dahn for his extensive support and guidance, great enthusiasm and patience. I would also like to thank my committee members, Mary Anne White, Mark Obrovac, and Ian Hill for their help and advice.

Most importantly I would like to give a thousand thanks to my wife for her loving support throughout the years of Ph.D. and two years of M.Sc. I would like to thank my son for simply being here and the many laughs we have had.

I would like to thank Lina Rotermund and Jordan Wentzell for their help with my projects during the summer internships they spent under my supervision.

I cannot forget the great help I have received from Robbie Sanderson and Simon Trusler in the design and making of the tools that greatly facilitated the progress made. I would also like to thank Tony Gozdz for the great help in obtaining a good electrolyte separation technique which fast-tracked my project.

CHAPTER 1. INTRODUCTION

1.1 Motivation

Li-ion cells are ubiquitous in present technologies, from portable electronics to ground and aerial transportation. Batteries for transportation such as electric vehicles (EV) have to meet high standards in terms of energy density, lifetime, charge-discharge rate capabilities, safety, and temperature range. Cycle performance (lifetime, and charge-discharge capacity retention) depends as much upon the electrolyte blend as the active material choice and particle morphology [1]. EV manufacturers such as Nissan and Tesla offer battery warranties ranging from 5 to 8 years. As a result, cell lifetime is an important research area in the electric vehicle industry.

Several researchers showed that electrolyte additives greatly affect cell lifetime [2–5]. Smith *et al.* [6,7], Burns *et al.* [5,8], and Sinha *et al.* [9] showed, using a combination of high precision coulometry (HPC) and open circuit voltage experiments, that this comes from a reduction of parasitic reactions at both the positive and the negative electrode surfaces. While the effects of additives on the rate of parasitic reactions are now recognized, the chemical origin of their effects is still poorly understood.

Figure 1.1 shows the discharge capacity *vs.* cycle number of Li-ion cells containing different initial additive (vinylene carbonate, VC) loadings. Figure 1.1 shows that all cells show a sudden capacity drop after a certain number of cycles. The cycle number onset for this sudden capacity-drop is pushed to higher and higher values with initial additive loading. Some researchers believe that this onset relates to a depletion of

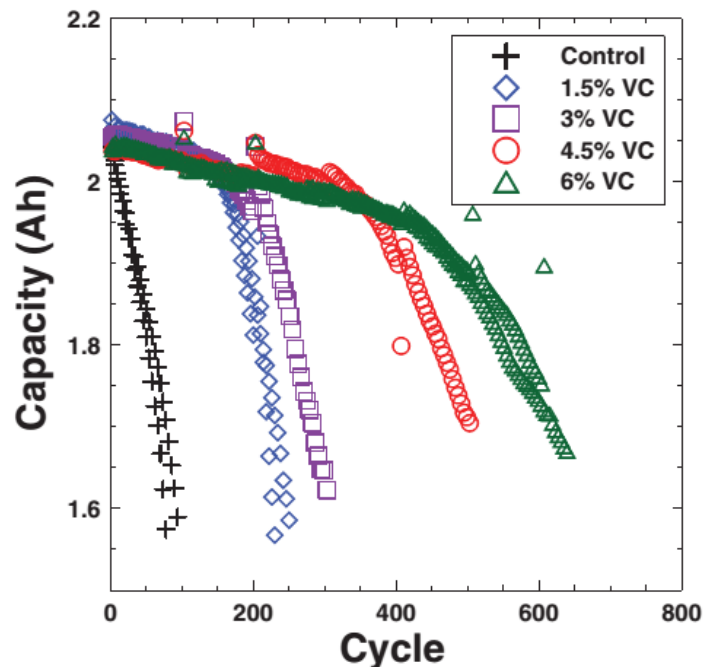


Figure 1.1. Capacity vs. cycle number for $\text{Li}[\text{Ni}_{0.33}\text{Mn}_{0.33}\text{Co}_{0.33}]\text{O}_2/\text{graphite}$ 18650 cells with varying VC concentrations cycling at 1C at 30°C. Reproduced with permission from *J. Electrochem. Soc.*, **160**, A1668-A1674 (2013). Copyright 2013, The Electrochemical Society.

the additive in the electrolyte [10]. A higher initial additive loading would then push the depletion of the additive to a higher cycle number. However, a publication from Burns *et al.* [5] seemed to indicate that this later onset with additive loading comes from a more pronounced reduction of parasitic reactions at the positive electrode. This clearly shows that the effects of additives are not completely understood. It is also very apparent that knowing the concentration-time profile of additives in Li-ion cells would settle this argument.

While designing long-lasting cells that operate to a potential cut-off of 4.2 to 4.3 V is still very difficult, a lot of effort is focused on developing Li-ion cells with higher operating voltage. However, such high voltages (4.4 – 4.8 V) give rise to poor capacity retention [11], high gas production during the first cycle and during subsequent cycles

[12,13], and high impedance [14]. Ma *et al.* [11] showed that typical electrolyte additives that are known to enhance cycle life in cells operating at 4.2 V and below, give little improvement when used in cells operating above 4.4 V. In another instance, Self *et al.* [13] showed that some additives produced a large amount of gas when cells were brought to voltages above 4.3 V for the first time. Knowing why such additives do not bring benefits at high potential and why their addition produces gas would help develop novel additives or additive blends that would enable the use of high voltage positive electrode materials.

There are now a substantial number of scientific publications showing the advantages of electrolyte additives [4,11,15–25]. However cells that can operate over large potential windows or large temperature ranges may need new electrolyte systems. For instance, low temperature performance cannot easily be improved with the use of electrolyte additives if freezing points need to be lowered or electrolyte conductivity needs to be improved. Similarly, there seems to be a limit to the improvements one additive or combination of additives can bring to cells cycled to high potential [26]. In these particular cases, new solvent blends in combinations with proper additives might be needed.

Designing new electrolytes is difficult since they need to be stable at high potential, provide good passivation of the graphite electrode (if a graphite electrode is used), have low viscosity, good conductivity, good separator wetting properties, be low cost, low toxicity, and give good performance at low and high temperature. This is the reason why most of the new electrolyte systems proposed in the literature [27–33] are unlikely to be commercialized in the near future. However, this thesis will show that new

electrolyte systems fulfilling most of these properties can be designed using a simple methodology.

Chapter 2 of this thesis presents an overview of the current understanding of passivation phenomena at both the positive and negative electrodes of Li-ion cells. Chapter 2 also presents a brief summary of the different classes of additives reported in the literature as well as how they are currently thought to function.

Chapter 3 gives a description of the experimental tools used throughout this work. Chapter 4 presents the two gas chromatography-based methods developed. The first method aims at extracting and analyzing the neutral components of the electrolyte of cycled Li-ion cells. The second method aims at extracting and analyzing the gas produced in cycled Li-ion cells.

Chapter 5 presents the results of additive quantification and gas analysis of Li-ion cells operated at both low voltage (*i.e.* < 4.2 V) and high voltage (*i.e.* 4.7 V). This Chapter will show the usefulness of the two GC-based methods in better understanding the reactivity of electrolyte additives as well as the reactivity of the solvents present in the electrolyte of Li-ion cells.

Chapter 6 presents initial results on phenyl carbonates used as electrolyte additives. Ultra-high precision coulometry, open circuit voltage storage and EIS were performed in order to evaluate their effectiveness in cells operated at 4.2 V and 4.3 V. Analysis of the electrolyte and gas produced will also present how these additives react at the graphite surface.

Chapter 7 shows that the two GC-based methods developed can also help reveal the failure mode of Li-ion cells using silicon alloy:graphite composite negative electrodes.

Chapter 8 demonstrates that using simple analytical measurements and the results of Chapter 5 can help understand how new electrolyte systems work. These new electrolyte systems consist of ethylene carbonate-free solvent blends using small amounts of additives.

Finally Chapter 9 proposes different avenues for future work and Chapter 10 gives concluding remarks.

Most of the results presented in this thesis were previously published in various peer-reviewed journals. The results were mainly published in:

- R. Petibon, L. Rotermund, K.J. Nelson, A.S. Gozdz, J. Xia, J.R. Dahn, Study of Electrolyte Components in Li-Ion Cells Using Liquid-Liquid Extraction and Gas Chromatography Coupled with Mass Spectrometry, *J. Electrochem. Soc.* 161 (2014) A1167–A1172. doi:10.1149/2.117406jes.

- R. Petibon, J. Xia, J.C. Burns, J.R. Dahn, Study of the Consumption of Vinylene Carbonate in $\text{Li}[\text{Ni}_{0.33}\text{Mn}_{0.33}\text{Co}_{0.33}]\text{O}_2/\text{Graphite}$ Pouch Cells, *J. Electrochem. Soc.* 161 (2014) A1618–A1624. doi:10.1149/2.0351410jes.

- R. Petibon, L. Madec, L.M. Rotermund, J.R. Dahn, Study of the consumption of the additive prop-1-ene-1,3-sultone in $\text{Li}[\text{Ni}_{0.33}\text{Mn}_{0.33}\text{Co}_{0.33}]\text{O}_2/\text{graphite}$ pouch cells and evidence of positive-negative electrode interaction, *J. Power Sources.* **313** (2016) 152–163. doi:10.1016/j.jpowsour.2016.02.054.

- R. Petibon, L.M. Rotermund, J.R. Dahn, Evaluation of phenyl carbonates as electrolyte additives in lithium-ion batteries, *J. Power Sources*. **287** (2015) 184–195. doi:10.1016/j.jpowsour.2015.04.012.

- R. Petibon, J. Harlow, D.B. Le, J.R. Dahn, The use of ethyl acetate and methyl propanoate in combination with vinylene carbonate as ethylene carbonate-free solvent blends for electrolytes in Li-ion batteries, *Electrochimica Acta*. **154** (2015) 227–234. doi:10.1016/j.electacta.2014.12.084.

- R. Petibon, V.L. Chevrier, C.P. Aiken, D.S. Hall, S.R. Hyatt, R. Shunmugasundaram, et al., Studies of the Capacity Fade Mechanisms of LiCoO₂ /Si-Alloy: Graphite Cells, *J. Electrochem. Soc.* **163** (2016) A1146–A1156. doi:10.1149/2.0191607jes.

The license agreements to reproduce the work previously published can be found in Appendix G.

1.2 Li-ion cells

1.2.1 General configuration

Figure 1.2 shows a simplified diagram of a Li-ion cell. Li-ion cells consist of a negative electrode and a positive electrode separated by a thin electronically insulating porous membrane called a “separator”. In Figure 1.2, the positive electrode is made from a lithium transition metal dioxide, and the negative electrode is made from graphite. These two materials have layered structures into which lithium can reversibly be inserted and de-inserted (intercalated and de-intercalated) between the layers without any substantial structural change [1]. The separator is soaked in an electrolyte consisting of a

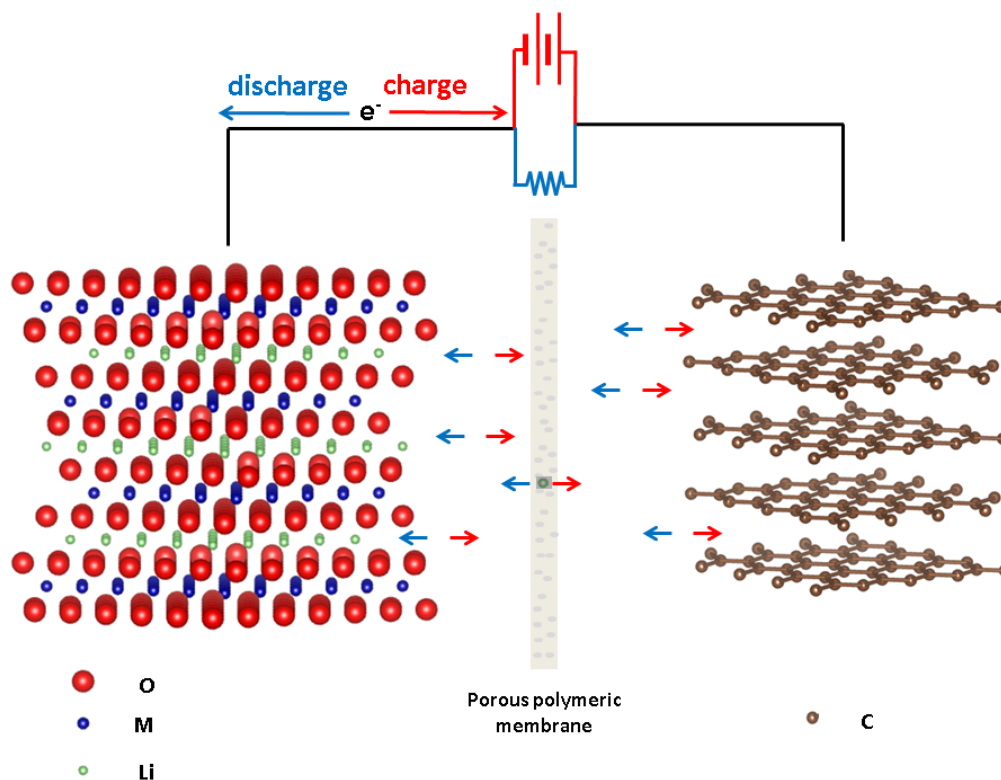


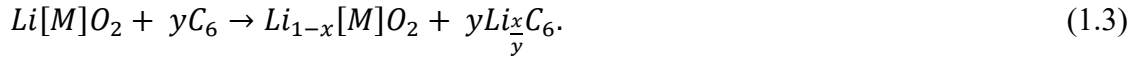
Figure 1.2. Schematic of a Li-ion cell with a graphite negative electrode (right) and $\text{Li}[M]\text{O}_2$ positive electrode where M is a transition metal (left). Taken with permission from R. Petibon, *Study of electrolyte additives in Li-ion batteries using electrochemical impedance spectroscopy on symmetric cells*, M.Sc. thesis, Dalhousie University, Halifax, NS (2013).

lithium salt dissolved in a blend of organic solvents. The active materials of both electrodes are typically micron-sized particles blended with a conductive additive and a polymeric binder [1]. During electrode manufacture, the active material, the conductive additive and the binder are mixed in a solvent thus forming a slurry. The slurry is then coated on a thin metallic foil acting as a current collector. For electrochemical stability and economic reasons, the positive electrode slurry is coated on an aluminum foil while the negative electrode material is coated on a copper foil [1]. The coated slurry is then dried until all the solvent evaporates.

The Li-ion cell depicted in Figure 1.2 is in a discharged state. During charge, a current is applied to force the thermodynamically un-favored reaction. During this process, an electron travels from the positive electrode to the negative electrode through an external circuit. In parallel, a lithium ion de-intercalates from the positive electrode and travels through the electrolyte towards the negative electrode into which it intercalates. The two half reactions during charge are given by:



The overall reaction is given by:



The value of x depends on the positive electrode material used and the upper cut-off voltage of the cell. For instance, the value of x is ~ 0.6 when $LiCoO_2$, or ~ 0.65 when $Li[Ni_{0.33}Mn_{0.33}Co_{0.33}]O_2$ (NMC(111)) are used with an upper cut-off voltage of 4.25 V. The mass of the negative electrode is usually adjusted so that the term $\frac{x}{y}$ reaches a value of about 0.9 or 0.95 when the cell is fully charged in order to prevent lithium from plating on the negative electrode.

During discharge, the thermodynamically favored reactions occur. A lithium ion de-intercalates from the negative electrode and travels from the negative electrode to the positive electrode through the electrolyte. An electron is transferred from the negative electrode to the positive electrode through an external circuit where useful work can be done. At the same time, a lithium ion intercalates into the positive electrode.

Figure 1.3 shows the galvanostatic lithiation profile of a graphite negative electrode (a) and the galvanostatic delithiation profile of a NMC(111) positive electrode (b) cycled vs. Li/Li^+ . In this figure, the amount of Li intercalated into the positive electrode decreases from left to right and the amount of lithium intercalated into the graphite electrode increases from left to right. The capacity of each electrode has been adjusted to present the potential vs. capacity profile (vs. Li/Li^+) that each electrode would experience during the galvanostatic charge of a 170 mAh NMC(111)/graphite full cell. Figure 1.3 shows that the potential vs. capacity profile of each electrode is dependent

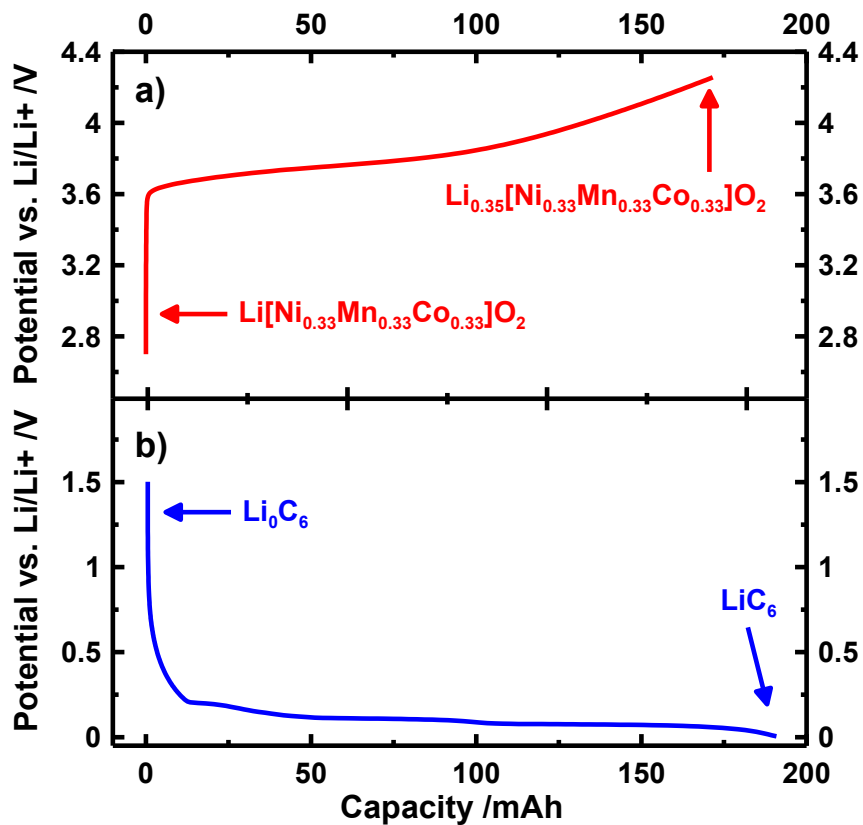


Figure 1.3. Galvanostatic charge-discharge curves for a $\text{Li}[\text{Ni}_{0.33}\text{Mn}_{0.33}\text{Co}_{0.33}]\text{O}_2$ positive electrode (a) and a graphite negative electrode (b) cycled vs. Li/Li^+ at a current of $\text{C}/20$. The currents are given in “ C/x - rate”, where x is the number of hours it would take to fully charge, or fully discharge the electrode.

upon the amount of Li intercalated in the electrode. The voltage of the cell would be the difference of the potential of the positive electrode and negative electrode:

$$V_{cell} = V_{(+)} - V_{(-)} \quad (1.4)$$

where V_{cell} is the cell voltage, $V_{(+)}$ is the potential of the positive electrode and $V_{(-)}$ is the potential of the negative electrode.

This thesis adopts the units that are commonly used in the Li-ion battery community as it renders comparison with the literature easier. For this reason, capacities (x-axis of Figure 1.3) are given in mAh rather than the IUPAC recommended coulomb units (1 mAh is equal to 3.6 C). The currents are given in “C/x - rate”, where x is the number of hours it would take to fully charge, or fully discharge the electrode.

1.2.2 Electrolyte systems

Typical electrolyte systems for Li-ion cells consist of a lithium salt dissolved in a mixture of organic carbonates [34,35]. Figure 1.4 shows the chemical structure of common lithium salts. Lithium hexafluorophosphate (LiPF_6) is typically used in Li-ion cells as it balances cost, ionic conductivity, and passivation of the aluminum current collector at high potential [34]. Other salts have been proposed in the literature, however they all have some disadvantages. For example, electrolytes using lithium bis(oxalate)borate (LiBOB) [36], and lithium tetrafluoroborate (LiBF_4) [37] have low conductivity when dissolved in organic carbonates [38–40], and sulfonyl imides such as LiFSi and LiTFSi are expensive and do not protect aluminum current collectors against corrosion at high potentials when used in typical concentrations (1 – 1.5 M) [41,42] or in

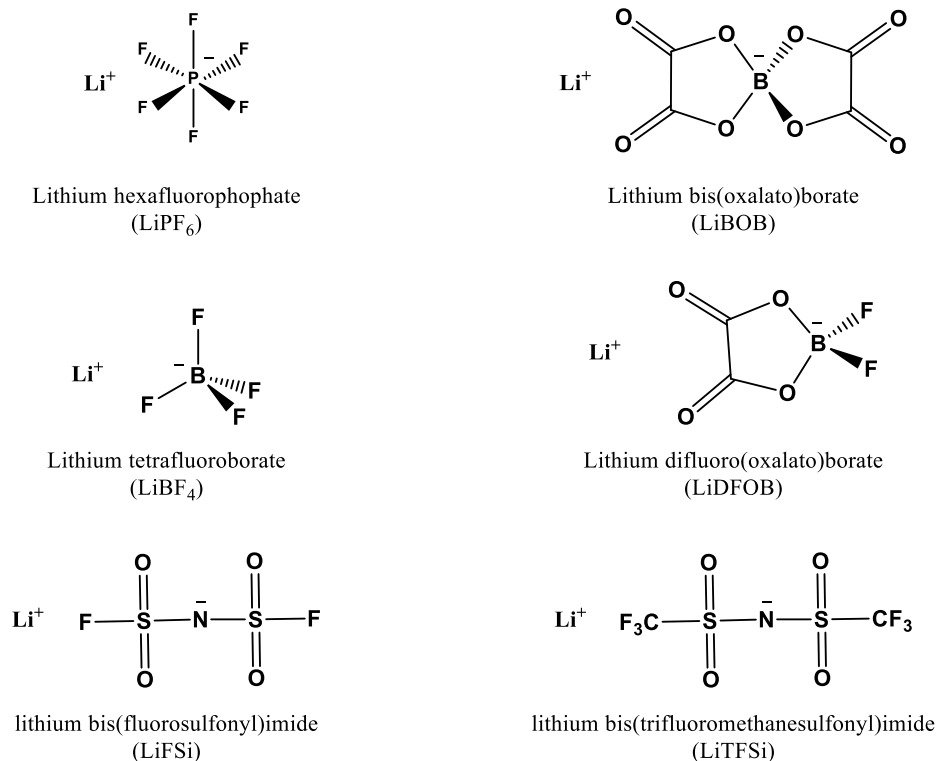


Figure 1.4. Chemical structures of common salts used in the formulation of electrolytes of Li-ion cells.

the presence of free chlorine contamination [43]. Some of these salts are however sometimes used as additives (see Section 2.3).

Figure 1.5 shows the chemical structures of solvents used in most Li-ion cells. Solvent mixtures typically use a cyclic carbonate, usually ethylene carbonate (EC), in combination with a linear carbonate such as dimethyl carbonate (DMC) or ethyl methyl carbonate (EMC). These particular combinations are used due to the high dielectric constant of cyclic carbonates, and the low viscosity of linear carbonates, which yields electrolytes with relatively high conductivity [1,35]. Typical carbonate-based electrolyte have conductivities on the order of 10^{-2} $\text{mS}\cdot\text{cm}^{-1}$ around room temperature [44]. Other organic solvents such as ethers and alcohols are usually not used due to their inadequate

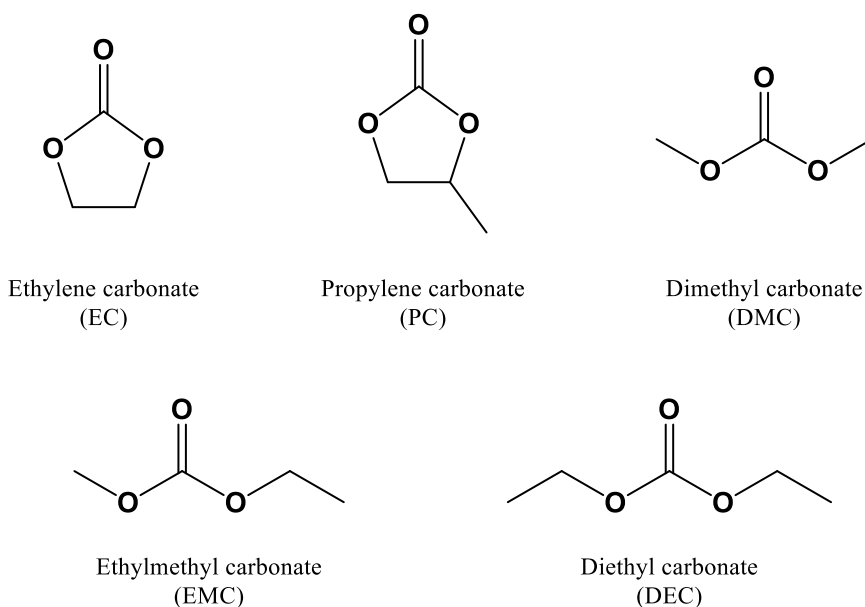


Figure 1.5. Chemical structure of common solvents used in electrolytes of Li-ion cells.

potential window of stability, limited high temperature stability and lack of film-forming properties [45].

1.2.3 Positive electrode materials

Numerous positive active materials have been developed for Li-ion cells. They usually adopt layered structures (see Figure 1.2), such as LiCoO_2 (LCO), $\text{LiNi}_x\text{Co}_y\text{Al}_{1-x-y}\text{O}_2$ (NCA) and $\text{Li}[\text{Ni}_x\text{Mn}_y\text{Co}_{1-x-y}]\text{O}_2$ (NMC), olivine type structures such as LiFePO_4 (LFP), or spinel structures such as LiMn_2O_4 (LMO) [1]. They have all advantages and drawbacks. For example, LFP has low energy density but high safety, LCO has high energy density but high cost and LMO is low cost but has poor high temperature performance [1]. The properties of NCA and NMC-type materials depend on

the transition metal composition, but generally present intermediate properties in terms of cost, safety and energy density [1].

Other materials are being investigated such as $\text{LiNi}_{0.5}\text{Mn}_{1.5}\text{O}_2$, commonly referred as high voltage spinel or LNMO, and lithium rich materials such as $\text{Li}[\text{Li}_{1/3-2x/3}\text{Ni}_x\text{Mn}_{2/3-x/3}]\text{O}_2$ materials [46]. However these suffer from electrolyte degradation due to their high nominal voltage [47–49], transition metal dissolution [50] and voltage fade due to gradual phase transformation [51]. Several researchers are investigating new additive systems [21,48,52,53], coatings [54,55] and core-shell designs [56] that might be able to solve these problems.

The potential cut-off of the positive electrode in commercial cells is typically limited to 4.3 V vs. Li/Li^+ to prevent sustained electrolyte oxidation. However batteries destined for consumer electronics that do not require long cycle-life have potential cut-offs as high as 4.45 V vs. Li/Li^+ [57].

1.2.4 Negative electrode materials

Several negative electrode materials are used in the industry. The most prominent one is graphite as it has relatively high volumetric capacity and a potential very close to Li metal (200 mV to 60 mV vs. Li/Li^+) [1]. The second most prominent electrode material is lithium titanium oxide ($\text{Li}_{4/3}\text{Ti}_{5/4}\text{O}_4$), however it suffers from high potential vs. Li/Li^+ [58] which yields Li-ion cells with low energy density [1].

Other negative electrodes are being introduced in commercial cells such as silicon-based electrodes, with which lithium alloys. This active material is being introduced due to its large volumetric capacity ($\sim 2200 \text{ Ah.L}^{-1}$ vs. $\sim 750 \text{ Ah.L}^{-1}$ for

graphite) [59] and relatively low average voltage (~ 0.3 V vs. Li/Li⁺) [60] which can potentially increase the energy density of Li-ion cells [59,60]. However Si-based electrodes can suffer from particle pulverization upon cycling (*e.g.* micron-sized silicon) [59,61–64], can have loss of electronic contact between particles after repeated expansion and contraction during cycling [60,65–67], can have high irreversible first cycle coulombic efficiency [68,69,69–72] and can have low coulombic efficiency (compared to graphite electrodes) during cycling [59,73,74]. The root cause of these challenges is the large volume expansion [59,75] of the material during lithiation and subsequent contraction during delithiation.

Several issues have been solved through the use of either nanosized Si or nanostructured Si. For instance the use of nanosized Si particles solves some of the pulverization problems common in micron-sized Si particles [59,61,68,76–78]. However, nanosized Si still suffers from inter-particle contact loss during cycling as well as low coulombic efficiency due to large specific surface area [59,73]. Other researchers have proposed micron-sized particles comprising nanodomains of Si scattered in an inactive alloy matrix [73,79–82]. Such microstructure seems to suppress particle pulverization and greatly reduces the surface area of Si exposed to the electrolyte. This approach appears to yield materials with lower first cycle irreversible capacity (IRC) loss, better coulombic efficiency (due to reduced surface area) as well as better capacity retention over 60 cycles compared to some nanosized Si particles in half cells.

1.2.5 Separators

Separators are an important feature of Li-ion cells. They allow the two electrodes to be physically separated, thus preventing any electrochemical short circuit. Separators also need to allow Li^+ ions to travel from one electrode to the other during cell use, need to be chemically inert and stable at both the negative electrode and positive electrode potentials, and allow good wetting of the electrolyte.

Polyethylene and polypropylene are usually the materials of choice due to their relative chemical stability, and relatively high melting point (above 100°C) [83]. Polyethylene or polypropylene separators are usually engineered to have a micro-porous structure in order to allow good Li^+ transport across it [1,83]. During cell manufacture, the electrolyte fills the pores of the separator thus creating a percolating pathway for the Li^+ ions.

In an effort to increase safety, separators consisting of a layer of polyethylene sandwiched between two layers of polypropylene have been used [83–85]. This particular configuration is used in order to have a lower melting point material held in place by two higher melting point materials. In case of a safety event such as short circuits, the temperature of the cells needs to be kept below the temperature at which thermal run-aways occur [84,85]. When the temperature of the cell rises above the melting point of the polyethylene layer (*i.e.* $> 130^\circ\text{C}$) [83,85], the melted polyethylene layer loses its microporous structure and prevents Li^+ from traveling from electrode to the other. This essentially disables the cell and prevents the temperature from rising further (as long as no thermal runaway occurred) and is referred as “separator shutdown” [86]. In this

particular separator structure, the polypropylene layers act as a structural support in order to keep the polyethylene layer in place [83].

Separators consisting of ceramic-coated porous polyethylene membranes have also been recently proposed and are commonly used in high voltage Li-ion cells [87]. These separators consist of particles of ceramic coated on one side or both sides of a porous polyethylene membrane. This design has enhanced safety properties compared to the tri-layer design described above as it does not suffer from shrinkage at high temperature and thus further hinders short-circuits [87]. Other ceramic containing separators where the ceramic particles are dispersed in the porous polymeric layer are also commercially available [88].

Separators made of different polymers such as polyvinylidene difluoride [89] or polyethylene terephthalate have been proposed [90], but will not be discussed.

CHAPTER 2. ELECTRODE-ELECTROLYTE INTERPHASE AND ELECTROLYTE ADDITIVES

2.1 Electrolyte reactivity

Several reports in the literature indicate that organic carbonates are thermodynamically unstable at potentials at which the negative electrode and positive electrode operate in Li-ion cells (60 mV to 4.45 V *vs.* Li/Li⁺). For instance solvent components have been shown to be reduced at the graphite surface at potentials as high as 1.3 V *vs.* Li/Li⁺ [91]. Other measurements on Al or Ni electrodes indicated that electrolytes show signs of oxidation at potentials as low as 3.8 V *vs.* Li/Li⁺ [92,93]. Fortunately, Li-ion cells can be operated over a period of a few years. This indicates that the electrolyte components are kinetically stable against both charged positive and charged negative electrodes.

In the 1970s, kinetic stability of several organic-based electrolyte systems was a known phenomenon for Li metal electrodes [94]. In 1979, Peled [94] proposed that the kinetic stability came from a passive film acting as a solid electrolyte which he called the “solid electrolyte interphase” (SEI). This SEI was proposed to be electronically insulating and ionically conducting. These particular properties would then prevent the direct transfer of electrons from the electrode to the electrolyte components whilst allowing Li ions to travel through the SEI. This proposed model was later adopted and confirmed for graphitic negative electrodes, and adopted for positive electrode materials.

2.2 Solid electrolyte interphase (SEI)

The SEI at the surface of the electrodes of Li-ion cells is still under investigation. Due to its thickness, in the order of nm - μm [95], the determination of the composition and physicochemical properties of this layer requires the use of a multitude of surface sensitive techniques. These techniques include X-ray photoelectron spectroscopy (XPS) [17,96–100], Fourier-transform infrared spectroscopy (FT-IR) [17,17,18,78,92,100], atomic force microscopy (AFM) [101–104], electrochemical impedance spectroscopy (EIS) [105–108], and time-of-flight secondary ion mass spectrometry (TOF SIMS) [50,98,109]. The two sections below present a brief overview of the present understanding of the SEI at the negative electrode (section 2.2.1) and positive electrode (section 2.2.2) in standard EC-based electrolytes.

2.2.1 Solid electrolyte interphase at the negative electrode in standard electrolyte

Substantial effort has been devoted to the study of interfacial reactions at the graphite electrode. It is now accepted that electrolyte consisting of LiPF_6 dissolved in a mixture of EC and other linear carbonates react early-on during the first charge of a Li-ion cell called the formation cycle. It was shown with a combination of FT-IR [95,110], nuclear magnetic resonance spectroscopy (NMR) [95] and XPS [95] that EC is the principle SEI forming agent and follows the reaction pathway presented in Figure 2.1. Since the lithium ethylene dicarbonate (LEDC) formed during the reduction of EC is only

sparsely soluble in the electrolyte, it precipitates at the surface of the graphite electrode. This precipitated film protects the electrolyte from further sustained reduction.

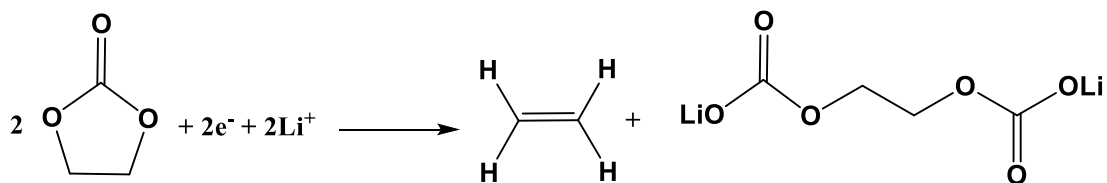


Figure 2.1. Reduction of EC at the graphite electrode of Li-ion cells.

The structure and solubility of the by-products of the reduction of EC are key in giving good passivation properties. Figure 2.2 shows the reduction pathway of propylene carbonate (PC) at a graphite electrode [111–114]. Figure 2.2 shows that the by-products of the reduction of PC are very similar to those from the reduction of EC. However their structures are different enough to result in a poorly passivating film [105,111–114]. As a result, when PC is used as co-solvent, EC or film forming additives are generally added to provide a satisfactory passivating film.

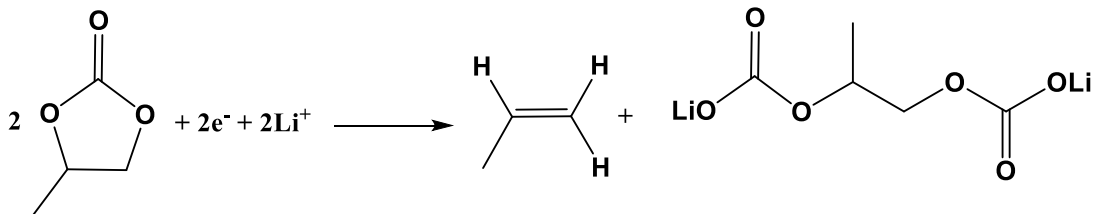


Figure 2.2. Reduction of PC at the graphite electrode of Li-ion cells.

Other products composing the SEI at the negative electrode include lithium alkyl carbonates (lithium hemicarbonates) [115,116], lithium carbonate [95], and lithium alkoxides [100,105,114,116–121]. These compounds result from the reduction of linear organic carbonates used as co-solvents as shown in Figure 2.3.

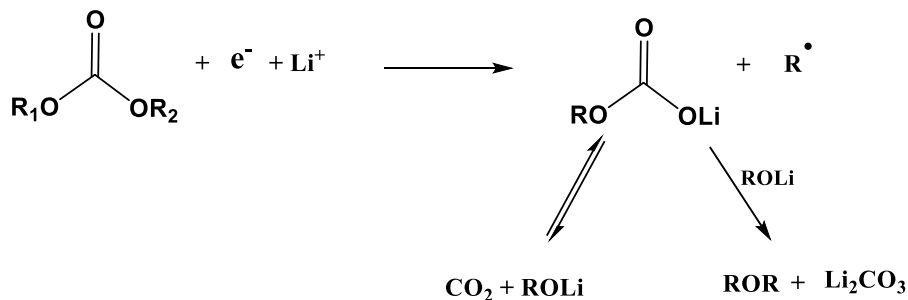


Figure 2.3. Reduction of linear dialkyl carbonates at the graphite electrode of Li-ion cells.

Inorganic compounds such as LiF [95,98,99] and organophosphates [19,95,120] resulting from the decomposition of LiPF₆ have also been identified as components of the SEI at the graphite electrode. These have been proposed to form following the pathways presented in Figure 2.4.

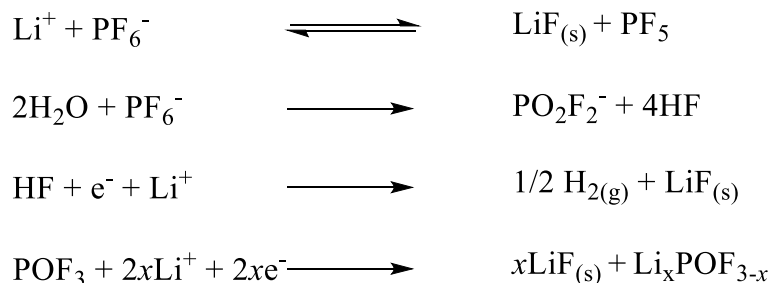


Figure 2.4. Proposed reaction pathways for the formation of LiF and fluorophosphates at the graphite electrode of Li-ion cells.

Evidence for the presence of polymeric substances such as polyethylene oxide or polyethylene carbonate [122] were also reported in the literature. These might form following the reaction pathways presented in Figure 2.5.

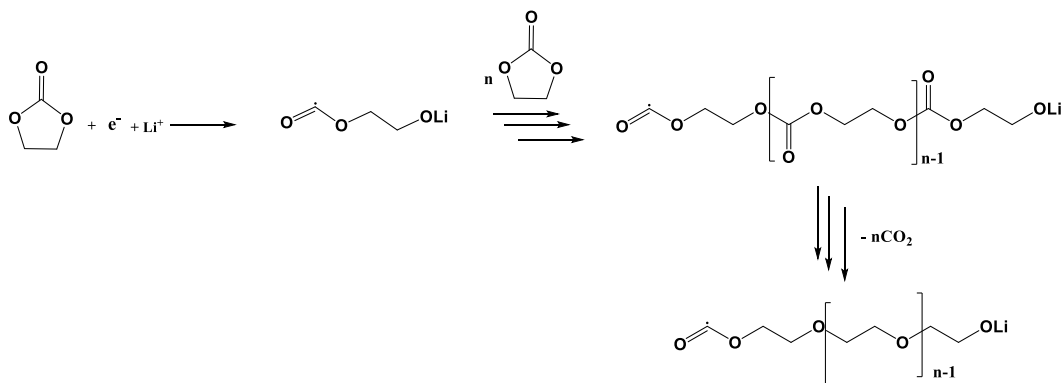


Figure 2.5. Proposed reaction pathways for the formation of polycarbonate and polyethylene oxide at the graphite electrode of Li-ion cells. Adapted from Ref [122].

Finally, high molecular weight compounds consisting of organophosphates have also been identified. Tochiara *et al.* [123] showed the products of thermally decomposed or hydrolyzed $LiPF_6$ and solvents can lead to structures similar to the one shown in Figure 2.6.

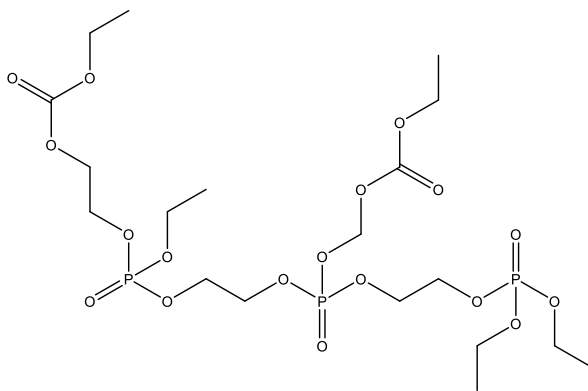


Figure 2.6. Example of high molecular weight organophosphate identified by Tochiara *et al.* in LCO/graphite cells cycled at $60^\circ C$ [123].

2.2.2 Solid electrolyte interphase at the positive electrode in standard electrolyte

In early publications, Aurbach *et al.* [124,125] showed that while noble metal electrodes presented high oxidation currents due to electrolyte degradation, positive electrode materials of Li-ion cells presented only small oxidation currents. They assigned this phenomenon to the existence of a passivating layer at the surface of the active material. The FT-IR spectra of the surface of positive electrodes (LCO and $\text{LiNi}_{0.8}\text{Co}_{0.2}\text{O}_2$) charged to 4.0 V showed peaks typical of lithium alkyl carbonates and also compounds with ether and carbonyl functional groups [124]. While ether and carbonyl structures could be consistent with oxidation of solvent molecules, the presence of lithium alkyl carbonates is most likely due to products of the reduction of the electrolyte at the negative electrode traveling to the positive electrode and precipitating at its surface. They also proposed that the formation of these alkyl carbonates might originate from a nucleophilic reaction between the terminal oxygens of the positive electrode surface and the organic carbonate of the electrolyte. Figure 2.7 presents a possible reaction pathway proposed by Aurbach *et al.* [125].

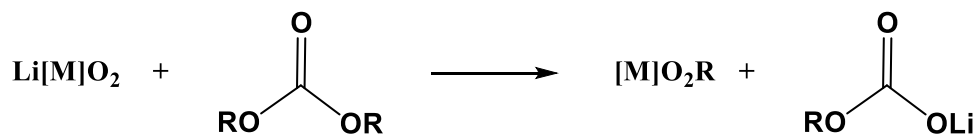


Figure 2.7. Reaction pathways proposed by Aurbach *et al.* [125] for the formation of lithium alkyl carbonates at the positive electrode of Li-ion cells.

Recent surface sensitive X-ray absorption experiments presented by Yogi *et al.* [20] indicated that a passive film does form as soon as a fresh positive electrode, LiCoO_2 in their case, was soaked in an electrolyte. They showed that the Co at the surface of the electrode was reduced from Co(III) to Co(II) with the formation of species that seemed to be Li_2CO_3 . While this is not consistent with the reaction pathway shown in Figure 2.7, it does show that some reactions between the uncharged electrode and the electrolyte occur. The same authors showed that after operating the cells for a few cycles, this Li_2CO_3 degrades and organic carbonyls (hemicarbonates, ketones, esters, and conjugate bases of carboxylic acids) appear.

Aurbach *et al.* [125,126] also showed evidence for the presence of polycarbonates. These may form through anionic polymerization of EC followed by precipitation at the positive electrode (Figure 2.5). They may also be formed via cationic ring-opening polymerization of EC following the pathway shown in Figure 2.8 [92].

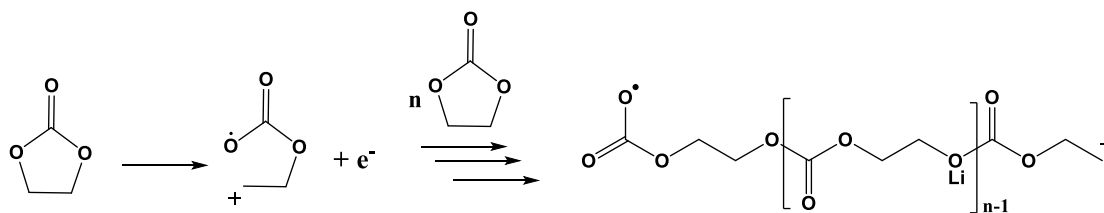


Figure 2.8. Proposed reaction pathways for the formation of polycarbonate through cationic ring opening polymerization as proposed in Ref [92].

Aurbach *et al.* [127] also showed evidence for the presence of LiF which might again come from the reaction of LiPF_6 at the negative electrode, or from the reaction of HF contamination with the positive electrode surface.

There seem to be two general mechanisms for the oxidation of the electrolyte. The first one appears to be a direct electro-oxidation between the charged positive electrode and the electrolyte as proposed by many researchers [92,128]. However density functional theory calculations predict oxidation potentials well above the ones of positive electrode materials used in practical Li-ion cell [129–131]. It may very well be that reduction by-product having low oxidation potential migrate towards the positive electrode and get oxidized at its surface. The second electrolyte oxidation mechanism may be of a chemical nature. For instance, Lin *et al.* [132] showed that the surface of charged layered NMC materials is prone to convert to a layered cubic rock-salt structure which involves the loss of oxygen. In this case, the oxygen may react with solvents or salt. The two main oxidation pathways of the electrolyte could be:



where *Slvt* represents a solvent molecule, *MO₂* represents the charged surface of a layered positive electrode, *Slvt⁺* represents the product of the oxidation of a solvent molecule, *Slvt-O* represents product of a pseudo combustion reaction between oxygen released from the charged positive electrode surface and a solvent molecule and *MO* represents a rock-salt structure resulting from the loss of oxygen from the surface of a charged positive electrode material.

2.3 Electrolyte additives

Electrolyte additives are organic or inorganic compounds added to the electrolyte in small quantities (0.2 – 5 wt. %) [34,35,133]. The study of electrolyte additives started

long ago in the battery community. For example, in 1991 Aurbach *et al.* [134] inspected the effect of small quantities of molecular oxygen and water on the plating efficiency of Li in batteries using Li metal as the negative electrode. Irish *et al.* [135] did a similar survey on the effect of CO₂ saturation of the electrolyte in 1995. In 2005 Broussely *et al.* [2] clearly demonstrated the effect of electrolyte composition on cell life-time and cycle performance. The results of cell testing over the course of several years (2 – 4 years) clearly showed that the use of additives could dramatically extend cell life-time and cycle performance.

Electrolyte additives are generally used in commercial cells to improve performance and/or improve cell safety [35,133]. Performance decline of Li-ion cells is generally assigned to active lithium loss through the ever thickening of the SEI at the negative electrode [6,136], electrolyte oxidation at the positive electrode [5,6,137], polarization growth [136,138,139], water contamination (for spinel type materials) [50,140] and active material loss [136,141]. Modern electrolyte additives or additive blends are designed to positively impact these five performance degradation mechanisms. The M.Sc. thesis of Kathlyne Nelson [142] describes 50 popular electrolyte additives in the introduction.

2.3.1 Electrolyte additives for improved cycle performance

Electrolyte additives designed for improved cycle-life are generally organic compounds of small molecular weight. These are generally unsaturated carbonates [3,143–145], alkyl or silyl phosphites [21,146–148], alkyl or silyl phosphates [146,149–152], organosulfates [19,153,154], sultones [22,155,156,156–158], or organoborates

[23,23,53,159,160], *etc.* Figure 2.9 shows some additives for improved cell performance proposed in the literature.

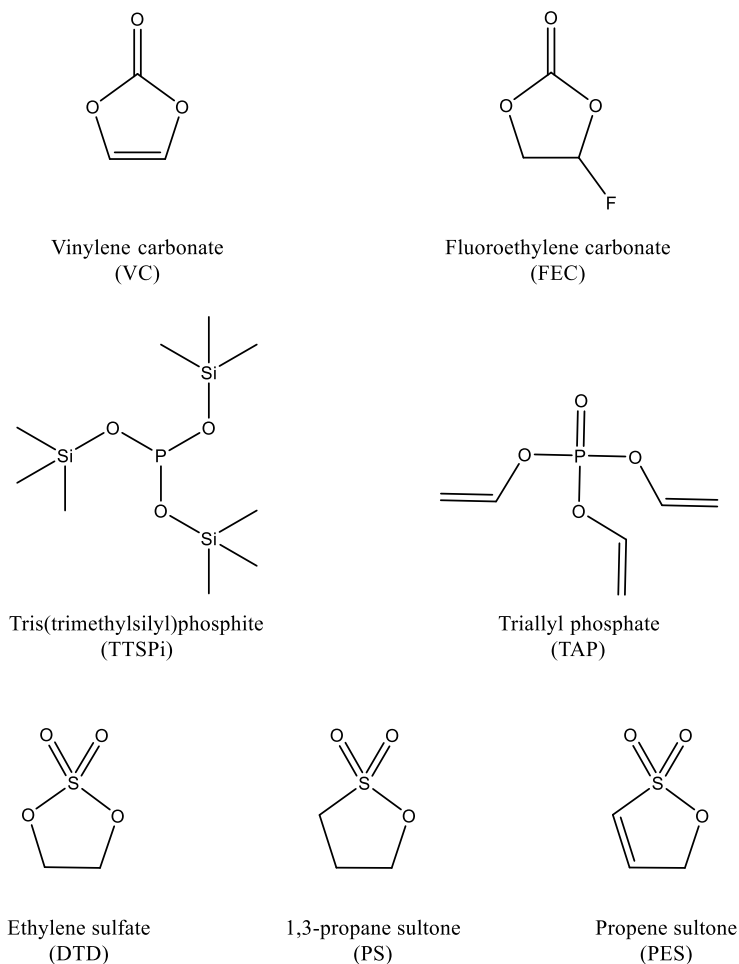


Figure 2.9. Chemical structures of some electrolyte additives for improved cycle performance of Li-ion cells.

Generally, additives are selected for their film forming or film modifying properties. For instance, unsaturated molecules such as VC and triallyl phosphate (TAP) can undergo ionic or radical polymerization [161] as shown in Figure 2.10. Other cyclic additives such as 1,3-propane sultone (PS), propene sultone (PES) and ethylene sulfite

(DTD) can undergo cationic or anionic ring-opening polymerization in the same manner as EC (see Figures 2.5 and 2.8). The polymeric products, being only sparsely soluble, precipitate at the surface of the electrodes providing a protective layer.

Film modifiers can alter the properties of oligomers formed from the polymerization of solvents or co-additives, or modify the composition of the SEI. The modification can consist of capping the terminal ends of polymeric chains [148] or co-polymerization, or the formation of insoluble salts. The altered SEI can then potentially modify some of the film properties such as Li^+ conduction, or decrease the diffusion coefficient of solvent molecules through the film. This would lower the impedance of the

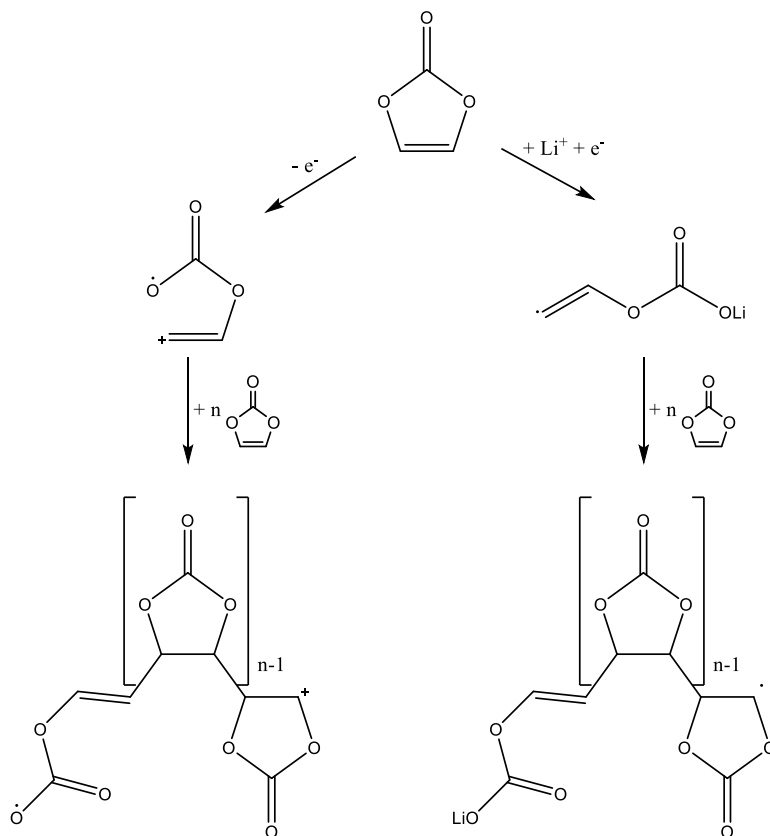


Figure 2.10. Proposed mechanisms of the cationic (left) and radical (right) polymerization of VC.

film, and lower the parasitic current associated with the reduction/oxidation of the electrolyte, respectively.

Hydrofluoric acid has been proposed to degrade the SEI and also some oxide based-materials. For this reason, additives able to capture HF or water contamination have been proposed [148,162,163].

Since LiPF_6 is in equilibrium with PF_5 in the electrolyte [122], researchers have developed additives that can stabilize PF_5 and prevent it from catalyzing electrolyte degradation. These compounds are generally Lewis bases such as nitrogen or phosphorus containing compounds [164] able to share a lone electron pair with PF_5 (Lewis acid).

Lastly, inorganic or ionic compounds have also been used as film forming or modifying additives, such as lithium salts (Li_2CO_3 [18], LiBOB [48,165], LiFSi [166]), gaseous compounds (SO_2) [167], and borates [168,169].

2.3.2 Study of electrolyte additives

The study of the effect of additives at the surface of both electrodes of Li-ion cells uses the same surface sensitive tools enumerated in section 2.2. Researchers often use these surface sensitive measurements in parallel with low precision coulometric or voltammetric measurements which can lead to inaccurate conclusions.

In the past, researchers were more concerned about the effect of additives at the negative electrode rather than the positive electrode. It was believed that most of the performance decline was caused by loss of active Li associated with the ever-growing SEI at the negative electrode. However, Burns *et al.* [5] clearly showed that using additives that minimize the parasitic currents at the positive electrode is as important as

additives that lower parasitic current at the negative electrode in order to obtain cells with long cycle life. The push towards Li-ion cells with higher nominal voltage makes this fact even more relevant.

The misconception about the importance of the effect of additives at the positive electrode comes from the fact that electrolyte oxidation does not lead to Li inventory loss [6]. As a consequence, mild electrolyte oxidation does not lead to noticeable capacity fade in the short term [6]. The effect of electrolyte oxidation is apparent only after long term cycling. Since most academic research focuses on a few weeks or months of cycling, the effect of parasitic currents at the positive electrode is not very apparent and often ignored.

However, the emergence of high voltage positive electrodes is shifting the focus of additive development towards the stabilization of the surface of positive electrode materials. These additives blends are designed to minimize electrolyte oxidation [16,48,53,143] and minimize impedance growth [11,138,170] through the formation of a protective SEI.

In 2010 Smith *et al.* [171] and in 2011 Sinha *et al.* [9] developed HPC and automated storage measurements of Li-ion batteries. These methods allow coulombic efficiency and parasitic currents at the positive electrode to be measured with high precision and accuracy in a matter of a few weeks. For this reason, the use of HPC measurements to compare the effect of additives is more relevant than low precision measurements.

In addition to low precision measurements, most researchers compare the effect of additives on synthetic electrodes with undisclosed and irreproducible electrolyte-volume-

to-active-material-mass ratio. Most academic cells use enormous electrolyte volume for a given active material mass compared to commercial cells. This high volume ratio is a direct consequence of the use of “coin cell” and “Swagelok cell” designs. These designs render the use of reproducible and commercially relevant electrolyte volumes extremely difficult. Burns *et al.* [143] showed that the effect of an additive strongly depends on the electrolyte-volume-to-active-material-mass ratio. It is then apparent that comparing the effect of additives with low precision coulometry, on cells with commercially irrelevant electrolyte-volume-to-active-material-mass ratio with low reproducibility may yield erroneous conclusions.

However some researchers have started using hand-made or machine-made dry pouch full cells (cell with graphite negative electrodes and $\text{Li}[M]\text{O}_2$ positive electrode) [16,146,172–176]. Machine-made pouch cells use commercial electrodes and their design allows the use of electrolyte-volume-to-active-material-mass ratios very close to those used in the industry. This leads to very low cell-to-cell variability and facilitates the comparison of the effect of additives. The reproducible electrolyte-volume-to-active-material-mass ratio of these pouch cells allows the additive concentration *vs.* time to be determined. It also allows the effect of additive type, and additive concentration on the gas produced during cell use to be assessed in a reliable manner. The development of such measurements using gas chromatography coupled with mass spectrometry (GC-MS) and GC coupled with thermal conductivity detectors (GC-TCD) and their preliminary results will be presented in the next chapters. These methods of analysis will also be used to understand new electrolyte systems developed as well as decipher the reduction mechanisms of various solvents.

CHAPTER 3. EXPERIMENTAL METHODS

3.1 Cell format and cell chemistry

Dry wound machine-made pouch cells were used throughout this thesis. Four different cell chemistries were used, mainly LCO/graphite (LCO/gr), $\text{Li}[\text{Ni}_{0.33}\text{Mn}_{0.33}\text{Co}_{0.33}]\text{O}_2/\text{graphite}$ (NMC(111)/gr), $\text{Li}[\text{Ni}_{0.4}\text{Mn}_{0.4}\text{Co}_{0.2}]\text{O}_2/\text{graphite}$ (NMC(442)/gr) and $\text{LiCoO}_2/\text{Si-alloy:graphite}$ (LCO/Si:gr). Table 3.1 shows the active material used, cell balance (maximum upper voltage cut-off), nominal capacity, and manufacturer for each of these cell types. Both NMC/gr pouch cells and LCO/Si:gr pouch cells had a size of 30 x 18 x 3 mm while the LCO/gr pouch cells had a size of 32 x 27 x 2.5 mm (see Figure A1 of the Appendix A). The pouch cells were vacuum sealed in China without electrolyte and then shipped to Dalhousie University (NS, Canada).

The negative electrode of the NMC pouch cells (NMC(111) and NMC(442)) and LCO pouch cells were made out of 15 - 30 μm and 10 - 25 μm artificial graphite flakes (determined by SEM imaging of the electrode), respectively. The size of the active particles of the positive electrode of both NMC and LCO pouch cells were 4 - 15 μm

Table 3.1. Dry pouch cell electrode active material, cell balance, capacity and manufacturer.

Cell notation	Active material (positive/negative)	Cell balance	Capacity	Manufacturer
LCO/gr	$\text{LiCoO}_2/\text{graphite}$	4.2 V	320 mAh	BAK
NMC(111)/gr	$\text{Li}[\text{Ni}_{0.33}\text{Mn}_{0.33}\text{Co}_{0.33}]\text{O}_2/\text{graphite}$	4.2 V	220 - 240 mAh	LiFun
NMC(442)/gr	$\text{Li}[\text{Ni}_{0.4}\text{Mn}_{0.4}\text{Co}_{0.3}]\text{O}_2/\text{graphite}$	4.7 V	180 - 220 mAh	LiFun
LCO/Si:gr	$\text{LiCoO}_2/\text{Si-alloy:graphite}$	4.35 V	200 mAh	LiFun/3M

(determined by SEM imaging of the electrodes).

The negative electrode of the LCO/Si:graphite cells used comprised a Si alloy (3M) with a specific capacity of 1180 mAh.g⁻¹, a density of 3.5 g.cm⁻³, a specific surface area of 6.9 m².g⁻¹ (determined by Brunauer–Emmett–Teller measurements at 3M, St. Paul, Minnesota 55144-1000, USA) and a mean particle size of 5.2 μm (determined by laser diffraction at 3M, St. Paul, Minnesota 55144-1000, USA), graphite (MAGE, Hitachi Chemical as well as Timrex KS6, IMERYS). The average specific surface area of the anode was 5.1 – 5.7 m².g⁻¹ (determined by Brunauer–Emmett–Teller measurements at 3M, St. Paul, Minnesota 55144-1000, USA) and the Si-alloy material represents about 40% of the total capacity of the negative electrode.

Table 3.2 shows the formulation of the composite electrodes of the four pouch cell types used. Table 3.2 shows that all electrode formulations used high active material

Table 3.2. Electrode formulations in the four pouch cell types used.

Cell notation	Negative electrode formulation /wt.%	Positive electrode formulation /wt.%
LCO/gr	96% graphite (1.2 g) + 2% carbon black + 2% polyvinylidene fluoride	96% LCO (2.1 g) + 2% carbon black + 2% polyvinylidene fluoride
NMC(111)/gr	96% graphite (0.8 g) + 2% carbon black + 2% carboxymethyl cellulose-styrene-butadiene rubber	96% NMC(111) (1.3 g) + 2% carbon black + 2% polyvinylidene fluoride
NMC(442)/gr	96% graphite (1g) + 2% carbon black + 2% carboxymethyl cellulose-styrene-butadiene rubber	96% NMC(442) (0.8 g) + 2% carbon black + 2% polyvinylidene fluoride
LCO/Si:gr	15% Si-alloy (0.1 g) + 72.3% MAGE graphite (0.5 g) + 10% KS6 graphite (0.06 g) + 2.7% carboxymethyl cellulose-styrene-butadiene rubber	95% LCO (1.4 g) + 2.5% carbon black + 2.5% polyvinylidene fluoride

loadings (> 95%). The areal capacity of all electrodes used was above 2 mAh.cm⁻². Table 3.2 also indicates the mass of active material of each electrode in parenthesis. Figure A2 of Appendix A shows the voltage vs. capacity curve of an early cycle of each pouch cell type used as well as the potential vs. capacity of the positive electrode and negative electrode as fitted using differential voltage analysis. Figure A2 shows that the negative electrode of each pouch cell type has extra capacity available when cells are charged up to their recommended upper voltage cut-off. This ensures that no Li plating occurs near the top of charge.

3.1.1 Cell preparation

The upper portion of the pouch bag of the pouch cells (see Figure A1 of Appendix A) was cut open and the cells were vacuum dried at 80°C for 10 - 14 h to remove most of the residual water. The NMC/gr (NMC(111) and NMC(442)) and LCO/Si:gr pouch cells were then filled with 0.75 mL of electrolyte while the LCO/gr cells were filled with 0.9 mL of electrolytes. The cells were then sealed under vacuum at a relative pressure of -85 kPa (relative to atmospheric pressure). After filling, the pouch cells were connected to a Maccor 4000 series charger and held at 1.5 V (NMC/gr cells and LCO/gr cells) or 2 V (LCO/Si:gr cells) for 12 - 24 h in a 40°C box to promote wetting. The NMC/gr and LCO/Si:gr cells were then charged to 3.5 V or 3.8 V at a current of C/20, respectively. In order to remove the gas formed early on during the formation charge [12,177] the pouch cells were then moved to an argon-filled glove-box to be opened and re-sealed under vacuum.

3.1.2 Electrolyte reagents

Reagents were obtained from a variety of manufacturers and used as received without further purification. Table A1 of Appendix A shows the supplier, purity and water level (when known) of each reagent used.

3.2 Electrochemical cell testing

3.2.1 Galvanostatic cycling

The capacity retention of cells was typically evaluated using galvanostatic cycling. That is, cells were charged and discharged using a constant current until the upper voltage cut-off (during charge) or the lower voltage cut-off (during discharge) was reached. The capacity of the cells was then calculated for each charge and discharge (done automatically using data processing software) using:

$$Q = I t \tag{3.1}$$

where Q is the capacity in mAh, I is the current applied to the cell in mA and t is the time the current was applied for in h.

3.2.2 High precision coulometry

High precision coulometry is a useful tool that allows the effect of additives or solvent composition on cell lifetime to be evaluated in a matter of a few weeks [5,6,8]. Selected cells were tested using high precision coulometry using the ultra-high precision chargers [178]. These chargers allow tracking coulombic efficiency and charge end-point

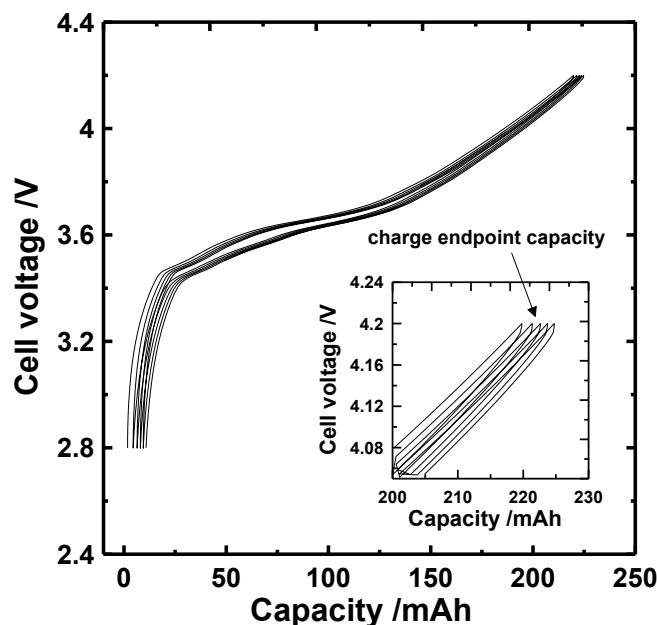


Figure 3.1. Voltage vs. capacity for a NMC(111)/graphite pouch cell filled with a 1M LiPF₆ EC:EMC (3:7) + 0.5% methyl phenyl carbonate, measured on the ultra-high precision charger at C/20 and 40°C. The insert shows an expanded view near the top of charge.

capacity slippage with high accuracy and precision (30 ppm and 10 ppm respectively) [178].

The coulombic efficiency (CE) is defined as the discharge capacity of a cycle divided by the capacity of the previous charge. The charge endpoint capacity is defined as the capacity value at the top of charge in the cell voltage vs. capacity plot (see Figure 3.1). Finally, the charge endpoint capacity slippage is defined as the slope of the charge endpoint capacity vs. cycle number plot [6].

Smith *et al.* [6] showed that the charge endpoint capacity slippage is related to the oxidation current of the electrolyte at the positive electrode, while CE encompasses parasitic reactions at both the negative electrode and the positive electrode. Lower charge endpoint capacity slippage and higher CE generally lead to longer lived cells [5].

Prior to UHPC testing, cells were first formed following the procedure described in Section 3.1.1. Cells were then moved to a $40. \pm 0.1^\circ\text{C}$ box and connected to an ultra-high precision charger [178]. Cells were then charged and discharged at a constant current of $C/20$ between 2.8 – 4.2 V for 16 cycles.

3.2.3 Open circuit voltage storage

Storing LCO/gr or NMC/gr cells in an open circuit state at a cell voltage where the graphite electrode is in a two-phase region allows electrolyte oxidation reactions at the positive electrode to be monitored [9]. During storage, the oxidation of the electrolyte changes the lithiation state of the positive electrode. Since the potential of lithium intercalation materials is dependent upon the amount of lithium intercalated (see section 1.2.1), the oxidation of the electrolyte will cause a decrease of the cell voltage (oxidation reactions increase the lithiation state of the positive electrode which lower its potential). In this case, a smaller cell voltage drop during open circuit voltage experiments is indicative of lower parasitic oxidation reaction rate.

3.2.3.1 Dumb open circuit voltage storage

Prior to “dumb” open circuit voltage (OCV) storage, cells were first formed following the procedure described in Section 3.1.1. Cells were then put back on the charger at $40.^\circ\text{C}$ to be cycled twice (two full charge-discharge cycles) between 2.8 V and the upper cut-off voltage at $C/20$. Cells were then charged to the upper cut-off voltage at $C/20$ and held at that voltage until the current dropped below $C/1000$. Cells were then moved to the storage station for their OCV to be monitored at $40.0 \pm 0.1^\circ\text{C}$ for a period

of 500 h. The OCV of each cell was monitored using a Keithley model 2750 scanning voltmeter. Cells were connected to the voltmeter only once every 15 min during the first 4 h of storage and then once every 6 hours for the remaining 494 h. The connection between the cells and the voltmeter was made through mechanical relays so that the cells experienced true open circuit condition during storage [9].

3.2.3.1 Smart open circuit voltage storage

Smart OCV storage is a technique very similar to the “dumb” OCV storage experiments. Figure 3.2 shows a typical voltage vs. time profile of a Li-ion cell during a smart OCV storage experiment. During smart OCV storage, the capacity of the discharge prior to a 500 h OCV storage period (D_0) is compared to the capacity of the 1st (D_1) and 2nd (D_2) discharge following the OCV storage period. The irreversible capacity loss

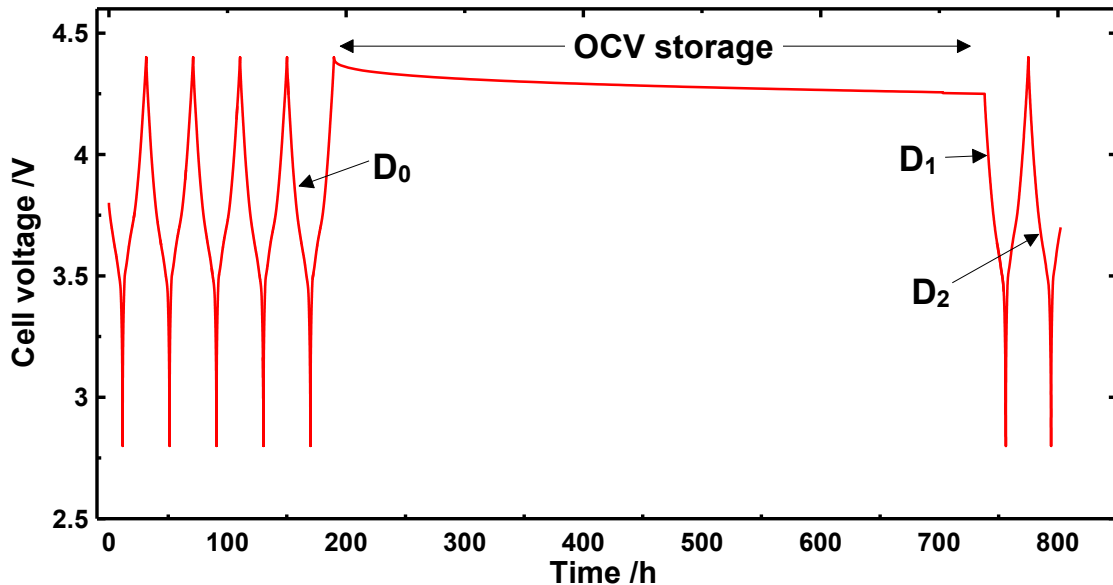


Figure 3.2. Typical cell voltage vs. time profile during a smart OCV storage experiment. Cells were cycled at C/20 before and after the OCV storage period.

(Q_{irrev}) during storage is then calculated as:

$$Q_{irrev} = D_0 - D_2. \quad (3.2)$$

The reversible capacity loss during storage (Q_{rev}) is calculated as:

$$Q_{rev} = D_2 - D_1. \quad (3.3)$$

Sinha et al. [9] showed that while the irreversible capacity loss was mainly due to electrolyte reduction at the graphite electrode, reversible capacity loss was mainly due to electrolyte oxidation at the positive electrode.

3.2.4 Electrochemical impedance spectroscopy

Electrochemical impedance spectroscopy (EIS) is a technique that allows the kinetics of different faradaic and non-faradaic processes to be evaluated [179]. Potentiostatic EIS consists of imposing a sinusoidal voltage signal of varying frequency on the cell and measuring the resulting current [179]. The frequency range probed for lithium ion cells is typically 100 kHz – 10 mHz. The voltage amplitude is kept small (1 – 10 mV) in order for the current response to be linear with the voltage signal [179]. The impedance at any given frequency is then calculated using [179]:

$$Z(\omega) = \frac{V(\omega, t)}{I(\omega, t)} = \frac{|V| \sin(\omega t)}{|I| \sin(\omega t + \varphi)} \quad (3.4)$$

where $Z(\omega)$ is the impedance at a frequency ω , $V(\omega, t)$ is the sinusoidal voltage of frequency ω , $I(\omega, t)$ is the current response, and φ is the phase shift between the alternating voltage and the current response. For practical reasons, the impedance is

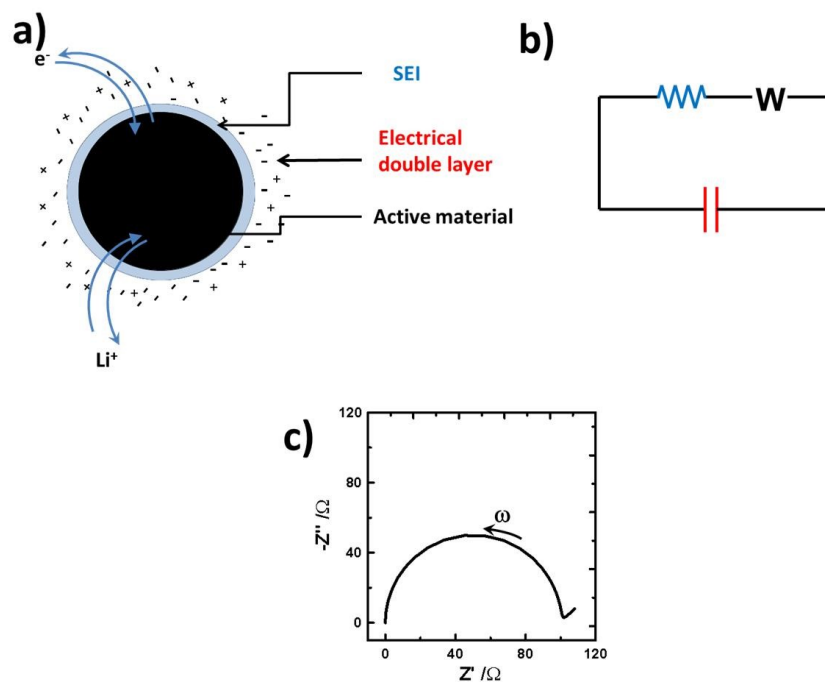


Figure 3.3. Schematic of a single active particle (a) along with its simplified equivalent circuit model (b) and Nyquist representation of its impedance (c). Adapted from R. Petibon, *Study of electrolyte additives in Li-ion cells using electrochemical impedance spectroscopy on symmetric*, M.Sc. thesis, Dalhousie University, Halifax, NS, Canada (2013).

always represented with complex numbers. The conversion of the impedance from trigonometric notation to complex number notation is performed using Euler's rule:

$$e^{j\omega t} = \cos(\omega t) + j\sin(\omega t). \quad (3.5)$$

Figure 3.3a shows a hypothetical active material particle. During EIS experiments, several processes will affect the amplitude and phase shift of the current response at characteristic frequencies. These processes include electrochemical double layer charging, electron transfer to and from the particle, lithium ion diffusion through the SEI, and diffusion of lithium into the bulk of the electrode.

The impedance of the hypothetical particle can be modeled using a simple equivalent circuit shown in Figure 3.3b. This equivalent circuit includes a resistance which models the electron transfer resistance as well as the diffusion of the lithium ions through the SEI, a Warburg resistance which models the lithium diffusion into the bulk of the particle in parallel with a capacitor which models the electrochemical double layer. Figure 3.2c shows the Nyquist representation of the impedance of this hypothetical particle. The impedance response has a semi-circular shape and a sloping tail at low frequency. The diameter of the semi-circle is equal to the charge transfer resistance (electron transfer and diffusion of lithium ion through the SEI) and the frequency corresponding to the apex of the semi-circle is inversely proportional to the product of the charge transfer resistance and capacitance of the double layer.

The electrodes of a Li-ion cell are made of many particles deposited on a current collector, held together by a polymer and electronically connected by a conductive additive. When the particles have good electronic contact and a narrow particle size distribution, the impedance of Li-ion cells can be modeled using the equivalent circuit shown in Figure 3.4. The equivalent circuit of the positive electrode and negative electrode are shown in red and blue, respectively. This particular equivalent circuit was adapted from the one proposed by Atebamba *et al.* [180] and assumes a good electronic pathway between active particles and negligible pore resistance. In this model, each electrode has a resistive component R_{cc} associated with the electron transfer from the current collector to the active particle, R_{ct} associated with the charge transfer (electron transfer from the conductive additive to the active material and lithium ion diffusion through the SEI) and W associated with the Li diffusion into the bulk of the active

material. The model also includes capacitive elements CPE and CPE_{cc} (constant phase elements here) associated with the electrochemical double layers at the surface of the active particles and current collector, respectively. Finally, the resistive component R_{el} accounts for the electrolyte conductivity.

Figure 3.4b shows the Nyquist plot of the impedance of a full LCO/graphite cell onto which the different contributions have been labeled. This thesis focuses on the effect of electrolyte composition which only affects the surface of the active material particles and electrolyte conductivity properties in the voltage range used (*i.e.* < 4.5 V) and particular electrolyte components used. For this reason, only the sum of the diameters of the overlapping semi-circles (current collector resistance, as well as lithium diffusion through the SEI of both the positive electrode and negative electrode particles) will be discussed and is referred as R_{ct} . The electrolyte conductivity properties will not be

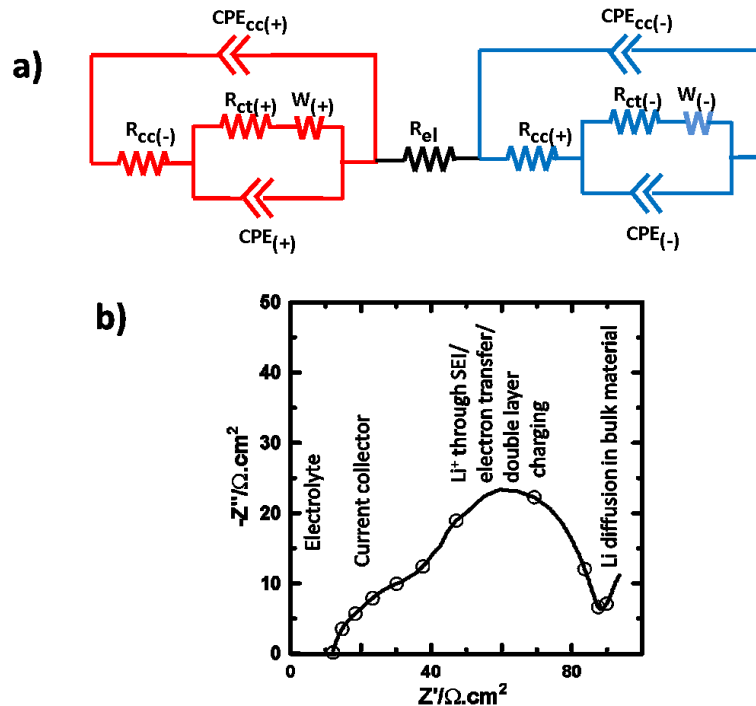


Figure 3.4. Equivalent circuit of a full lithium cell derived from reference [180] (a) and Nyquist representation of the impedance of an LCO/graphite pouch cell (b).

analyzed from impedance spectra due to irreproducible cable and connection resistances between the instrument and the cells.

All EIS spectra were measured using a Biologic VMP3 electrochemical test station at a temperature of $10^{\circ}\text{C} \pm 0.2^{\circ}\text{C}$ and with an excitation amplitude of 10 mV. Prior to EIS measurements, cells were charged or discharged to 3.80 V and held at that voltage until the current dropped below $C/1000$ (unless stated otherwise).

3.2.5 Electrolyte conductivity measurements

Electrolyte conductivity measurements were made using a Mettler Toledo FG3 conductivity meter equipped with an InLab 710 (Mettler Toledo) four platinum pole conductivity probe. The conductivity probe was inserted into a machined Teflon jar and sealed using an ultra torr Swagelok nut fitted with two viton O-rings. This setup allows the probe to be sealed into the electrolyte-containing Teflon compartment and prevents air and water from contaminating the cell and prevents solvent evaporation. The conductivity probe was calibrated with a single point calibration using a conductivity standard of $12.88 \text{ mS}\cdot\text{cm}^{-1}$ at 25°C (Mettler Toledo).

The conductivity of the electrolyte was measured every 5 - 10°C between $-20 - 60^{\circ}\text{C}$. To do this, the conductivity cell was immersed in a temperature controlled bath with a temperature fluctuation of $\pm 0.5^{\circ}\text{C}$ and a temperature accuracy of $\pm 1^{\circ}\text{C}$. A 20 - 30 min waiting period was used between cell temperature stabilization and conductivity measurement.

3.3 Cell volume change measurements

Using cell designs comprising soft enclosures such as pouch cells allows the volume of gas produced during cell operation to be measured. Cell volume changes were measured using Archimedes' principle. The weight of the cells when submerged in water was measured before and after cycling. The weight of the cells was measured by suspending the cell underneath a balance (some balances are equipped with a weight sensor underneath its base) using a thin wire. The weight of the submerged cell was then equal to the tension on the wire and measured by the balance. The difference in wire tension before and after cell operation is directly proportional to the volume change of the cell following:

$$F = (m - \rho V_{cell})g \quad (3.6)$$

$$\Delta V_{cell} = \frac{-F_{final} + F_{initial}}{\rho g} \quad (3.7)$$

where F is the tension in the wire, m is the mass of the cell, g is the gravitational acceleration, ρ is the density of the water, V_{cell} is the volume of the cell and the subscripts *initial* and *final* refer to before and after cell testing, respectively.

3.4 Gas chromatography coupled with mass spectrometry and thermal conductivity detection

In the work presented here, gas chromatography (GC) coupled with electron impact mass spectrometry (MS) and GC coupled with thermal conductivity detection (TCD) were used in order to analyze liquid and gas components of Li-ion cells.

3.4.1 Gas chromatography

Gas chromatography is a technique that allows volatile compounds to be separated. Figure 3.5 shows a schematic of a gas chromatograph. A basic chromatograph includes a carrier gas supply, a heated injector, a temperature programmable oven housing the separation column and a detector.

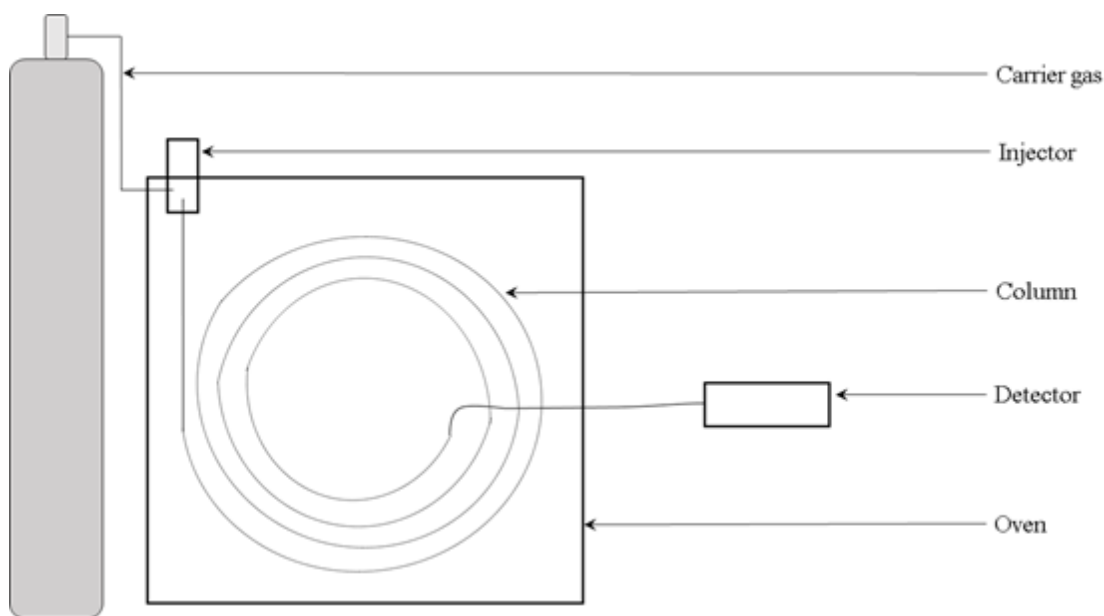


Figure 3.5. Simplified schematic of a gas chromatograph.

The carrier gas is called the “mobile phase”, and typically is either N_2 , He, or H_2 [181]. Analytical columns are usually made of silica with a polymeric film on the outside of the column for tensile strength. The inner walls of the column are coated either with a liquid phase or with porous particulates. The coating on the inner walls of the column is called the “stationary phase”. The length of the column can typically vary from 15 m to

100 m, its inner diameter from 0.05 mm to 0.55 mm, and the coating thickness from 0.2 μm to 5 μm [181]. The dimensions of the column and coating thickness depend on a variety of factors such as detector used, sample loading, and most importantly the analytes needing to be separated. The liquid phase coating consists of functionalized polysiloxanes. The type of functional group used and degree of functionalization of the liquid phase depend on the chemical structures of the analytes to be separated.

3.4.2 Separation principles

The sample is usually diluted in a volatile solvent and introduced in the injector. The injector temperature is set to about 10°C above the highest boiling point of the least volatile analyte [181]. Inside the injector, the mixture is volatilized and carried through the column by the carrier gas. Inside the column, each analyte is in equilibrium between the stationary and the gas phase following:

$$i_s \rightleftharpoons i_m \quad (3.8)$$

where i_s is the analyte i in stationary phase, and i_m is the analyte i in the mobile phase (gas phase).

The equilibrium constant for analyte i between the stationary phase and the gas phase is called the partition coefficient and is given by:

$$K_i = \frac{[i]_m}{[i]_s} \quad (3.9)$$

where $[i]_m$ is the concentration of the analyte i in the mobile phase (gas phase), and $[i]_s$ is the concentration of the analyte i in the stationary phase. For columns with liquid

coatings, both $[i]_m$ and $[i]_s$ are in mol/L. Usually, K is smaller than 1 in order to have adequate separation between analytes.

The retention time is defined as the time an analyte takes to elute out of the column. The retention time is closely related to the partition coefficient and given by [181]:

$$t'_{r,i} = \frac{1}{K_i} t_m \frac{V_s}{V_m} \quad (3.10)$$

$$t'_{r,i} = t_{r,i} - t_m \quad (3.11)$$

where $t'_{r,i}$ is the corrected retention time of analyte i , t_m is the time an unretained compound takes to elute out of the column (no interaction with the column coating), V_s is the volume of the stationary phase, V_m the volume of the mobile phase and $t_{r,i}$ is the time analyte i takes to elute out of the column. The volume of the stationary phase in analytical columns is typically 50 – 100 smaller than the volume of the mobile phase (the gas in the case of GC). Differences in partition coefficients from one analyte to the next are the very foundation of any chromatographic separation methods.

A discussion for columns with solid coatings would be very similar. In this particular case, adsorption isotherms would have to be taken into account instead of partition coefficient.

Many detection methods can be employed with gas chromatography. Amongst them are thermal conductivity detectors (TCD), flame ionization detectors (FID), FT-IR detectors, and mass spectrometric (MS) detectors.

3.4.3 Electron impact mass spectrometry

Mass spectrometry is a qualitative and quantitative detection method. For this reason, it is often used in tandem with gas chromatography. Figure 3.6 shows a basic schematic of a MS. Every MS has four basic components, a sample inlet, an ionization chamber, a mass analyzer and an ion detector [181]. The sample is introduced through the sample inlet and directed towards the ionization chamber where it is ionized.

Several ionization methods can be used. Among them are electron impact ionization (EI), chemical ionization (CI) or electrospray ionization (ESI) [181]. Most mass spectrometers used as detectors in gas chromatography have either an EI module or a CI module.

Electron impact ionization uses electrons accelerated to a set energy, usually 70 eV [181,182]. The electrons are thermionically generated using a heated tungsten filament and a strong electric field. The sample flows into the ionization chamber where

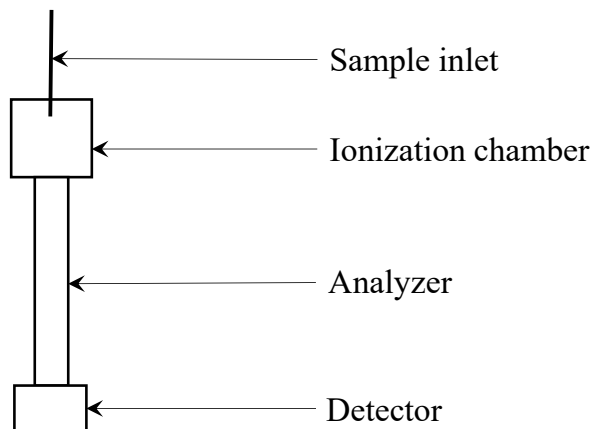


Figure 3.6. Simplified schematic of a mass spectrometer.

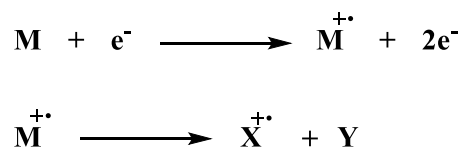


Figure 3.7. Ionization mechanism in electron ionization modules.

the molecules collide with the generated electrons. As a result of these collisions, the molecules can lose one or more electrons, giving positively charged species as shown in Figure 3.7, where M is a molecule from the sample [181,182]. The cation $M^{+\bullet}$ is referred to as the “molecular ion”. Figure 3.7 also shows that once the molecules are ionized, the cations have generally enough internal energy to undergo several fragmentations.

Since each given molecule has a specific fragmentation pattern, an unknown molecule can be identified by comparing its mass spectra to a database of fragmentation patterns of known compounds [181,182]. If a reference fragmentation pattern is not available for the identification of an unknown compound, the chemical formula and structure can sometimes be assessed by inspecting the isotopic distribution of each fragment, the mass of the molecular ion, and the particular fragmentation pattern [181,182].

Once the sample is ionized, it is directed towards the mass analyzer. Common analyzers in mass spectrometry used with GC are quadrupole analyzers, and time-of-flight analyzers, although other analyzers exist [181]. Quadrupole analyzers use two sets of rod-shaped electrodes arranged in parallel. Both a constant voltage and an alternating voltage are applied to the electrodes. Figure 3.8 shows a simplified schematic of a quadrupole mass analyzer [183].

The trajectory of each ion through the quadrupole depends on its m/z ratio (where m and z are the mass and the charge of the ion, respectively) for given sets of constant and alternating voltages. This means that only ions with a particular m/z value will successfully pass through the mass analyzer and reach the detector. Ions with an m/z that is too low or too high will eventually collide with one of the electrodes. When analyzing a sample, the value of the constant voltage as well as the amplitude and frequency of the alternating voltage are varied to scan through the m/z range set by the user.

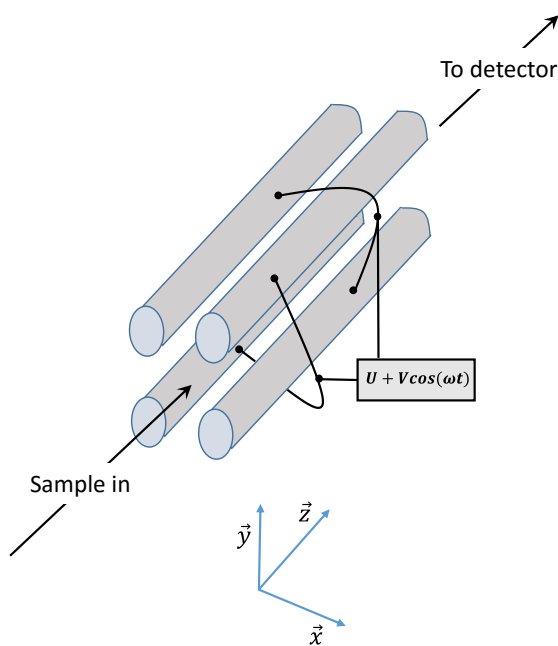


Figure 3.8. Simplified schematic of a quadrupole mass analyzer.

In typical measurements, the analyzer is set to screen through a given m/z range in discrete increments at specific time intervals. Each data point is a record of the signal intensity of each m/z scanned, called “mass spectra”. The time separating each data point

is determined by the time the mass spectrometer takes to scan through the m/z range set by the user.

3.4.4 Thermal conductivity detection

Since the MS used in this work could not detect H_2 , a thermal conductivity detector (TCD) was used for selected analyses of gases produced in Li-ion cells.

Figure 3.9 shows a simplified schematic of a thermal conductivity detector with a Wheatstone design [184]. Figure 3.9 shows that the TCD comprises 4 cells. Two of these cells act as references and the two others act as analytical cells. The four cells consist of heated chambers containing a filament whose electrical resistivity depends on its temperature. The filaments are heated to a temperature above the one of the chamber temperature. A reference gas (same as the carrier gas) flows through the reference cells and the gas coming out of the column is directed through the analytical cells. The flow rate of the reference cells is typically adjusted to be the same as the flow rate of the

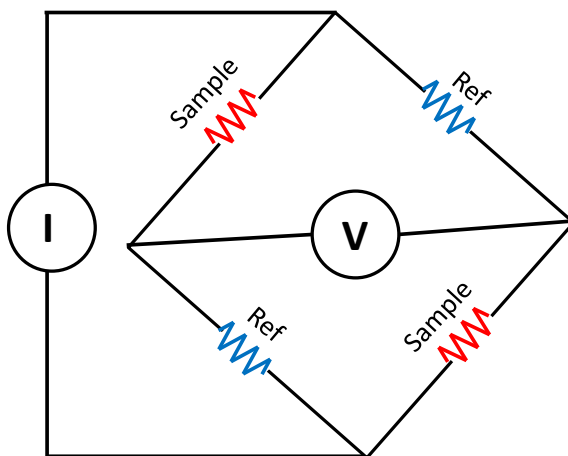


Figure 3.9. Simplified schematic of a thermal conductivity detector with a Wheatstone design.

analytical cells. A current is applied at two opposing intersection points between the sets of reference and analytical cells. The voltage across the bridge is then monitored.

When there is no compound eluting out the column, all filaments have the same resistivity and the voltage across the bridge is zero (the current flows equally through the reference and analytical cells). When a compound elutes out of the column, the thermal conductivity of the gas passing through the analytical cell changes causing the filament temperature to change slightly. Since the resistance of the filaments is temperature dependent, the current distribution through the analytical cells will differ from that passing through the reference cells. This will in turn induce a voltage change across the bridge which is then recorded. The sensitivity of TCDs then strongly depends on the thermal conductivity differences between the gases analyzed and the carrier gas chosen.

3.4.5 GC-MS settings for liquid component analysis

The GC-MS used was a Bruker 436-GC equipped with two split/split-less injectors, an EI single quadrupole MS and a TCD.

For the analysis of liquid components of the electrolyte of Li-ion cells, a BR-5MS column (Bruker, 30m, 0.25 mm ID, 1 μ m coating) was used. Helium was used as carrier gas at a constant flow rate of 1.3 mL/min. The GC was coupled to the MS. The injector temperature was set to 250°C and the oven temperature was programmed to get the best component separation in the shortest amount of time (see Table A2 of Appendix A). This particular column provides good separation for organic carbonates and esters. However small alcohols such as methanol and ethanol as well as ethers and ester of formates are

not separated and elute either before or at the same time as the dilution solvent used (CH_2Cl_2 here).

The transfer line was set to 250°C , the ion source to 250°C and the electron energy to 70 eV. The mass spectrometer was set to a single ion monitoring mode (SIM) for the measurement of EC, EMC, DMC, DEC, VC and known by-products of the dimerization of EC with either EMC, DMC, or DEC [122,185,186]. The by-products of the dimerization of EC with DMC, DEC, or EMC were monitored in the eventuality that they would form during formation. After the SIM mode measurements, most solutions were re-measured with the MS set to a full scan mode to check if no other compounds were present.

Calibration solutions were made and analyzed during quantitative analysis of electrolyte components. The calibration solutions were made by diluting known amounts of electrolyte solvents and additives in CH_2Cl_2 . A minimum of five solutions of known concentration were used to obtain an external calibration curve with a squared correlation coefficient of at least 0.998.

3.4.6 GC-MS settings for the analysis of gaseous compounds and high vapor pressure liquid compounds

The column used for GC-MS analysis of the gases as well as high vapor pressure liquid compounds produced during Li-ion cell operation was a Q-PLOT column (Bruker, 30m, 0.25 mm ID, 8 μm coating). Helium was used as carrier gas at a constant flow rate of 1.3 mL/min. This column gives good separation of volatile hydrocarbons and organic compounds with low boiling points such as mono-ethers, ketones, esters, alcohols and

formates of small molecular mass (*i.e.* smaller than $100 \text{ g}\cdot\text{mol}^{-1}$). However, this column provides very poor retention and/or separation of H_2 , CO , and N_2 .

The injector temperature was set to 100°C and the oven temperature was programmed to get the best component separation in the shortest amount of time (see Table A3 of Appendix A). The transfer line temperature, source temperature and electron energy were kept the same as for the liquid component analysis of the electrolyte.

The gas sample transfer method allows some ambient air to enter the syringe needle; as a consequence, the O_2 and N_2 detected during analysis were ignored. This is not troublesome since O_2 is unlikely to be generated during the early first charge of the pouch cells, and since no nitrogen-containing components or chemicals are present in the cell.

3.4.7 GC-TCD settings for gas components analysis

The analysis of gas products formed during Li-ion cell operation was also performed using GC-TCD. The TCD used was a Wheatstone type detector (Bruker). A custom-made capillary column that allows for permanent gases (H_2 , O_2 , N_2 , CO) and light hydrocarbons (CH_4 , C_2H_6 , C_2H_4 , etc.) as well as CO_2 to be well separated in a single injection was used. The column consisted of a 5A molecular sieve column (Bruker, 10m, 0.32 mm ID, 30 μm coating), in parallel with a Q-PLOT column (Bruker, 50 m, 0.53 mm ID, 20 μm coating). This particular column used with a TCD does not allow good separation and detection of heavier compounds such as ethers, alcohols, ketones, esters and formates.

Argon was used as the carrier gas at a flow rate of 9 mL.min⁻¹. In order to maximize the sensitivity of the detector, the reference cell flow rate of the TCD was set to 30 mL.min⁻¹ and the make-up flow rate of the analytical cell was set to 5 mL.min⁻¹. The TCD temperature was set to 230°C while the filament temperature was set to 370°C. The oven temperature program was adjusted to get the best separation in a minimal amount of time (see Table A4 of Appendix A).

A custom gas mixture of known composition was obtained from Praxair. This gas mixture was used for retention time determination and signal calibration. The gas mixture used was 7.48% butane, 7.55% carbon dioxide, 7.72% carbon monoxide, 7.55% ethane, 7.55% ethylene, 7.44% hydrogen, 7.56% methane, 7.49% propane, 7.48% propylene and 32.18% nitrogen with all % as volume (at atmospheric pressure) percents. All gas volumes reported in this thesis are at atmospheric pressure.

3.5 Error calculation

All results presented in this thesis are the average of the measurements of two samples unless indicated otherwise. The error bars shown in the various figures were calculated as the range of the two samples. This provides a good idea of the repeatability of the measurements.

CHAPTER 4. NOVEL METHODS FOR THE EXTRACTION OF LIQUID AND GASEOUS COMPONENTS FROM LI-ION CELLS AND SUBSEQUENT GC ANALYSIS¹

4.1 Gas chromatography experiments for the study of electrolytes and gas composition in Li-ion cells

Gas chromatography has been previously used in the Li-ion battery research community. This analysis method has been primarily used for qualitative analysis of the volatile components of the electrolyte after cell use [92,122,126,187,188], or the analysis of the composition of the gases produced after the first cycle and after cell use [15,18,185,189,190].

4.1.1 GC-MS measurements of the electrolyte

Several qualitative GC-MS measurements of the electrolyte have been reported. For instance, Moshkovich *et al.* [92] used GC-MS to analyze the electrolyte after it was exposed to high potentials. Using this method, they found evidence of oxidative degradation products. Aurbach *et al.* [126] also measured the composition of the liquid components of the electrolyte of aged commercial cells and saw evidence of the transesterification of linear carbonates. In a similar manner, Sloop *et al.* [122] not only saw

¹ Some of the results presented in this Chapter were published in R. Petibon, L. Rotermund, K.J. Nelson, A.S. Gozdz, J. Xia, J.R. Dahn, J. Electrochem. Soc. **161** (2014) A1167–A1172 and R. Petibon, L.M. Rotermund, J.R. Dahn, J. Power Sources. **287** (2015) 184–195 for which the candidate wrote the first draft of the entire manuscript. The contribution of the co-authors (other than the candidate) is indicated in the captions of the figures where appropriate.

evidence of trans-esterification of linear carbonates, but also trans-esterification between cyclic carbonates and linear carbonates. The presence of trans-esterification products allowed the authors to show that lithium alkoxides were one of the products of the reduction of carbonates at the graphite surface as will be shown later. Later, GC-MS studies by Eom *et al.* [191], Sasaki *et al.* [192] and Kim *et al.* [193] showed that the use of certain additives can suppress such trans-esterification reactions. Kim *et al.* [193] also used semi-quantitative GC-MS analysis to pinpoint the potential at which linear carbonates get reduced at the graphite electrode by following the trans-esterification products of the solvents.

The use of GC-MS in battery research does not seem to go beyond showing evidence of the presence or absence of trans-esterification. This occurs for two reasons, the first one being the particular cell design used in academic research and the second being an intrinsic limitation of GC-MS. Common cell designs used in academic research do not allow for a reproducible electrolyte volume for a given active material mass as indicated in Chapter 2. However, quantification and semi-quantification of reaction by-products and additive consumption requires the use of reproducible electrolyte-volume-to-active-material-mass ratio. This arises from the fact that the passivation of each electrode requires a finite amount of reaction by-products. If the electrolyte-volume-to-active-mass ratio used is not reproducible, then quantification of the electrolyte components will not yield meaningful results. At the same time, GC can only separate compounds that are volatile (boiling point below 300°C). Since the oxidation and reduction of solvents produce ionic species along with molecular compounds, GC can

only see half of the picture. Nevertheless, GC-MS has not been used to its full potential in the Li-ion battery community.

While there are several reports on the use of GC for the analysis of electrolytes, only a few give a detailed description of the method of extraction. For instance, when in presence of moisture or heat, the salt used in most Li-ion cells decomposes and forms HF and PF₅ respectively [188]. Since most GC injectors are made of borosilicate glass and most analytical columns have functionalized silicate-based walls, the presence of HF and PF₅ produces volatile fluorinated and silicated compounds and degrade the column coating over time. The presence of multiple silicon-containing compounds might make the identification of products of the degradation of the electrolyte difficult if silicon containing additives or silicon-based electrodes are used.

4.1.2 GC and GC-MS measurements of the gas composition

Gas chromatography has also been largely used in order to assess the composition of the gas evolved during the first cycle (formation cycle) of Li-ion cells. For instance Yoshida *et al.* [185] evaluated the composition of gas evolved during the initial charge of LCO/graphite full cells filled with an electrolyte containing a variety of cyclic and linear carbonate blends. Kumai *et al.* [189] used GC to analyze the composition of the gas produced during cycling of LCO/graphite cells under various conditions such as different charging currents, over-discharge conditions, or overcharge conditions. Eom *et al.* [191] used similar analysis techniques to evaluate the gas evolved during high temperature storage of LCO/graphite cells containing VC. Many other instances of GC uses for the evaluation of the composition of the gas have been published [15,18,115,190,194].

Usually mass spectrometry is not used as detection tool during gas analysis. This is because the lower mass limit of common quadrupole mass analyzers is about 10 a.m.u. This means that dihydrogen usually cannot be detected with most MS detectors used with GC. Thermal conductivity detectors are usually used instead. While TCD are sensitive to hydrogen, their limit of detection is higher (worse) than MS [181,195] and they do not provide any chemical information. However it is apparent that one could use the high sensitivity of MS to detect reduction or oxidation by-products with low molecular weight and high vapor pressure through the analysis of the gas evolved in pouch cells. This can be understood by evaluating Raoult's law of ideal mixtures:

$$p_i = p_i^* x_i \quad (4.1)$$

where p_i is the partial pressure of component i of the mixture, p_i^* is the partial pressure of the pure component i , and x_i is the molar fraction of the component i . Equation 4.1 shows that if the vapor pressure of a by-product is high enough, a small amount of that compound will be present in the head space of the cell. Since the limit of detection of MS is incredibly low, around 50 fg, compounds in the head space can be detected, even if the vapor pressure of the pure compound is low. Given that the molar volume of an ideal gas is around 22 L.mol⁻¹, MS could potentially detect volumes as low as 5 x 10⁻¹¹ mL of a volatile compound with molecular weight of 50 g.mol⁻¹ (assuming room temperature and atmospheric pressure).

Despite the availability of such methods, there are no systematic reports on the effect of additives on the composition of the gas produced during formation and cell use. Doing such measurements would greatly help understanding how these additives work.

This chapter will present two GC-MS measurement methods developed. The first method deals with the analysis of the liquid components of the electrolyte following the removal of the potentially corrosive salt, and the second deals with the extraction and GC-MS or GC-TCD analysis of gases produced in cycled cells.

4.2 Method for extracting the liquid components of Li-ion cells

Results of GC analyses of electrolytes have been previously presented in the literature [122,188,189,191,196–198] without giving specific details about the extraction method. Some do not disclose any information on the extraction method [126], some indicate a simple dilution in acetonitrile [193] or dichloromethane [187] without further separation. Here a simple GC-MS method for the analysis of the fate of additives in any small Li-ion cell format (smaller than about 10 Ah) is reported. This method separates the LiPF_6 from the solvent, thus protecting the instruments from the aggressive HF or PF_5 formed in the presence of water or heat as well as from the buildup of the salt itself, or LiF, in the GC column.

4.2.1 Experimental procedure

Figure 4.1 shows a schematic of the electrolyte extraction procedure prior to GC-MS analysis. The cells were first discharged to an open circuit potential near 0.0 V, to ensure safety during opening, and opened rapidly outside the glove box. The jelly roll was then immediately put in a vial, preferably polytetrafluoroethylene or perfluoroalkoxy polymer, containing 10 mL of dichloromethane. These particular vials were used because glass vials react with HF and polyethylene or polypropylene-based vials release

oligomers into the sample. Interested readers are invited to consult Figure B1 of Appendix B which shows a comparison of the effect of using glass vials and polymer vials on the chromatograms. The vial was then shaken for 10 - 15 min. The supernatant was then filtered using a syringe filter with a polytetrafluoroethylene membrane with 0.2 - 0.45 μm pores to remove any particles that may have dislodged from the electrodes. A few drops of the filtrate were then added to a vial containing 10 - 15 mL of dichloromethane and 0.2 - 0.5 mL of distilled water, shaken for 5 - 10 min and then centrifuged at 300 g-acceleration for 10 - 15 min to eliminate any potential emulsion. The organic layer (the lower layer) was then injected in the GC-MS.

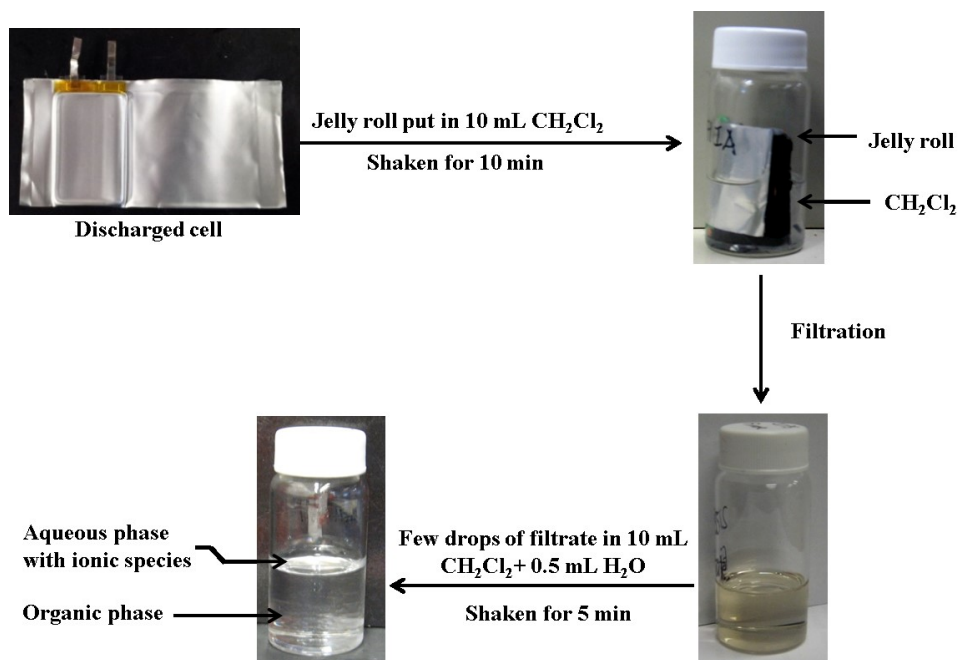


Figure 4.1. Schematic of the electrolyte extraction method used for the analysis of the electrolyte components by GC-MS. The vials shown in the pictures are clear glass vials for illustration purposes. The extraction method was developed with the help of A.S. Gozdz, A123 Systems LLC, 200 West Street, Waltham, Massachusetts, USA 02451. Present address: MarkForged, Inc., 950 Winter St., Waltham, MA.

The exact volume and weight of filtrate added were not measured. During short term cycling at ambient temperature (less than a year) and modest potentials, the amount of EC and linear alkyl carbonate consumed is expected to be small. During each GC-MS measurement, EC, EMC, the additive studied, along with known trans-esterification products of EMC and EC were quantified. As the exact volume (or weight) of the filtrate was not measured, the quantification gives a relative mass percent of each compound quantified. The results presented in this thesis are then weight percent of the additive relative to the total mass of EC, EMC, known trans-esterification products of EMC or EC and the additive.

This quantification method gives reliable results as long as the total weight of EC and linear alkyl carbonate consumed, from which by-products that cannot be measured by GC-MS, is less than 10%. Following the partial derivative rule of error propagation, the error in the final weight of additive left in the electrolyte can be approximated as the total percent of by-products of EC and EMC reactions that cannot be measured (*e.g.* ionic or polymeric compounds). This is true for additives that are added in small quantities. For instance if 5 % of the combined weight of EC and EMC reacts and gives by-products that cannot be measured, this will cause a 5% relative error (5% of the relative amount of additive measured) in the calculated weight of additive left in a cell. This error is acceptable and probably within the cell to cell reproducibility.

4.2.2 Recovery tests

In order to evaluate the recovery efficiency of the extraction method, NMC(111)/gr cells were filled with a known amount of 1M LiPF₆ EC:EMC (3:7)

electrolyte. Cells were then opened and their electrolyte extracted following the procedure described in Section 4.2.1. A known amount of n-nonane was added to the CH₂Cl₂ used for the extraction and used as internal standard for the quantification of the mass of solvent extracted from the cell. The use of an internal standard during electrolyte extraction allows one to have truly quantitative measurements of the solvents extracted.

Table 4.1 presents the results of the extraction and recovery efficiency of the extraction. Table 4.1 shows that the recovery efficiency of the extraction procedure is around 90%. The electrolyte that was not extracted was likely lost during the extraction of the jelly roll from the pouch bag (some electrolyte might be adsorbed on the pouch bag or on the tweezers used to extract the jelly roll). Table 4.1 shows that the recovery efficiency is very good. For instance, Grützke *et al.* [173] recently reported on an extraction procedure using supercritical CO₂, acetonitrile and propylene carbonate with a recovery efficiency of 89%. While this extraction procedure is equally efficient, it is more complex because of its use of supercritical CO₂.

Table 4.1. Recovery efficiency results of the extraction of the electrolyte from NMC(111)/graphite pouch cells using the extraction procedure described in Section 4.2.1.

Cell	mass of electrolyte added to the cell /g	mass of solvent added to the cell (EC + EMC) /g	mass of solvent measured by GC-MS /g	Recovery efficiency /%	Average recovery efficiency /%	Standard deviation recovery efficiency /%
1	0.845	0.74	0.65	88	91	4
2	0.849	0.74	0.71	95		
3	0.830	0.73	0.66	90		

4.2.3 Proof of concept

In order to determine the amount of residual LiPF_6 salt in the organic layer injected into the column of the GC-MS, a simple experiment was carried out. One vial was filled with a mixture of 10 mL of CH_2Cl_2 and 1 mL of H_2O and another vial was filled with a mixture of 10 mL of CH_2Cl_2 and 3 mL of H_2O . The volumes of water used here were chosen so that the aqueous layer would be large enough to be able to extract a few drops.

Two different volumes of water were tested to determine if the ratio of CH_2Cl_2 to H_2O influences the amount of LiPF_6 remaining in the organic phase. To each vial, 40 drops (~ 0.2 mL) of a 1 M LiPF_6 EC:EMC (3:7) electrolyte were added. The volume of electrolyte introduced in the vials was chosen to represent a worst case scenario and to obtain measurable quantities of LiPF_6 with the instruments used. The vials were shaken

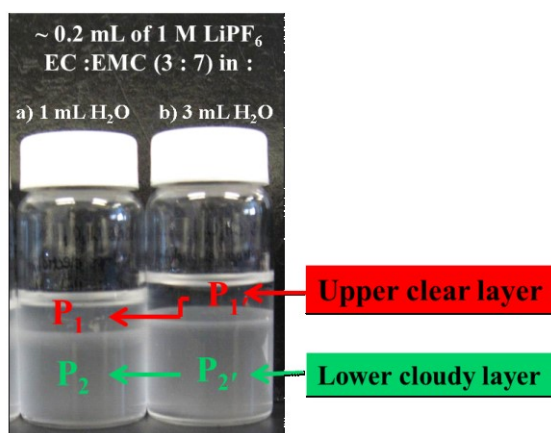


Figure 4.2. Picture of a vial containing 40 drops of a 1 M LiPF_6 EC EMC (3:7) electrolyte in 10.0 mL of CH_2Cl_2 and 1.0 mL of H_2O (a) and of a vial containing 40 drops of a 1 M LiPF_6 EC EMC (3:7) electrolyte in 10.0 mL of CH_2Cl_2 and 3.0 mL of H_2O (b). Sample prepared by Lina Rotermund, 1st Year B.Sc. student, Physics & Atmospheric Science, Dalhousie University (2013).

for 15 min. The two phases were allowed to settle for another 15 min. Figure 4.2 shows the picture of the vials after the 15 min settlement period. Figure 4.2 shows that each vial contained two phases, a clear phase on top (aqueous phase) and a cloudy phase at the bottom. The cloudy phase consists of an emulsion between the organic phase and some of the aqueous phase. The emulsion can be easily eliminated by centrifuging the mixture at 300 g-acceleration for 15 min or by adding unreactive salts such as sodium chloride.

In order to assess if any LiPF_6 remained in the organic layer, a few drops of each phase in the two vials were deposited on silicon wafers. [The emulsion was not eliminated in order to present a worst case scenario.] The wafers were then put in a 250°C oven for 15 min in order for the H_2O , CH_2Cl_2 , EMC, and EC to either evaporate or decompose. At elevated temperature, LiPF_6 starts to decompose into PF_5 and LiF following equation 4.2 [122]:



Since PF_5 is a gas and the sample was in a ventilated oven, the equilibrium is displaced to the product side. LiF is a crystalline compound and is left behind on the silicon wafer.

The Si wafers were weighed before the drops of each phase were added and then again after the heating step. Any positive mass difference after the heating step indicates the presence of residual LiPF_6 and LiF . It is important to point out that the presence of some HF is expected (see Figure 2.4). Hydrofluoric acid is known to react with silicon forming volatile tetrafluorosilane which would create a mass loss of the wafer. However since the wafer is directly put in a 250°C oven, HF is expected to evaporate before

reacting with silicon in a significant way. Table 4.2 shows the mass difference of the silicon wafers on which several drops of each phase were deposited.

Table 4.2 shows that heating the silicon wafer with a few drops of the aqueous phase yielded a positive mass difference, while heating the silicon wafer with a few drops of the organic phase did not cause a significant mass difference (the mass difference was close to the limit of detection of the balance which explains the large error). This indicates that the water phase contains the majority of the LiPF_6 . It ensures that a negligible amount of LiPF_6 is injected into the GC thus preventing damage to the instrument. Moreover, over the course of two years and a half of use and more than 3000 injections, the column has not shown any signs of degradation, and the chromatograms have always been free of fluorosilicates. The absence of peaks characteristic of fluorosilicates and the absence of signs of column degradation further emphasize the fact

Table 4.2. Mass difference of the silicon wafers after depositing a few drops of each phase in the vials shown in Figure 4.2 and then after heating the same sample at 240°C for 15 min. Samples and measurement were made by Lina Rotermund, 1st Year B.Sc. student, Physics & Atmospheric Science, Dalhousie University (2013).

	Layer in vial	Average mass difference /mg	Error /mg
P_1	Upper aqueous layer from the vial containing 1 mL H_2O	3.0	0.7
P_2	Lower organic layer (emulsion) from the vial containing 1 mL H_2O	0.07	0.07
$P_{1'}$	Upper aqueous layer from the vial containing 3 mL H_2O	1.0	0.2
$P_{2'}$	Lower organic layer (emulsion) from the vial containing 3 mL H_2O	0.07	0.04

that the organic layer does not contain any significant amounts of HF or LiPF₆.

In order to verify the complete recovery of the organic components of the electrolyte in the CH₂Cl₂ phase during the extraction, a drop of electrolyte of known composition was extracted in a 10 mL CH₂Cl₂/0.2 mL H₂O mixture. The measured composition of the extracted electrolyte matching the composition calculated from the mass of the different components acts as a proof of total recovery. For instance Table 4.3 shows the measured composition of a drop of two different electrolytes extracted in a CH₂Cl₂/H₂O mixture. Table 4.3 shows that the measured composition of the electrolytes extracted matched the expected composition within error. This indicates that the partition coefficient of the liquid components of the electrolyte greatly favors the organic phase. The relative volume of the water phase was still minimized in case an additive studied has a partition coefficient that favors the water phase.

Table 4.3. Expected and measured composition of a drop of electrolyte extracted in a mixture consisting of 10 mL of CH₂Cl₂ and 0.2 mL of H₂O and measured by GC-MS.

Electrolyte	Expected composition	Measured composition
1M LiPF ₆ EC:EMC (3:7)	30% EC + 70% EMC	30.5 ± 0.6% EC + 69 ± 0.7 % EMC
1M LiPF ₆ EC:EMC (3:7) + 2.0 wt.% PES	29.3% EC + 68.3% EMC + 2.4% PES	28.6 ± 0.5% EC + 68.2 ± 0.4 % EMC + 2.39 ± 0.06% PES

4.3 Extraction method for gaseous and volatile components of Li-ion cells

4.3.1 Experimental procedure

The analysis of the qualitative and quantitative composition of the gas produced during the first charge of Li-ion pouch cells was analyzed using GC-MS and GC-TCD

and a simple extraction method. After cycling, pouch cells were discharged to 1 V and put in a gas extraction device. Figure 4.3 shows a picture of the gas extraction device.

The gas extraction device consists of a brass chamber fitted with a screw top. An O-ring allows good sealing between the screw top and the brass chamber. A shaft with a sharp point was fitted through the screw top. The screw top opening was also lined with two O-rings providing a good seal to the shaft. The brass chamber was fitted with a Swagelok quick-connect on one side and a GC natural rubber septum on the other side.

Once the pouch cell was put in the chamber, the screw-top was screwed on and the chamber evacuated to at least 13 Pa (absolute pressure) through the Swagelok quick-connect for a period of 20 – 30 min. The vacuum line was removed and the shaft lowered, piercing a hole through the pouch cell. The pressure differential between the



Figure 4.3. Picture of the gas extraction device designed for the extraction of gaseous and volatile components of Li-ion cells. Designed with the help of Simon Trussler, Physics & Atmospheric Science, Dalhousie University (2014). The outer diameter of the chamber was 7.5 cm.

brass chamber and the inside of the pouch cell allows for the extraction of the gas during the puncturing step. The chamber was allowed to rest for 5 min to ensure a complete gas extraction from the pouch bag and jelly roll of the cell. The brass chamber was back-filled using ultra-pure Ar through the quick connect at a pressure of 150 kPa (~1.5 atm). The gas inside the chamber was then mixed by pumping a 1 mL gas tight syringe (Hamilton) fitted through the septum. The gas from the chamber was then extracted through the septum using a gas-tight syringe (250 μ L gas-tight syringe SGE or Hamilton). The gas was then injected into the GC.

4.3.2 Proof of concept

In order to evaluate the range of compounds that this method can extract, separate and detect, the gas produced in NMC(111)/gr cells filled with a 1M LiPF₆ EC:EMC (3:7) electrolyte and charged to 3.5 V at 40°C was analyzed using GC-MS.

Figure 4.4 shows the chromatogram of the gas extracted. Figure 4.4 shows that the gas extraction method allows gas compounds as well as liquid compounds such as ethyl formate, methyl acetate and ethanol to be detected. This comes about because of the moderate to high vapor pressure of these compounds in combination with the low pressure step during the extraction procedure and the very low limit of detection of the mass spectrometer. The signal to noise ratio of these liquid compounds appears high. This is due to the low abundance of these compounds in the gas phase and to the fact that the total ion count (10 - 250 a.m.u.) is shown. Figure 4.4 also shows the ion count of fragments characteristic of the compounds listed (red trace). The selected ion count shows an improved signal to noise ratio.

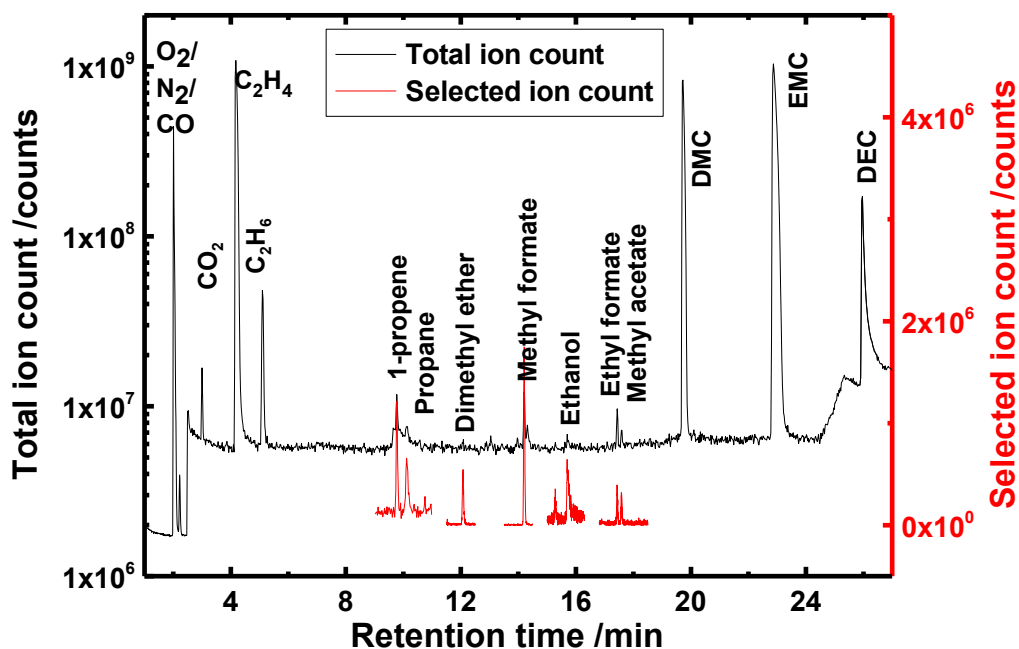


Figure 4.4. Chromatogram of the gas extracted from a NMC(111)/graphite pouch cell charged to 3.5 V at 40°C. Left axis shows the total ion count (10 – 250 amu), right axis shows the ion count of fragments specific to the low abundance volatile compounds listed in the figure.

Figure 4.4 shows that the main gas formed in cells filled with a control electrolyte is ethene (C_2H_4). This is expected since it is one of the main by-products of the reduction of EC at the graphite surface [112–114,116,185,190] following the reaction pathways shown in Figure 2.1. Figure 4.4 also shows that many gases and other volatile compounds form during the very first charge to 3.5 V. These compounds include saturated hydrocarbons (C1 to C4), carbon dioxide, alcohols, esters, formates, and ethers. Most of these compounds can be traced back to the reduction of EMC as will be shown in Chapter 5.

In order to evaluate the gas extraction efficiency, NMC(442)/gr cells vacuum dried at various temperatures before electrolyte filling with a 1M $LiPF_6$ EC:EMC

electrolyte were charged to 3.5 V. The gas volume produced during this first charge was measured ex-situ using Archimedes' principle (see Section 3.3). The gas from the cells was then extracted using the method described in Section 4.3.1 and analyzed by GC-TCD.

Figure 4.5 shows the results of this comparison. Figure 4.5 shows that the total volume measured by TCD is consistently greater than the volume measured ex-situ. This is consistent with the partial solubility of the various gases produced during the graphite passivation in the carbonate based electrolyte as reported by Anouti *et al.* [199] and Dougassa *et al.* [200–202]. Figure 4.5 then strongly suggests that the extraction procedure not only extracts the gas trapped in the gas bag of the pouch cells but also

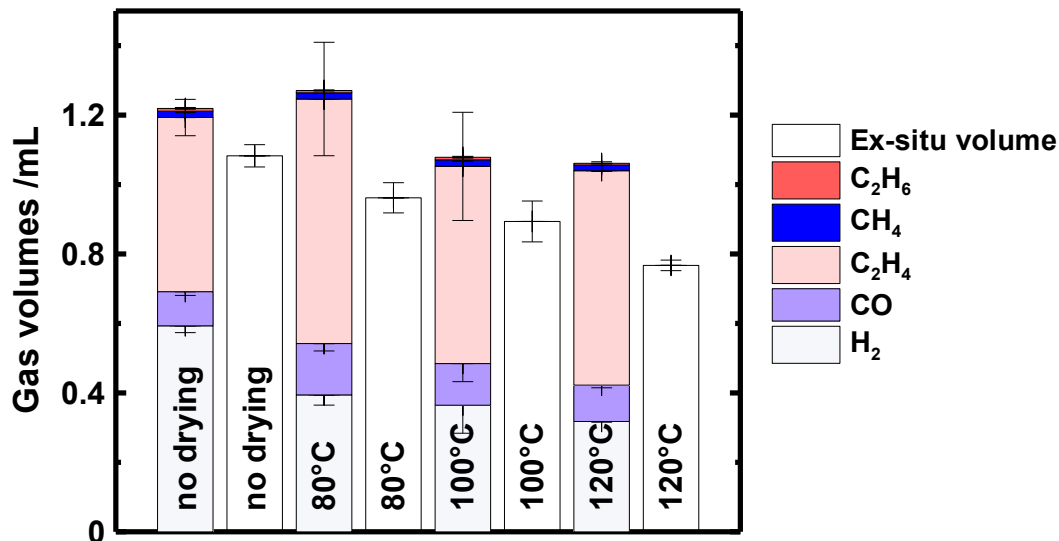


Figure 4.5. Comparison of the gas volume measured ex-situ and gas volume (and composition) measured using the extraction method described in Section 4.3.1 and GC-TCD for NMC(442)/graphite pouch cells vacuum dried at various temperature prior to electrolyte filling. All cells were filled with a 1M LiPF₆ EC:EMC (3:7) electrolyte and charged to 3.5 V at 40°C and C/20. The data shown is the average of two cells. The error of the ex-situ volume is the range of the two cells and the error of the gas composition is the square root of the sum of the squared of the range of two cells and squared standard deviation of the TCD sensitivity measured during calibration runs.

partially or totally extracts the gas dissolved in the electrolyte. This is made possible by the low pressure step added to the extraction procedure. This low pressure, added to the large chamber size (compared to the jelly roll volume) drives the equilibrium of the gas dissolved in the electrolyte towards the gas phase.

Figure 4.5 also shows that drying cells prior to electrolyte filling has a great impact on gas production during the formation of full cells to low voltage (*i.e.* 3.5 V). For instance, vacuum-drying cells at 80°C decreases the amount of H₂ produced by about 30%, consistent with removal of residual water present in the electrodes and separator. Figure 4.5 also shows that increasing the drying temperature from 80°C to 120°C further decreases the amount of H₂ produced by another 20%. This indicates that while drying cells at 80°C does remove some of the residual moisture present in the cell, it does not completely remove it.

4.4 Concluding remarks on the extraction procedures

Chapter 4 presented two extraction procedures. The first extraction procedure allows the liquid components of the electrolyte to be analyzed and quantified and which recovery efficiency was shown to be upward of 90%. The subsequent chapters of this thesis will show how this method can be used to evaluate the concentration *vs.* time profile of an additive as well as to evaluate at which electrode an additive is consumed during cell use.

The second extraction method presented allows the gas composition as well as small molecular weight organic compounds to be detected and measured. This method was shown to quantitatively extract the gas in the cell headspace as well as some/all of

the gas dissolved in the electrolyte. The subsequent chapters of this thesis will show how this method can be used to determine the reduction pathways of solvents and some additives.

CHAPTER 5. ANALYSIS AND QUANTIFICATION OF ADDITIVE CONSUMPTION AND GAS GENERATION DURING OPERATION OF LI-ION CELLS CONTAINING VINYLENE CARBONATE OR PROP-1-ENE-1,3-SULTONE²

5.1 Additive consumption and gas production during the first charge of NMC/graphite cells to low voltage containing VC or PES

This chapter mainly deals with NMC/gr cells filled with a 1M LiPF₆ EC:EMC (3:7) base electrolyte to which no additive has been added (called control) and to which VC or PES has been added. The gas produced during the first charge to low voltage (< 3.5 V) and high voltage (> 4.2 V), as well as the additive consumption during the first charge and subsequent cell use to moderate voltages (< 4.2 V) will be presented. Vinylene carbonate was chosen for its wide use and extensive prior study in the Li-ion battery literature [3,111,150,172,190,191,203–206]. Prop-1-ene-1,3-sultone was chosen because it is similar to VC in terms of CE improvement, low gas production properties during cell formation, film forming properties and low rate of electrolyte oxidation in EC-based and PC-based electrolytes in cells cycled to 4.2 V and below [155,157,207–209].

² Some of the results presented in this Chapter were published in R. Petibon, J. Xia, J.C. Burns, J.R. Dahn, , J. Electrochem. Soc. **161** (2014) A1618–A1624 and in R. Petibon, L. Madec, L.M. Rotermund, J.R. Dahn, J. Power Sources. **313** (2016) 152–163 for which the candidate wrote the first draft of the entire manuscripts. The contribution of the co-authors (other than the candidate) is indicated in the captions of the figures where appropriate.

5.1.1 Gas production in NMC/graphite cells charged to 3.5 V

Figure 5.1 shows a summary of the gas extracted from NMC(111)/gr cells filled with various electrolytes and charged to 3.5 V. Figure 5.1 shows again that the procedure

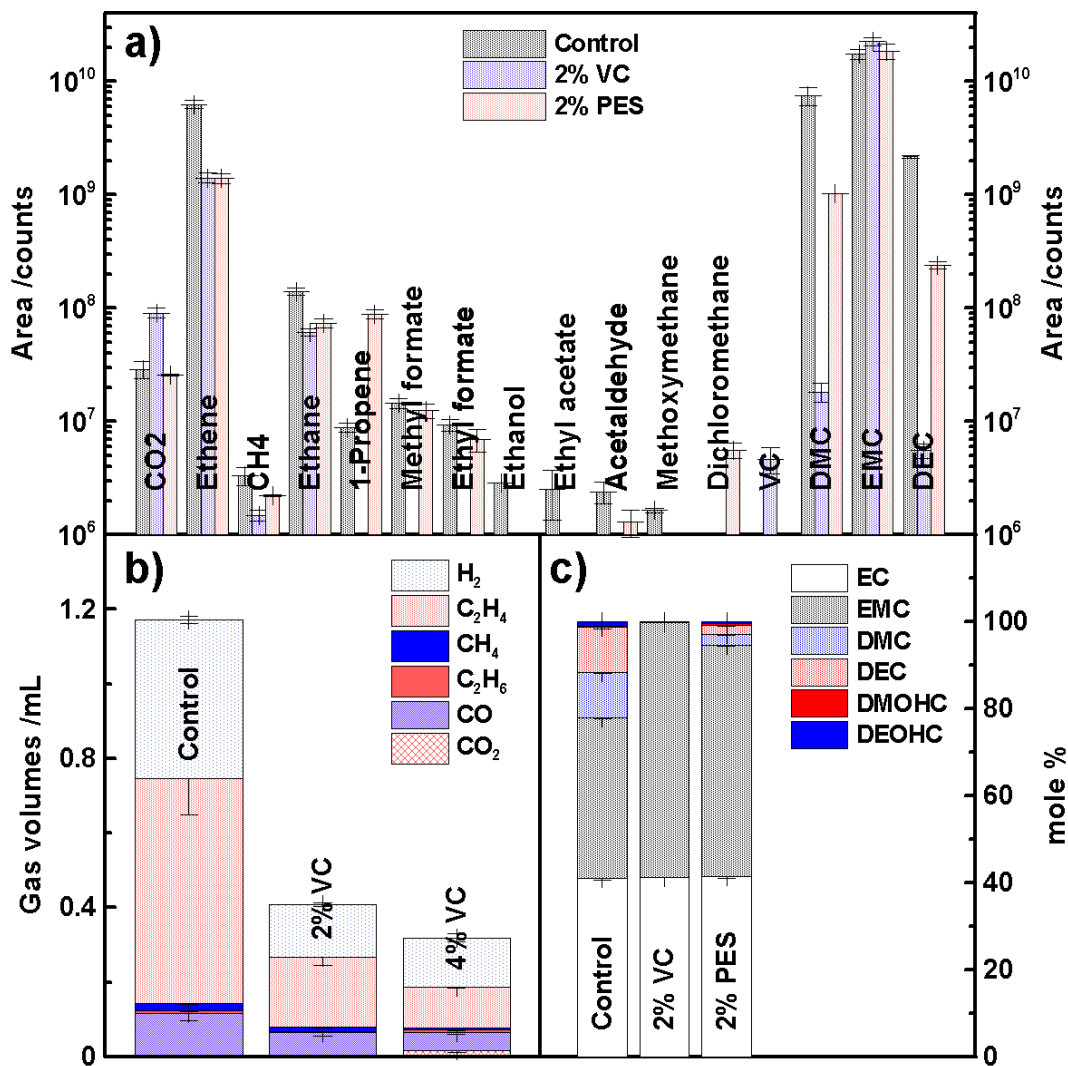
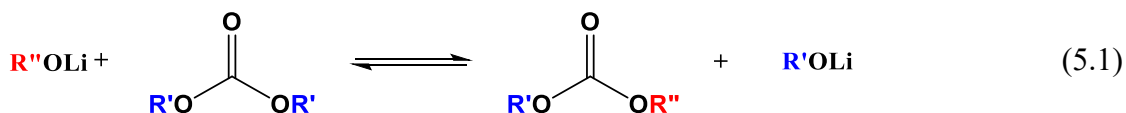
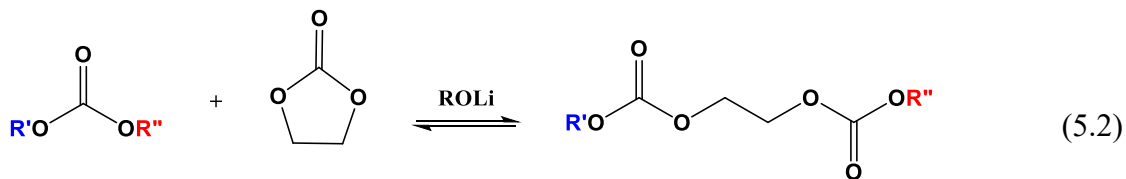


Figure 5.1. Peak area of compounds detected by GC-MS analysis (a) and volume of gases detected by GC-TCD analysis of the gas (b) and GC-MS analysis of the solvents (c) extracted from NMC(111)/graphite pouch cells filled with various electrolytes and charged to 3.5 V at 40°C and C/20. The data shown are the average of two cells and the error was calculated as the range of the two cells. Cells used for panel a) were prepared by Lénaïc Madec, Post-doctoral fellow, Physics & Atmospheric Science, Dalhousie University (2014).

shown in Section 4.3 allows the extraction of gases (*e.g.* ethene, ethane, etc.) and liquids with high vapor pressure (*e.g.* dimethyl ether, methyl formate, *etc.*). The identification of these compounds helps elucidate the reduction pathway of EC and EMC.

Figures 5.1a and 5.1b show that the major gases produced in cells without additive are ethene, CO and H₂. Ethene is a product of the reduction of EC following the mechanism shown in Figures 2.1 and 5.2 [95,110] while H₂ is a product of the reduction of residual water present in the electrodes, separator and electrolyte. Carbon monoxide may come from the 2-electron reduction of EC and EMC as proposed by Ota *et al.* [190] and Kumai *et al.* [189], although the results presented by Onuki *et al.* showed that it most likely only comes from the 2-electron reduction of EC [115]. Figure 5.1 also shows that ethane and methane are produced which both result from the reduction of EMC [115,189]. Finally, Figures 5.1a and 5.1c show that cells containing no additive show large quantities of DMC and DEC and small quantities of dimethyl-2,5-dioxahexane carboxylate (DMOHC), diethyl-2,5-dioxahexane carboxylate (DEOHC), and ethylmethyl-2,5-dioxahexane (EMOHC, not quantified) when the starting electrolyte contained no additive. Dimethyl carbonate and DEC are generated via the transesterification of EMC while DMOHC, EMOHC, DEOHC are generated via the dimerization of EC and a linear carbonate. The formation of these compounds is activated by the presence of lithium alkoxides as shown by many researchers [19,122,126,185,191,193,210] and following:





where $ROLi$ is a lithium alkoxide.

The presence of ethers, esters, aldehydes, methyl or ethyl formate, and EMC trans-esterification indicates that the reduction of EMC can follow various reduction pathways and that the by-products can further react. The GC-MS analysis of the gas then allows the reduction pathway shown in Figure 2.3 to be completed and the subsequent reaction of the by-products of the reduction to be determined. Figure 5.2 shows proposed reactions resulting from the reduction of EC, linear carbonates and water which accounts for the gases and high vapor pressure compounds detected in NMC/gr cells charged to 3.5 V as shown in Figure 5.1.

Figure 5.2 shows that the reduction of EMC can lead to the formation of a lithium alkoxide and a RCO_2 radical, or a lithium hemcarbonate and an aliphatic radical. This is consistent with some of the pathways of the reduction of linear carbonate (DEC in this case) determined by low temperature radiolysis and presented by Shkrob *et al.* [116]. The formation of methyl acetate, methyl formate and ethyl formate is consistent with the prior formation of a RCO_2 -type radical followed by a radical recombination.

Onuki *et al.* [115] showed using ^{13}C labeled EC, and ^{13}C labeled DEC, that the reduction of DEC leads to the formation of C_2H_6 (ethane) during the initial charge of $\text{LiNi}_x\text{Co}_y\text{Al}_{1-x-y}\text{O}_2/\text{graphite}$ cells. It is then very likely that the reduction of EMC leads to the formation of C_2H_6 and CH_4 through the reduction pathways shown in Figure 5.2. The formation of these two gases would then originate from the 1-electron reduction of

EMC followed by hydrogen abstraction. The source of the hydrogen radical may be from other linear carbonates as shown by Shkrob *et al.* [116] or H₂ resulting from the reduction of water. It is also probable that RCO₂ radicals can abstract hydrogen from linear alkyl carbonates and H₂ in the same manner. This would explain the presence of methyl formate and ethyl formate.

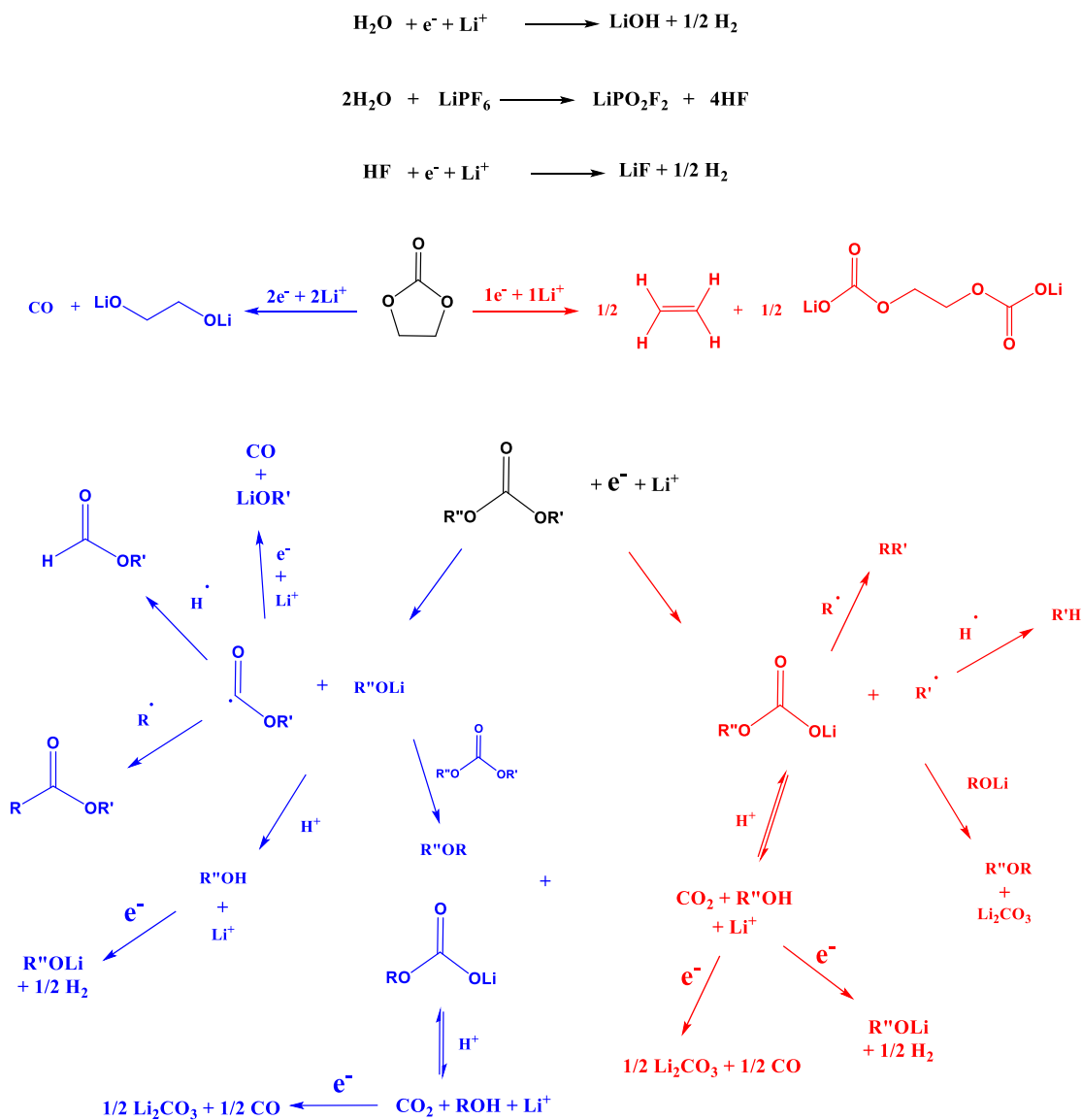


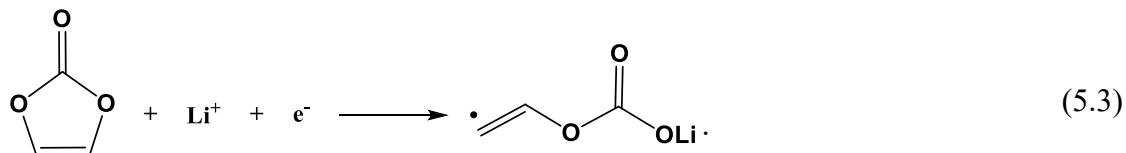
Figure 5.2. Proposed reaction schemes for the reduction of water, HF, EC and linear carbonates based on the results shown in Figure 5.1.

Since the reduction of EMC leads to the formation of lithium alkoxides, it is very likely that the observed ethyl methyl ether and dimethyl ether are formed from the reaction of these alkoxides with EMC and lithium hemicarbonates via a simple nucleophilic substitution reaction. Finally, the reduction of some of the CO₂ produced as well as the 2-electron reduction of EC or linear carbonates would explain the presence of CO seen in Figure 5.1b as proposed by Aurbach *et al.* [105] and Ota *et al.* [190]. Hemicarbonates are also prone to CO₂ loss in presence of acids [211] such as H₂O or HF. This would explain, in part, the generation of CO₂ and alcohols seen in Figure 5.1a.

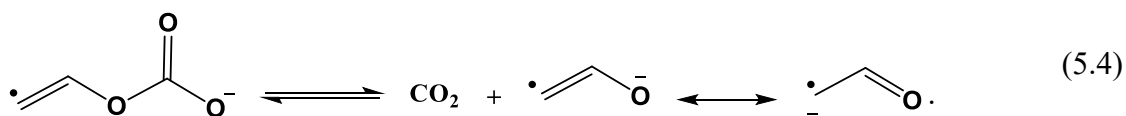
Figure 5.1 also shows that the presence of either VC or PES affects the gases produced during the formation of NMC/gr cells formed to 3.5 V (readers are reminded that the y-axis of Figure 5.1a is a logarithmic scale). For instance, the intensity of all compounds detected is lowered upon addition of these additives with the exception of CO₂ in the presence of VC and propene in the presence of PES. This is consistent with the formation of a passivating film resulting from the reduction of the additives as reported by many researchers [3,155,157,190,203–205,208,209]. The gases produced being dependent on the additive added to the electrolyte allows the reduction pathways of the additives to be inferred.

Figure 5.1 shows that the addition of VC leads to a higher CO₂ production. This is consistent with the findings presented by Ota *et al.* [190] and Zhang *et al.* [158]. This indicates that either the reduction of VC leads to the formation of CO₂ or that some of the by-products of its reduction decompose or react with other chemicals leading to the formation of CO₂. In an earlier publication, Wang *et al.* [212] proposed that the first

reduction of VC leads to the ring opening of the molecule forming an ethenolate radical substituted hemicarboxylate following:

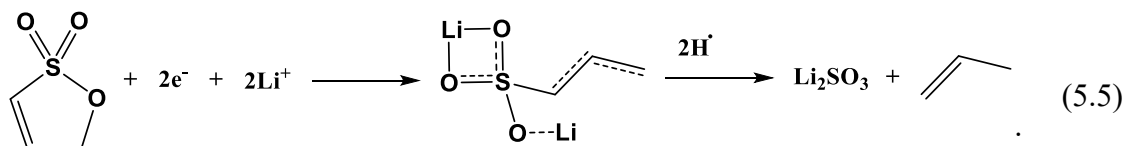


This product would be prone to CO₂ loss since the ethenolate radical would be stabilized by resonance as proposed by Zhang *et al.* [158] following:



The presence of CO₂ then suggests that the mechanism proposed by Zhang *et al.* [212] is plausible (other mechanisms may also explain the production of CO₂).

Figure 5.1 also shows that cells containing PES produced more propene than cells without. This indicates that the reduction of PES leads to the formation of propene. Self *et al.* [209] computed the reduction of PES resulting in the formation of propene following:



In an earlier publication, Li *et al.* [155] proposed a reduction pathway for PES that would lead to the formation of propyne. The absence of propyne in Figure 5.1 allows this proposed pathway to be rejected and further supports the one proposed by Self *et al.* [209].

Finally, Figures 5.1a and 5.1c show that the amount of DMC and DEC, ethers, methyl or ethyl formate generated during the first charge of NMC/gr cells to 3.5 V is a lot

smaller in the presence of PES and VC. This is consistent with the passivation of the graphite surface by these additives before the electrode reaches a potential below the reduction potential of EC and EMC. This pre-passivation limits the amount of EC and EMC which is reduced and limits the amount of alkoxide produced which then lowers the amount of EMC and EC undergoing trans-esterification or dimerization. The presence of small quantities of ethylene, ethane and methane in cells containing VC and PES indicates that there is still some EC and EMC that has been reduced which then leads to a small amount of lithium alkoxides. These alkoxides produced may then be trapped by VC and PES thus preventing them from catalyzing the trans-esterification and dimerization of EMC and EC as proposed by Sasaki *et al.* [192] (in the case of VC).

Guyomard *et al.* [213] and Smart *et al.* [45] showed that ethers and esters have lower oxidation potentials than organic carbonates. Alcohols and lithium alkoxides might also have a low oxidation potential. It is then very likely that VC and PES lower the electrolyte oxidation rate at the positive electrode of LCO/gr cells and NMC/gr cells operated to 4.2 V [143,214] because of the modified positive electrode SEI [203,204,208] as well as due to a lower generation rate of compounds with poor oxidative stability at the graphite electrode.

Finally, Figure 5.1a shows that the gas extracted from cells filled with an electrolyte containing PES contains small quantities of dichloromethane. This dichloromethane is likely to come from the solvent used to synthesize the compound.

5.1.2 Additive consumption during the first charge of NMC/graphite cells containing VC or PES

Figure 5.3 shows the percentage of VC and PES left in cells initially containing 2.2% VC or 2.2% PES charged to different voltage cut-offs during the first charge of NMC(111)/gr cells, shown alongside the voltage *vs.* capacity curves (a) and shown alongside the differential capacity *vs.* voltage curves (b). In order to obtain each data point shown in the additive remaining *vs.* cell capacity plot, pair cells were stopped at a pre-defined cut-off voltage. Their electrolyte was then extracted and analyzed by GC-MS following the procedure described in Section 4.2. Figure 5.3b shows that cells were stopped at differential capacity minima. This ensures that pair cells were stopped around the same state of charge, regardless of any difference in cell impedance.

The differential capacity plot of the first charge of cells containing VC shows a peak around 2.8 V while the dQ/dV *vs.* V curve for cells containing PES shows a peak around 2.4 V (see inset in Figure 5.3b). These two peaks correspond to the reduction of VC [3,143,215] and PES [157,207] at the graphite surface, respectively.

Generally, the consumption profile of PES during the first charge is very similar to that of VC. That is, the largest concentration drop occurs between 1.5 V and 3.0 V as the cell is charged. This is expected since in this potential range the graphite electrode potential (*vs.* Li/Li⁺) drops below the reduction potential of the additives. Based on the assumption that the reduction of the additive leads to the formation of a passivating layer, one would expect that the rate of consumption of the additive would dramatically slow down past this 1.5 – 3 V range. However, Figure 5.3 clearly shows that both VC and PES continue reacting in a significant manner beyond the peak corresponding to their

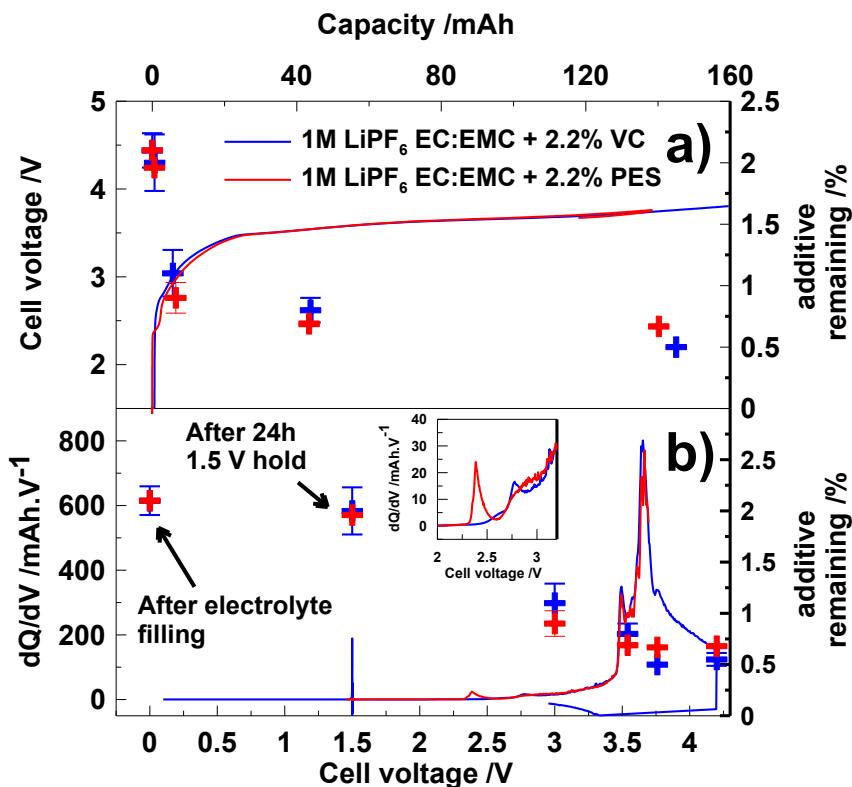


Figure 5.3. VC and PES remaining in NMC(111)/graphite pouch cells initially containing 2.2 % VC or 2.2 % PES, charged to different voltage cut-offs during formation, shown alongside the voltage vs. capacity curves (a) and shown alongside the differential capacity vs. voltage curves (b). Each data point shown is the average of two cells. The PES containing cells were prepared and analyzed by Lina Rotermund, 2nd year B.Sc. student, Physics & Atmospheric Science, Dalhousie University (2014).

electrochemical reduction. This sustained consumption may originate from an incomplete graphite passivation (partial passivation), or from reactions between the remaining additives and nucleophilic by-products commonly generated during reductive processes [78,114,193,208,209,216] (see Section 2.2.1 and Figure 5.2).

The main difference between PES and VC seems to be that PES consumption slows down significantly between 3.5 V and 3.75 V (no significant consumption) while VC consumption still occurs. Figure 5.3 clearly shows that the reduction peak of the

additive in the differential capacity vs. voltage plot during the first charge of a cell (formation cycle) only partially reflects the reactivity of an additive.

In order to evaluate the effect of temperature and initial additive loading on additive consumption, NMC(111)/gr cells containing various additive loadings were prepared, formed and their electrolyte analyzed by GC-MS. Figures 5.4a and 5.4b show that, generally, higher initial VC or PES loading leads to higher consumption. However this increased consumption does not lead to complete consumption of the extra added additive. This may relate to accelerated consumption kinetics due to increased additive

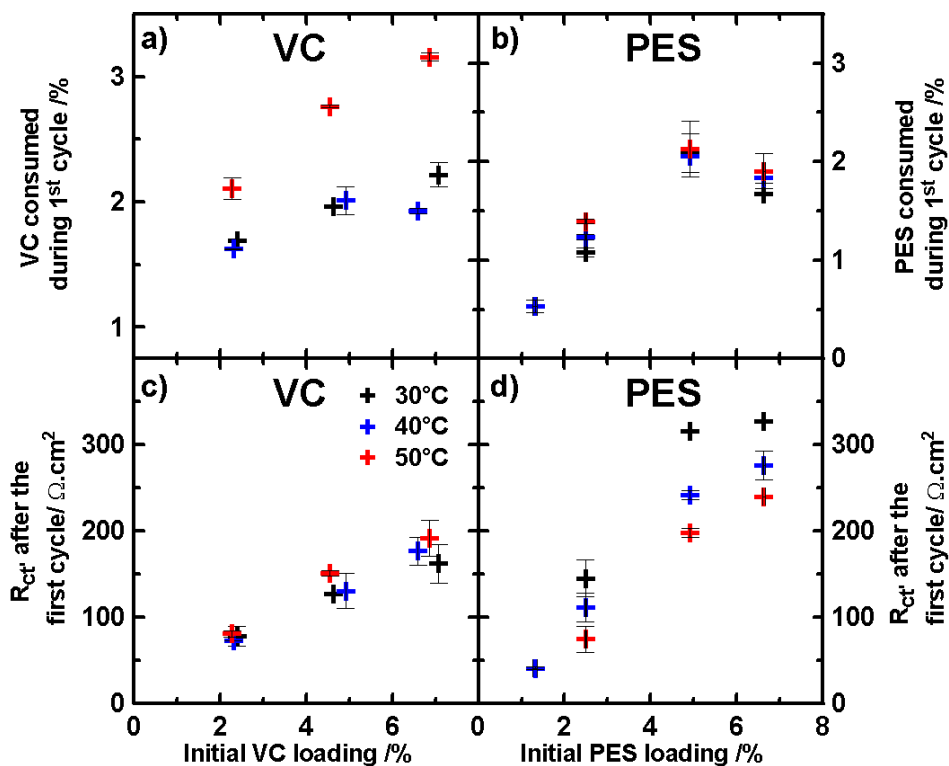


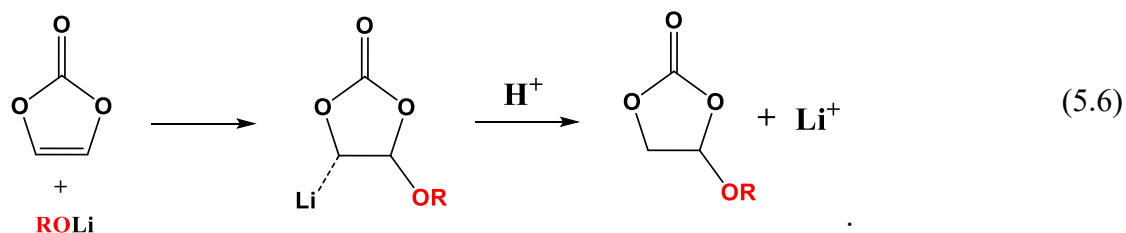
Figure 5.4. Amount of VC (a) and PES (b) consumed as a function of initial additive loading during the first cycle of NMC(111)/graphite pouch cells containing a 1M LiPF_6 EC:EMC (3:7) base electrolyte, magnitude of the impedance (R_{ct}) after the first charge and partial discharge to 3.8 V of VC-containing cells (c) and PES containing cells (d) as a function of initial additive loading. The PES-containing cells were prepared and analyzed by Lina Rotermund, 2nd year B.Sc. student, Physics & Atmospheric Science, Dalhousie University (2014).

concentration. Figures 5.4a and 5.4b also show that while the formation temperature does not impact the amount of PES consumed, forming VC-containing cells at 50°C significantly increases the amount of additive consumed compared to cells formed at 30°C and 40°C. This may indicate that formation temperature may impact the composition of the SEI at the graphite electrode of cells containing VC. Figure 5.4b also shows that the consumption in PES-containing cells stops increasing with increasing initial loading past 4%. This may indicate a near complete graphite passivation.

Figures 5.4c and 5.4d show the magnitude of the impedance, R_{ct} (see Section 3.2.4 for a definition of R_{ct}) after the first cycle. Figures 5.4c and 5.4d show that the magnitude of the impedance of both VC-containing and PES-containing cells increases with increasing initial additive loading. This is consistent with the findings presented by Petibon *et al.* [215], Burns *et al.* [143] and Nelson *et al.* [214] in earlier publications. It is then apparent from Figures 5.4a-d that the more VC or PES is consumed, the more resistive the SEI of either electrode becomes. Petibon *et al.* [107,215] and Xia *et al.* [207] [207] showed that this increased impedance comes from the negative electrode. This indicates that increased VC or PES reduction at the negative electrode leads to the formation of a more resistive SEI at the negative electrode.

5.1.3 Prevention of trans-esterification in presence of VC

The results in Section 5.1.1 showed that VC may prevent the trans-esterification of EMC by lowering the amount of EMC that is reduced as well as by trapping lithium alkoxides that may have been produced. In an earlier publication, Sasaki *et al.* [192] proposed that VC might trap lithium alkoxides via a simple addition reaction following:



They made this assumption based on the detection of the neutral compound of the addition reaction by GC-MS analysis. However they did not report any quantification which means that this product might very well result from a minor pathway. Moreover, alkoxides may be able to initiate anionic polymerization of VC or at least its oligomerization. In order to verify this hypothesis, lithium methoxide as well as lithium ethoxide were added to EMC solutions with or without 10% VC.

Figure 5.5 shows the mole ratio of EMC, DMC and DEC as a function of time after adding lithium methoxide (LiOMe) or lithium ethoxide (LiOEt) to EMC as

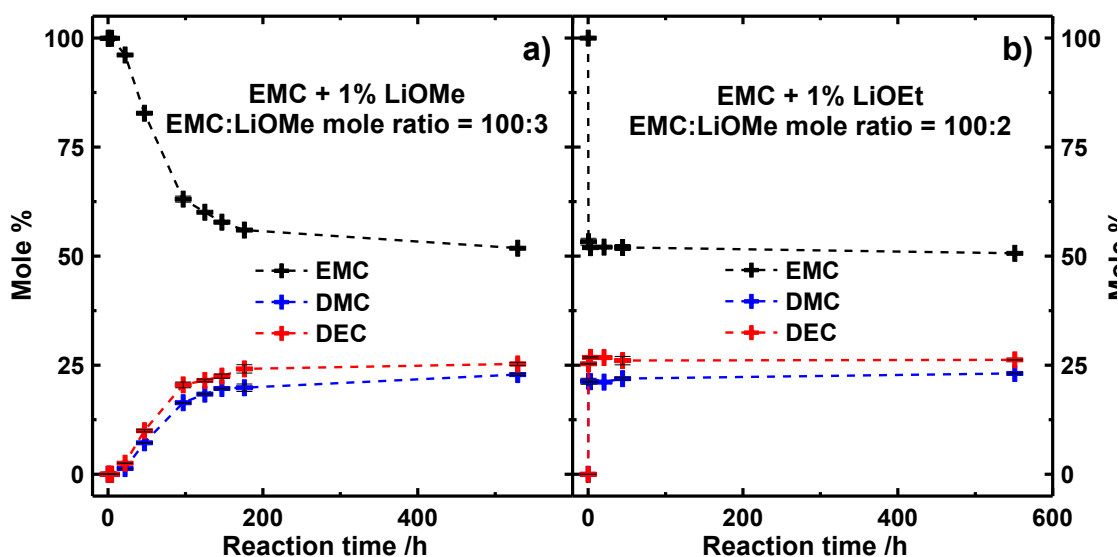


Figure 5.5. EMC, DMC, and DEC mole ratio as a function of time after adding lithium methoxide (LiOMe, (a)) or lithium ethoxide (LiOEt, (b)) to EMC. Reactions were carried in closed high density polyethylene vial under mild agitation in an Ar-filled glovebox at a temperature of $25^{\circ}\text{C} \pm 5^{\circ}\text{C}$.

determined by GC-MS. Figure 5.5 shows that EMC undergoes transesterification in the presence of lithium alkoxides, consistent with the results presented by Kim *et al.* [193] and Sasaki *et al.* [186]. Figure 5.5 shows that the trans-esterification reaction reaches equilibrium once about 50 mole% of EMC has been converted to DMC and DEC. The experiment was carried out again in an EC:EMC mixture and the equilibrium was reached at the same EMC mole% (see Figure C1 of Appendix C). Finally, Figure 5.5 shows that the trans-esterification reaction reaches equilibrium with LiOEt much faster than with LiOMe. For instance, the reaction reaches equilibrium after ~ 100 h with LiOMe compared to < 20 h with LiOEt. This may relate to faster kinetics or higher solubility of LiOEt compared to LiOMe.

Figure 5.6 shows the EMC, DMC and DEC mole% as well as amount of VC left (normalized to the starting VC content) as a function of time after addition of LiOMe or LiOEt to mixtures of EMC:VC (90:10). Figure 5.6 shows that very little transesterification occurs in the presence of VC consistent with the results presented by Kim *et al.* [193] and Sasaki *et al.* [192] as well as with the results presented in Figure 5.1. Figure 5.6 shows that small quantities of products of the addition reactions between VC and lithium methoxide or lithium ethoxide (EC-OMe and EC-OEt, see Equation 5.6 and Figure C2 of Appendix C for their structure) have been detected. In addition, Figure 5.6 shows that 50% of the initial VC content is consumed upon addition of alkoxides. Based on the relative mole ratio of alkoxide and VC added, this indicates that the reaction happens with a VC:alkoxide stoichiometry of around 2-3:1. The addition of LiOMe and LiOEt lead to the formation of a brownish insoluble compound. This then indicates that the pathway proposed by Sasaki *et al.* [192] (see equation 5.6) is only a minor pathway.

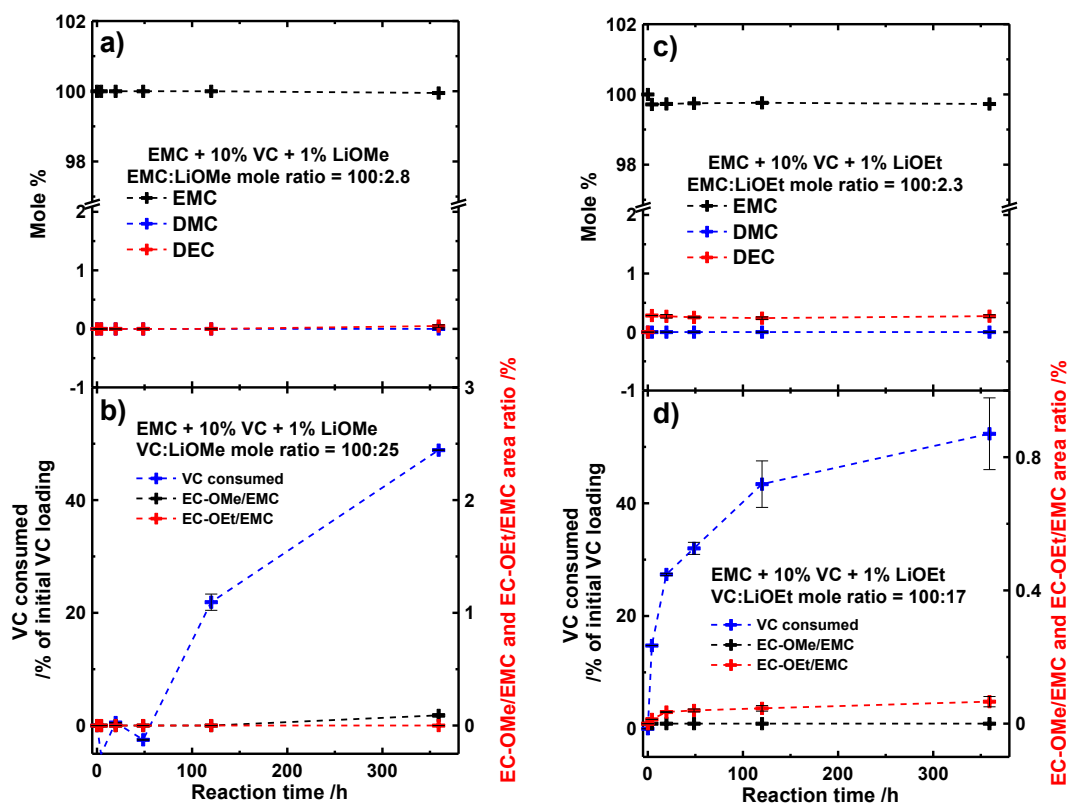


Figure 5.6. EMC, DMC and DEC mole ratio (a, c) and amount of VC left (normalized to the starting content) (b, d) as a function of time after adding lithium methoxide (a,b) or lithium ethoxide (c,d) to EMC + 10% VC mixtures. Reactions were carried out in closed high density polyethylene vials under mild agitation in an Ar-filled glovebox at a temperature of $25^{\circ}\text{C} \pm 5^{\circ}\text{C}$.

This also indicates that lithium alkoxides are able to initiate the oligomerization of VC. This also shows that the consumption of VC observed in Figure 5.3 may correspond to the reaction of VC and nucleophilic products present in the electrolyte in addition to its consumption due to electrochemical reduction followed by polymerization.

Figure 5.7 shows various pathways that may lead to the consumption of VC in the presence of lithium alkoxides. Figure 5.7 shows that several pathways may lead to VC oligomerization (others may exist). Some of these pathways may lead to the formation of compounds prone to lose CO_2 under mild heating. Further analysis of the reaction would

be necessary using liquid chromatography (LC)-MS, NMR, or thermogravimetric analysis in order to assess which of these pathways are the favoured ones.

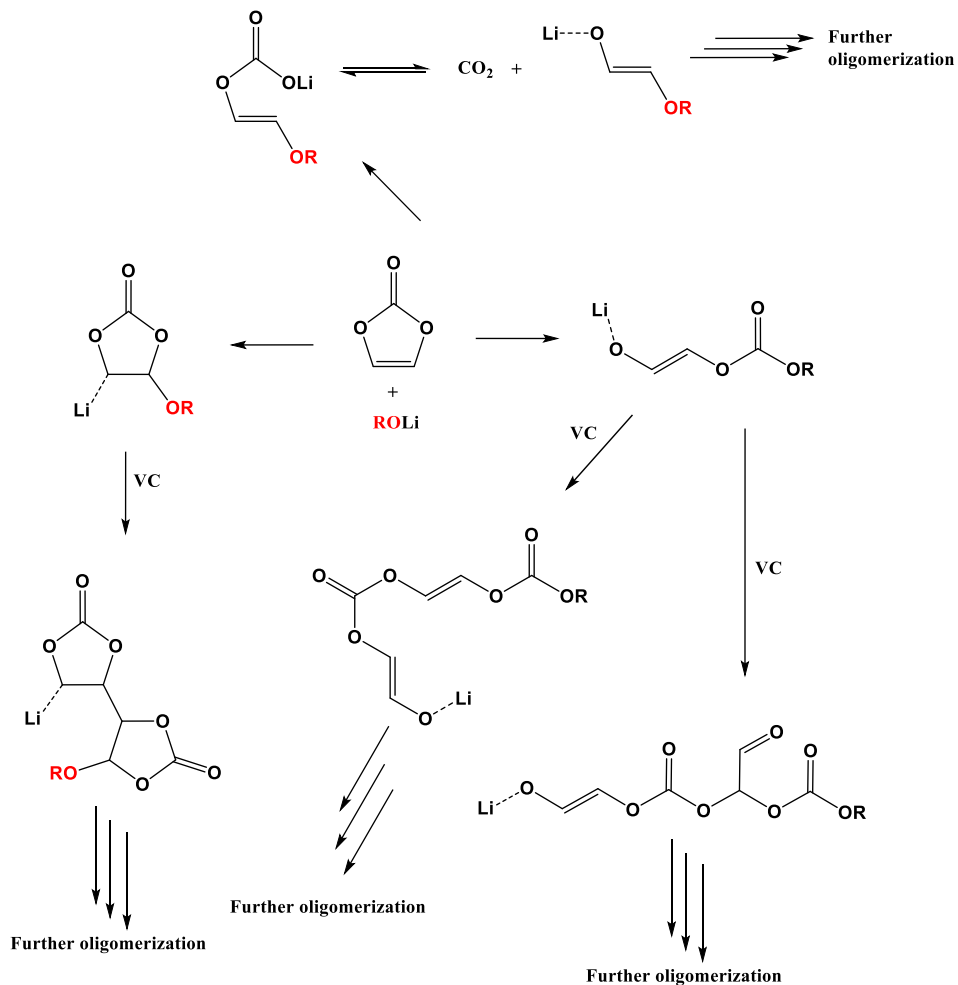


Figure 5.7. Possible reaction pathways between VC and lithium alkoxides and subsequent VC oligomerization.

5.2 Additive consumption during 4.2 V operation

5.2.1 Additive consumption at the negative and positive electrodes

In order to probe at which electrode VC or PES reacts during cycling or storage, NMC(111)/graphite pouch cells initially containing 2% and 4% VC or PES underwent a constant voltage hold period at either 3.9 V or 4.2 V for a period of 250 h at 40°C. The same experiment was conducted at 50°C for which results can be found in Figure C3 of Appendix C. Figure 5.8 shows the voltage vs. specific capacity curve of the fourth cycle of a NMC(111)/graphite pouch cell alongside the potential vs. specific capacity curves of

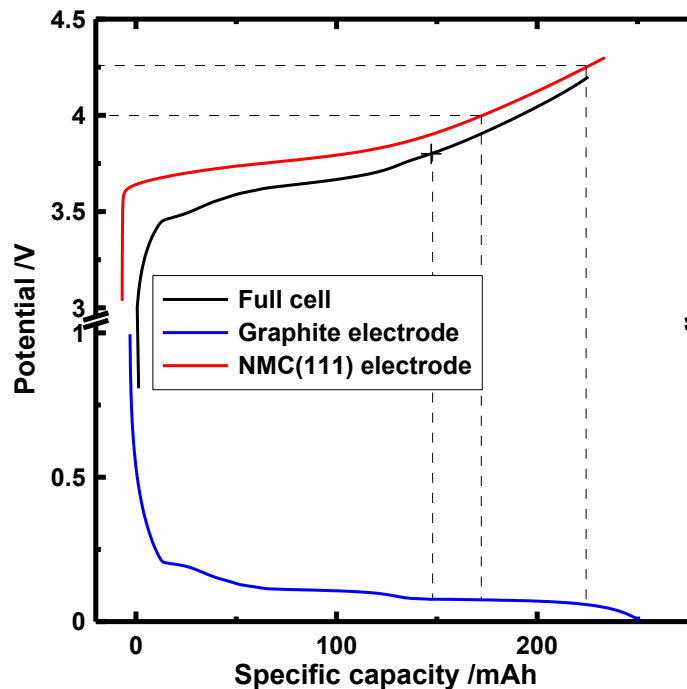


Figure 5.8. NMC(111)/graphite pouch cell voltage (“full cell”) vs. specific capacity of the fourth cycle shown alongside the fitted NMC(111) electrode and graphite electrode potential vs. specific capacity obtained using the differential voltage analysis freeware as described in reference [217]. The data were collected by Chris Burns, Ph.D. candidate, Physics & Atmospheric Science, Dalhousie University (2013).

a reference positive and a reference negative electrode vs. Li/Li^+ . The negative and positive reference potential vs. specific capacity curves were obtained using the differential voltage vs. capacity fitting freeware described in reference [217]. Figure 5.8 shows that at full cell voltages of 3.9 V and 4.2 V, the negative electrode potential is nearly fixed (~ 73 mV vs. Li/Li^+). On the other hand, the positive electrode potential changes by 250 mV (4.00 V vs. 4.25 V). Since only the positive electrode potential changes between a full cell voltage of 3.9 V and 4.2 V, any difference in the amount of VC or PES consumed in cells held at 3.9 V and cells held at 4.2 V should indicate that some VC or PES reacts at the positive electrode.

Figures 5.9a and 5.9b show that additive consumption occurs in most cells held at 3.9 V. [In Figure 5.9a and 5.9b, a consumption of 2.5 % of additive in cells initially containing 2.5% of VC or PES would indicate a total consumption of the additive.] This consumption comes primarily from SEI growth at the negative electrode. Additive oxidation is ignored here since the positive electrode potential is quite low (3.97 V vs. Li/Li^+) and should result in a slow oxidation rate. This is supported by the low rate of voltage decay during open circuit voltage storage of VC-containing and PES-containing NMC/gr cells presented by Xia *et al.* [207]. Figures 5.9a and 5.9b also show that while the consumption of VC during the 3.9 V hold increases at higher initial VC-loading, the consumption of PES actually decreases at higher initial content. This indicates that while increasing the initial VC loading does not lead to an SEI with a lower VC permeation rate, increasing initial PES loading affects the SEI in such a way that it slows the permeation rate of PES thus lowers its consumption.

Figure 5.9a also shows that the consumption of VC is not greater in cells held at 4.2 V compared to cells held at 3.9 V. This suggests that during the hold period, VC is

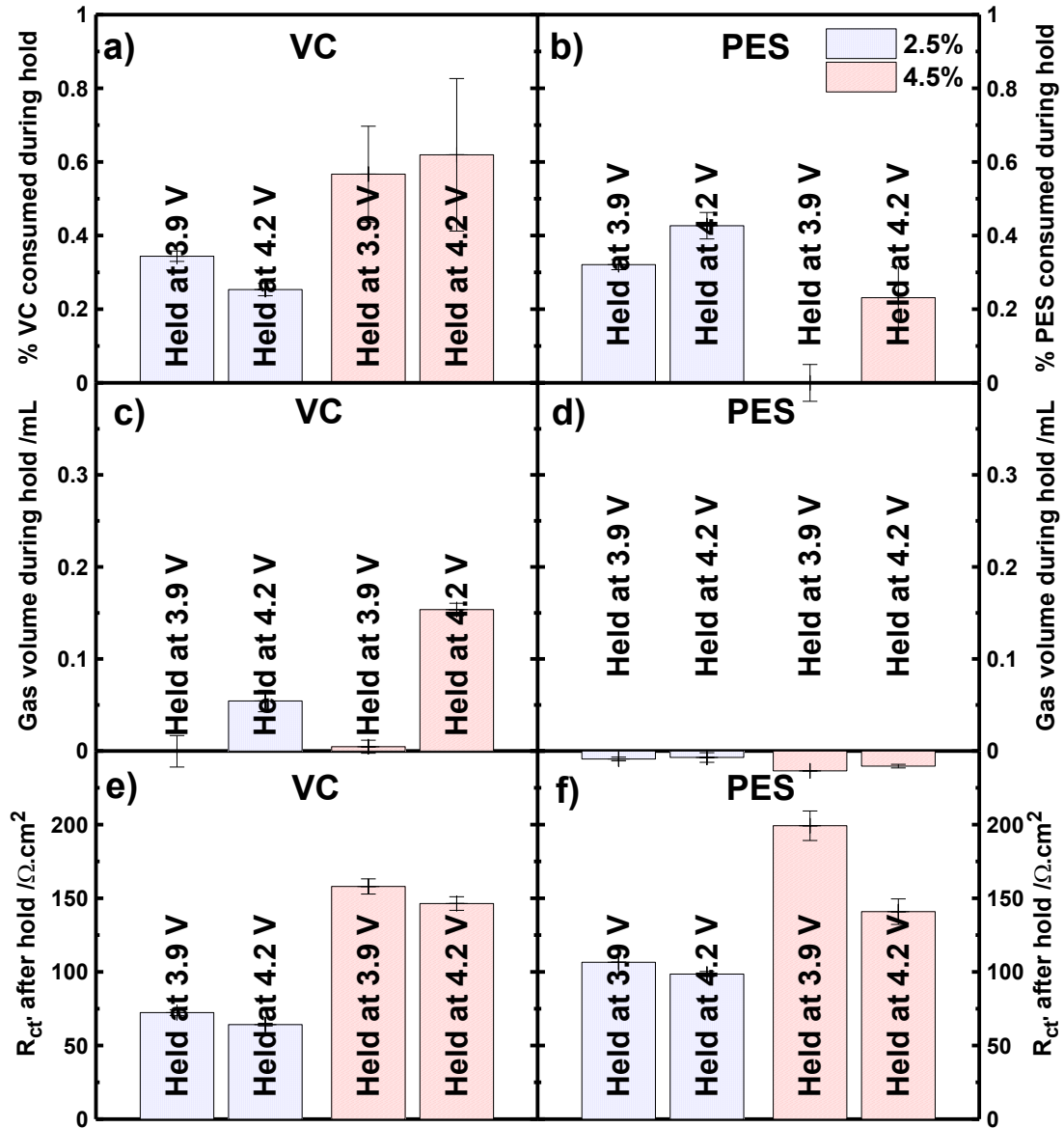


Figure 5.9. Amount of VC (a) and PES consumed (b), volume of gas produced in cells containing VC (c) and PES (d), and magnitude of the impedance of cells containing VC (e) and PES (f) for NMC(111)/graphite pouch cells held for 250 h and 40°C at either 3.9 V or 4.2 V. Each data point is the average of two cells. Some of the PES-containing cells were prepared and analyzed by Lina Rotermund, 2nd year B.Sc. student, Physics & Atmospheric Science, Dalhousie University (2014).

consumed primarily at the negative electrode, or that if some reacts at the positive electrode, the quantities are too small to be detected with the method used. Figure 5.9a also shows that the consumption of VC is actually smaller in cells initially containing 2% VC and held at 4.2 V compared to cells held at 3.9 V (a similar trend was observed in cells held at 50°C, see Figure C3 of Appendix C). It may be that an electrode-electrode interaction occurs which modifies the SEI of the negative electrode thus lowering the consumption of VC. In this case, oxidation by-products may travel to the negative electrode and affect its SEI composition. On the contrary, Figure 5.9b shows that the amount of PES consumed is greater in cells held at 4.2 V than in cells held at 3.9 V. This suggests that PES is consumed at the positive electrode in measureable amounts in NMC/gr cells operated to 4.2 V. In the case of PES, the amount of additive consumed at the positive electrode during the 4.2 V hold is of the same order of magnitude as its consumption at the negative electrode.

In a recent publication Self *et al.* [209] presented the results of density function theory (DFT) calculations on PES oxidation. Their results indicated that the oxidation of PES is unlikely to be caused by direct electron transfer. They indicated that PES is likely to react at the positive electrode surface of partially delithiated layered materials following a partial combustion reaction as described in Equation 2.2 of Section 2.2.2. This reaction occurs between the delithiated NMC (MO_2 , where M is Ni, Mn, Co) surface and the additive resulting in the formation of a rock salt layer (MO , where M is Ni, Mn, Co) at the electrode surface and various organic by-products. The results presented in Figure 5.9b suggest that this reaction may occur at 4.27 V vs. Li/Li^+ with NMC(111)

electrodes. This also suggests that PES can alter the passivation layer at the positive electrode which was confirmed by XPS analysis presented by Madec *et al.* [208].

Figures 5.9c and 5.9d show that no cell held at 3.9 V produced any significant amount of gas. This indicates that the reduction of the solvents of the electrolyte and additives at the graphite surface during the hold (once the graphite SEI is formed during the first charge) does not lead to the formation of significant amounts of gas. This may suggest that the reduction of solvents after graphite passivation does not follow the same pathway as during the first charge (see Section 5.1.1) or that the gases produced are consumed at the same rate. For instance, in a recent publication, Self *et al.* [13] showed that NMC/gr cells containing certain electrolyte blends showed significant gas consumption.

Figures 5.9c and 5.9d also show that cells containing VC and held at 4.2 V produced a significant amount of gas and that the higher the initial VC content, the more gas produced. Since the graphite is at the same potential during the 3.9 V and 4.2 V hold period, the gas is certainly produced at the positive electrode or at least results from oxidation reactions. This is consistent with the results of gas volume measurements on VC-containing cells stored at open circuit voltage at 4.2 V and 40°C [207]. Figure 5.9c then suggests that some of the VC remaining in the electrolyte is oxidized at the positive electrode. If each molecule of VC oxidized produced one molecule of CO₂, the formation of 0.1 mL of gas (volume created in cells initially containing 2.3% VC and held at 4.2 V and 40°C) would be the result of the oxidation of 0.04% of VC. This number is close to the uncertainty of the measurements. As a consequence, if any consumption of VC

happens at the positive electrode, it would not be statistically distinguishable from the range in the measurements. This is consistent with the results shown in Figure 5.9a.

Figure 5.9d shows that all cells initially containing PES did not produce any significant amount of gas. This suggests that the oxidation of PES does not lead to the generation of gas or that the gas produced is consumed at the same rate. The low gassing of PES containing cells during operation was previously reported by Xia *et al.* [207] and is a significant advantage over VC.

Figures 5.9e and 5.9f show the magnitude of the impedance, R_{ct} (see Section 3.2.4 for a definition of R_{ct}) after the hold period. Figures 5.9e and 5.9f show that cells held at 4.2 V have smaller impedance than cells held at 3.9 V. Cells held at 50°C showed similar behavior (see Figure C3 of Appendix C). It then seems that the reduction of impedance during cycling and storage at 4.2 V observed by Xia *et al.* [207] and Nelson *et al.* [214] in cells containing PES originates from electrolyte oxidation. In order to determine whether the impedance reduction during the 4.2 V hold originates from a smaller positive electrode impedance or negative electrode impedance, symmetric cells were constructed from pouch cells initially containing PES. The impedance plots of the symmetric cells can be found in Figure C4 of Appendix C.

The symmetric cell study of electrodes extracted from pouch cells initially containing PES showed that while the positive electrode impedance is similar between 3.9 V and 4.2 V hold, the impedance of the negative electrode is significantly smaller after the 4.2 V hold than after the 3.9 V hold. The fact that between 3.9 V and 4.2 V only the positive electrode potential changes strongly suggests a positive-negative electrode interaction. These types of interactions have now been reported by several researchers

[5,218–220]. X-ray photoelectron spectroscopy of the surface of the positive electrode and negative electrode of cells held at 3.9 V and 4.2 V also showed that the negative electrode SEI is strongly affected by the high potential of the positive electrode. Interested readers can find a schematic of the SEI as determined by XPS analysis in Ref [221]. The XPS analysis further supports the existence of this positive-negative electrodes interaction.

5.2.2 Correlation between impedance and VC consumption

Figure 5.10 shows the magnitude of the impedance, R_{ct} of NMC/gr cells (see Section 3.2.4 for a definition of R_{ct}) at 3.8 V as a function of the amount of VC

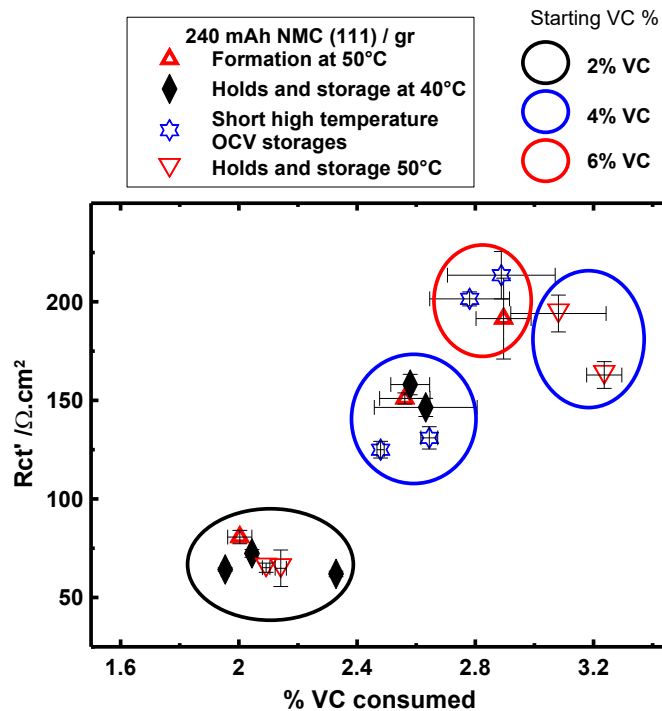


Figure 5.10. Magnitude of the impedance (R_{ct}') vs. amount of VC consumed in NMC(111)/graphite pouch cells filled with electrolytes initially containing various VC contents after various cycling and storage protocols.

consumed in cells initially containing various amounts of VC (2 - 6%), after formation, hold or storage at various temperatures and various voltages.

Figure 5.10 shows that there is a general linear trend between the magnitude of the impedance and the amount of VC consumed for all cells, no matter their starting additive concentration. However, the data points do not align on a perfect line indicating that cell history has noticeable influence on the magnitude of the impedance. The existence of a general trend between the amount of VC consumed and R_{ct} with some data points that deviate from the trend indicates that R_{ct} is mainly controlled by the amount of VC consumed, as well as by the cell history (potential during storage and holds, temperature during holds) to a minor extent. Burns *et al.* [143] showed that higher VC loading leads to lower electrolyte oxidation, however, it also leads to higher impedance. If one wants to fill cells with high VC loading while keeping the impedance low, the addition of co-additives limiting the consumption of VC or modifying the SEI slightly would then, in theory limit impedance growth whilst lowering electrolyte oxidation.

Figure 5.11a shows the magnitude of the impedance, R_{ct} (see Section 3.2.4 for the definition of R_{ct}) of cells containing various initial VC loadings, with or without 1% ethylene sulfite (ES) or 1% ES + 1% tris(trimethylsilyl)phosphite (TTSPi). Figure 5.11 shows that while the addition of 1% ES to VC-containing electrolytes leads to higher VC consumption during the first cycle, it also leads to lower cell impedance compared to cells containing VC only. Figure 5.11b also shows that ES gets slightly consumed. This indicates that the addition of ES modifies the SEI generated by the reduction of VC (confirmed by XPS analysis presented by Madec *et al.* [204]) which leads to lower impedance. Figure 5.11 also shows that adding 1% ES + 1% TTSPi to VC-containing

cells maintains low VC consumption even at high initial VC loading which result in low cell impedance. This suggests that the lower cell impedance at higher VC loading originates mainly from a reduction of the amount of VC consumed as well as a modified SEI due to the consumption of the co-additives.

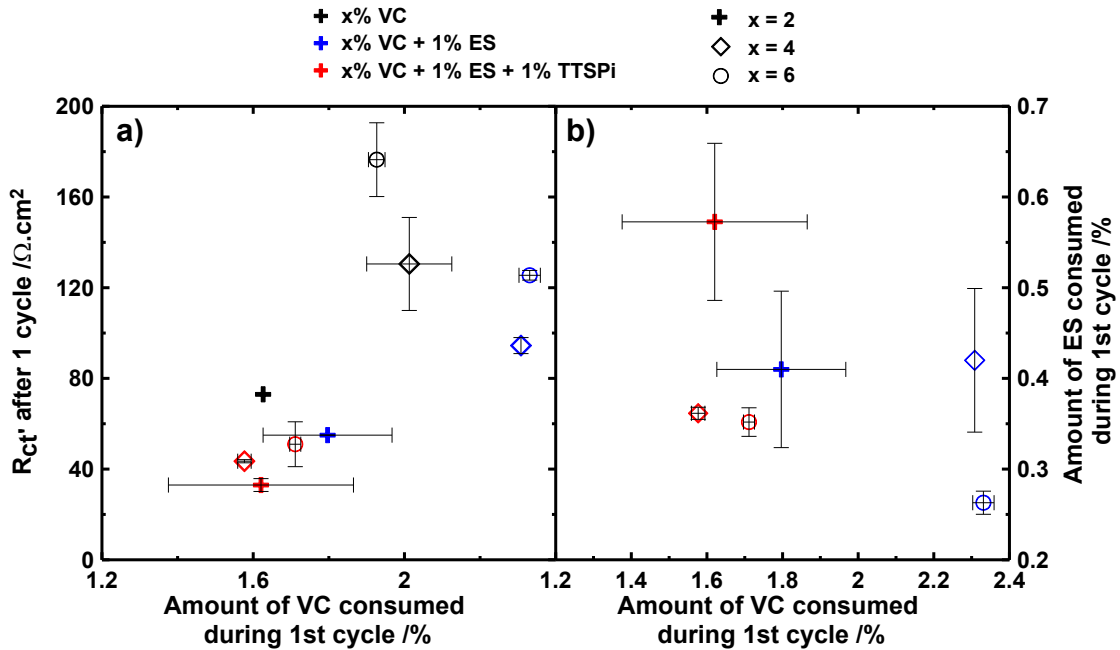


Figure 5.11. Magnitude of the impedance ($R_{ct'}$) (a) and amount of ES consumed (b) vs. amount of VC consumed after the first cycle of NMC(111)/graphite pouch cells filled with electrolytes initially containing various VC, ES and TTSPi contents. Cycling was performed at 40°C and C/20 between 2.8 V and 4.2 V. Cells were prepared by Jian Xia, visiting student, Physics & Atmospheric Science, Dalhousie University (2013).

Figure C5 of Appendix C shows the results of storage at 4.2 V and 60°C of cells initially containing 2% VC or 4% VC + 1% ES + 1% TTSPi. Figure C5 shows that cells containing the largest amount of VC had the lowest voltage drop during storage. This indicates that electrolyte oxidation was less severe with higher VC amount even in the presence of ES and TTSPi. Therefore adding ES and TTSPi allows the use of high initial VC loadings whilst maintaining low cell impedance. It is then probable that the

synergetic effects of ternary additive blends containing VC, a sulfur-containing additive and TTSPi in cells cycled to moderate voltage (*i.e.* up to 4.2 V) observed by Wang *et al.* [16] and Ma *et al.* [222] originates in part from a lower VC consumption at the graphite electrode, leading to lower impedance which also leaves larger amount of VC for the passivation of the positive electrode (lower electrolyte oxidation). Synergetic effects also probably come from a modified SEI at both the negative and positive electrodes. However, cells with the VC + ES + TTSPi blend produced a substantial amount of gas which might indicate a slight oxidation of the VC remaining in the electrolyte as discussed in Section 5.2.1.

Measuring the consumption of additives in electrolytes containing various additive blends allows one to detect whether a change in electrolyte composition will result in a change of SEI composition. For instance, Madec *et al.* [204,208] showed that the consumption of additives measured by GC-MS in NMC/gr cells cycled to 4.2 V containing various combinations of VC, PES, and ES correlated well to the SEI composition measured by XPS. For instance, in cells containing VC and ES, where consumption of both additives was confirmed by GC-MS, the SEI at the graphite electrode was shown by XPS analysis to be a convolution of the SEI of cells containing VC only and ES only. This indicates that measuring the consumption of additives is a simple and rapid qualitative assessment of the participation of an additive to the formation of the SEI layers.

5.3 Gas generation in cells cycled to high voltage

In a previous publication, Aiken *et al.* [12] and Self *et al.* [13] showed that Li-ion cells with layered positive electrode material (*e.g.* LCO and NMC) produced gas during the first charge to high voltage. This gas production occurred around a cell voltage of 4.25-4.5 V depending on the additive used and electrode chemistry. Some of their results are shown in Figure 5.12. Figure 5.12 shows the cell volume *vs.* cell voltage for NMC(442)/gr cells charged to 4.7 V at C/10 and then left at open circuit at 4.7 V for 8 h. Figure 5.12 shows that the volume of the cells increased between 2.4 and 3.5 V which corresponds to the passivation of the graphite surface and associated gas production (see Section 5.1.1). Cells also show a gas production event between 4.25 - 4.5 V depending on

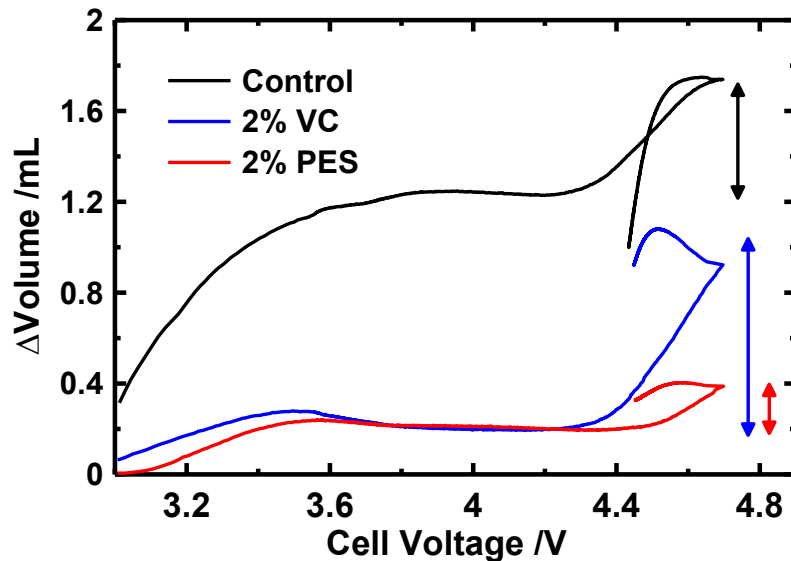


Figure 5.12. In-situ volume measurements during the first charge to 4.7 V at C/10 and 40°C followed by an OCV period of 8 h of NMC(442)/graphite pouch cells filled with electrolytes containing various additive blends. Cells were prepared and analyzed by Connor Aiken, 4th year B.Sc. honor's student, Physics & Atmospheric Science, Dalhousie University (2014). Adapted from Ref. [12] and [13].

the additive used. This presumably corresponds to the oxidation of the electrolyte and probably to the formation of a new passive layer. Figure 5.12 shows that the addition of VC leads to the production of more gas during the first charge to high voltage while the addition of PES leads to smaller gas production, compared to cells without additive. Figure 5.12 also shows that the volume of cells decreases during the rest period (the cell voltage also decreases as the electrolyte is being oxidized). This volume decrease corresponds to gas consumption at either electrode. Cells with control electrolytes undergo faster gas consumption at high voltage than cells with VC or PES. This indicates that the gas analyzed by GC-TCD corresponds to the gas produced at high voltage, minus the gas consumed during the period separating the cell charging and gas analysis.

In order to attempt to determine the origin of this gas evolution, NMC(442)/gr cells were filled with electrolytes containing various amounts of VC or PES and charged to 4.7 V. The gas was generated was then analyzed either by GC-TCD or GC-MS.

Figures 5.13a and 5.13b show the results of the GC-TCD and GC-MS analysis of the gas produced in cells containing various amounts of VC and PES, respectively. Figures 5.13a and 5.13b show that cells with no additive produced small amounts of CO, C₂H₄, C₂H₆, CH₄, H₂, methyl or ethyl formate as well as esters. These gases and volatile compounds are consistent with the by-products generated during the passivation of the graphite surface as shown in Section 5.1.1. Figure 5.13b also shows that cells filled with a control electrolyte produced some CO₂. The CO₂ is not apparent in Figure 5.13a probably due to differences in time delays between cell charging and gas analysis for the GC-TCD and GC-MS analyses which would result in different gas consumption in both sets of cells. Figure 5.13b also shows that cells charged to 4.7 V also produce small

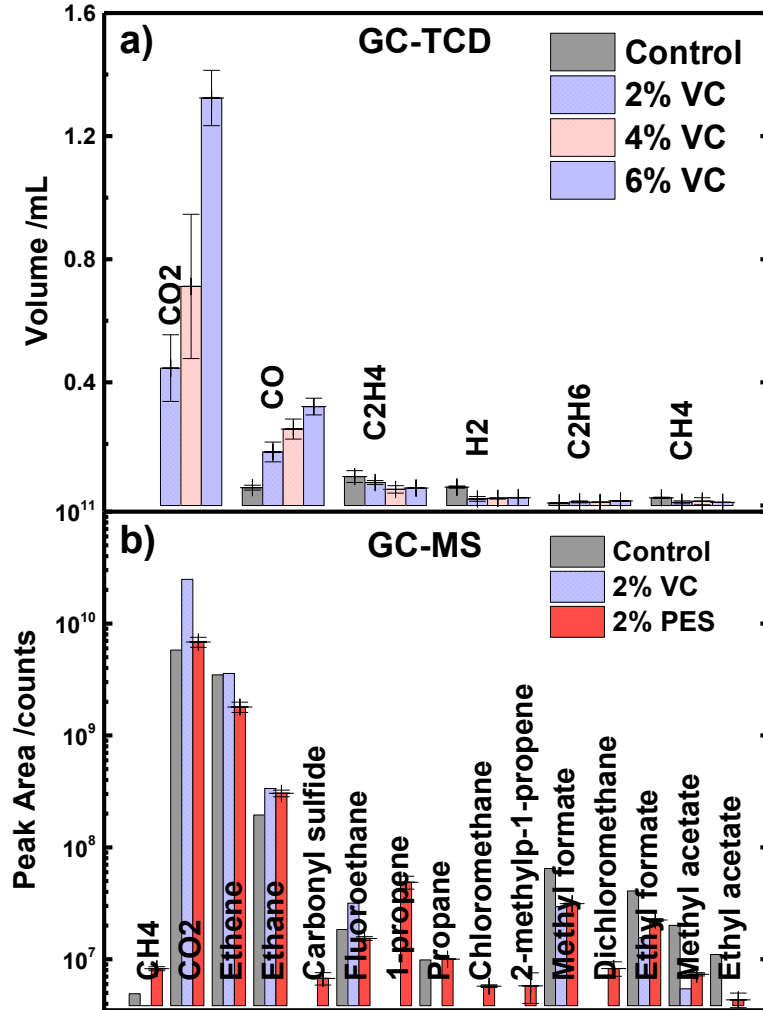


Figure 5.13. Summary of GC-TCD (a) and GC-MS (b) analysis of the gas extracted from NMC(442)/graphite pouch cells containing various additive contents and charged to 4.7 V for the first time at 40°C. Cells in panel a) were degassed at 3.5 V before being charged to 4.7 V while cells in panel b) were not. Cells in panel b) were prepared by Connor Aiken, 4th year B.Sc. honnor's student, Physics & Atmospheric Science, Dalhousie University (2014).

quantities of fluoroethane. The formation of CO, CO₂ and fluoroethane is consistent with the oxidation of organic carbonates. Figure 5.14 shows reaction pathways adapted from ones proposed by Zhang *et al.* [223], Borodin *et al.* [131] and Moshkovich *et al.* [92].

Figure 5.14 shows that the oxidation of EC and EMC can lead to the formation of both CO and CO₂, consistent with the gases measured by GC-MS and GC-TCD. Figure

5.14 also shows that some of the by-products can abstract fluorine from PF_6^- present in the electrolyte leading to the formation of the fluoroethane observed in Figure 5.13b. This would lead to loss of salt over time which was observed by Day *et al.* [224] using differential thermal analysis of NMC/gr cells cycled to high voltage. Figure 5.14 also shows that the by-products of the oxidation of EC and EMC can lead to the formation of H^+ . The H^+ formed may then travel to the negative electrode and be reduced to form some of the H_2 observed in Figure 5.13a. The formation of protic compounds at the positive electrode and their transfer to the negative electrode and subsequent reduction leading to the formation of H_2 was recently demonstrated by Metzger *et al.* [225].

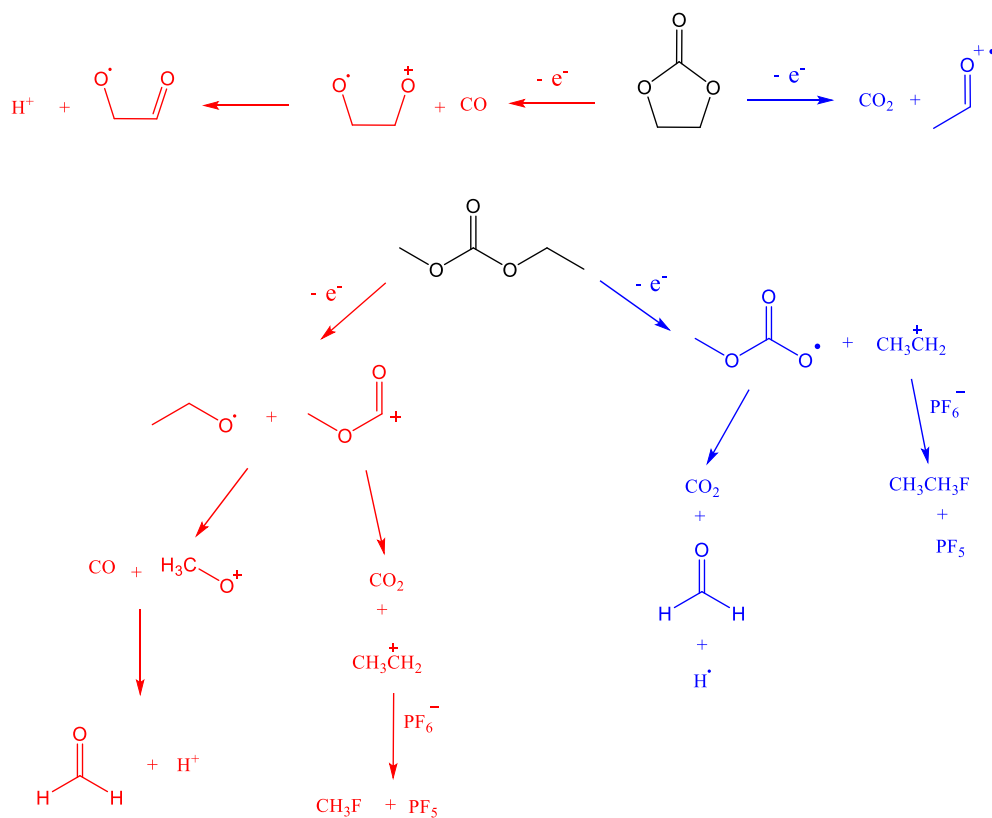
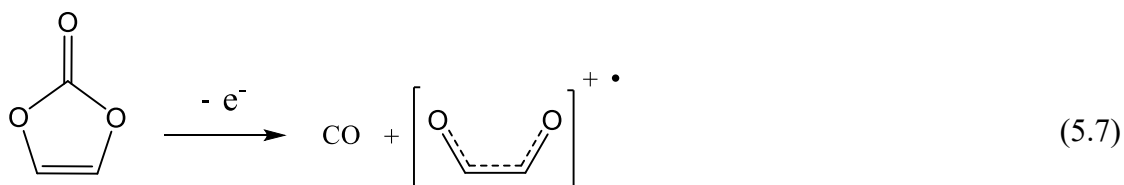


Figure 5.14. Possible oxidation pathways for EC and EMC. Adapted from pathways proposed in Ref [87, 126, 217].

Figure 5.13a clearly shows that increasing the initial amount of VC leads to larger gas production during the first charge to high voltage. This strongly suggests that the VC remaining in the electrolyte after the passivation of the graphite electrode is oxidized at the positive electrode. In an earlier publication, Zhang *et al.* [223] presented the results of a DFT calculation which predicted that the oxidation potential of VC would be close to 4.1 V vs. Li/Li⁺. Based on in-situ volume measurements, it appears that this oxidation potential is closer to 4.5 V vs. Li/Li⁺. The calculation of Zhang *et al.* [223] predicted that the oxidation of VC leads to the formation of CO following:



The presence of CO₂ suggests that the oxidation of VC can follow a second oxidation pathway which could be:

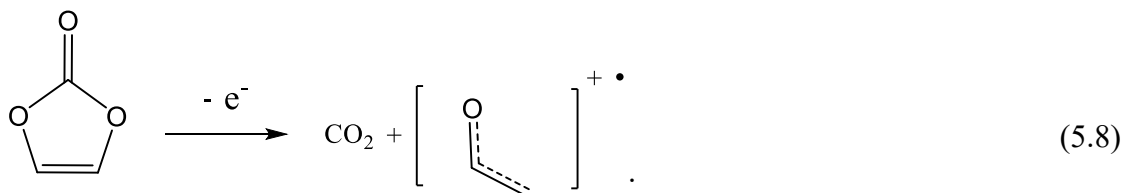
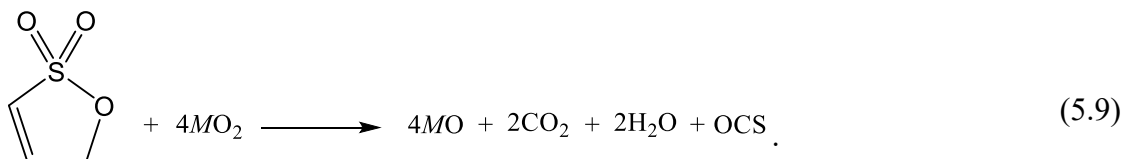


Figure 5.13b shows that cells containing PES produced a small amount of carbonyl sulfide. The carbonyl sulfide then comes from the oxidation of PES at the positive electrode. Self *et al.* [209] showed that this oxidation probably happens through a pseudo-combustion reaction as discussed in Section 5.1.3 following:



where MO_2 is the delithiated or partially delithiated NMC electrode surface.

Figures 5.12 and 5.13 show that while the oxidation of VC is very pronounced, the oxidation of PES seems to be limited (evidenced by the small gas volume generation). It then seems that while PES appears to passivate the positive electrode surface at high potential, VC continuously oxidizes, or the SEI it creates breaks down at high potential. This may explain why PES is a superior additive to VC in NMC/gr cells cycled to high voltage (*i.e.* > 4.2 V) as shown by Ma *et al.* [11].

5.4 Concluding remarks

The analysis of the gas and liquid components of the electrolyte using the methods described in Chapter 4 provided a great deal of information. The analysis of the gas produced during the first charge to 3.5 V of NMC/gr cells allowed the complete reduction pathways of EC and EMC to be determined. The reduction pathway of VC and PES as well as the reaction pathway between VC and lithium alkoxide were also proposed.

The measurement of additive consumption during holds at various voltages suggested that VC is primarily consumed at the negative electrode during cell operation while PES is consumed at both the negative and positive electrodes. At higher potential, VC oxidizes at the positive electrode leading to the generation of gaseous products.

The measurement of the amount of VC consumed in cells that had undergone different cycling protocols allowed the correlation between the amount of additive consumed and the magnitude of the cell impedance to be determined. It showed that the magnitude of the impedance of NMC/gr cells containing VC was strongly correlated with

the amount of VC consumed. Measurement of the consumption of VC in the presence or absence of co-additives was also performed. These measurements indicated that high VC loadings can be used when co-additives that either modify the SEI formed at the graphite surface or additives that limit the amount of VC consumed are added. This allows one to obtain Li-ion cells with low impedance and low electrolyte oxidation when operated at moderate voltage (*i.e.* < 4.3 V).

Finally, the gas produced during the first charge of NMC/gr cells to high voltage (*i.e.* 4.7 V) was also analyzed. The results showed that cells without additives produced mainly CO₂, CO and H₂, consistent with the oxidation of EC and EMC. The results also showed that VC is heavily oxidized at the positive electrode at cell voltages higher than 4.5 V. The gases produced mainly consisted of CO and CO₂, consistent with the oxidation of VC or the oxidation of the SEI made by VC at the positive electrode. This indicates that VC is inadequate for cells cycled to high voltage due to its oxidative instability. Finally the addition of PES to the electrolyte resulted in small gas evolution. Carbonyl sulfide and CO₂ were detected in cells containing PES which indicated that PES is likely oxidized at the positive electrode following a pseudo-combustion reaction as proposed by Self *et al.* [209].

CHAPTER 6. CYCLING PERFORMANCE, GAS GENERATION AND ADDITIVE CONSUMPTION IN CELLS CONTAINING PHENYL CARBONATES³

Electrolyte additives can also be used to improve cell safety in overcharge conditions. In this particular application, additives can act as redox shuttles [226,227] and/or gas producers [228–230]. The latter safety feature is applicable for hard-can cells such as 18650-type cells equipped with a pressure activated electric disconnect device. This device disconnects the jelly roll from the cell terminals once a set internal pressure is reached. During overcharge, the additive oxidizes at the positive electrode and produces gas. The internal pressure increases until the set pressure is reached at which point the cell is disconnected.

Choosing suitable additives to trigger pressure activated disconnects can be difficult as they may affect the charge-discharge cycle life and calendar life of the cell. It is crucial to carefully choose the combination of additives introduced in a cell and make sure they do not interact in a negative manner.

Figure 6.1 shows the chromatogram of the solvent extracted from a commercial 18650 Li-ion cell (NCA positive electrode and graphite negative electrode) made by a reputable manufacturer. Figure 6.1 shows an expected solvent blend consisting of ethylene carbonate (EC) mixed with dimethyl carbonate (DMC) and ethyl methyl

³ Some of the results presented in this Chapter were published in R. Petibon, L.M. Rotermund, J.R. Dahn, *J. Power Sources*. **287** (2015) 184–195 for which the candidate wrote the first draft of the entire manuscript. The contribution of the co-authors (other than the candidate) is indicated in the captions of the figures where appropriate.

carbonate (EMC). Figure 6.1 also shows that the electrolyte from this commercial Li-ion cell contains methyl phenyl carbonate (MPC). Mitsubishi Chemical Corporation filed a

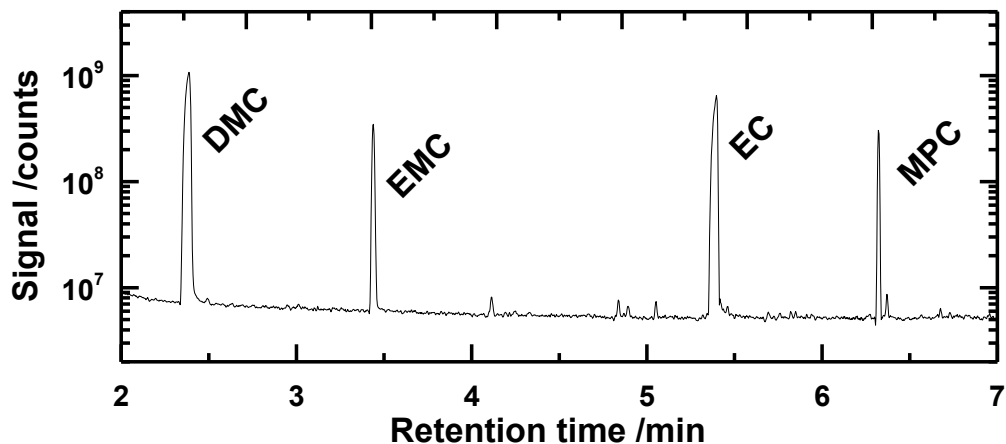


Figure 6.1. Chromatogram of the electrolyte extracted from a commercial 18650 Li-ion cell produced by a major manufacturer.

patent on such chemicals [231] which described them as additives for enhanced cell storage properties and better safety. This particular patent indicates that when MPC is added to an electrolyte containing VC, the cell produces a large amount of gas during overcharge to 5 V. Cells with MPC and VC also show good capacity retention during continuous charge-discharge tests at 60°C to an upper cut-off voltage of 4.25 V. Table 6.1 summarizes some of the results in the patent filed by Nakagawa *et al.* [231]. Table 6.1 shows that cells filled with electrolyte with only VC, or only MPC produced relatively small volumes of gas during overcharge to 5 V (25°C) while cells filled with electrolytes containing both VC and MPC produced a large amount of gas.

Since phenyl carbonates are used in Li-ion cells made by a major manufacturer and potentially provide good safety and storage properties, studies of phenyl carbonates are worthwhile, leading to a better understanding of how they function.

Table 6.1. Summary of some of the results presented in the patent filed by Nakagawa *et al.* [226].

Electrolyte formulation	Gas generated during 5 V overcharge test /mL	OCV after 5 V overcharge test / V	Gas generated during continuous charge test /mL	Capacity after continuous charge test /%
1M LiPF ₆ EC:EMC:DMC (2:3:3) + 2% VC	0.13	4.54	0.53	97
1M LiPF ₆ EC:EMC:DMC (2:3:3) + 1% MPC	0.24	4.52	0.29	92
1M LiPF ₆ EC:EMC:DMC (2:3:3) + 1% MPC + 2% VC	0.92	4.44	0.48	97

In this chapter, the results of high precision coulometry testing, OCV storage, gas analysis during formation as well as electrolyte composition during formation and after cycling are reported. Further results from EIS measurements on full cells, as well as EIS measurements on symmetric cells are also described. NMC(111)/graphite pouch cells filled with electrolytes containing different phenyl carbonates, either singly or in combination with VC were used as the test vehicle. Figure 6.2 shows the structure of the additives used in this study.

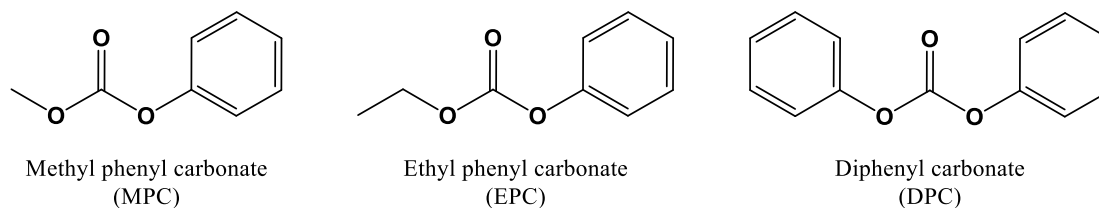


Figure 6.2. Chemical structure of phenyl carbonates studied.

6.1 Electrochemistry and gas volume generation

Figure 6.3a shows the differential capacity vs. cell voltage of NMC(111)/graphite pouch cells filled with a control electrolyte (1M LiPF₆ EC:EMC (3:7)) and control electrolyte in combination with small wt% of MPC, ethyl phenyl carbonate (EPC) and diphenyl carbonate (DPC). Figure 6.3a does not show any noticeable difference in the differential capacity plot of the early first charge between cells filled with the additive-free electrolyte and cells containing phenyl carbonates. The plot shows a characteristic peak around 2.8 V (graphite potential around 0.85 ± 0.1 V vs Li/Li⁺) which corresponds to the reduction of EC at the surface of the graphite electrode [3,91,114,118,232] (see Sections 2.2.1 and 5.1.1). This indicates that MPC, EPC and DPC do not electrochemically react at the graphite electrode before EC to a noticeable extent. This is in contrast with so-called “passivating additives” such as (VC) [3,143,215] or PES

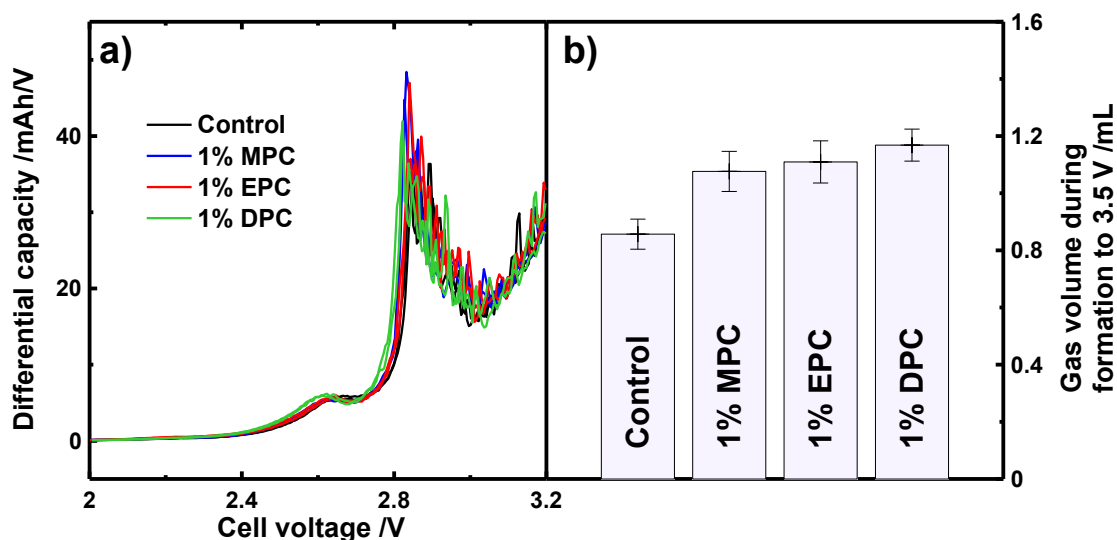


Figure 6.3. Differential capacity vs. cell voltage during the first 10 mAh of the first charge (a) and gas volume produced during the first charge to 3.5 V (b) for 220 mAh NMC(111)/graphite pouch cells filled with different electrolyte blends.

[155,157,207,208]. The electrochemical reduction of such additives show a clear peak in the differential capacity plot at potentials higher (vs. Li/Li^+) than that of EC (lower full cell voltage). The reduction of such additives also lowers the intensity of the differential capacity peak from EC through the partial passivation of the graphite surface. The phenyl carbonates tested obviously do not show such passivation properties.

Figure 6.3b shows the gas volume produced during the first charge to 3.5 V of the same cells. Cells filled with the control electrolyte produced 0.9 mL of gas. This gas primarily comes from the reduction of EC at the graphite electrode [18,115,185,233], and trace water [233,234] as shown as shown in Chapter 2 and Chapter 5. Figure 6.3b shows that all phenyl carbonate-containing cells produced slightly more gas than cells filled with the control electrolyte (1.1 mL vs. 0.9 mL). From the differential capacity plot, it is expected that the phenyl carbonate-containing cells produce at least the same amount of gas as cells filled with the control electrolyte (due to the reduction of EC). The additional gas volume is likely to come from several factors such as water content of the additive, partial reduction of the additive, or increased reactivity of EC due to the presence of the additives.

6.2 Additive consumption during formation to 3.5 V

Figure 6.4 shows the results of the GC-MS analysis of the solvent composition of the electrolyte of NMC(111)/graphite pouch cells filled with control electrolyte and control electrolyte in combination with 2% VC, 1% MPC or 2% VC + 1% MPC, after the cells were charged to 3.5 V. Figure 6.4a shows the mass percent of VC consumed, assuming negligible EC and EMC consumption. Figure 6.4a shows that at 3.5 V

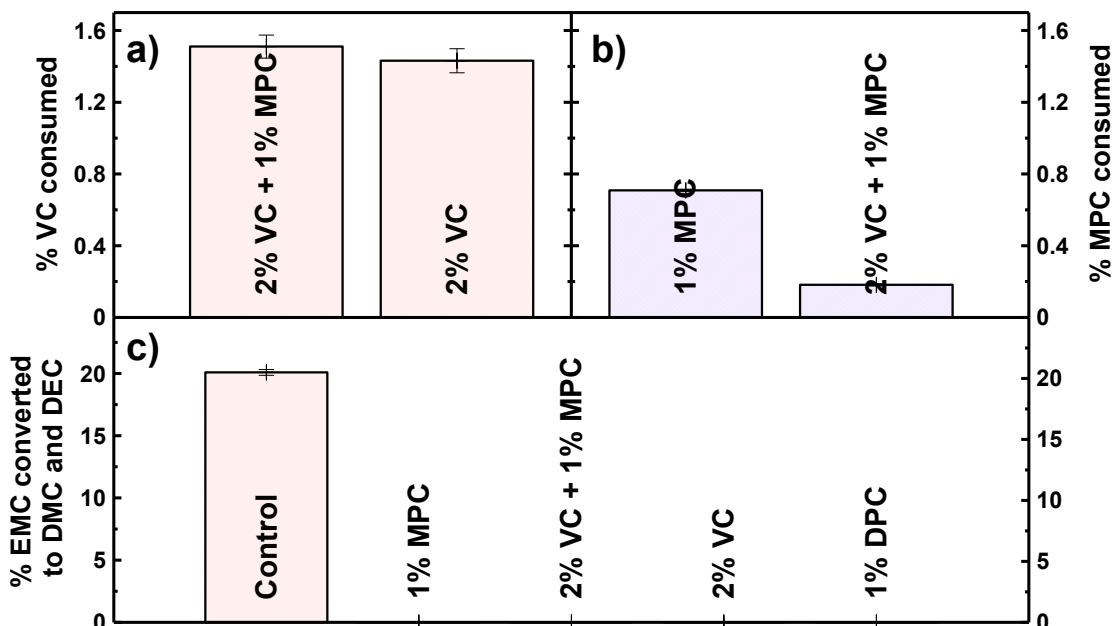


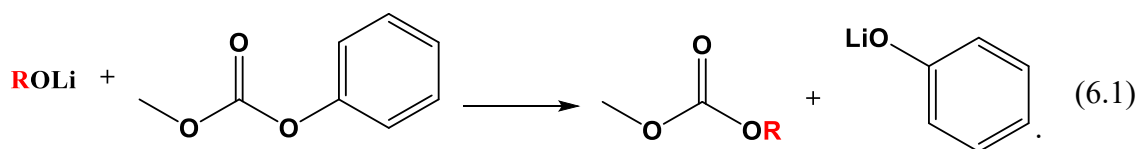
Figure 6.4. Mass percent (relative to total electrolyte mass) of VC consumed (a); mass percent (relative to total electrolyte mass) of MPC consumed (b) and mass percent of EMC converted into DMC and DEC (c) in 220 mAh NMC(111)/graphite pouch cells filled with 1M LiPF₆ EC:EMC (3:7) electrolyte (control), control electrolyte + 1% MPC, control electrolyte + 2% VC + 1% MPC (2% VC + 1% MPC), and control electrolyte + 2% VC (2% VC), after the first charge to 3.5 V and 40°C. Each data set is the average of two cells.

approximately 1.5% VC reacted out of the initial 2%, consistent with the results shown in Chapter 5. Figure 6.4a shows that the VC consumption in cells containing 2% VC + 1% MPC is not statistically different from cells containing only 2% VC.

Figure 6.4b shows the amount of MPC consumed prior to 3.5 V in cells filled with electrolyte containing 1% MPC or 2% VC + 1% MPC. Figure 6.4b shows that approximately 0.7 % of MPC, out of the initial 1%, reacted early on during the first charge. However, such cells did not show any characteristic peak in the differential capacity plot presented in Figure 6.3a. This indicates that MPC either reacts chemically with the by-products of the reduction of the solvents, salt, and trace water or that it reacts

electrochemically at the graphite surface after EC (in which case it might not be seen in the differential capacity plot).

Figure 6.4c shows the amount of EMC converted to DEC and DMC after the first charge to 3.5 V by trans-esterification (see Section 5.1). Figure 6.4c shows that early on during the first charge, 20 % of the EMC in cells filled with control electrolyte was converted into DEC and DMC. By contrast, cells filled with 2% VC, 1% MPC and 2% VC + 1% MPC showed no sign of EMC conversion. Figure 6.4c then clearly shows that phenyl carbonates can trap lithium alkoxides thus preventing trans-esterification of EMC, similarly to VC (see Section 5.1.3). Lithium phenoxide is a less nucleophilic compound than lithium methoxide or lithium ethoxide. It is then probable that MPC suppresses the trans-esterification reaction following:



This reaction pathway is supported by the detection of small amounts of phenol in an EMC:MPC (90:10) solution to which 1% lithium ethoxide was added (see Figure D1 of Appendix D). The reaction of MPC with lithium alkoxides would explain some of its consumption as seen in Figure 6.4b. The lower MPC consumption in the presence of VC may be due to a higher reactivity of VC towards lithium alkoxides if consumption is primarily caused by the presence of alkoxides. In addition the passivation of graphite by VC could also limit the production of alkoxides as well as limit the amount of MPC that eventually gets reduced at the graphite surface.

6.3 Qualitative composition of the gas generated at 3.5 V

Figure 6.5 shows the compounds detected by GC-MS in the gas formed after the first charge to 3.5 V of NMC(111)/graphite pouch cells filled with 1M LiPF₆ EC:EMC (3:7) base electrolyte containing no additive, containing 1% MPC or 1% DPC. Hydrogen was not detected due to instrument limitations. Since the sensitivity of the mass spectrometer to each gas was not calibrated, Figure 6.5 shows a qualitative gas composition.

Figure 6.5 shows that the presence of small loadings of phenyl carbonates leads to very similar gas composition as cells without phenyl carbonates. Figure 6.5 also shows that cells containing MPC and DPC produced a small quantity of benzene. At the same

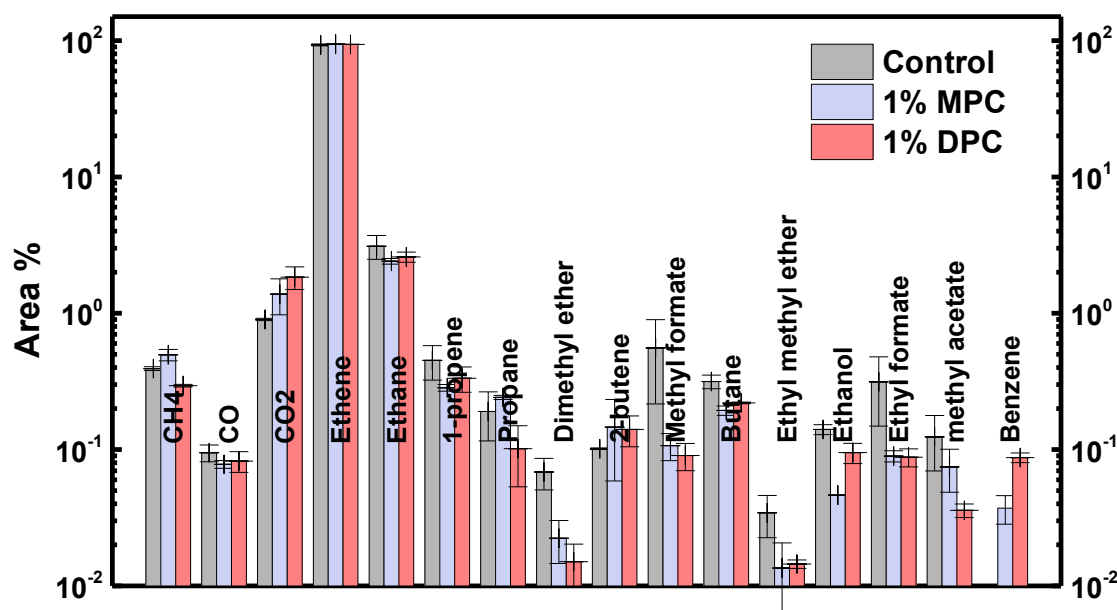


Figure 6.5. Relative peak area of the GC chromatogram of the gas extracted from 220 mAh NMC(111)/graphite pouch cells filled with control electrolyte, control electrolyte + 1% MPC (1% MPC), and control electrolyte + 1% DPC (1% DPC) after being charged to 3.5 V at C/20 and 40°C (H₂ was not measured due to instrument limitations). Each dataset is the average of two cells.

time, cells containing MPC seemed to produce more CH₄ than cells filled with control electrolyte, while cells containing DPC produced less CH₄ than cells filled with control electrolyte. Figure 6.5 also shows that cells containing the phenyl carbonates produced more CO₂ than cells filled with control electrolyte.

The presence of benzene, the variation of CH₄, CO₂ production and the large MPC consumption as shown in Figure 6.4b seem to indicate that the phenyl carbonates get reduced at the graphite surface to some extent. Therefore, the reduction of MPC and DPC would likely follow the pathways described in Figure 6.6. The reduction of these phenyl carbonates might not be seen in the dQ/dV vs. voltage plot (Figure 6.3a) due to a low rate of the redox reaction or a reduction potential lower than EC (vs. Li/Li⁺). The alkyl phenyl ethers, phenyl esters, and phenols shown in Figure 6.6 would not be detected in the gas analysis due to low content and low partial pressures. The added gas volume generated in the presence of phenyl carbonates would then likely come from their reduction. If we assume as a first approximation that the CO₂ and methane generated from phenyl carbonate reduction follows the ideal gas law and is responsible for the

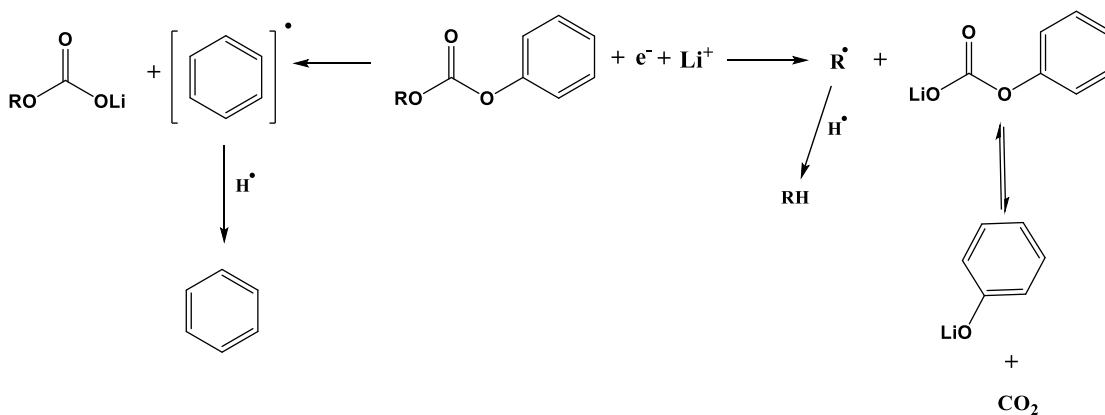


Figure 6.6. Proposed reduction mechanisms of phenyl carbonates and subsequent reactions of the reduction by-products.

added 0.2 mL of gas generated (Figure 6.3b), about 0.15 % out of the initial 0.8% of phenyl carbonate that reacted, would have done so through one of the pathways present in Figure 6.6.

6.4 High precision coulometry of cells containing MPC, EPC, and EPC + VC

Figure 6.7 shows a summary of the results of the cycling between 2.8 – 4.2 V of NMC(111)/graphite cells filled with electrolyte containing low loadings of MPC, EPC or 2% VC + 1% EPC, measured using the UHPC. The raw data can be found in Figure D2 of Appendix D. The testing used a current density of $C/20$ between 2.8 V and 4.2 V at 40°C. Smith *et al.* [6] showed that charge-end-point capacity slippage is proportional to the oxidation current of the electrolyte at the positive electrode, while coulombic

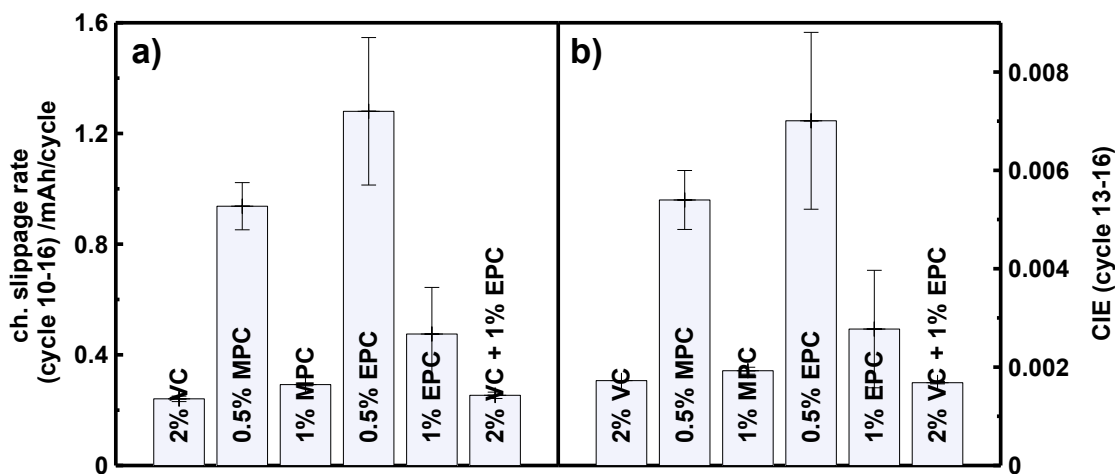


Figure 6.7. Charge endpoint capacity slippage rate (a) and CIE (b) of NMC(111)/graphite pouch cells containing various electrolytes and cycled between 2.8 – 4.2 V at $C/20$ and 40°C. The charge endpoint capacity slippage rate was calculated based on the slope of the charge endpoint capacity vs. cycle number of the cycles 11-15 and the CIE was calculated as the average of the CIE of the data points of cycles 11-15. Each data set is the average of two cells.

inefficiency (CIE, $CIE=1-\text{coulombic efficiency}$) encompasses parasitic reactions at both the negative electrode and the positive electrode. Lower charge-end-point capacity slippage (slope of charge-end-point capacity vs. cycle number) and CIE generally lead to longer lived cells [5].

The results of the UHPC cycling of cells containing phenyl carbonates were compared to cells containing 2% VC. Figure 6.7a shows that while cells containing 0.5% of MPC or 0.5% of EPC have high charge-end-point capacity slippage, cells containing 1% MPC or 1% EPC have charge-end-point capacity slippage rate slightly higher than cells with 2% VC. Burns *et al.* [143] and Petibon *et al.* [215] showed that the addition of 2% VC in LCO/gr or NMC/gr pouch cells greatly reduces the charge slippage and increases the CE compared to cells containing no additives. This then indicates that alkyl phenyl carbonates slow down the parasitic reactions at the positive electrode compared to a control electrolyte, but not as much as 2% VC, when present in concentration higher than 0.5%. This was confirmed by 4.2 V open circuit voltage storage of cells filled with MPC-containing and MPC-free electrolytes. Interested readers can see such results in Figure D3 of Appendix D. Figure 6.7a also shows that cells containing 2% VC + 1% EPC have exactly the same charge-end-point capacity slippage as cells containing 2% VC only.

Figure 6.7b shows that while cells with 0.5% MPC or 0.5% EPC have higher CIE, cells with 1% MPC and 1% EPC have CIE that is only slightly higher than cells containing 2% VC. Figure 6.7b also indicates that cells with 2% VC + 1% EPC have CIE values that are identical to cells with 2% VC only.

Figures 6.7a and 6.7b show that cells with 1% MPC or 1% EPC have parasitic reaction rates at the positive electrode and negative electrode close to cells containing 2% VC. As a consequence, small loadings of phenyl carbonates should give cells with lifetime comparable to cells containing 2% VC. Figures 6.7a and 6.7b also show that the addition of small loadings of phenyl carbonates in cells containing 2% VC does not affect the parasitic reaction rate at either electrode, compared to 2% VC alone. This indicates that using electrolytes containing 2% VC + 1% MPC for overcharge protection in metal-can or cylindrical cells will also yield cells with lifetime very close to cells containing 2% VC only.

6.5 Additive consumption after extended storage at 4.2 V and 40°C

Figure 6.8 shows the amount of additive left in NMC(111)/graphite pouch cells containing different initial MPC loadings, 2% VC, or 2% VC + 2% MPC after 1000 h of OCV storage at 4.2 V and 40°C. [In Figure 6.8, the additive consumption is relative to the total weight of the electrolyte. A consumption of 2% would indicate that the weight of additive consumed was equal to 2% of the total weight of the electrolyte.] If the presence of MPC is required for the gas to be generated during an eventual overcharge event, knowing the concentration of this additive with cell use is crucial. Figure 6.8 shows that while cells initially containing 2% VC had barely any additive left, cells initially containing 1% MPC still have some. Figures 6.4a and 6.4b showed that 1.5% VC and 0.8% MPC are consumed during the first charge to 3.5 V of cells initially containing 2% VC or 1% MPC, respectively. This indicates that while 0.5 % VC ($2\% - 1.5\% = 0.5\%$) is consumed during cell use (1000 h of storage in this case), only about 0.1% of MPC is

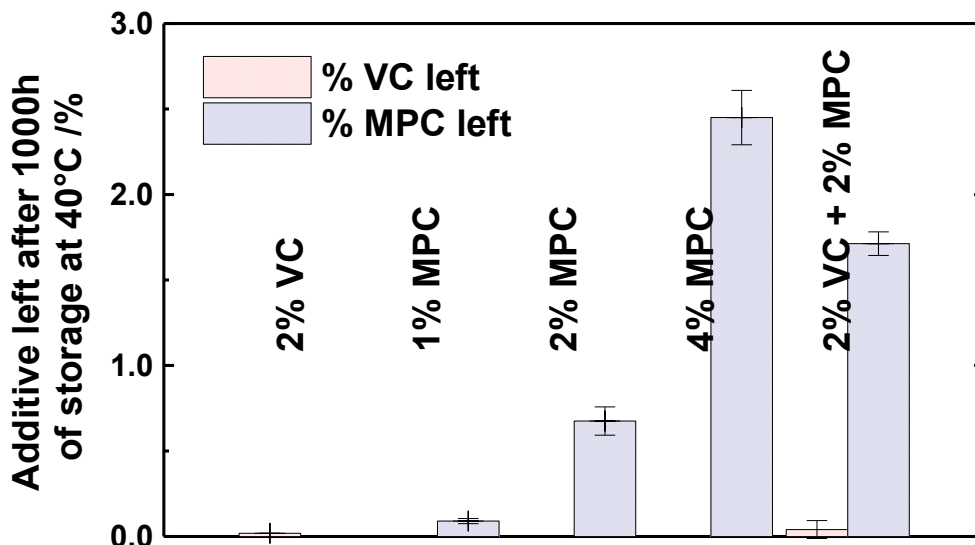


Figure 6.8. Amount of additive left in 220 mAh NMC(111)/graphite pouch cells filled with 1M LiPF₆ EC:EMC (3:7) base electrolytes with MPC alone or in combination with 2% VC, after two 500 h of open-circuit voltage storage at 4.2 V and 40°C.

consumed (1% - 0.8% - 0.1% = 0.1%). Figure 6.8 also shows that cells initially containing 2% MPC and 4% MPC, have 0.75% or 2.5% MPC left, respectively. This corresponds to a consumption of 1.25% and 1.5%, respectively. It then seems that the consumption of MPC does not strongly depend on concentration. This is expected since increasing the MPC loading from 1% to 4% does not affect the impedance or the voltage drop during storage (see Figure D3 of Appendix D).

Figure 6.8 shows that the presence of MPC in a 2% VC-containing electrolyte does not affect the consumption of VC. This again suggests that MPC does not significantly participate in the formation of passive films at either electrode when VC is present. The fact that MPC is barely consumed when 2% VC is present (see additive left after storage for cells containing 2% VC + 2% MPC), and the fact that the addition of EPC to 2% VC, or MPC to 2% VC did not affect the CIE (Figure 6.7b), charge slippage

(Figure 6.7a), and voltage drop (Figure D3 of Appendix D) point towards the same conclusion. Figure 6.8 clearly demonstrates that if the presence of residual MPC is necessary for gas generation during overcharge of cells initially containing VC + MPC (which remains to be confirmed), then prolonged cell use seems not to be a problem since MPC remains after use.

6.6 Storage at 4.2 V and 40°C of cells containing VC, MPC or DPC

Figure 6.9 shows the results of 40°C, 4.2 V open circuit voltage storage experiments of 220 mAh NMC(111)/graphite cells containing diphenyl carbonate (1% or 2%), 2% methyl phenyl carbonate or 2% VC. If phenyl carbonates are to be used as a single additive in Li-ion cells, then comparing the performance of diphenyl carbonate is useful. This is because symmetric esters of carbonic acid (such as DPC) are cheaper compared to asymmetric esters of carbonic acids (such as MPC).

Figure 6.9a shows the cell voltage vs. time during 500 h of storage. Again, the self-discharge profiles of cells containing VC and the phenyl carbonates are very similar. Figure 6.9a shows that the voltage drop of cells containing 1% DPC is statistically the same as the voltage drop of cells containing 2% DPC. This indicates that there is no added benefit in adding higher loadings of DPC in terms of parasitic reactions at the positive electrode. This is very similar to the results of storage experiments with MPC at loadings between 1 and 4% (Figure D3 of Appendix D). Figure 6.9a also shows that the voltage drop of cells containing 2% DPC or 2% MPC were the same, in the same manner that EPC had the same effect in terms of CIE and charge endpoint capacity slippage compared with MPC (see Figures 6.7). This suggests that the effect of phenyl carbonates

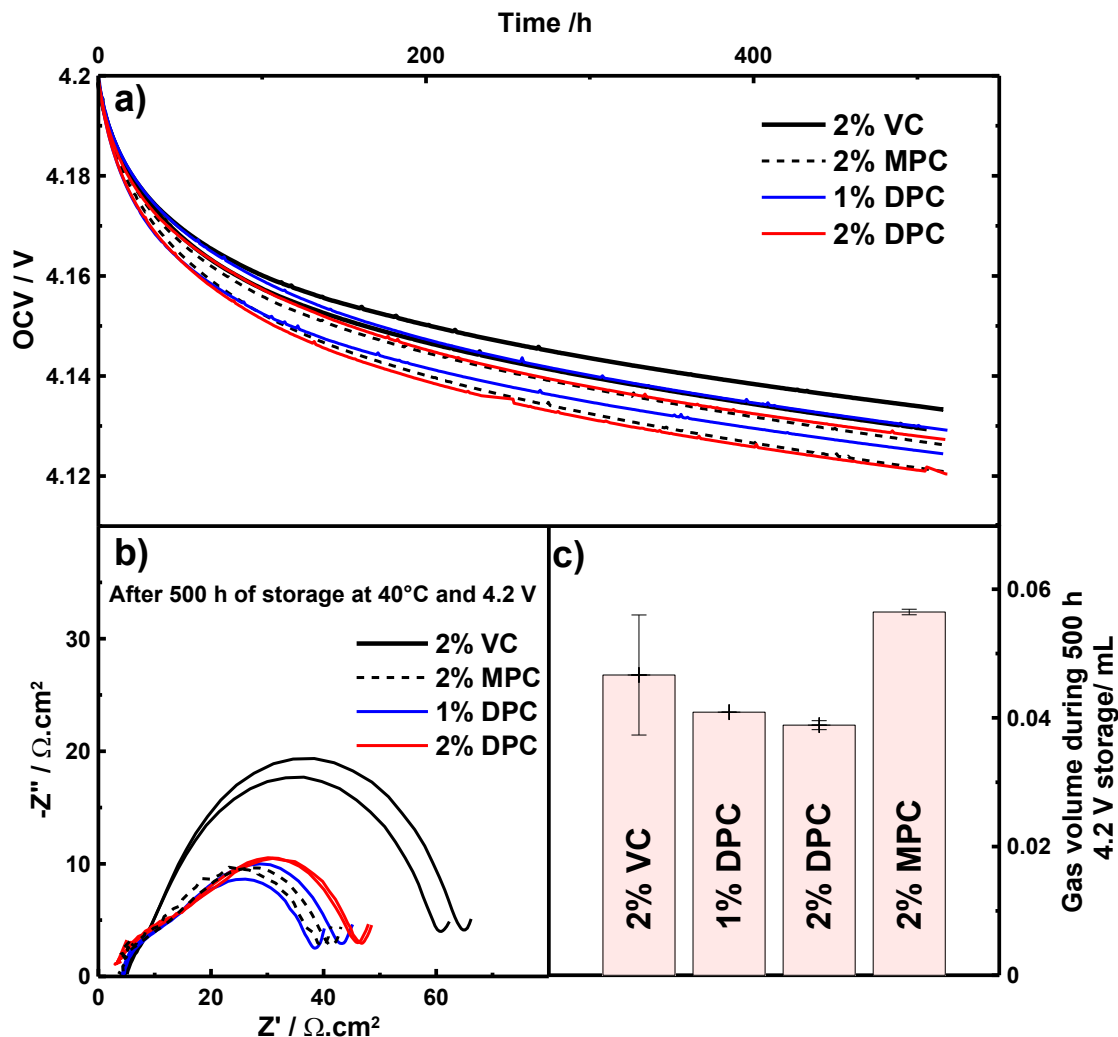


Figure 6.9. OCV vs. time of 220 mAh NMC(111)/graphite pouch cells filled with control electrolyte in combination with various additive blends stored at 40°C at 4.2 V (a); impedance spectra measured at 10°C and 3.80 V after the storage period (c) and gas volume produced during the first charge to 3.5 V and during the 500 h storage period (d). Cells were prepared by Lina Rotermund, 2nd year B.Sc. student, Physics & Atmospheric Science, Dalhousie University (2014).

are the same whether the ester groups of the carbonate are one or two phenyls, as long as the non-phenyl substitute is a saturated alkyl.

Figure 6.9b shows the impedance spectra measured at 10°C and 3.8 V after the storage period. Figure 6.9b shows that cells containing phenyl carbonates have impedance that is significantly lower than cells with 2% VC. Figure 6.9b also shows that

the impedance spectra of cells containing 1% DPC, 2% DPC or 1% MPC are very similar both in shape and magnitude. This indicates that the effect of different amounts of phenyl carbonates past a certain loading (1% here) is the same, and that again the effect of phenyl carbonates are the same whether the carbonate group is substituted with one or two phenyls.

Figure 6.9c shows the volume of gas produced during the 4.2 V, 500 h storage period. Figure 6.9c shows that within error, cells with phenyl carbonates produced the same amount of gas as cells containing 2% VC. Figure 6.9c also shows that cells with DPC produced less gas during the storage period than cells with MPC which might be an advantage for pouch-type cells using phenyl carbonates as single additives.

6.7 Symmetric cell construction from pouch cells containing 1% MPC

Figure 6.10 shows the impedance spectra measured at 10°C of negative electrode symmetric cells (a) and positive electrode symmetric cells (b) reconstructed from NMC(111)/graphite pouch cells initially filled with control electrolyte and an electrolyte containing 1% MPC. Both pouch cells had been cycled for 200 h at 40°C between 2.8 V and 4.2 V at C/10. As shown in earlier publications by Petibon *et al.* [107,108], symmetric cell reconstruction from full pouch-type, or prismatic-type cells allows the contributions of the positive electrode and the negative electrode to the impedance of the full cell to be clearly separated. This technique was later used to evaluate the effect of a multitude of additives on the impedance of the positive electrode and negative electrode in commercially relevant cell formats [108,143,215,235,236].

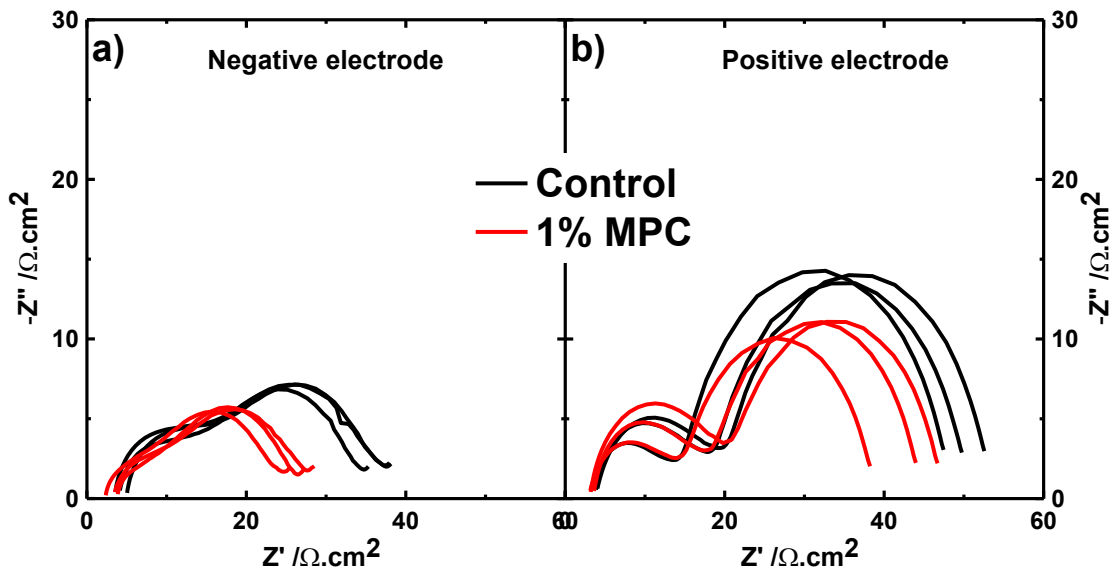


Figure 6.10. Impedance spectra measured at 10°C of negative electrode symmetric cells (a) and positive electrode symmetric cells (b), reconstructed from 220 mAh NMC(111)/graphite pouch cells filled with control electrolyte and control electrolyte + 1% MPC. The pouch cells were cycled at C/10 between 2.8 V and 4.2 V at 40°C for 200 h before being opened for symmetric cell construction. The pouch cells were opened at 3.65 V, about 45% state-of-charge.

Figures 6.10a and 6.10b clearly show that MPC affects both the negative electrode and positive electrode impedances. Since the impedance of Li-ion cell electrodes is closely related to the SEI formed at the surface of the active material, Figure 6.10 shows that MPC affects the formation of the passivating film of both electrodes. This was expected since the addition of MPC provided reduced parasitic reactions at the positive electrode (evidenced by the low charge endpoint capacity slippage during cycling and low voltage drop during storage) and at the negative electrode (evidenced by the high coulombic efficiency). Petibon *et al.* [107,108,215] and Burns *et al.* [143] showed that in cells with similar active mass-to-electrolyte ratio, while the addition of 2% VC decreased the impedance of the positive electrode compared to a control electrolyte, it increased the impedance of the negative electrode. Figure 6.10 then clearly explains why the impedance of cells containing 1 – 4% MPC have significantly lower impedance

than cells containing 2% VC as seen in Figure 6.9b. This comes from a lowering of both the negative and positive electrode impedance.

In an earlier publication, Petibon *et al.* [108] presented the effect of several additives on the impedance of the graphite electrode of NMC/graphite and LCO/graphite prismatic cells. In that study, they showed that the majority of additives increased the impedance of the negative electrode. Figure 6.10 shows that additives that lower the impedance of the negative electrode do exist. This is very advantageous since low negative electrode impedance is necessary to achieve high charging rates without lithium plating. Such additives would be useful for the electric vehicle industry where fast battery charging is key for the success of their commercialization.

6.8 Storage at 4.3 V and 40°C of cells containing DPC

Figure 6.11a shows the results of 500 h OCV storage experiments at 4.3 V and 40°C of 220 mAh NMC(111)/graphite cells filled with a 1M LiPF₆ EC:EMC (3:7) electrolyte containing 2% DPC or 2% PES + 1% methylene methanedisulfonate (MMDS) + 1% TTSPi. The electrolyte with the ternary additive blend was chosen as comparison based on the results presented by Ma *et al.* [11] and Nelson *et al.* [138]. In earlier publications they showed that ternary additive blends containing PES, a sulfur containing additive and TTSPi provided better performance in terms of capacity retention, impedance growth rate, solvent oxidation rate and gas generation to NMC/gr cells cycled to high voltage (*i.e.* > 4.2 V). Figure 6.11 shows that cells filled with an electrolyte containing 2% DPC have a voltage drop that is statistically the same as the one for cells filled with an electrolyte containing the ternary additive blend.

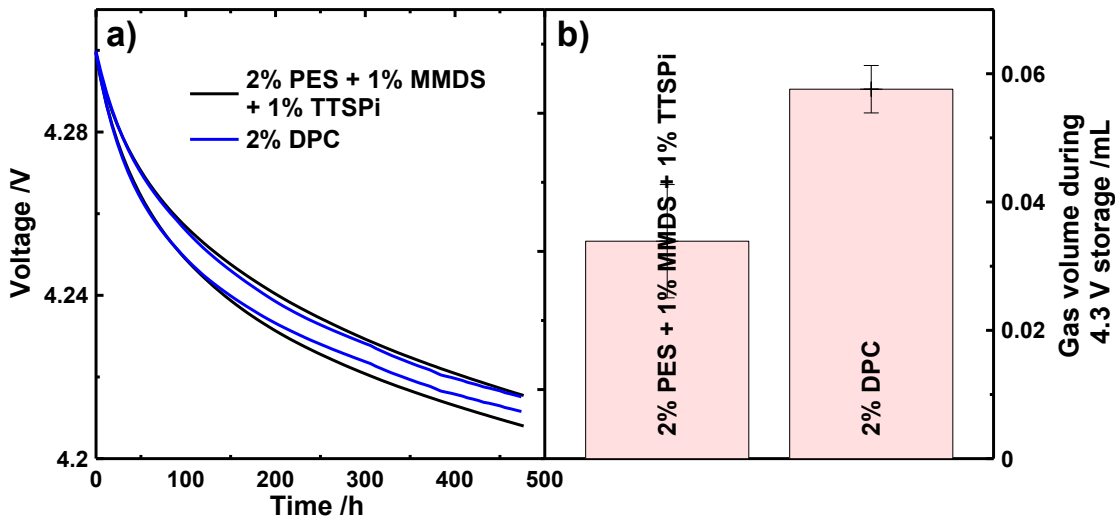


Figure 6.11. Cell voltage vs. time during a 500 h open circuit voltage storage at 4.3 V and 40°C of 220 mAh NMC(111)/graphite pouch cells filed with a 1M LiPF₆ EC:EMC (3:7) electrolyte containing 2% diphenyl carbonate or 2% PES + 1% MMDS + 1% TTSPi.

Figure 6.11b shows the gas produced during the 500 h OCV storage at 4.3 V and 40°C. Figure 6.11 shows that while the volume of gas produced in cells containing DPC is slightly larger than the one produced in cells containing the ternary additive blend, it is still very small. For instance, the initial volume of the NMC/gr pouch cell was around 2 mL. The 0.06 mL of gas produced in cells containing DPC then represents only a volume expansion of 3%.

Figure 6.11 clearly shows that phenyl carbonate may be useful in cells cycled to at least 4.3 V. While the electrolyte oxidation rate and gas volume production can always be lowered, further optimization would be necessary. Further testing such as long term cycling and high precision coulometry also need to be performed in order to clearly assess their effectiveness at high voltage.

6.9 Performance of NMC(811)/graphite cells containing DPC

Figure 6.12 shows the discharge capacity and cell polarization (difference of the average charge voltage and average discharge voltage) of NMC(811)/graphite pouch cells filled with 1M LiPF₆ EC:EMC (3:7)-based electrolyte with various additive blends and cycled at 40°C and C/2.5 between 2.8 – 4.3 V. Figure 6.12 shows that all cells containing no additive, VC, or a ternary additive based on VC, MMDS and TTSPi have poor

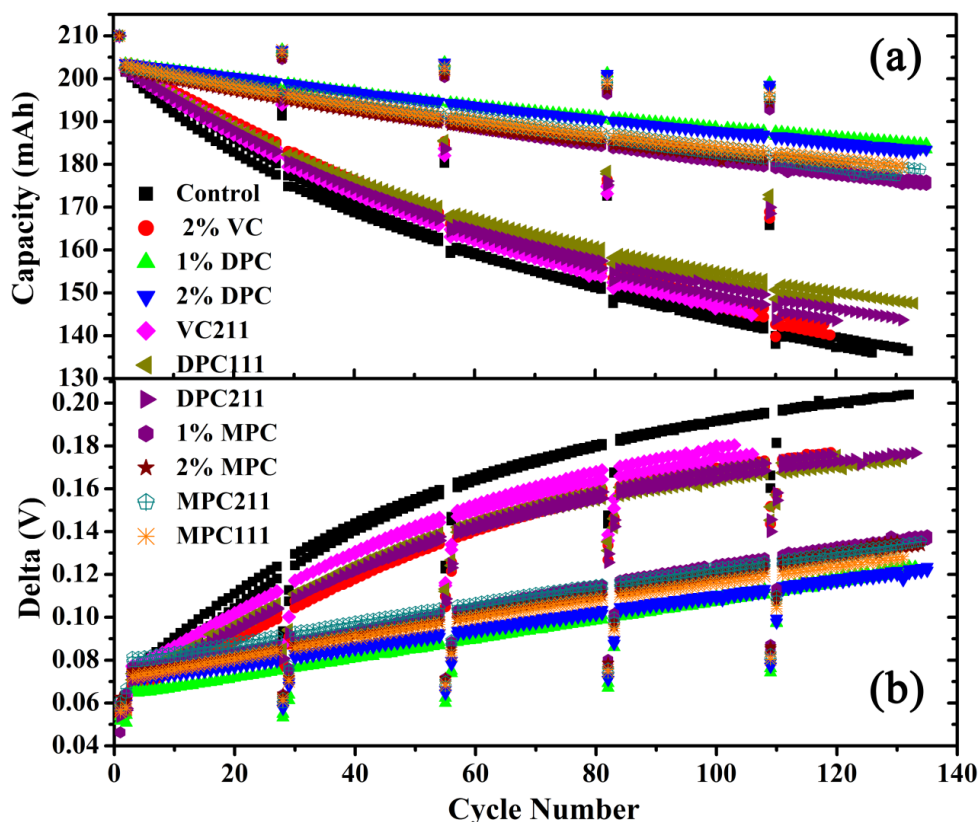


Figure 6.12. Discharge capacity (a) and difference between average charge and discharge voltage (delta V, b) vs. cycle number for 200 mAh NMC(811)/graphite pouch cells cycled with clamps at C/2.5 (80 mA) at 40°C between 2.8 and 4.3 V. The electrolyte compositions VC211, MPC211, DPC111 refer to control electrolyte plus 2%VC + 1% MMDS + 1% TTSPi, 2% MPC + 1%MMDS + 1% TTSPi, 1%DPC + 1%MMDS + 1%TTSPi, respectively. Cells were prepared and the data analyzed by Wenda Qiu, visiting student, School of Chemistry and Chemical Engineering, Sun Yat-sen University, Guangzhou 510275, China (2015).

capacity retention (the ternary additive blend was chosen based on findings published by Wang et al. [16]). Figure 6.12b seems to indicate that some of the capacity loss in these cells originates from polarization growth. However, Figures 6.12a and 6.12b show that cells containing MPC or DPC have better capacity retention and lower polarization growth rate than cells with VC or a ternary additive blend. For instance, while cells containing VC have only 68% capacity retention after 120 cycles, cells containing DPC have close to 90% capacity retention. This once again strongly suggests that phenyl carbonates are valuable additives.

6.10 Concluding remarks on phenyl carbonates

The effects of the addition of phenyl carbonates to the electrolyte of NMC(111)/graphite pouch cells were evaluated. High precision cycling and OCV storage experiments indicated that the addition of 1 to 4% phenyl carbonates as a single electrolyte additive yielded cells with parasitic reactions at the positive electrode and negative electrode on the same order as cells containing 2% VC. Electrochemical impedance spectroscopy also showed that the use of these compounds as single additives led to cells with very low impedance.

The impedance of symmetric cells constructed from full cells showed that phenyl carbonates lower the impedance of both the positive electrode and negative electrode compared to the situation with 2% VC. This proved that phenyl carbonates constitute promising additives for Li-ion cells with layered metal oxide positive electrode material and graphite negative electrode material. It has also been shown that the addition of phenyl carbonates to cells containing 2% VC does not affect parasitic reaction rates at

either electrode, gas generation during cell use, and cell impedance. This suggests that adding these compounds as gas generators during overcharge in cells containing 2% VC will not affect cycle life.

All the tests performed indicated that MPC, DPC and EPC had the same effect in terms of parasitic reaction rates, impedance at both electrodes and gas generation during formation and cell use. This is advantageous since DPC would be a very low cost single additive compared to VC, MPC or EPC. This comes from the fact that unsaturated cyclic carbonates such as VC, or asymmetric carbonates such as MPC or EPC, are difficult to synthesize because of the many reaction and purification steps compared to a symmetric carbonate such as diphenyl carbonate. Current bulk pricing from Chinese suppliers shows that DPC is about 10% of the cost of VC.

The differential capacity plot of the first few mAh of the first charge did not show any visible feature when phenyl carbonates were added while solvent analysis by GC-MS showed that 0.8 % of phenyl carbonates were consumed. This showed that these molecules do not get reduced before EC, or at least not to a great extent. They most likely react with the by-products of the reduction of EC and EMC, and are reduced at a potential (vs Li/Li⁺) lower than EC. Analysis of the gas produced in cells formed to 3.5 V showed that the addition of phenyl carbonates does not significantly affect the composition of the gas formed during the first charge indicating the gas mainly comes from the reduction of EC. This indicates that the addition of this class of additive does not affect how much EC is reduced at the graphite electrode during the first charge. However EIS on symmetric cells, high precision coulometry and storage experiments revealed that phenyl carbonates affect the surfaces of both the positive electrode and the

negative electrode. This seems to indicate that phenyl carbonate act as SEI modifiers as opposed to SEI formers.

Open circuit voltage storage at 4.3 V of cells containing DPC indicated that phenyl carbonates may be useful additives for cells cycled to high voltage. Further testing, optimization and co-additive survey are necessary in order to assess their full potential.

Finally, phenyl carbonates were shown to be superior to VC or ternary additive blends consisting of VC, MMDS and TTSPi in NMC(811)/gr cells. Cells containing MPC or DPC were shown to have much better capacity retention and much smaller polarization growth rate when cycled at 40°C with an upper cut-off voltage of 4.3 V than cells containing VC.

CHAPTER 7. ANALYSIS OF THE FADE MECHANISM OF LCO/SILICON ALLOY-GRAPHITE POUCH CELLS⁴

7.1 Why studies of Si-containing full cells is important

Cost reduction and an increase in the volumetric energy density of Li-ion cells can possibly be attained using silicon-based negative electrodes [59,60,237]. While these benefits have been known for many years, commercial implementation remains limited due to silicon's inherent challenges. The root cause of these challenges is the large volume expansion [59,75] of the material during lithiation and subsequent contraction during delithiation (see Section 1.2.4).

In a recent publication, Chevrier *et al.* [73] presented a rational way to design commercially relevant Si-based negative electrodes. Chevrier *et al.* [73] and Du *et al.* [238] showed that composite electrodes made of Si-alloy particles blended with graphite can achieve many charge-discharge cycles without dramatic capacity loss using commercially-relevant active mass loadings (*i.e.* 3 - 4 mAh/cm²). In these composite electrodes, graphite acts as a Li-intercalation material, conductive network between the Si-alloy particles, lubricant during electrode calendaring and reduces the total volume expansion of the electrode.

While the academic literature has an abundance of cycling data on Si-based half-cells using a Li metal counter electrode [25,68,69,72,80,239–247], it is very difficult to

⁴ Some of the results presented in this Chapter were published in R. Petibon, V.L. Chevrier, C.P. Aiken, D.S. Hall, S.R. Hyatt, R. Shunmugasundaram, et al., *J. Electrochem. Soc.* 163 (2016) A1146–A1156 for which the candidate wrote the first draft of the entire manuscript. The contribution of the co-authors (other than the candidate) is indicated in the captions of the figures where appropriate.

find data for complete Li-ion cells. This is a direct consequence of the poor coulombic efficiency of many Si-based electrode designs. In a full cell configuration, the amount of active lithium is limited by the capacity of the positive electrode. As a result, any active lithium lost in the formation or thickening and repair of the SEI of the negative electrode in a full cell will translate into a loss in capacity. By contrast, in a half cell, this lithium loss will be recovered from the lithium foil and will not appear as capacity loss. Therefore it is common to see Si negative electrodes in the literature that perform well in half cells. It is much more difficult to build practical Si-based full cells that cycle well with limited capacity loss. For this reason, most full cells using nanosized silicon or micron sized silicon negative electrodes show poor capacity retention [74,176,240,248–252].

Studies of the failure mechanisms of full cells with Si-containing negative electrodes need to be performed. Studying full cells can identify further challenges faced by Si-based negative electrodes and quite possibly guide researchers towards electrode and electrolyte designs that are more commercially relevant.

In this chapter, the capacity loss mechanisms of LiCoO₂/Si-alloy:graphite (LCO/Si:gr) full pouch cells are investigated. Machine-made pouch cells were used to ensure cells with high reproducibility. Such cells have an electrolyte volume to active mass ratio close to those used in commercial cells. This further helps identify failure mechanisms such as electrolyte dry-out that cells with excess electrolyte such as coin cells or Swagelok cells might not experience. Since FEC-containing electrolytes appear to be the best performing electrolytes for Si-based electrodes [25,109,239,253–255], all cells used in this study used a 1M LiPF₆ EC:EMC:FEC (27:63:10) electrolyte. Cells were

cycled between 4.35 V and 3.0 V using a constant current-constant voltage (CCCV) charge and constant current discharge protocol unless stated otherwise. The constant voltage portion at the top of charge was maintained until the current dropped below $C/20$. The rates of the constant current charge and constant current discharge are indicated in the figure captions.

7.2 Room temperature cycling of LCO/Si-alloy:graphite pouch cells filled with FEC-containing electrolytes

Figure 7.1 shows the discharge capacity vs. cycle number of 200 mAh LCO/Si:gr pouch cells formed and cycled at room temperature (22°C) between 2.75 V and 4.35V using a current of $C/2$ and the CCCV protocol described above with an additional $C/20$ cycle every 50 cycles. Cell C (black crosses) shows the typical discharge capacity vs. cycle number of a LCO/Si:gr full cell containing FEC. In the particular dataset shown here, cells also contained 2% of pyridine boron trifluoride (PBF). However cells without co-additives also presented a similar behavior. Cells show a gradual capacity loss during the first 300 - 400 cycles followed by a sudden capacity fade. In order to investigate the origin of this sudden failure, three sister cells were cycled under identical conditions. Cell A was cycled for 100 cycles (red circles), cell B was stopped right before the sudden failure (blue diamonds), and cell C was cycled through failure. The three cells (cells A, B and C) were then discharged and their electrolyte was extracted to be analyzed by GC-MS.

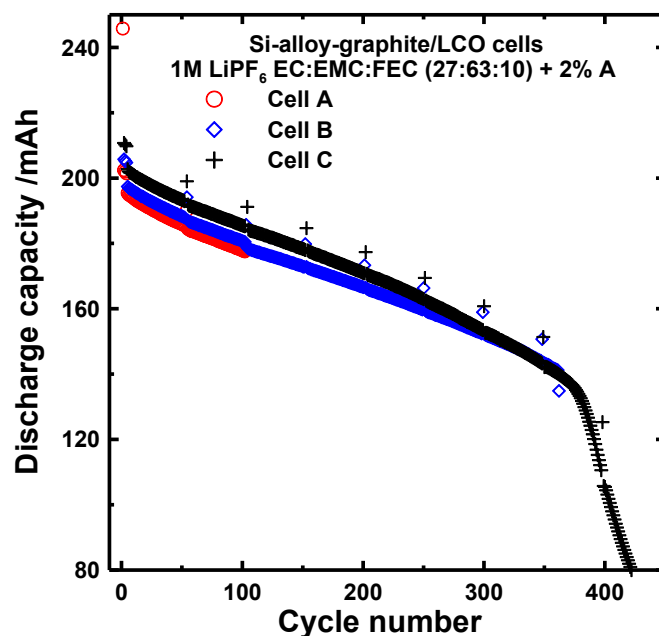


Figure 7.1. Discharge capacity vs. cycle number of 200 mAh LCO/Si-alloy-graphite pouch cells cycled at room temperature (22°C) between 2.75 V and 4.35V using a current of C/2. A constant voltage step at the top of charge was applied until the current dropped below C/20. A C/20 cycle without a constant voltage step was performed every 50 cycles. Cells were filled with a 1M LiPF₆ EC:EMC:FEC (27:63:10) + 2% PBF electrolyte. Cells were prepared and cycled by Vincent Chevrier, research scientist, Corporate Research Materials Laboratory, 3M Center, St. Paul, Minnesota 55144-1000, USA.

Table 7.1 shows the results of the GC-MS analysis of the electrolyte of cells A, B and C after the testing shown in Figure 7.1. Table 7.1 shows that out of the initial 10% FEC present in the cells, cell A has 5.3% left after 100 cycles. Table 7.1 also shows that cell B, which is about to undergo sudden failure has only 0.9% FEC left after 360 cycles and that the cell that has undergone sudden failure (cell C) has no FEC left. Table 7.1 clearly shows that FEC is consumed during cycling. It also strongly suggests that the sudden failure of LCO/Si:gr full cells happens once the FEC is fully consumed. This suggests that the continuous presence of FEC is required for Si-based full cells to cycle fairly well.

Table 7.1. Results of the GC-MS analysis of the electrolyte extracted from cells A, B and C shown in Figure 7.1.

Cell	Failed/did not fail during cycling	Avg FEC left /%	EMC /%	DMC /%	DEC /%
Cell A	Did not fail	5.32 ± 0.2	70.2 ± 0.1	0.00 ± 0.01	0.17± 0.01
Cell B	On the brink	0.91 ± 0.01	74.1 ± 0.1	0.00 ± 0.01	0.17± 0.01
Cell C	Failed	0.00 ± 0.01	39.12± 0.03	12.5± 0.1	23.6± 0.1

During cycling, the Si-alloy particles experience a ~ 135% volume change based on the alloy composition and theoretical molar volume Li occupies in the Si domains [59,60]. Similarly to pure Si particles, this volume change is likely to cause SEI damage and expose fresh alloy surface to the electrolyte. This exposed surface then needs to be protected with a new SEI which consumes FEC, solvents and salt. It is well known that EC-based FEC-free electrolyte provides only poor passivation to Si particles [25,109,239,253–255]. It is then likely that once FEC has been fully consumed, the alloy surface exposed to the electrolyte during particle expansion cannot be well passivated. At this point, the cell would undergo sudden failure.

Table 7.1 also shows that the sudden failure is also associated with the appearance of DMC and DEC. As mentioned in Chapter 5, the generation of DMC and DEC from EMC is caused by trans-esterification of linear carbonates [122,126,185,189,191,193,210,216,256]. At temperatures below 70°C, these trans-esterification reactions are catalyzed by the presence of lithium alkoxides generated by the reduction of linear and cyclic carbonates [78,105,116,186,190,193,216] (see Equation 5.1 and Section 5.1.3).

7.2.1 Prevention of trans-esterification in presence of FEC

Section 5.1.3 showed that VC prevents trans-esterification of EMC by lowering the amount of EMC that gets reduced and by trapping lithium alkoxides. It is then possible that the trans-esterification of EMC occurs during the sudden failure of the LCO/Si:gr cells because of the absence of FEC. For instance, Kim *et al.* [193] showed that FEC can effectively prevent the formation of ethylene-bis-carbonates which are generated through similar reaction mechanisms as the formation of DEC and DMC from EMC.

In order to determine whether the alkoxide trapping by FEC is energetically favorable or not, DFT calculations were performed. Figure 7.2a shows the possible

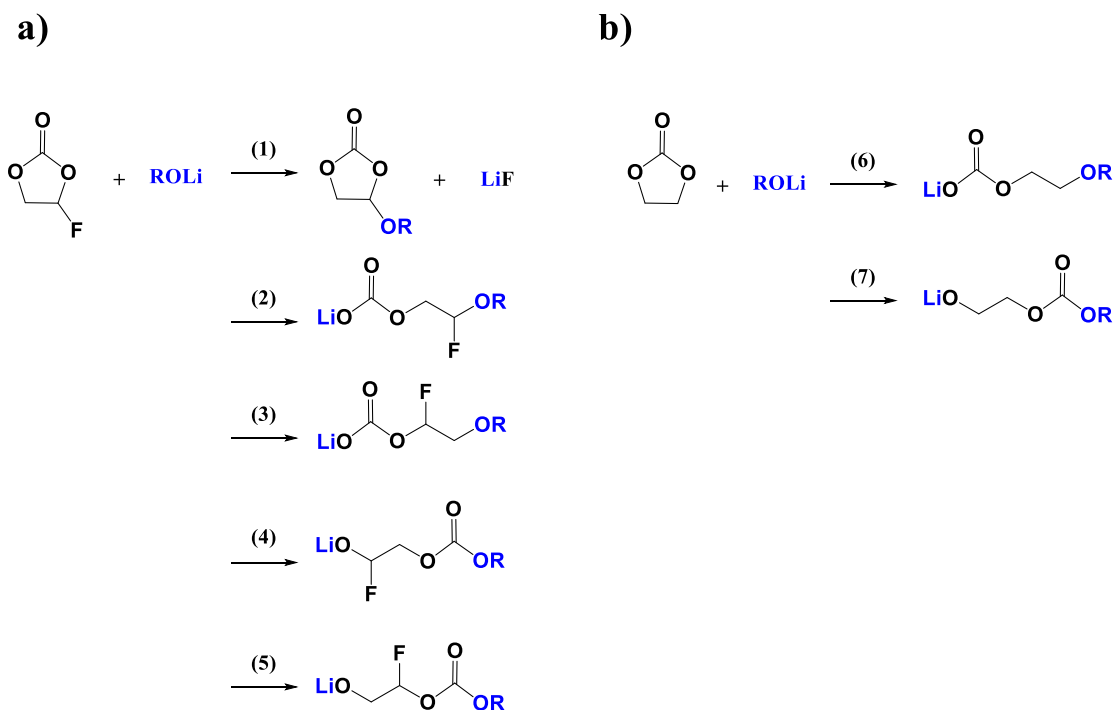


Figure 7.2. Proposed reaction pathways between lithium alkoxides and FEC (a) and between lithium alkoxides and EC (b).

reactions between FEC and lithium alkoxides while Figure 7.2b shows the possible reactions between EC and lithium alkoxides. All DFT calculations were made using lithium methoxide and lithium ethoxide in order to assess the effect of alkyl chain length of the alkoxides on the energies of the reactions. Interested readers can refer to Appendix E for a description of the method used to perform these calculations.

Table 7.2 shows the energies of reactions (1) through (7) presented in Figure 7.2. Table 7.2 shows that almost all reactions have negative free energy change which indicates that they are favorable. Out of the 5 possible reactions between FEC and lithium alkoxides, reactions (1), (2), (3), and (5) are the most energetically favorable. Reaction (4) has a small negative free energy which indicates that this reaction is likely to be in equilibrium and not unidirectional. Table 7.2 also indicates that there is only a small reaction free energy difference between lithium methoxide and lithium ethoxide. This indicates that FEC is as energetically likely to react with lithium ethoxide or lithium methoxide. Table 7.2 also shows that both reactions between EC and lithium alkoxides

Table 7.2. Calculated free energies of reactions (1) to (7) shown in Figures 7.2. Calculations were performed by David Hall, Post-doctoral fellow, Physics & Atmospheric Science, Dalhousie University (2015). The method used to compute the reaction energies is described in Appendix E.

Reaction	ΔG (kJ mol ⁻¹)	
	R = Me	R = Et
(1)	-112.0	-111.2
(2)	-110.0	-107.1
(3)	-103.1	-102.8
(4)	-9.4	-2.9
(5)	-58.1	-54.0
(6)	-92.2	-83.7
(7)	-1.5	2.7

are favorable. Reaction (6), which generates an ethereal semi-carbonate, has a negative free energy of reaction of the same magnitude as reactions (1), (2) and (3). This indicates that if FEC traps lithium alkoxides, it is for kinetic reasons and not for energetic reasons.

The energies of reaction presented in Table 7.2 indicate that they are all likely to occur and that FEC is likely preventing the transesterification of linear carbonate for kinetic reasons. This means that if the reaction between FEC and alkoxides happens in a faster fashion than between EC and alkoxides, then trans-esterification reactions will not occur. In order to assess which of these reactions have the fastest kinetics, lithium methoxide and lithium ethoxide were added to EMC:FEC (90:10 w:w) mixtures and analyzed by GC-MS similarly to the experiments presented in Section 5.1.3.

Figure 7.3 shows the mole% of EMC, DMC and DEC, as well as the amount of FEC remaining (relative to the initial FEC loading) and relative peak intensity for the products of reaction (1) of Figure 7.2 (EC-OMe and EC-OEt) and EMC as a function of time after the addition of LiOMe (7.2a) or LiOEt (7.2b) to a EMC:FEC (90:10, w:w) solution. Similarly to the data shown in Figures 5.5 and 5.6, Figure 7.3 shows that the kinetics of the reaction are faster with LiOEt than with LiOMe. Figure 7.3 also shows that the addition of lithium alkoxides to FEC-containing EMC does not lead to the formation of DMC and DEC. This reaction was performed in an EC:EMC:FEC mixture and trans-esterification was not observed either (see Figure E1 of appendix E). This indicates that FEC traps lithium alkoxides. Figure 7.3 also shows that the amount of EC-OEt and EC-OMe (see Figure C2 of Appendix C for their structure) generated in FEC containing solution is greater than the amount generated in VC-containing solution (see Figure 5.6). The reaction was accompanied by the formation of a white solid and a

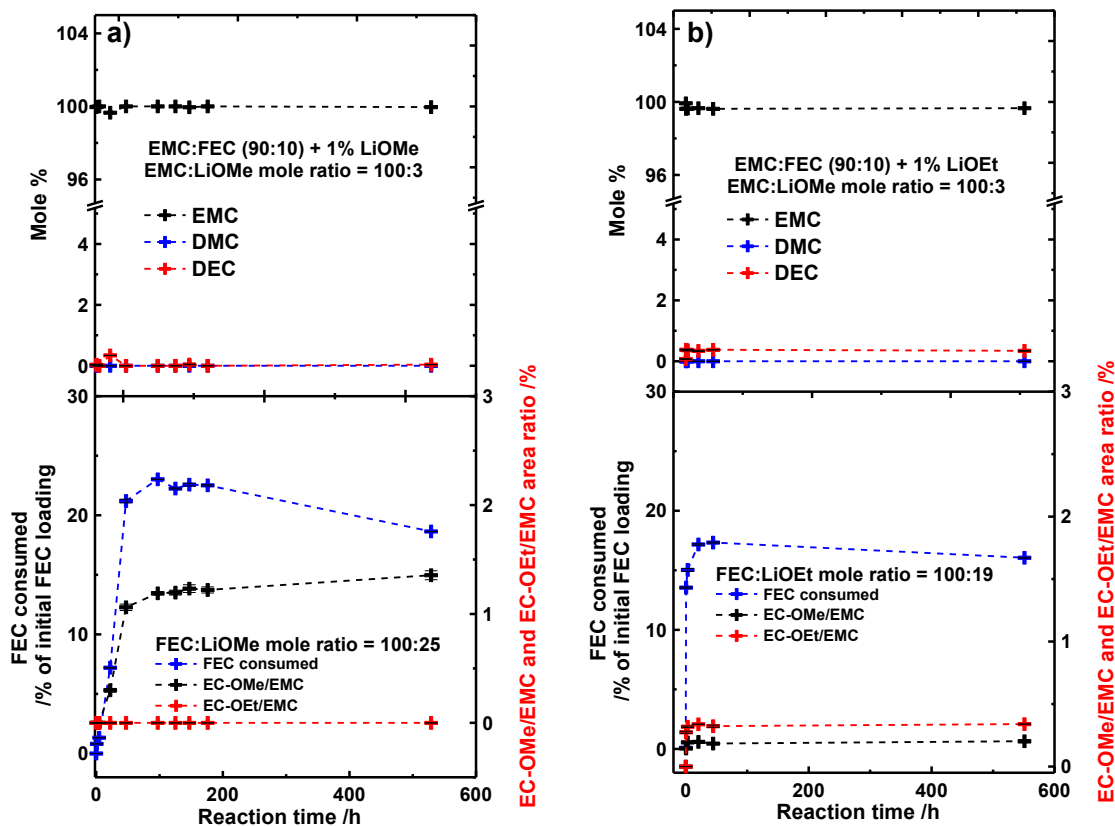


Figure 7.3. EMC, DMC, and DEC mole ratio (a, c) and amount of FEC left (normalized to the starting content) (b, d) as a function of time after adding lithium methoxide (a,b) or lithium ethoxide (c,d) to EMC + 10% FEC mixtures. Reactions were carried out in closed high density polyethylene vial under mild agitation in an Ar-filled glovebox at a temperature of $25^{\circ}\text{C} \pm 5^{\circ}\text{C}$.

soluble orange compound. The white solid was confirmed to be LiF by x-ray diffraction (XRD) measurements (see Figure E2 of Appendix E). Figure 7.3 also shows that the reaction stoichiometry is close to 1:1 (lithium alkoxide:FEC). This indicates that contrary to the case of VC, lithium alkoxides do not initiate the oligomerization of FEC. Figure 7.3 and the detection of LiF indicates that FEC traps lithium alkoxide following reaction (1) shown in Figure 7.2. This also indicates that, similarly to VC, FEC prevents transesterification reactions by lowering the amount of EMC getting reduced as well as by trapping the remaining lithium alkoxides generated.

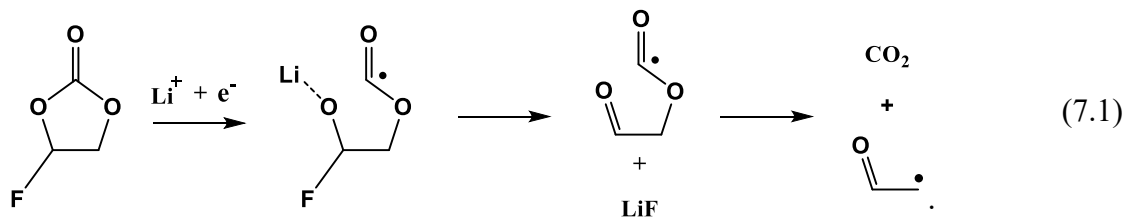
7.3 Gas generated during the first charge of LCO/Si-alloy:graphite pouch cells filled with FEC-containing electrolytes

Table 7.3 shows the composition of the gas produced during the first full cycle of LCO/Si:gr pouch cells filled with a 1M LiPF₆ EC:EMC:FEC (27:63:10) electrolyte (cells used here were not degassed at 3.8 V). Table 7.3 shows that the gas is composed of 8% H₂, 92% CO₂ and traces of CO. The amount of hydrogen produced is consistent with the water level present in the initial electrolyte (< 20 ppm). The absence of measurable amounts of ethylene (the limit of detection of the GC-TCD method was about ~ 2 μL) indicates that FEC prevents most of the reduction of EC. In an earlier publication, Leung *et al.* [257] presented the results of DFT and ab-initio molecular dynamics calculations of the reduction of FEC at the surface of Si electrodes. In this paper, they indicated that while both the 1-electron and 2-electron reduction of FEC leads to the formation of the well documented LiF [109,239,253,258], they lead to the formation of different gaseous products. Their calculations showed that the 1-electron reduction of FEC leads to the formation of CO₂ while the 2-electron reduction leads to the production of CO. The

Table 7.3. Composition of the gas produced during the first cycle between 4.35 V and 3.0 V at C/20 and 40°C of LCO/Si-alloy:graphite pouch cells filled with a 1M LiPF₆ EC:EMC:FEC (27:63:10) electrolyte. The cells used here were charged to 4.35 V and discharged to 2.8 V at C/20 without a degassing step at 3.8 V. The total volume of gas evolved during the first cycle was 0.17 mL.

Gas	Average Concentration /%
H ₂	7.9 ± 2.3
CO ₂	92.1 ± 2.3
CO	Traces

presence of CO₂ in LCO/Si:gr cells then indicates that FEC is likely to be reduced following a 1-electron reduction pathway following [257]:



While the nature of the gas evolved suggests a consumption pathway for FEC, other pathways cannot be excluded. For instance, the results presented in Figure 7.3 and Table 7.2 indicate that FEC may be consumed through reactions with generated lithium alkoxides. In a recent publication, Ma *et al.* [259] also showed using DFT calculations that FEC may be reduced following 2-electron reduction pathways that do not generate gaseous products. In their calculations, they showed that FEC may readily be reduced at the surface of Si clusters with a low lithiation state following pathways with very low energy barriers. Amongst these 2-electron pathways, they identified three mechanisms that do not involve the formation of volatile products.

7.4 FEC consumption and irreversible capacity during the first cycle of LCO/Si-alloy:graphite pouch cells

Figure 7.4 shows the cell voltage as well as FEC consumption vs. specific capacity (a) and % FEC consumed vs. irreversible capacity (b) for 200 mAh LCO/Si:gr pouch cells cycled once to various states of charge at 40°C. Cells were charged up to 3.2 V (7 mAh), 3.75 V (66 mAh), 4.06 V (180 mAh) and 4.35 V (240 mAh) and then discharged to 3.0 V at C/20. These cell voltages were chosen to be soon after the dQ/dV

peak corresponding to the reduction of FEC (3.2 V), at about 30% of the first charge (3.75 V), at 75% of the first charge (4.06 V) and at 100% state of charge (4.35 V). These voltages allow the voltage range at which most of the first cycle irreversible capacity (IRC) occurs to be roughly determined as well as evaluating when FEC is consumed during the first cycle. Readers need to be reminded that some consumption of FEC may occur during the discharge portion. The FEC consumption points were placed at the top of charge in Figure 7.4a for clarity.

Figure 7.4a shows that 1.0% out of the initial 10% of FEC reacts between 0 V and 3.2 V. This early consumption may correspond to the passivation of the graphite surface as well as the early passivation of the Si-alloy surface. Figure 7.4a also shows that FEC is still consumed above 3.2 V. For instance, an additional 1.5% FEC is consumed between 3.2 V and 4.06 V. Figure 7.4a also shows that the consumption of FEC then

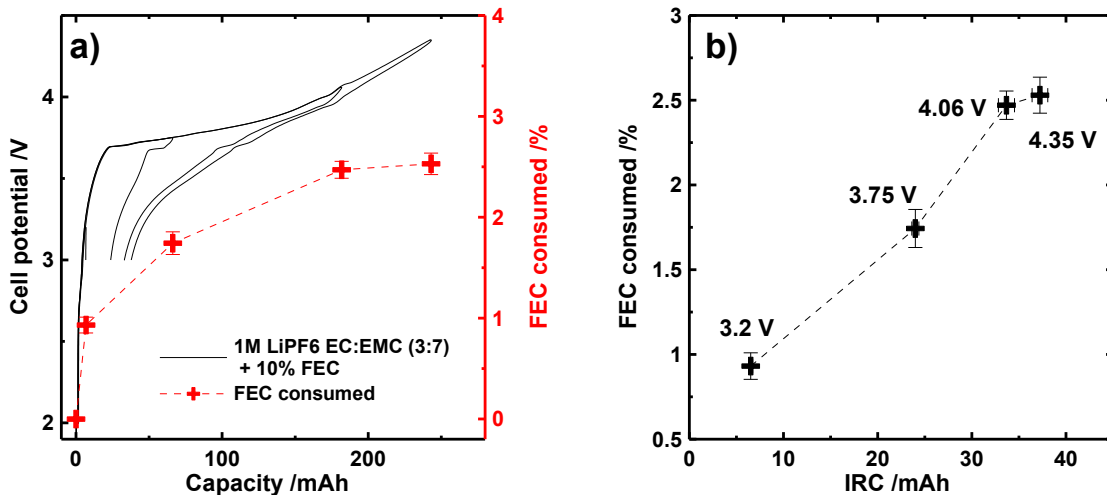


Figure 7.4. Cell voltage (left axis) and FEC consumption (right axis) vs. capacity (a) and FEC consumption vs. irreversible capacity (b) during the partial charging of 200 mAh LCO/Si-alloy:graphite pouch cells. The experiment was performed at 40°C. The amounts of FEC consumed are shown at the top of charge although they were measured at the bottom of discharge.

slows down between 4.06 V and 4.35 V. It is tempting to assign the entire consumption of FEC between 3.2 V and 4.06 V to the expansion of the Si-alloy particles and corresponding SEI damage. However Section 5.1.2 showed that in NMC(111)/gr cells containing 2% VC or 2% PES and charged to 4.2 V, VC and PES were consumed during the span of 60% of state of charge during the first cycle. It is then likely that FEC consumption occurring between 3.2 V and 4.06 V during the first cycle of LCO/Si:gr cells is from the SEI aging at the surface of the graphite and Si-alloy particles as well as due to SEI cracking/repair related to the expansion of the Si-alloy particles.

Figure 7.4b shows the amount of FEC consumed as a function of irreversible capacity. Figure 7.4b shows an almost linear relationship between the amount of FEC consumed and the irreversible capacity between 3.2 V and 4.06 V of the first charge. However the IRC does not arise only from the reduction of FEC since 30 mAh (4.06 V) of IRC would represent the reduction of 20% FEC (twice the initial amount) assuming a 1-electron reduction when only 2.5% was consumed. If all the FEC consumed at 4.06 V was reduced via a 1-electron mechanism, the consumption of FEC would account for about 5 mAh out of the 30 mAh of IRC. The other losses are likely due to the reduction of solvents, salt, functional groups at the surface of the graphite and carbon black particles, reduction of the by-products of the 1-electron and/or 2-electron reduction of FEC, as well as possible reaction of surface oxides likely present at the surface of the pristine Si-alloy particles with lithium. It is also important to note that the analysis of the gas produced during the first cycle did not contain any detectable ($> 2 \mu\text{L}$) amounts of methane, ethane or ethylene. This indicates that if the solvents have been reduced, their reduction mechanism did not follow the major pathway (producing gaseous compounds)

observed during the initial lithiation of graphite electrodes [185,189,216,260,261] (see Section 5.1).

Since FEC is needed for the cell to cycle, Figure 7.4 shows that out of the initial 10% FEC present in the cell, 7.5% is left after the first cycle. The rate at which this 7.5% FEC is consumed will dictate the cycle number to failure.

7.5 Cycling of LCO/Si-alloy:graphite cells at 40°C

Figure 7.5 shows the discharge capacity vs. cycle number (a), cell polarization (difference of the average charge voltage and average discharge voltage) vs. cycle number (b), and results of differential voltage analysis after 7 cycles (c), 12 cycles (d), 52 cycles (e), and 112 cycles (f) of LCO/Si:gr pouch cells cycled at 40°C between 4.35 V and 3.0 V at C/2. Figure 7.5 shows that LCO/Si:gr cells have similar behaviour when cycled at 40°C and room temperature (see Figure 7.1). Mainly, LCO/Si:gr cells have a gradual capacity loss for the first 250 cycles followed by a sudden capacity loss. Based on the results shown in Table 7.1, the sudden capacity loss can be associated with the depletion of FEC. It is also apparent that the consumption of FEC is accelerated at 40°C since cells cycled at room temperature underwent sudden failure at cycle number 400 and cells cycled at 40°C underwent sudden failure at cycle number 250.

Figure 7.5b shows that the Si-based full cells have a gradual polarization growth during the first 250 cycles followed by a sudden increase. Impedance measurements of positive and negative symmetric cells showed that this gradual polarization growth originates from increased positive electrode impedance (see Figure E3 of Appendix E). Gradual impedance growth was also observed by Wang *et al.* [262] in LCO/gr cells filled

with FEC-containing electrolytes and operated to 4.2 V. It is then apparent that if LCO electrodes are to be cycled with Si-based negative electrodes, new electrolyte compositions providing low and stable impedance to the positive electrode are needed.

The sudden polarization growth observed in Figure 7.5b occurs at the same time as the sudden capacity loss after 250 cycles. This corresponds well with the formation of

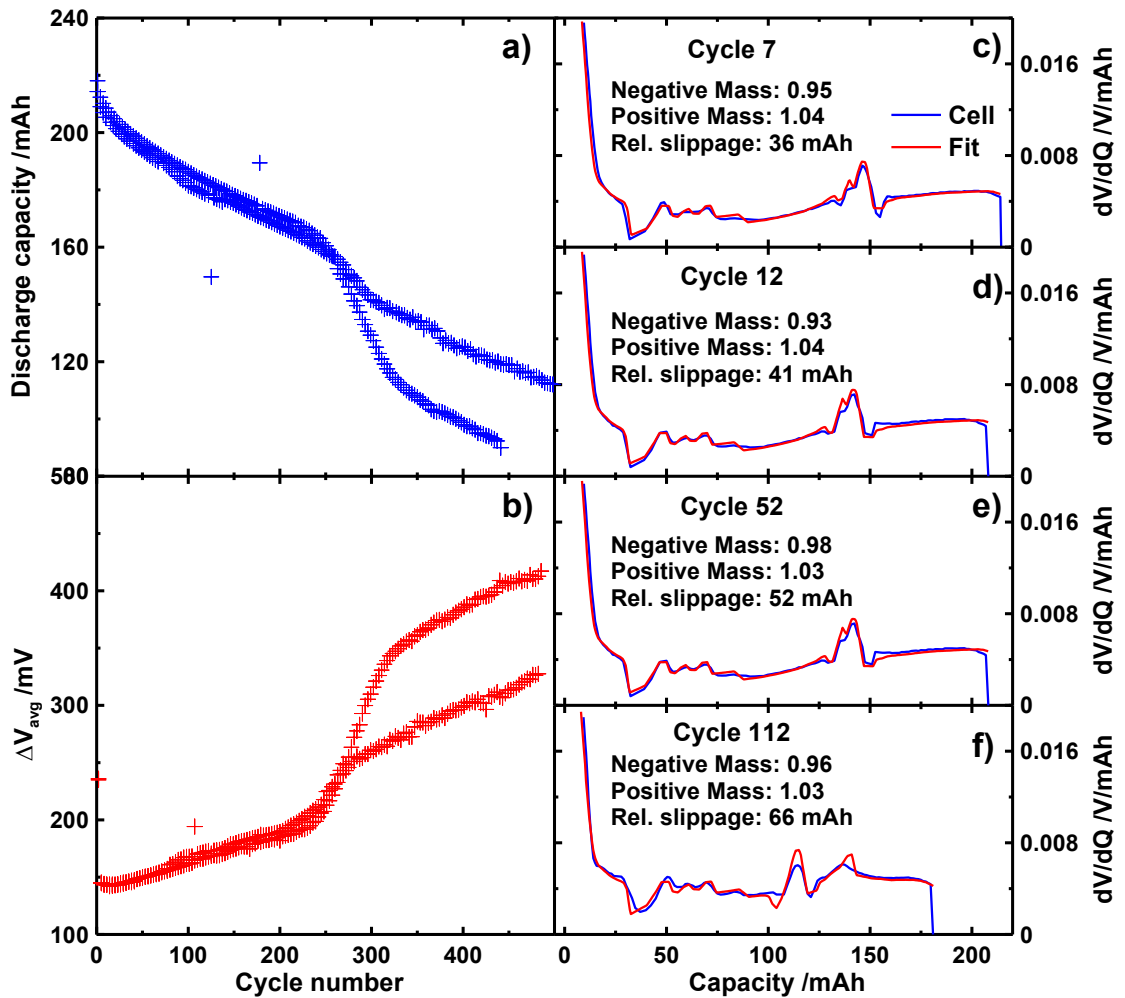


Figure 7.5. Discharge capacity vs. cycle number (a), cell polarization vs. cycle number (b) and fitting of the differential voltage vs. capacity curve (c-d) of the 7th cycle (c), 12th cycle (d), 52nd cycle (e) and 112th cycle (f) of 200 mAh LCO/Si-alloy:graphite pouch cells filled with a 1 M LiPF₆ EC:EMC:FEC (27:63:10) electrolyte cycled at 40°C between 3.0 V and 4.35V and a current of C/2. A constant voltage step at the top of charge was applied until the current dropped below C/20.

an SEI made from the reduction of an additive-free electrolyte. For instance, several researchers [239,254,255] showed that Si-based half cells filled with an additive-free electrolyte presented higher impedance than cells filled with an FEC-containing electrolyte. This suggests that once the FEC has been depleted, the new SEI created during the volume change of the Si-alloy particles might be similar to the one made by an additive-free electrolyte. Figure 7.5b suggests that the capacity loss during the sudden failure is likely a mixture of kinetic hindrance and active lithium loss.

In order to assess whether the gradual loss before sudden failure is due to Li loss due to SEI growth and repair or to active material loss, differential voltage analysis was performed on LCO/Si:gr cells after various cycle numbers. In an earlier publication, Dahn *et al.* [217] reported on a differential voltage analysis freeware that allows the relative slippage of the positive and negative electrodes, the negative electrode active mass and the positive electrode active mass to be determined based on the analysis of the differential voltage curves of a full cell. These parameters were fitted using reference differential voltage curves of LCO/Li and Si-alloy:graphite/Li half cells. In the particular cells studied here, the relative slippage is caused mostly by the lithium loss at the negative electrode. For instance, a relative slippage of 0 mAh indicates that when the cell reaches its discharge cut-off, the negative electrode is totally delithiated and the positive electrode is totally lithiated. A relative slippage greater than 0 mAh indicates that when the cell reaches its discharge cut-off, the negative electrode is completely delithiated while the positive electrode is not fully lithiated. This latter scenario occurs when active Li is consumed for the SEI formation, growth and repair at the negative electrode [217,263]. The greater the relative slippage, the more active Li has been consumed for

SEI formation. If a cell had no active material loss, then the capacity loss would be equal to the relative slippage.

Figures 7.5c – 7.5f show that the negative electrode active mass as well as the positive electrode active mass do not vary significantly between cycles 7 and 112 (variation within the accuracy of the method). However, the relative slippage varies greatly and changes from 36 mAh to 66 mAh between cycle number 7 and 112. Figures 7.5c – 7.5f then indicate that the major part of the capacity loss prior to sudden failure is due to SEI growth and SEI repair at the surface of the graphite and Si-alloy particles. The cycling of a Si-alloy:graphite/Li half-cell at 40°C also indicated little active material loss (0 - 8%) over 80 cycles and 3000 h of cycling (see Figure E4 of Appendix E).

7.6 Modeling the capacity fade and consumption of FEC in LCO/Si-alloy:graphite cells cycled at 40°C

In order to evaluate the time dependence and cycle number dependence of the capacity fade and FEC consumption, LCO/Si:gr pouch cells were cycled at different rates. Figure 7.6a shows the normalized charge capacity as a function of cycling time for cells cycled at C/2, C/4, C/8 and C/16 (the charge capacities were normalized to the second cycle).

Figure 7.6a shows that for an equal cycling time, cells cycled the fastest (*i.e.* with a higher cycle count) experienced a higher capacity loss. This indicates that the fade of LCO/Si:gr cells has both a time dependence and a cycle number dependence. In order to decouple these two dependences, a simple model was developed. The capacity of the LCO/Si:gr cells cycled at various rates were fit using:

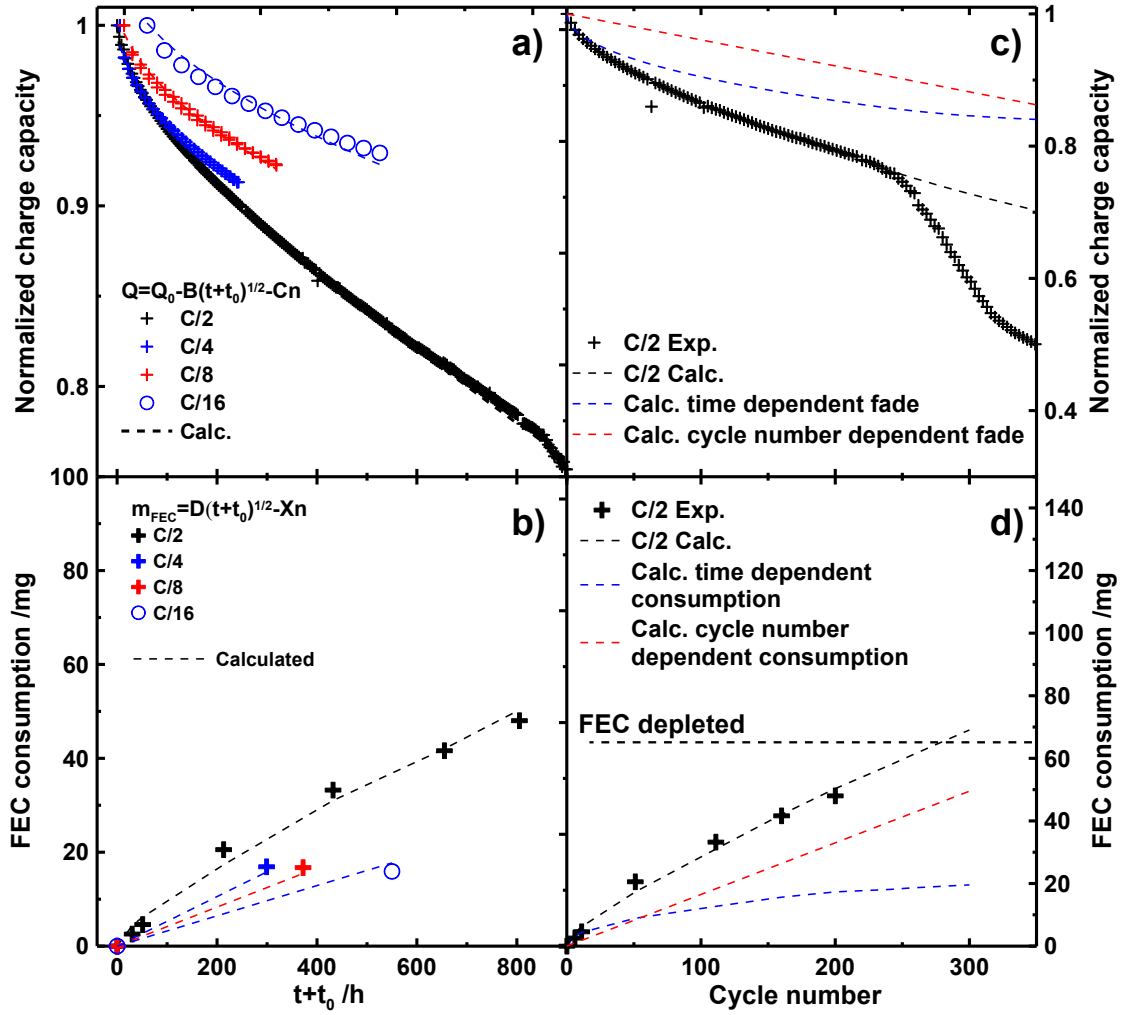


Figure 7.6. Experimental and fitted normalized charge capacity (a), experimental and fitted FEC consumption (b) as a function of cycling time at various rates, as well as experimental normalized charge capacity (c) and FEC consumption (d) for cells cycled at C/2 shown alongside the fitted time dependent and cycle number dependent capacity fade and FEC consumption of 200 mAh LCO/Si-alloy:graphite pouch filled with a 1 M LiPF₆ EC:EMC:FEC (27:63:10) electrolyte, cycled at 40°C between 3.0 V and 4.35V and a current of C/2. A constant voltage step at the top of charge was applied until the current dropped below C/20.

$$Q = Q_0 - B(t + t_0)^{\frac{1}{2}} - Cn \quad (7.2)$$

where Q corresponds to the normalized capacity, Q_0 corresponds to the capacity of the reference cycle (cycle 2, set to ~ 1 and allowed to deviate from 1 by less than ± 0.02), B is

a constant related to the time dependence of the capacity fade, t is the cycling time, t_0 is a constant to account for the time of the degassing step and C is a constant related to the cycle number dependence of the capacity fade. The time dependence was set to be proportional to the square root of time as reported by several researchers [2,7,264–267]. The cycle number dependence can originate from the SEI repair at the surface of the Si-alloy particles due to the volume changes upon lithiation and delithiation. In these fits, the possibility of lithium plating was ignored since no plating was visually observed in cells cycled at $C/2$ after 112 cycles. Figure 7.6a shows that the simple model fits the data very well with single values for the B and C parameters allowing simultaneous agreement with experiments across a wide range of cycling rates. The model then shows that both the ever-growing SEI at the surface of the graphite and Si-alloy particles as well as the SEI repair due to the large volume expansion of the alloy accounts for the fade of LCO/Si:gr cells.

Table 7.4 shows the parameters extracted from the fit of the data in Figure 7.6a using equation 7.2. While the model used is very simplistic and unlikely to account for all the contributions to the loss of capacity (*i.e.* loss due to polarization), it gives an understanding of the most prominent losses.

Table 7.4. Parameters obtained from the fitting of the data presented in Figure 7.6a using Equation 7.2.

$B / h^{-1/2}$	C / cycle^{-1}	$t_0 C/2 / h$	$t_0 C/4 / h$	$t_0 C/8 / h$	$t_0 C/16 / h$
		0	5.4	14	60
4.8×10^{-3}	0.39×10^{-3}	$Q_0 C/2$	$Q_0 C/4$	$Q_0 C/8$	$Q_0 C/16$
		1.00	1.00	1.01	1.04

Table 7.5 shows a comparison of the time dependences extracted from long term cycling data at 40°C available in the literature [2,7,264]. Table 7.5 shows that at a cycling temperature around 40°C, the normalized time dependence of Li loss varies between 0.3 h^{-1/2} and 4 h^{-1/2}. Table 7.5 also shows that the normalized time dependence of the capacity fade is within the same order of magnitude of the values reported in the literature. In an earlier publication, Smith *et al.* [7] showed that the time dependence of Li loss at graphite-based electrodes is directly proportional to the weighted average surface area of the electro-active materials (graphite and conductive additive) composing the negative electrode. This indicates that the time dependent capacity fade of LCO/Si:gr cells can be minimized through the use of graphite and Si-alloy particles with smaller specific surface area and with electrolyte blends minimizing Li loss. For instance, Table 7.5 shows that the surface area normalized time dependence of the fade of LCO/Si:gr cells is similar to the surface area normalized time dependence of irreversible Li loss in graphite/Li half cells cycled at 40°C reported by Smith *et al.* [7]. This suggests that the

Table 7.5. Comparison of the time dependence of lithium loss with values available in the literature.

Authors	Ref	Cell chem.	Temp.	Upper voltage cut-off	Time dep. / h ^{1/2}	Surface area/ m ² .mAh ⁻¹	Surface area normalized time dependence /h ^{-1/2} .mAh
Petibon et al.	This thesis	LCO/Si-alloy:gr	40°C	4.35 V	5x10 ⁻³	1x10 ⁻²	0.5
Broussely et al.	[2]	NCA/gr	40°C	3.9 V	3x10 ⁻⁴	NA	NA
Fathi et al.	[248]	LCO/gr	37°C	4.075 V	1x10 ⁻³	NA	NA
Smith et al.	[7]	Gr/Li	40°C	1.2 - 0.005 V	4x10 ⁻³	9x10 ⁻³	0.4

time dependent Li loss mechanisms in Si-alloy:graphite composite electrodes are similar to the ones in graphite only electrodes. The reader should be reminded that 40°C and a 4.35 V cut-off are relatively aggressive cycling conditions and that electrolyte oxidation at the positive electrode may contribute to the time-dependent Li loss through an electrode/electrode interaction. It is therefore highly encouraging for Si implementation, that despite having these aggressive cycling conditions, the time dependent Li loss of the LCO/Si-alloy:gr cells is similar to other values in Table 7.5.

Figure 7.6b shows the FEC consumption as a function of cycling time for LCO/Si:gr cells cycled at various C-rates. In order to evaluate the time dependence and cycle number dependence of the consumption of FEC, the electrolyte of LCO/Si:gr cells cycled at C/2, C/4, C/8 and C/16 and 40°C was analyzed using GC-MS. Each data point shown in Figure 7.6b is the average of two cells. In total, the electrolyte of 24 cells was analyzed at various cycle numbers and cycling rates. Similarly to the capacity fade, Figure 7.6b shows that the consumption of FEC has both a time dependence and a cycle number dependence. Since FEC is involved in the passivation of both the surface of the graphite and the Si-alloy particles, the consumption of FEC was modeled using an expression similar to the capacity fade using:

$$m_{FEC} = D(t + t_0)^{\frac{1}{2}} + Xn \quad (7.3)$$

where m_{FEC} is the mass of FEC consumed, D is a constant related to the time dependence of the consumption of FEC and X is a constant related to the cycle number dependence of the consumption of FEC.

Figure 7.6b shows the model fits the experimental data well across a wide range of cycling rates. Again, the time dependence of the consumption of FEC corresponds to

the ever-growing SEI at the surface of the graphite and Si-alloy particles and the cycle number dependence of the consumption corresponds to the SEI repair at the surface of the Si-alloy particles due to the large volume variation during lithiation and delithiation. Table 7.6 shows the parameters extracted from the fit of the data of Figure 7.6b using equation 7.3. Figure 7.6d also fairly accurately predicts the cycle number to failure. For instance, the fitted parameters predict the depletion of FEC at the 270th cycle while the cells experience failure at the 250th cycle.

Table 7.6. Parameters obtained from the fitting of the data presented in Figure 7.6b using Equation 7.3. In the fits of the data to equation 7.3, the parameters for t_0 were fixed at those given in Table 7.4, determined by the fits to equation 7.2.

D /mg.h ^{-1/2}	X /mg.cycle ⁻¹	t_0 C/2 /h	t_0 C/4 /h	t_0 C/8 /h	t_0 C/16 /h
0.61	0.16	0	5.4	14	60

Figures 7.6c and 7.6d show the normalized discharge capacity and FEC consumption as a function of cycle number alongside the time dependent and cycle number dependent portions of the capacity fade and FEC consumption obtained from the fitting of the data in Figures 7.6a and 7.6b. Figures 7.6c and 7.6d show that while the time dependence is the major contributor to the fade during the first 250 cycles, the cycle number dependence is the major contributor to the consumption of FEC.

The results presented in Figures 7.6c and 7.6d are quite important as a combination of two simple models is able to predict both the capacity fade and the sudden failure of Si-alloy-containing full cells. These figures indicate that the time dependence as well as the cycle number dependence of the fade should be minimized.

Lowering the time dependence of the fade will help minimizing the capacity loss before the depletion of FEC while minimizing the cycle number dependence of the fade will delay the depletion of FEC and the associated sudden failure. A good electrolyte system would ultimately allow the use of an FEC-free electrolyte while having low time dependent fade in order to eliminate the sudden failure altogether. One should recall that these cells are being cycled to high voltage at elevated temperature, which will have significant impact in increasing the time-dependence of the fade.

7.7 Concluding remarks on the fade and FEC consumption in LCO/Si-alloy:graphite pouch cells

The capacity fade of LCO/Si:gr full cells cycled at room temperature and 40°C was studied using galvanostatic cycling, GC-MS, GC-TCD, EIS on symmetric cells and differential voltage analysis. LCO/Si:gr cells filled with FEC-containing electrolytes showed gradual failure followed by a sudden failure. This sudden failure is attributed to the depletion of FEC and is accompanied by a large cell polarization growth and EMC trans-esterification.

The onset of the alkoxide catalyzed trans-esterification of EMC was caused when all the FEC was consumed. It was shown that FEC prevents the trans-esterification of EMC through a simple substitution reaction with lithium alkoxides. The reaction between FEC and lithium alkoxides was shown to produce a cyclic carbonate with an ether group as well as LiF.

The analysis of the gas produced during the first cycle of LCO/Si:gr cells filled with an electrolyte containing 10% FEC indicated that FEC is reduced following a 1-

electron pathway and other possible pathways that do not lead to the generation of gaseous products. The absence of significant quantities of methane, ethane and ethylene indicated that the presence of FEC prevented most of the initial reduction of EMC and EC. The analysis of the electrolyte throughout the first cycle also indicated that the consumption of FEC is not limited to the initial portion of the charge. Fluoroethylene carbonate was shown to be continuously consumed throughout the first 80% of the first charge.

Both the capacity fade and the consumption of FEC were shown to have a time dependence and a cycle number dependence. The time dependence was proportional to the square root of time consistent with the SEI thickening at the surface of the graphite and Si-alloy particles. The cycle number dependence was consistent with the SEI fracturing at the surface of the Si-alloy particles due to volume changes upon lithiation and delithiation. A simple model describing the consumption of FEC as a function of time and cycle number predicted the depletion of FEC and associated sudden cell failure within 20 cycles of the real value. This model indicated that the cycle number dependence of the consumption was the main contribution to the consumption of FEC.

EIS on symmetric cells showed (see Figure E3 of Appendix E) that while the impedance of the Si:graphite composite electrode varies only slightly during cycling (prior to sudden failure), the impedance of the LCO electrode increases in a rapid manner. This showed that FEC-containing electrolytes are not best suited for cells using an LCO electrode with the charge cut-off voltages used in this study.

As a whole, the results presented here show that new electrolyte systems have the potential to dramatically improve the performance of Si-based negative electrodes in

commercial Li-ion cells. These should be electrolytes that provide good passivation of the graphite and Si-based particles in order to limit the time dependence of the fade. If FEC is to be used, the other components of the electrolyte should limit the consumption of FEC in order to delay the sudden failure. In a full cell configuration, the electrolyte should not only limit the reduction of the electrolyte at the negative electrode but also limit the oxidation at the positive electrode. This is required in order to obtain cells with long life-time [5]. The new electrolytes should then also provide good passivation to the positive electrode with stable impedance and low electrolyte oxidation.

The results presented in this study also show the importance of studying Si-based electrodes in a full cell configuration with an electrolyte-to-active material mass ratio close to commercial cells. In a half cell configuration, the fade of the Si-based electrode is less pronounced than in a full cell configuration. The use of coin cells where the volume of electrolyte used is large compared to the active mass of the electrode would not demonstrate the sudden failure associated with the depletion of FEC.

CHAPTER 8. DESIGN OF NEW ELECTROLYTE SYSTEMS⁵

8.1 Ester-based electrolytes

Most electrolytes for Li-ion cells use a mixture of EC (and occasionally PC) and other linear organic carbonates such as DEC, EMC, or DMC with LiPF_6 as the conductive salt (see Section 1.2.2). The use of such electrolytes, in combination with small weight percentages of electrolyte additives can yield quite long lived cells [2] with low parasitic currents when cycled up to 4.2 V [16,268]. However, the presence of EC increases the viscosity of the electrolyte (see Table 8.1 for the viscosities of some pure solvents) which lowers its conductivity compared to EC-free electrolytes, especially at low temperatures. The electrolyte conductivity can still be tuned to some extent by using higher weight fractions of low viscosity linear carbonate co-solvents as demonstrated by Smart *et al.* [269].

In order to further lower the viscosity of EC-based electrolytes, co-solvents having even lower viscosity than linear carbonates have been used. For instance, Smart *et al.* [45,270] demonstrated that the use of low molecular weight organic esters in EC:DMC:DEC:ester quaternary solvent blends improved the electrolyte conductivity (especially at low temperature) compared to ternary EC:DMC:DEC blends. They also showed that the resistivity and the stability of the SEI films created by the addition of esters depended on the ester introduced. Sazhi *et al.* [271] also developed electrolytes

⁵ Some of the results presented in this Chapter were published in R. Petibon, J. Harlow, D.B. Le, J.R. Dahn, *Electrochimica Acta*. 154 (2015) 227–234 for which the candidate wrote the first draft of the entire manuscript. The contribution of the co-authors (other than the candidate) is indicated in the captions of the figures where appropriate.

containing ternary solvent blends with EC:EMC:ethyl propanoate (EP) and EC:DEC:EP. Even though the electrolyte conductivity was greatly enhanced, these electrolyte blends still contained 20 - 30 % of EC.

Table 8.1. Physical characteristics of selected organic carbonates and esters. Data were compiled from Ref [1] (a), [272] (b) and [273] (c).

Chemical name	Abbreviation	Viscosity at 25°C /cP	Melting point /°C	Boiling point /°C
Ethylene carbonate	EC	1.86 (40°C) ^a	39 ^a	248 ^a
Propylene carbonate	PC	2.5 ^a	-48 ^a	242 ^a
Diethyl carbonate	DEC	0.75 ^a	-43 ^a	126 ^a
Ethyl methyl carbonate	EMC	0.65 ^a	-55 ^a	109 ^a
Dimethyl Carbonate	DMC	0.59 ^a	4 ^a	90 ^a
Ethyl acetate	EA	0.441 ^b	-84 ^b	77 ^b
Methyl propanoate Also known as Methyl propionate	MP	0.43 ^c	-87 ^b	80 ^b

The inability of most solvents to form a protective layer at the surface of graphite requires the use of additives if no EC is added. Several researchers, for example, used additives that are known to form surface films at the lithiated graphite surface to design new solvents blends. Ein-Eli *et al.* [274] showed that the addition of SO₂ allows the use of different single solvents such as methyl formate, propylene carbonate, DMC and DEC with graphite, without the use of EC. In another instance, Zhang *et al.* [91] showed that the use of 5% VC in PC allows graphite to be cycled without any EC. Many other examples have been presented in detail in other references [4,145,165,275–279].

Based on the previous studies mentioned above, low molecular weight esters such as ethyl acetate (EA) and methyl propanoate (MP) are good solvent candidates from an electrolyte conductivity standpoint. The use of known film forming additives in combination with these esters should make such blends suitable for their use in Li-ion cells with a lithiated graphite negative electrode. Table 8.1 lists some physical characteristics of common cyclic and linear organic carbonates and two organic esters (ethyl acetate and methyl propanoate, also called methyl propionate). Table 8.1 shows that the two esters have lower viscosity and lower melting point than any of the linear carbonates. This makes them suitable for low temperature applications. For instance, Figure 8.1 shows the conductivity as a function of temperature for various esters to which 1M LiPF₆ has been added. Figure 8.1 shows that methyl acetate (MA), EA and MP solutions have better conductivity than 1M LiPF₆ EC:EMC (3:7) solution at temperatures below 30°C.

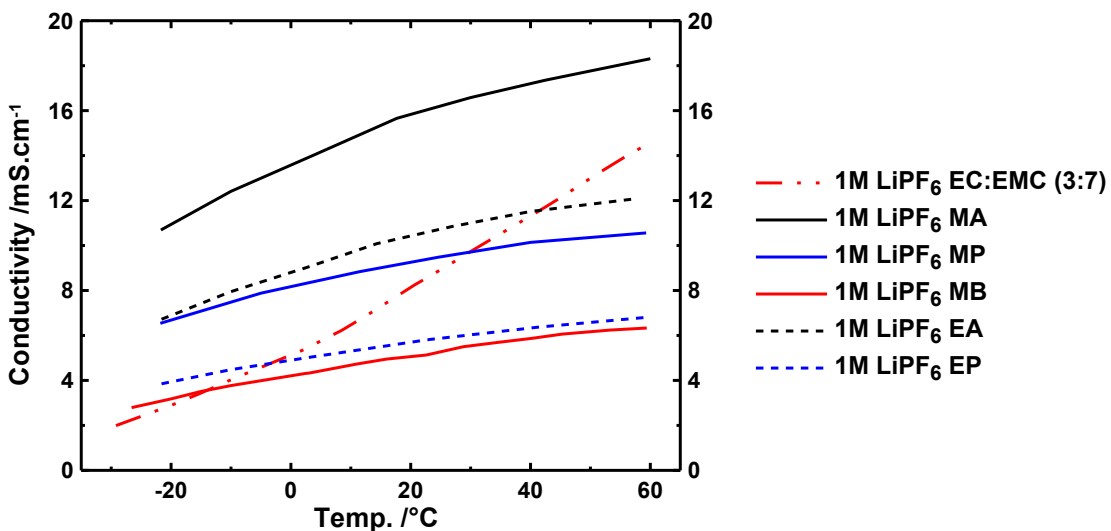


Figure 8.1. Conductivity vs. temperature for various esters containing 1M LiPF₆.

The additive VC is a very well-known and extensively studied additive [3,91,111,127,143,161,190–192,203,212,275,280–283] (see Section 2.3). It has been shown to form an SEI film at the lithiated graphite surface which enables the use of PC-based electrolytes without any EC. It then stands to reason that electrolytes consisting of a blend of an ester with VC should be kinetically stable against lithiated graphite and should show good rate performance at low temperature.

8.1.1 Formation of NMC/graphite cells filled with ester-based electrolytes

Figure 8.2 shows the cell voltage vs. capacity (a) and differential capacity vs. cell voltage (b) for the first charge to 3.5 V of 220 mAh NMC(111)/graphite pouch cells filled with

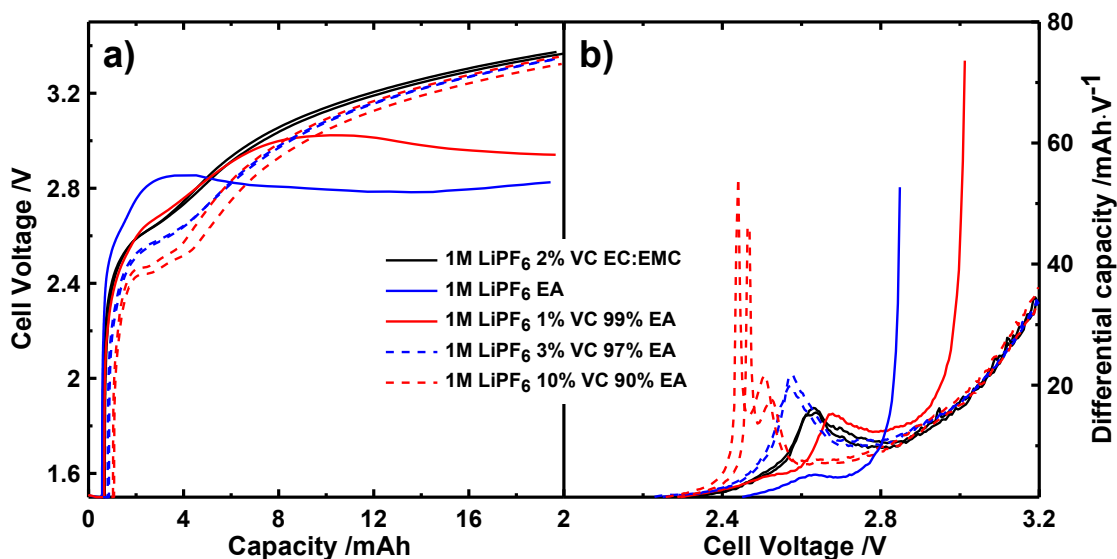


Figure 8.2. Cell voltage vs. capacity (a) and differential capacity vs. cell voltage (b) during the first charge of NMC(111)/graphite pouch cells filled with ester-based electrolytes with or without VC. Cells containing 1M LiPF₆ EC:EMC (3:7) + 2% VC are shown in each panel for comparison. Cells were charged at a current of C/20 and 40°C. Some of the ester-containing cells were prepared by Lina Rotermund, 2nd year B.Sc. student, Physics & Atmospheric Science, Dalhousie University (2014).

with 1 M LiPF₆ in EC:EMC + 2% VC or various ester-based electrolytes with or without VC. Cells filled with an EC-based electrolyte show the expected voltage-capacity curve and differential capacity curve for an NMC(111)/graphite pouch cell filled with an electrolyte containing compounds providing a passivating layer on the graphite electrode surface. That is, cells show a rapidly increasing voltage profile from 0 V to around 3 V followed by a short plateau (peak in the differential capacity plot), followed by a gradually increasing voltage between 3 V and 3.5 V (end of the first formation step). The length of the plateau around 3 V in the voltage vs. capacity plot depends on the amount of passivating agent reduced to provide a satisfactory graphite passivation. The voltage at which this plateau occurs depends on the reduction potential of the passivating agent. In the case of Figure 8.2, in cells containing an EC-based electrolyte containing VC, VC is the passivating additive with a reduction potential around 0.9 V vs. Li/Li⁺ (full cell voltage of around 2.6 V) [3,205,215]. Figure 8.2 shows that cells containing esters without VC never reach voltages above 3.2 V. This is because the graphite electrode is never passivated and the solvent is continuously being reduced. Cells were filled with other esters (MA, MP, MB, and PA) and did not show any signs of graphite passivation either (see Figure F1 of Appendix F).

Figure 8.2 shows that the addition of more than 1% VC to cells containing an EA-based electrolyte do reach voltages above 3.2 V. These cells also have a differential capacity peak at a cell voltage close to that of cells filled with an EC-based electrolyte containing VC. This peak then most likely corresponds to the reduction of VC at the partially lithiated graphite surface. The voltage at which this peak occurs shifts to lower cell voltage (higher graphite potential) with higher VC contents, consistent with that of

cells filled with EC-based electrolytes containing VC as presented by Petibon *et al.* [215]. Figure 8.2 also shows that cells containing 1% VC in EA show a sharp rise in the differential capacity plot around 3 V. This corresponds to the reduction of EA (see Figures 8.2a and 8.2b). This indicates that there is a minimal initial VC loading necessary to properly passivate the graphite surface. In the cells used here, this minimal amount seems to lie between 1% and 3% VC.

8.1.2 Reduction mechanism of various esters

In order to assess the reduction mechanism of esters at the graphite surface, NMC/gr cells were filled with various additive-free ester-based electrolytes and charged to a fixed capacity. The gas produced in these cells was then analyzed by GC-MS using

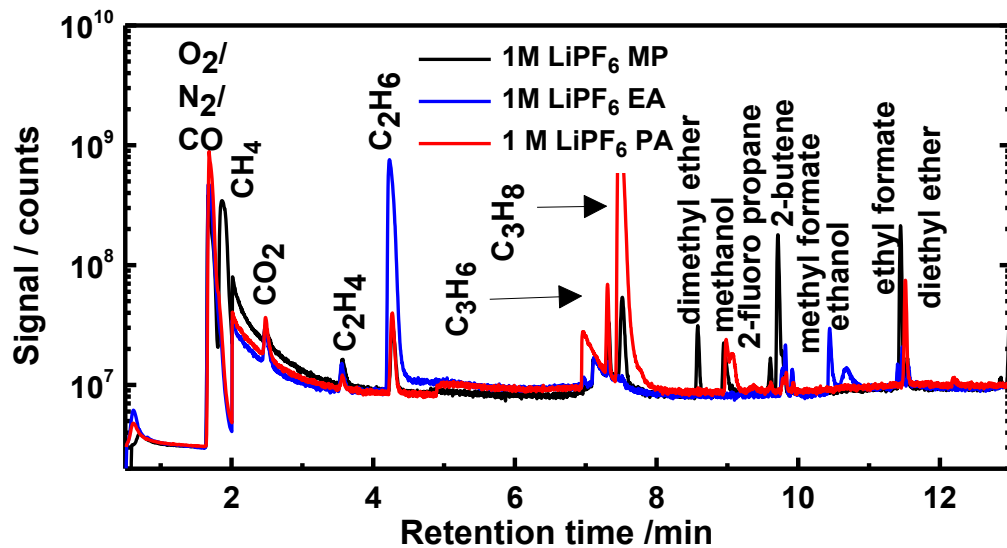


Figure 8.3. Chromatogram (total ion counts) of the gas extracted from NMC(111)/graphite pouch cells containing various ester-based electrolytes and charged to 20 mAh at C/20 and 40°C. Cells were prepared and the gas analyzed by Lina Rotermund, 2nd year B.Sc. student, Physics & Atmospheric Science, Dalhousie University (2014).

the method described in Section 4.3. Figure 8.3 shows the chromatogram of the gas analyzed by GC-MS from cells filled with MP-based, EA-based and propyl acetate (PA)-based electrolytes. These experiments were repeated with cells filled with methyl acetate (MA)-based and methyl butyrate (MB)-based electrolytes (see Figure F2 of Appendix F).

Figure 8.3 shows that the main gas produced in cells containing MA is methane while the main gas produced in cells containing EA is ethane and the main gas produced in cells containing PA is propane. The main gas produced in cells containing MP and MB-based electrolytes was methane (see Figure F2 of Appendix F). This strongly suggests that the main reduction pathway of these esters results in the cleavage of the oxygen-carbon bond of the alkoxide part of the ester functional group. The presence of methanol and dimethyl ether in cells containing MA, MP, and MB also suggests that the

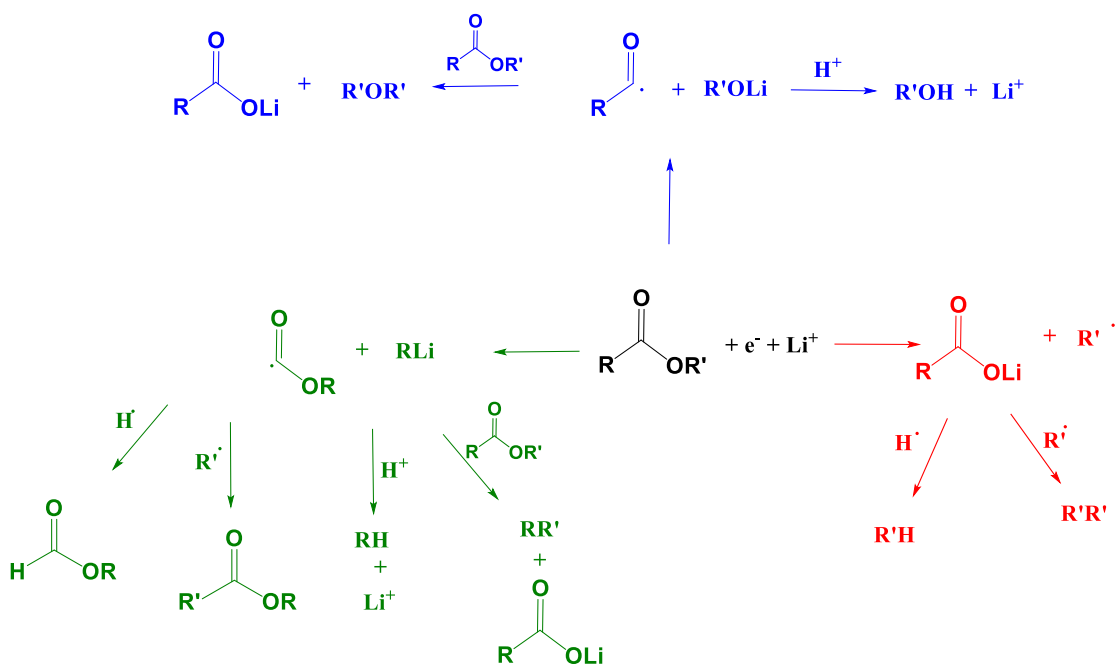


Figure 8.4. Proposed reduction pathways for organic esters at the graphite surface and subsequent reactions of the reduction by-products. The pathways proposed are based on the results of the gas analysis presented in Figure 8.3 and Figure E1.

reduction of esters can also lead to the cleavage of the carbon-oxygen bond of the carbonyl part of the ester functional group. The presence of ethyl or methyl formate also indicates that esters can follow a third reduction pathway. Figure 8.4 shows proposed reduction mechanisms and reaction pathways of the various by-products which account for the presence of aliphatic gases, alcohols, ethers, and formates.

Based on the results presented in Figure 8.2, it is clear that the various by-products resulting from the reduction of esters are non-passivating. It is likely that the various lithium carboxylates and other CO_2R -type radicals are too soluble in esters to precipitate at the surface of the graphite electrode and prevent further solvent reduction.

8.1.3 High precision coulometry measurements of cells filled with ester-based electrolytes

In order to compare ester-based electrolytes to EC-based electrolytes, NMC(111)/gr cells were filled with various electrolyte blends and cycled on the UHPC (see Section 3.2.2). Figure 8.5 shows a summary of the charge end-point capacity slippage (a) and coulombic inefficiency (CIE, $\text{CIE}=1-\text{coulombic efficiency}$, b). In an earlier publication, Burns *et al.* [5] showed that cells with lower CIE and charge endpoint capacity slippage generally have longer cycle life. In other publications they showed that NMC/gr cells containing VC had low CIE and low charge slippage compared to cells without additive [143,172]. They then suggested that comparing new electrolyte blends destined for cells operated to 4.2 V and below to cells containing an EC-based electrolyte and VC present a fair comparison as opposed to comparing it to an electrolyte without

additive. For this reason, the performance of cells filled with various ester-based electrolytes was compared to cells filled with an EC-based electrolyte containing 2% VC.

Figure 8.5a shows that cells filled with 1M LiPF₆ in MP:VC (95:5) or 1M LiPF₆ in MB:VC (95:5) have charge endpoint capacity slippage that is very similar to cells containing EC:EMC + 2% VC electrolyte. This indicates that parasitic currents due to electrolyte oxidation in MP + VC and MB + VC-based electrolytes are of similar magnitude compared to those in cells filled with 1M LiPF₆ EC:EMC + 2% VC electrolytes.

Figure 8.5b shows that cells with MP:VC (95:5) or MB:VC (95:5) electrolytes have a CIE that is on par with the CIE of cells filled with EC:EMC + 2% VC. Figure 8.5b also shows that cells filled with EA:VC (95:5) have higher CIE compared to cells

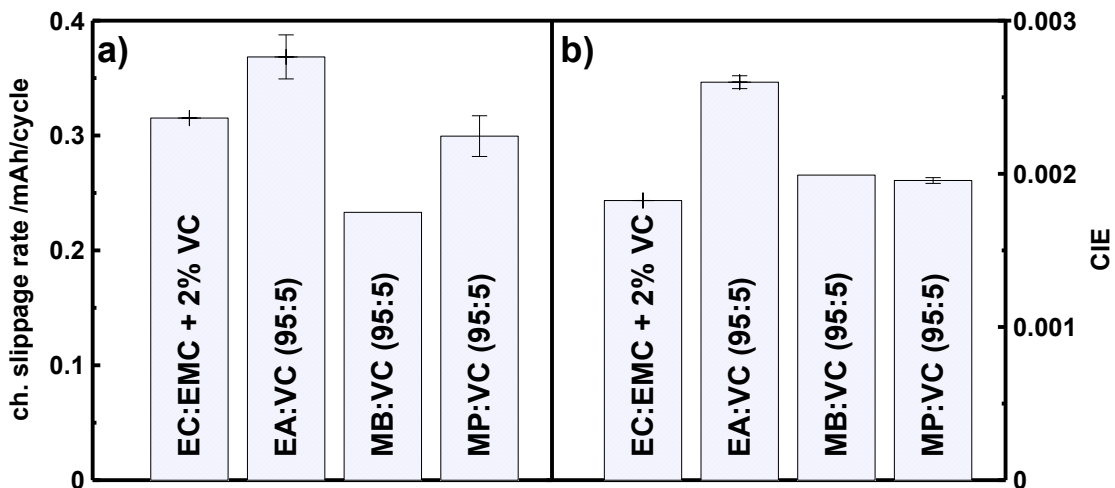


Figure 8.5. Charge endpoint capacity slippage rate (a) and CIE (b) of NMC(111)/graphite pouch cells containing various electrolytes and cycled between 2.8 – 4.2 V at C/20 and 40°C. The charge endpoint capacity slippage rate was calculated based on the slope of the charge endpoint capacity vs. cycle number of the cycles 11-15 and the CIE was calculated as the average of the CIE of the data points of cycles 11-15, and. Cells were prepared by Lina Rotermund, 2nd year B.Sc. student, Physics & Atmospheric Science, Dalhousie University (2014).

filled with MB:VC or MP:VC (95:5). Since the charge endpoint capacity slippage is comparable between EA:VC and MP:VC electrolytes, this indicates that the electrolyte reduction is more severe in cells with an EA:VC electrolyte. This shows that even though these three electrolyte blends are very similar (same additive loading, same chemical nature of solvent), the parasitic reactions are different. Figure 8.5 implies that cells filled with MP:VC or MB:VC (95:5) have parasitic reactions at both the positive electrode and negative electrode very similar to cells filled with EC:EMC + 2% VC. This indicates that the MP:VC or MB:VC (95:5) blends are competitive electrolytes in terms of electrolyte degradation rate, compared to EC-based electrolyte with 2% VC, at least at 40°C and 4.2 V.

8.1.4 Long term cycling of cells filled with ester-based electrolytes

Figure 8.6 shows the discharge capacity of NMC(111)/gr cells filled with MP-based electrolytes with 5% or 10% VC during cycling at 40°C and C/5 between 2.8 - 4.2 V. All electrolytes contained 1M LiPF₆. Only every second cycle is shown for clarity. The discharge capacity vs. cycle number plot for cells filled with EA-based electrolytes is shown in Figure F3 of Appendix F.

Figure 8.6 shows that cells with MP:VC (95:5) [the pair cell that showed erratic discharge capacity values had connection problems] have very similar capacity retention compared to cells filled with EC:EMC + 2% VC, which is consistent with the CIE and charge endpoint capacity slippage data presented in Figure 8.5. Figure 8.6 also shows that cells with MP:VC (90:10) have a higher fade rate than cells containing only 5% VC. Based only on discharge capacity data, it is not possible to tell if this higher fade rate is

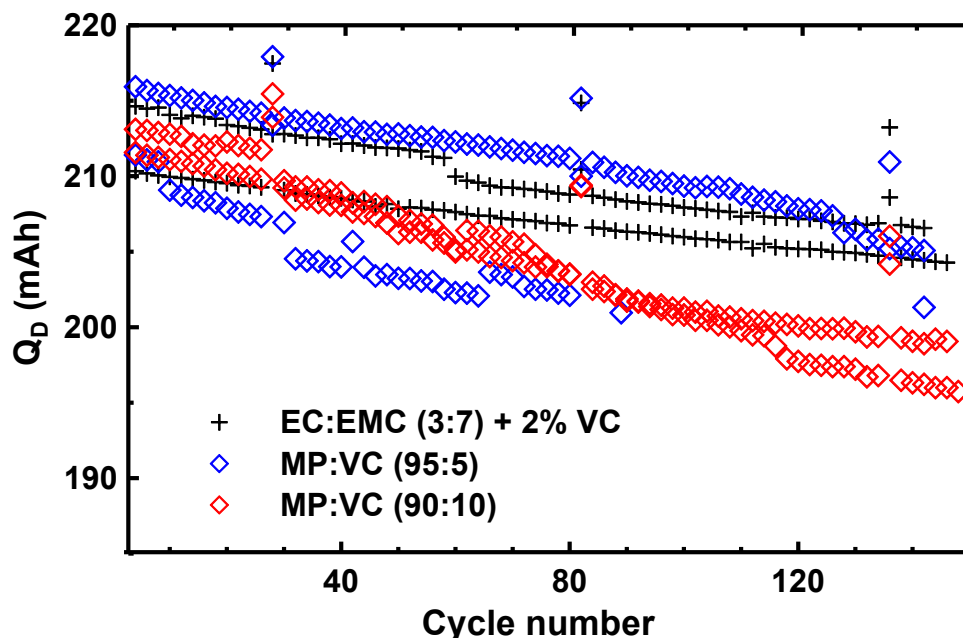


Figure 8.6. Discharge capacity vs. cycle number of 240 mAh NMC(111)/graphite pouch cells filled with 1M LiPF₆ x% MP + 100-x% VC electrolytes, cycled at C/5 between 2.8 V and 4.2 V at 40°C. Only every second cycle is shown for clarity. A cycle at C/20 was performed every 20 cycles. The discharge capacity vs. cycle number of cells filled with 1M LiPF₆ EC:EMC + 2% VC is shown in each panel for comparison. Cells were cycled without clamps.

due to electrolyte reduction, polarization growth, or loss of stack pressure due to gas formation. Figures 8.6 clearly shows that with the proper amount of VC, esters such as MP and EA (see Figure F3 of Appendix F) can be used as EC-free solvents and can yield impressive capacity retention, even after 1700 h of cycling at 40°C.

Figure 8.7 shows the impedance spectra (a) and gas volume formed (b) after 1700 h of cycling at 40°C and between 2.8 – 4.2 V for NMC(111)/gr cells containing MP-based electrolytes. Data for cells filled with EA-based electrolytes containing VC are presented in Figure F4 of Appendix F. Figure 8.7 shows that cells with the highest VC loadings (10% VC in MP) had the largest impedance and generated the largest volumes of gas which might explain their higher capacity fade. This is consistent with cells filled

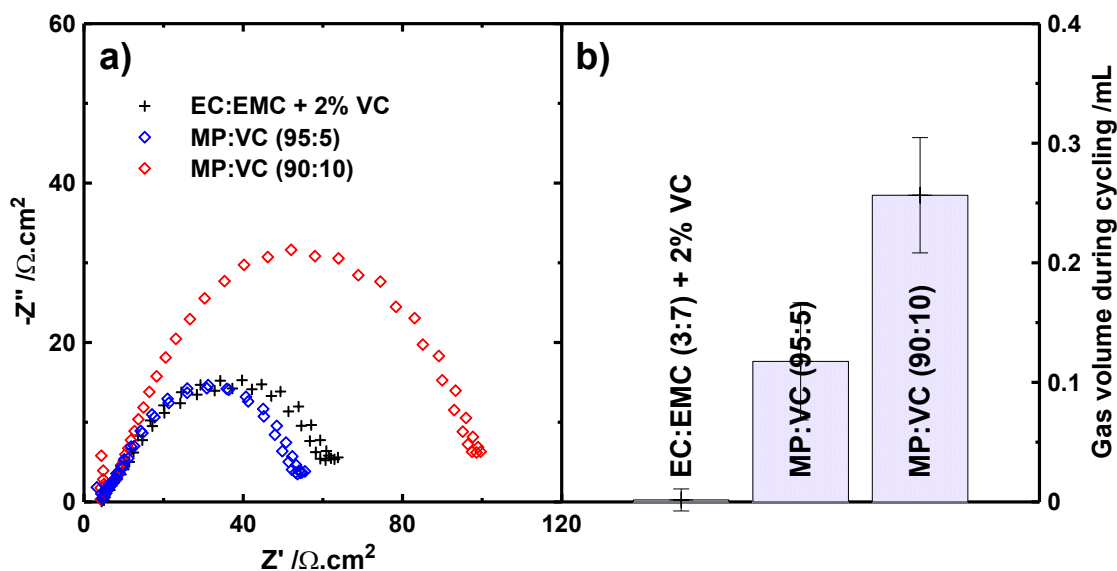


Figure 8.7. Impedance spectra (a) and gas volume formed (b) for 240 mAh NMC(111)/graphite pouch cells filled with 1M LiPF_6 x% MP + 100-x% VC electrolytes, cycled at C/5 between 2.8 V and 4.2 V at 40°C for 1700 h. Data for cells filled with 1M LiPF_6 EC:EMC + 2% VC is shown in each panel for comparison. Impedance spectra were measured at a cell voltage of 3.80 V and at 10°C.

with EC-containing electrolytes with increasing amounts of VC, as shown in Section 5.2. This gas generation might also explain, in part, the higher capacity fade of cells containing 10% VC. Gas generation reduces the stack pressure that the jelly roll is subjected to which hinders the use of all the active material. This effect is even more severe when using medium to high rates (cells were not clamped here). The cells shown in Figures 8.6 and 8.7 were subjected to C/5 rates. Figure 8.7 shows that cells filled with electrolyte consisting of 5% VC in MP or EA (see Figure F4 of Appendix F) produced relatively small gas volumes after 1700 h of cycling at 40°C especially considering the small passivating agent loading and the absence of EC. This gas volume might not be manageable for cells with soft enclosures such as pouch cells, but should be manageable

for cells with metal casings such as 18650 type cells. It is also likely that the gas volume produced can be minimized by optimizing the initial VC loading.

Comparing Figures 8.7a and F4a shows that cells filled with MP-based electrolytes have lower impedance than cells filled with EA-based electrolytes, at equivalent VC loading. This indicates that the film created by VC + MP at the surface of either the positive electrode or the negative electrode (or both) is less resistive to Li^+ transfer than the film created by VC + EA. Figure 8.7a also shows that cells filled with 5% VC + 95% MP have lower impedance than cells filled with EC:EMC + 2% VC. This is somewhat surprising since Section 5.2 showed that increasing VC loading (above 2%) leads to increasing impedance in EC-based electrolytes. This suggests that the SEI created by VC is slightly different in ester-based solvents than in EC-based solvent blends. However, the effect of VC loadings in ester-based electrolytes seems to be the same as in EC-based electrolytes. That is, higher VC loadings lead to higher impedance and higher gas generation during cell operation.

Figure 8.8 shows the amount of VC consumed (a) and the amount of VC remaining (b) in 240 mAh NMC(111)/graphite pouch cells filled with various MP:VC and EA:VC-based electrolytes, after 1700 h of cycling at C/5 between 2.8 V and 4.2 V at 40°C. Figure 8.8 shows that cells filled with 10% VC have a larger amount of VC consumed compared to cells filled with 5% VC for both EA and MP-based electrolytes. Section 5.2 showed that the impedance of cells filled with EC-based electrolyte was roughly proportional to the amount of VC consumed. It seems that this phenomenon is similar for cells containing ester-based electrolytes with increasing VC loading. Figure 8.8 also shows that cells filled with MP have lower amounts of VC consumed than cells

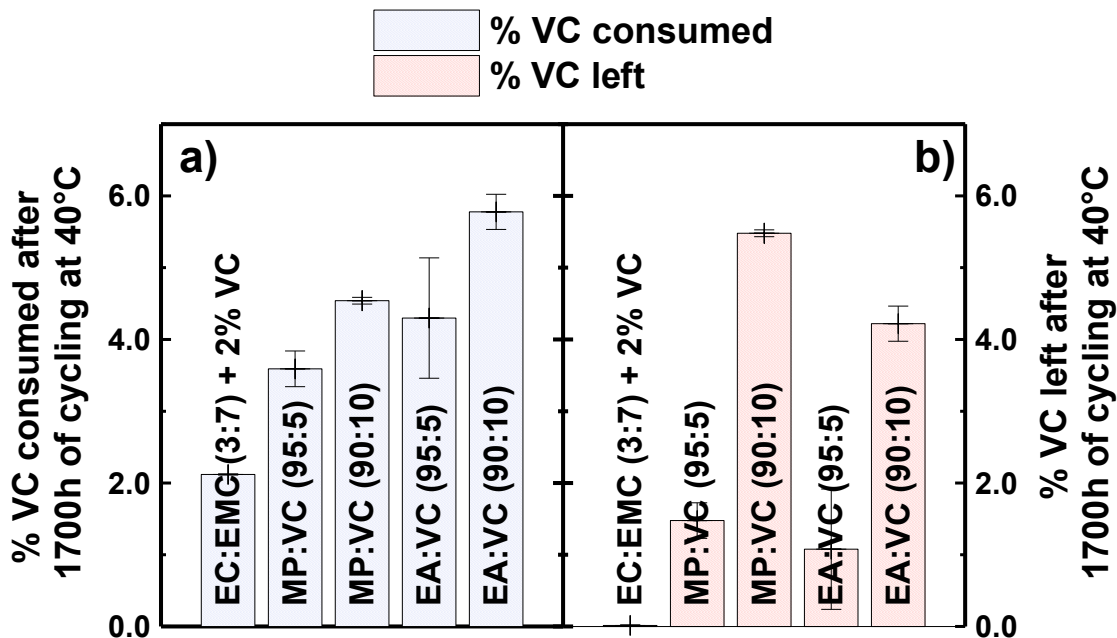


Figure 8.8. Amount of VC consumed (wt.% of total weight of EA + VC, or MP + VC, a), and amount of VC left (b) in 240 mAh NMC(111)/graphite pouch cells filled with electrolytes filled with various MP + VC electrolyte blends, after 1700 h of cycling at C/5 between 2.8 V and 4.2 V at 40°C.

with EA, at equivalent initial VC loading. This might explain why cells with MP have generally lower impedance than cells with EA.

Figure 8.8 also shows that cells filled with MP:VC (95:5) have twice as much VC consumed as cells filled with EC:EMC + 2% VC even though they have lower impedance. This seems to indicate that the impedance of the SEI film created by VC depends strongly on the solvent present. It also might indicate that EC, EMC, MP and EA participate in the formation of the SEI film, although it is not apparent on the differential capacity vs. cell voltage plot during the first charge of the cell (see Figure 8.9). Kang Xu *et al.* [284] showed that the impedance of Li-ion electrodes is also highly dependent on the desolvation energy of Li^+ . It is then also possible that the lower impedance of cells filled with ester-based electrolytes at equivalent VC consumption comes from a

difference in desolvation energy of Li^+ between an EC-based electrolyte and an ester-based electrolyte.

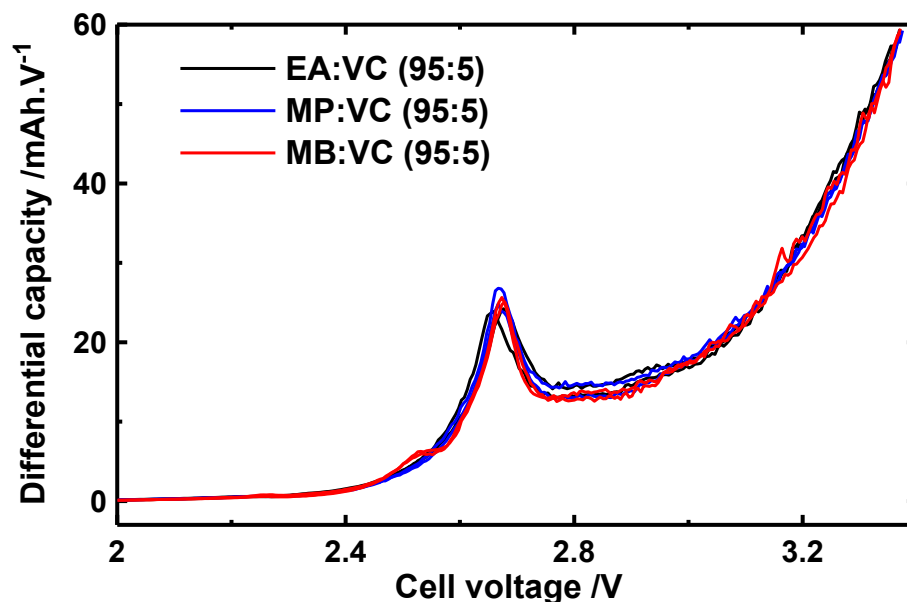


Figure 8.9. Differential capacity vs. cell voltage during the first charge to 3.5 V at 40°C and C/20 of 220 mAh NMC(111)/graphite pouch cells filled with various ester:VC blends. All blends contained 1M LiPF_6 .

8.1.5 Low temperature rate performance of cells filled with ester-based electrolytes

Figure 8.10 shows the discharge energy at -14°C at various currents of 240 mAh NMC(111)/graphite pouch cells previously cycled at C/2 at 40°C for 1700 h and filled with either EC:EMC + 2% VC or MP:VC (95:5) electrolytes. All electrolytes contained 1M LiPF_6 . This temperature was chosen to evaluate the low temperature rate performance of both electrolyte systems. In order to avoid lithium plating, the charge current was kept at C/40. Figure 8.10 shows that cells filled with MP:VC (95:5) have

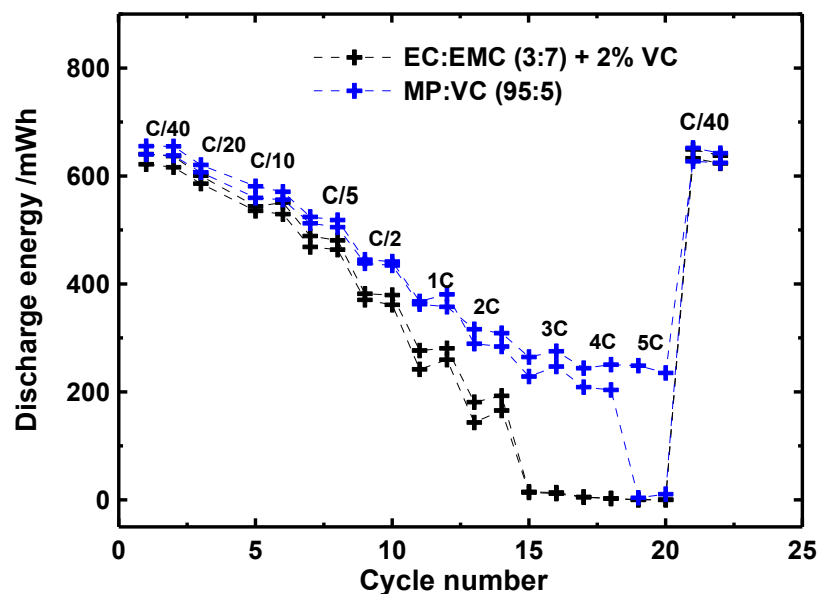


Figure 8.10. Discharge energy at -14°C and various rates of 240 mAh NMC(111)/graphite pouch cells previously cycled at C/2 at 40°C and filled with either 1M LiPF_6 EC:EMC + 2% VC or 1M LiPF_6 MP:VC (95:5) electrolytes. All charges were performed at C/40. Duplicate cells are shown for all electrolyte blends.

better rate capability than cells filled with EC:EMC + 2% VC at -14°C , from currents corresponding to C/2 up to currents corresponding to 4C, even after 1700 h of cycling at 40°C . Figure 8.10 shows that while cells filled with the EC-based electrolyte failed to deliver any energy starting from 3C, cells filled with the ester-based electrolyte delivered up to 40% of the discharge energy (as measured at C/40 and -14°C) at 4C. This clearly shows the advantage of using electrolyte blends that use only solvents with low viscosity.

8.1.6 High temperature performance of cells filled with ester-based electrolytes

Figure 8.11 shows the discharge capacity of NMC(111)/gr cells filled with various electrolytes and cycled at 55°C between 2.8 – 4.2 V at C/10. Figure 8.11 shows that cells filled with a 1M LiPF₆ MP:VC (95:5) electrolyte have very poor capacity retention when cycled at high temperature compared to cells filled with an EC-based electrolyte containing VC. In an earlier publication, Wang *et al.* [166] showed that the addition of LiFSi (Figure 1.4 shows the structure of LiFSi) improved the high temperature performance of NMC/gr cells filled with EC-based electrolytes and operated to 4.2 V. In an attempt to improve the high temperature performance of cells filled with

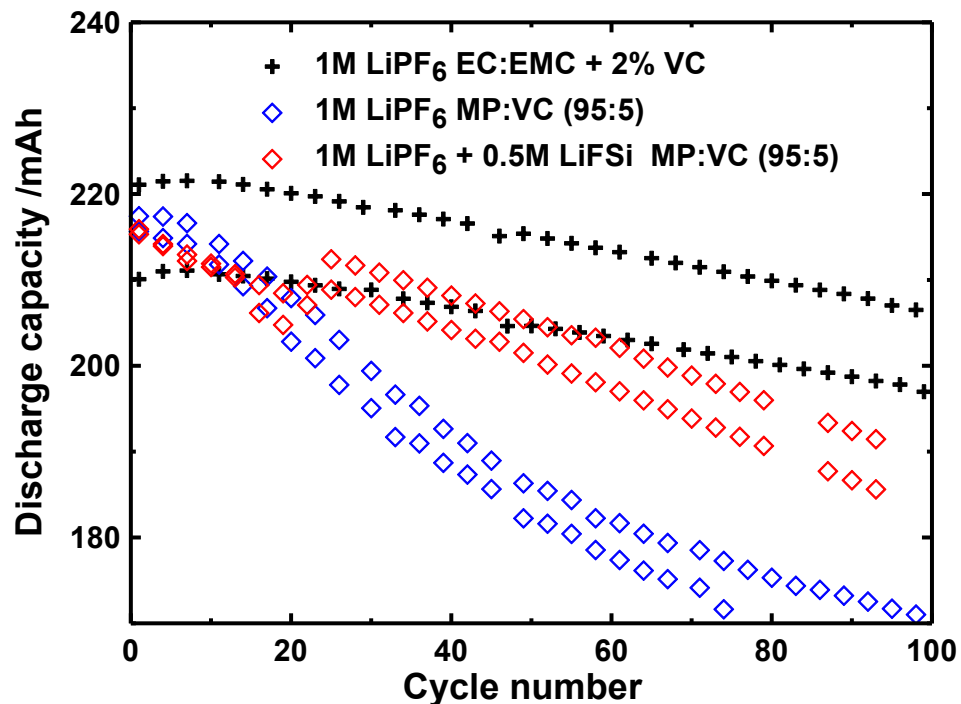


Figure 8.11. Discharge capacity of NMC(111)/graphite pouch cells filled with various electrolyte blends and cycled between 2.8 – 4.2 V at 55°C and C/10. Cells underwent a 800 h open circuit voltage period at 40°C and 4.2 V prior to cycling at 55°C.

ester-based electrolytes, electrolytes based on LiPF_6 , LiFSi, MP and VC were formulated and tested. Similar MB-based electrolytes were tested for which data are presented in Figure F5 of Appendix F. Figure 8.11 clearly shows that the addition of LiFSi greatly improves the capacity retention of NMC/gr cells filled with MP:VC (95:5) electrolytes and cycled to high temperature. A similar trend was observed for cells filled with MB-based electrolytes (see Figure F5). Moreover, the addition of LiFSi enhances the conductivity of MP-based and MB-based electrolytes (see Figure F6 of Appendix F). Even though the capacity retention at high temperature is improved, it is still worse than that of cells filled with the EC-based electrolyte containing VC. This indicates that further VC loading optimization is necessary. It might very well be that the addition of co-additives would also improve the high temperature cycle-ability of cells filled with ester-based electrolytes. For instance, the addition of small quantities of PES to 1M LiPF_6 MP:VC-based electrolyte proved to greatly improve the capacity retention of NMC/gr cells cycled at 40°C (see Figure F7 of Appendix F). It is then possible that adding both LiFSi and PES to ester-based cells would yield NMC/gr cells with ester-based electrolytes with capacity retention at high temperature similar to that of cells filled with EC-based electrolytes containing VC.

8.1.7 Other passivating agents allowing the use of esters

In order to assess whether other additives could act as passivating agents in ester-based electrolytes, NMC(111)/gr cells were filled with electrolytes containing 1M LiPF_6 in various esters to which 10% of a variety of additives were added (Figure F8 of

Appendix E shows the name and structure of the additives tested). Figure 8.12 shows the cell voltage vs. capacity during the first charge to 3.8 V at 40°C.

Figure 8.12 shows that at 3.5 V, cells show a voltage drop followed by a voltage increase. The voltage drop is due to the degassing step. At 3.5 V, cells were removed from the charger, their volume measured and degassed before being put back on the charger again. A large voltage drop indicates substantial lithium loss from the graphite electrode due to reduction of the electrolyte [at low lithiation state the potential of the graphite electrode increases with decreasing Li content causing the full cell voltage to decrease, see Figure 1.3]. A cell with a well passivated graphite electrode typically has a voltage drop smaller than 100 mV. Figure 8.12 shows that out of the eight additives

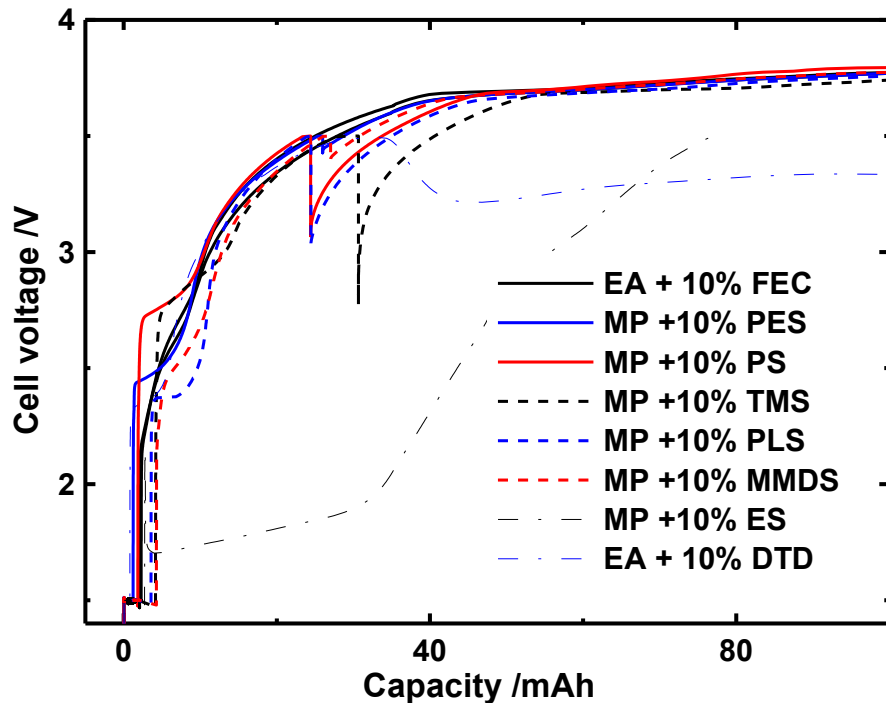


Figure 8.12. Cell voltage vs. capacity during the first charge at 40°C and C/10 of NMC(111)/graphite pouch cells filled with ester-based electrolytes containing various additives. All electrolytes containing 1.2 M LiPF_6 . Some of the cells were prepared by Lina Rotermund, 2nd year B.Sc. student, Physics & Atmospheric Science, Dalhousie University (2014).

tested only three provide a low cell voltage drop during the degassing step. These additives are FEC, PES and MMDS. Cells containing DTD and ES never reached 3.5 V indicating that they did not provide any kind of passivation. Cells with PS, TMS, and PLS did reach 3.5 V. This indicates that these three additives provided some kind of passivation. However, the voltage drop during the degassing step indicates that this passivating layer still allows substantial solvent reduction. These additives are then not good passivating agents on their own.

The results presented in Figure 8.12 are quite important. For instance, Wrodnigg *et al.* [4,277] and Zuo *et al.* [156] showed that both ES and PS are passivating additives in carbonate-based electrolytes. The fact that these additives do not provide sufficient passivation in ester-based electrolytes indicates that either the passivation of the graphite surface in presence of ES or PS requires the co-reaction of organic cyclic carbonates, or that esters can permeate through the layer resulting from the reduction of these additives.

While PES and MMDS seemed to be good passivating agents, a 10% loading leads to cells with very high impedance (see Figure F9 of Appendix F). Their loadings would then need to be optimized to give proper graphite passivation while keeping the cell impedance low.

8.1.8 Performance of ester-based electrolyte in cells operated to 4.3 V

Table 8.2 shows the volume of gas produced in NMC(111)/gr cells containing a 1 M LiPF₆ + 0.5 M LiFSi MP:VC (95:5) electrolyte stored at 40°C at an open circuit voltage of 4.2 V or 4.3 V. Table 8.2 shows that the gas volume produced during storage at 4.3 V is 6 - 7 times greater than the volume produced during storage at 4.2 V. This

Table 8.2. Gas volume produced in NMC(111)/graphite pouch cells containing a 1M LiPF₆ + 0.5 M LiFSi MP:VC (95:5) electrolyte stored for 800h at open circuit and 40°C.

Storage voltage	Gas volume during 800 h of storage /mL
4.2 V	0.09 ± 0.01
4.3 V	0.66 ± 0.05

indicates that ester-based electrolytes might not be suitable for high voltage operation. This might be due to either the oxidative instability of esters as reported by Smart *et al.* [45] or due to the oxidation of the VC remaining in the electrolyte (see Chapter 5).

8.1.9 Concluding remarks on ester-based electrolytes

EC-free electrolytes using esters such as MP, EA or MB in combination with VC have been shown to function well in Li-ion cells. A minimum amount of VC was required in order to partially passivate the lithiated graphite against ester reduction. In the cells used here, this minimum seemed to lie between 1% and 3%.

High precision measurements, long term cycling at 40°C, impedance measurements and a rate capability evaluation at -14°C showed that MP:VC (95:5) was competitive with EC:EMC + 2% VC electrolyte, if not better. High precision coulometry measurements showed that MP:VC (95:5) and MB:VC (95:5) electrolytes had parasitic currents due to SEI growth and electrolyte oxidation very close to those in EC:EMC + 2% VC electrolytes. These particular ester-based electrolytes also had similar capacity retention at 40°C, slightly better impedance, and far better rate capability at -14°C than EC:EMC + 2% VC electrolyte. The high temperature performance of these ester-based

blends was shown to be quite poor. However, the addition of LiFSi greatly improved the capacity retention of cells containing these EC-free blends when cycled at 55°C.

High precision coulometry also showed the CE depended on the ester used at an equivalent VC loading. Long term cycling showed that cells with ester-based electrolytes with 10% VC had worse capacity retention than cells with ester-based electrolytes with 5% VC. This increased capacity fade with increased VC content seemed to come from a combination of impedance growth and stack pressure loss due to gas generation.

Electrolyte characterisation by GC-MS showed that while cells with MP:VC (95:5) electrolytes had a larger amount of VC consumed after 1700 h of cycling compared to EC:EMC + 2% VC, their impedance was slightly lower. This indicated that the amount of VC consumed does not dictate the impedance of a cell if electrolytes with different chemical classes of solvents are compared.

Cells containing ester-based electrolyte stored at 4.3 V produced large amounts of gas compared to cells stored at 4.2 V. This indicated that ester-based electrolyte might not be suitable for high voltage operation or that the amount of VC should be optimized or other passivating agent used.

This work shows that ester based solvents can be used without any EC, as long as enough VC is added. However EC could also be added to the mixtures if tuning of properties was desired. The work by Smart *et al.* [45,270,285] showed the advantages of adding esters to EC-containing electrolytes, but the ester content was not increased beyond 60%. The work here shows that the ester content can be as large as 95% even if no EC is used. This gives more flexibility in electrolyte design for Li-ion cells destined for various applications.

8.2 Linear alkyl carbonate-based electrolytes

Typical layered materials used in commercial cells are not used through their entire potential range of structural stability. For instance, NMC(442) material is used with a potential cut-off of 4.28 V vs. Li/Li^+ despite being structurally stable up to 4.78 V vs. Li/Li^+ [286]. The limitation of the upper cut-off is used in order to limit electrolyte oxidation and polarization growth [132,138,287] in order to extend cell lifetime [5]. Figure 8.13 shows that increasing the potential cut-off of NMC(442) material from the typical 4.28 V to 4.48 V or to 4.78 V vs. Li/Li^+ leads to an energy density gain (of the positive electrode material) of 18% and 36%, respectively.

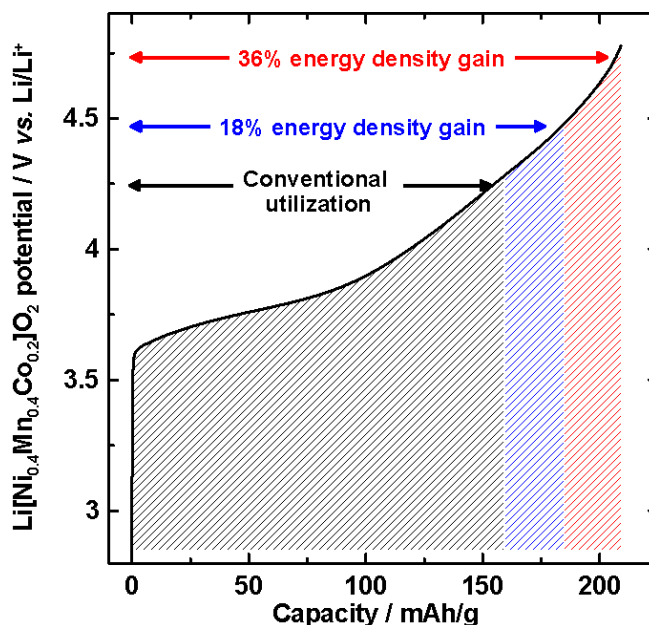


Figure 8.13. Potential vs. capacity of a $\text{Li}[\text{Ni}_{0.4}\text{Mn}_{0.4}\text{Co}_{0.2}]\text{O}_2$ cycled at 40°C and C/20 using Li foil as counter and reference electrode.

Surface coatings [288–290], use of electrolyte additives [11,151,152,160], or new solvent systems [27,28,32,291–293] have been used to allow layered materials to be charged to high potentials. For instance, Figure 8.14 shows the impact of additive blends

added to NMC(442)/graphite cells with a typical electrolyte of LiPF_6 dissolved in EC and EMC, cycled to 4.4 V and 4.5 V. Figure 8.14 clearly shows the performance improvement when vinylene carbonate is substituted by PES in a ternary additive blend. While the improvement in Figure 8.14 is substantial, it is still not enough for applications such as EVs or grid energy storage.

Successfully operating Li-ion cells to high voltage may require the use of a combination of new solvent blends, additives and coatings. It is generally believed that new solvent blends should have oxidation potentials higher than that of alkyl carbonates (*i.e.* $> 5 \text{ V vs. Li/Li}^+$) [294]. Most proposed solvent blends consist of fluorinated compounds [27,291,293], dinitriles [292], or sulfones [28,32]. However these new systems can suffer from inadequate wettability of typical olefin separators [28], high

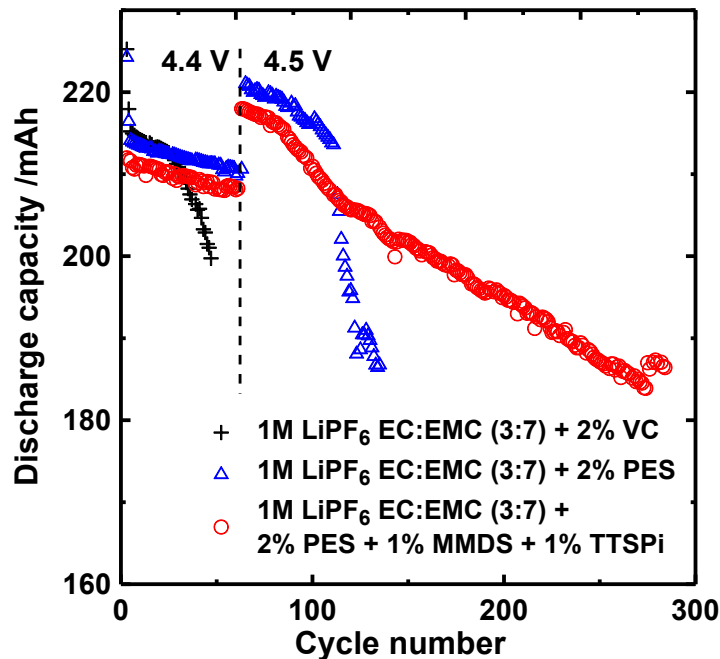


Figure 8.14. Discharge capacity vs. cycle number of 220 mAh NMC(442)/graphite pouch cells cycled at 40°C at a current of C/5 between 2.8 – 4.4 V for the first 50 cycles and then between 2.8 – 4.5 V. Cells were prepared and cycled by Kathlyne Nelson, 2nd year Ph.D. student, Physics & Atmospheric Science, Dalhousie University (2014).

viscosity [28,292], high gas production and high impedance [291] or potential cost and safety concerns (*e.g.* fluorinated solvents).

Section 8.1 showed that esters can be used if adequate passivating agents are added to the electrolyte. While these electrolytes were shown to function well in cells operated at 4.2 V, storage experiments seemed to indicate that they would not perform well at high voltage. In this regard, linear-carbonate based EC-free electrolytes would, in principle perform better than ester-based electrolytes in cells operated to high voltage.

Using DFT calculations, Borodin *et al.* [129] indicated that decreasing the dielectric constant of an electrolyte would create opposing effects in terms of oxidation potential of the electrolyte components. They indicated that decreasing the dielectric constant would increase the oxidation potential of isolated organic carbonates while it would decrease the oxidation potential of complexes formed of organic carbonates and PF_6^- . This indicates that if the oxidation of isolated organic carbonate molecules is the main reason for solvent oxidation, removing EC from carbonate-based electrolyte would increase the cycle-ability of NMC/gr cells operated to high voltage. Similarly, if the oxidation of solvent and PF_6^- complexes is the main reason for solvent oxidation, then removing EC from carbonate-based electrolyte would decrease the cycle-ability of NMC/gr cells operated to high voltage.

8.2.1 Conductivity of linear alkyl carbonate-based electrolytes

Figure 8.15 shows the conductivity of linear alkyl carbonate-based electrolytes as a function of temperature. In typical electrolyte, EC is used for its graphite passivation properties and high dielectric constant [34]. Figure 8.15a shows that a 1M LiPF_6 EMC

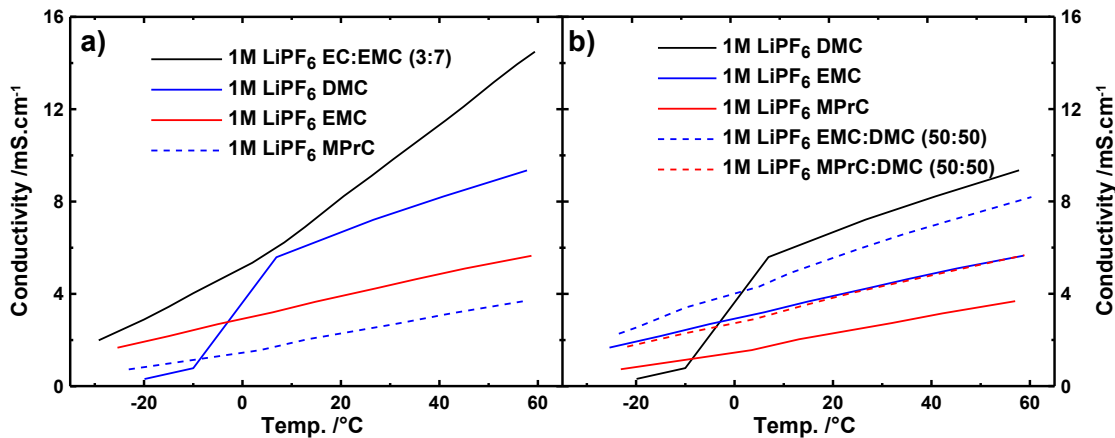


Figure 8.15. Conductivity vs. temperature of 1M LiPF₆ in pure linear alkyl carbonate solution (a) and in blends of linear alkyl carbonates (b).

electrolyte has a conductivity ranging from 2 mS.cm⁻¹ to 6 mS.cm⁻¹ between -20°C and 60°C, respectively. Figure 8.15 also shows that the addition of EC to the solvent blend is only advantageous in terms of conductivity at temperatures higher than -10°C. For instance, 1 M LiPF₆ EMC has similar conductivity to 1M LiPF₆ EC:EMC (3:7) below -15°C. The conductivity range of the EMC-based electrolyte presented here is acceptable for energy storage cells where high C-rate capability is not needed. Figure 8.15a also shows that the length of the alkyl chain greatly affects the conductivity. For instance, the conductivity decreases going from DMC to EMC to methyl propyl carbonate (MPrC). This is most probably a consequence of the increased viscosity of the solvents (see Table 8.1).

Figure 8.15b also shows that blending DMC with EMC or MPrC improves electrolyte conductivity. For instance adding 50% DMC to EMC gives a conductivity improvement of about 30% throughout the temperature range tested. Electrolytes of LiPF₆ dissolved in pure DMC show better conductivity than EMC or MPrC or EMC:DMC mixtures at temperatures higher than 5°C. The break in the conductivity vs.

temperature profile corresponds to the liquid/solid phase transition of the electrolyte. Electrolyte with DMC only would be suitable in cells used where temperatures do not go below 5 - 10°C and should yield cells with better rate capabilities than cells filled with an EMC-based electrolyte.

8.2.2 First cycle of NMC(442)/graphite cells with linear alkyl carbonate-based electrolytes

Figure 8.16 shows the differential capacity vs. cell voltage during the first charge to 3.5 V at 40°C and C/20 of NMC(442)/gr cells filled with various EMC-based electrolytes with or without additives. Figure 8.16 shows that cells filled with a 1M LiPF₆ EMC electrolyte have a large peak in the differential capacity plot around 3.1 V. This

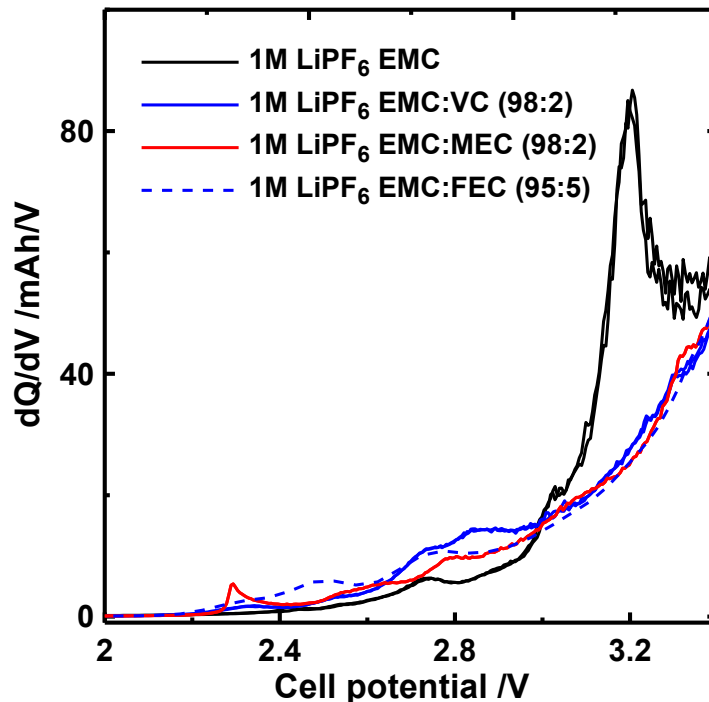


Figure 8.16. Differential capacity vs. cell voltage during the first charge to 3.5 V at 40°C and C/20 of 180 mAh NMC(442)/graphite pouch cells filled with various EMC-based blends. For comparison the cell volume before cycling is about 2 mL. Cells filled with the EMC:FEC electrolyte were prepared by Jian Xia, Post-doctoral fellow, Physics & Atmospheric Science, Dalhousie University (2016).

peak corresponds to the reduction of EMC at the graphite surface. This peak was associated with a large production of gas (1.2 mL, representing a 50% cell volume expansion). The large area under the peak indicates that the reduction of EMC does not form an effective passivating layer or at least that its passivation requires the reduction of a large amount of EMC. This is consistent with the results presented by Nie *et al.* [95]. Figure 8.16 also shows that the addition of very small amounts of VC, FEC or methylene ethylene carbonate (MEC) suppresses the peak corresponding to the reduction of EMC. This indicates that the reduction of these additives, evidenced by the presence of small differential capacity peak at 2.3 V, 2.5 V and 2.8V for MEC, FEC and VC, respectively, produces a good passivating layer. The passivation of the graphite was also evidenced by the small amount of gas (*i.e.* < 4% expansion) produced during the first charge to 3.5 V (see Figure F10 of the Appendix F).

8.2.3 Open circuit performance of cells filled with linear alkyl carbonate-based electrolyte vs. ester-based electrolyte

Figure 8.17 shows the cell voltage vs. time and gas volume produced in NMC(111)/gr cells filled with a linear alkyl carbonate-based electrolyte or an ester-based electrolyte during 500 h open circuit voltage storage at 4.3 V and 40°C. Figure 8.17 clearly shows that cells containing the MPrC-based electrolyte have smaller parasitic oxidation currents at the positive electrode. This is evidenced by the lower voltage drop during storage. At the same time, at similar initial VC content, the volume of gas produced in cells with the MPrC-based electrolyte is only a quarter of the volume produced in cells with the ester-based electrolyte. This reinforces the fact that linear alkyl

carbonate-based electrolytes outperform ester-based electrolytes if cells are to be operated at high voltage (*i.e.* > 4.2 V).

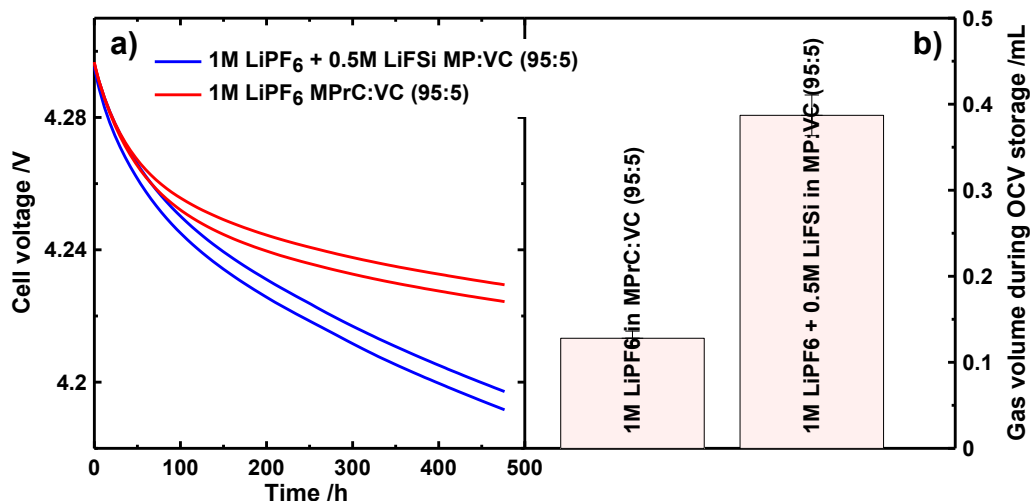


Figure 8.17. Cell voltage vs. time (a) and gas volume produced (b) for NMC(111)/graphite pouch cells filled with various electrolyte blends during a 500 h open circuit voltage storage at 4.3 V and 40°C. Cells were prepared by Jordan Wentzell, 4th year B.Sc. student, Chemistry Department, Lakehead University (2015).

8.2.4 Optimization of the initial VC content in linear alkyl carbonate-based electrolyte

The result presented in Chapter 5 and Section 8.1 indicated that the amount of VC needs to be tuned in order to obtain cells with good graphite passivation (in the case of EC-free blends), low impedance and low gas generation. That is, the amount of VC needs to be high enough to properly passivate the graphite electrode yet low enough to limit the amount of VC reduced to ensure low impedance. At the same time, the amount of VC left in the electrolyte once the cell reaches a high voltage (*i.e.* > 4.2 V) needs to be minimized in order to limit gas generation through oxidation during cell operation.

Figure 8.18 shows the amount of VC left (a) and the amount of EMC having undergone trans-esterification (b) after the first cycle to 4.4 V at 40°C and C/20 for NMC(442)/gr cells filled with EMC-based electrolyte containing various initial VC loadings (all electrolytes contained 1M LiPF₆). Figure 8.18a shows that cells initially containing 1.7 - 3% VC have very little additive left after the first cycle. This is probably the reason why cells filled with EMC:VC-based electrolytes with low initial VC loading have low gas evolution during the first charge between 3.5 - 4.5 V and during subsequent cycling (see Table F10 of Appendix F).

Figure 8.18b shows that EMC reduction/transesterification is mostly suppressed at an initial VC loading between 1.8 and 3%. This shows that the minimal VC loading required to passivate the graphite surface and prevent substantial EMC reduction lies between 1.8-3%. This also explains why cells with 2% VC generated such small amounts of gas during the first charge to 3.5 V compared to cells filled with a 1M LiPF₆ EMC (no VC) electrolyte (see Figure F10 of Appendix F).

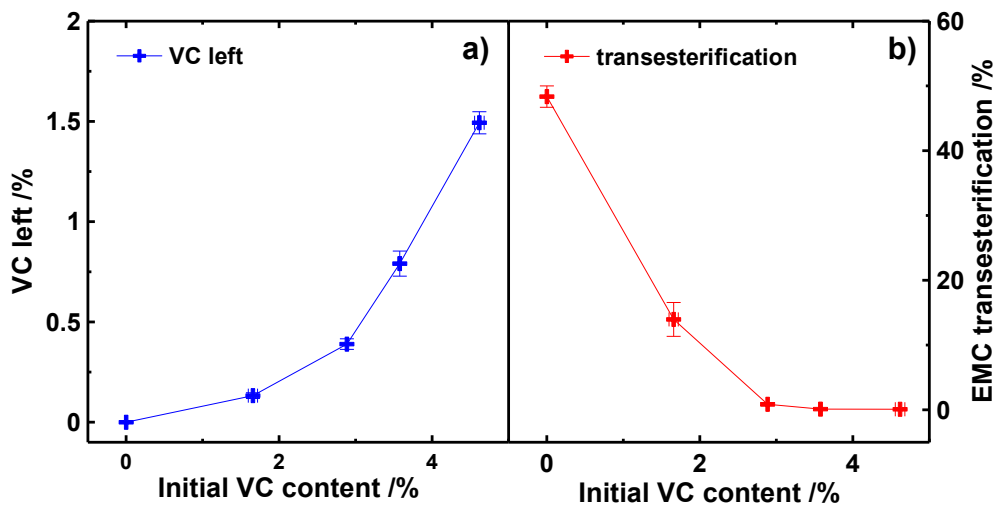


Figure 8.18. Amount of VC left (a) and % EMC trans-esterification (b) vs. initial VC content in NMC(442)/graphite pouch cells that underwent one full cycle between 2.8 – 4.4 V at 40°C and filled with 1M LiPF₆ EMC + x% VC electrolytes. The lines are a guide to the eyes.

Figure 8.19 shows the amount of VC remaining as a function of cycling time during the first charge to various voltage cut-offs of NMC(442)/graphite cells filled with a 1M LiPF₆ EMC:VC (98.2:1.8) electrolyte. Figure 8.19 shows that a large portion of the consumption of VC occurs between 0 – 3.1 V which is the cell voltage window where VC is expected to be reduced at the graphite surface [32] (see Section 5.1). Figure 8.19 also shows that once the cell reaches 3.62 V, only a small amount of VC is left in the cell (~ 0.25%). This small amount of VC remaining minimizes the gas produced during the first charge to high voltage and subsequent cycling (*i.e.* minimizes the amount of VC remaining in the electrolyte that can oxidize at the positive electrode, see Section 5.3).

In order to evaluate the impact of VC loading and the nature of the linear carbonate chosen on electrolyte oxidation and reduction, cells were put on a smart storage station (see Section 3.2.3 for a description of smart storage experiments). Figure 8.20

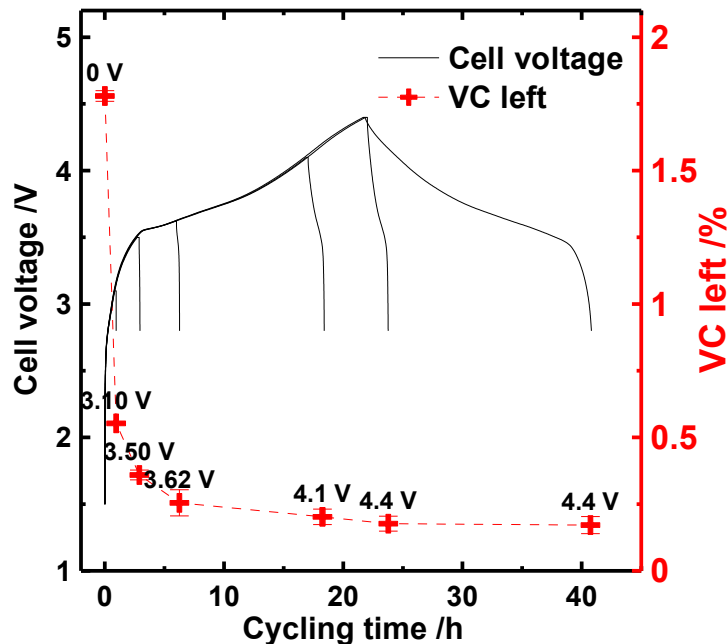


Figure 8.19. Amount of VC left vs. cycling time during the first cycle at 40°C in NMC(442)/graphite pouch initially filled with a 1M LiPF₆ EMC + 1.8% VC electrolyte.

shows a summary of the reversible capacity loss (a), irreversible capacity loss (b), magnitude of the impedance after storage (R_{ct} , c) and gas volume generated (d) as a function of initial VC loading during 500 h of storage at 4.4 V and 40°C. The red dashed line shows the results for a cell filled with a 1M LiPF₆ EC:EMC (3:7) + 2% PES +1% DTD + 1% TTSPi electrolyte (Figure 2.9 shows the structure of PES, DTD and TTSPi). This EC-based electrolyte was chosen based on the comparison of more than 300-500 different additive blends [11,16,26,138,143,151,153,214,222,236,268,287,295,296]. These extensive additive studies showed that cells with EC-based electrolytes containing this particular ternary additive blend have better overall performance (*i.e.* electrolyte oxidation rate, electrolyte reduction rate, polarization growth, gas production) compared to other additive mixtures in EC-based electrolytes.

Figure 8.20 clearly shows that there is an optimal VC loading. Figures 8.20a and 8.20b show that too low or too high an initial VC loading in both EMC or MPrC-based blends leads to higher reversible capacity losses (more electrolyte oxidation) and higher irreversible capacity losses (more electrolyte reduction) during storage. The higher losses at the low end of VC loading may originate from a poor graphite electrode passivation leading to higher lithium loss due to electrolyte reduction. Section 5.1 showed that the reduction of linear carbonates produces compounds with poor oxidative stability such as ethers and esters. These compounds may travel to the positive electrode and be oxidized leading to higher reversible capacity losses during storage at high voltage. The higher losses at the high end of initial additive loading may originate from a larger amount of VC left over in the electrolyte. The VC remaining may permeate through the SEI of the graphite electrode and be reduced similarly to the case of EC-based electrolytes (see

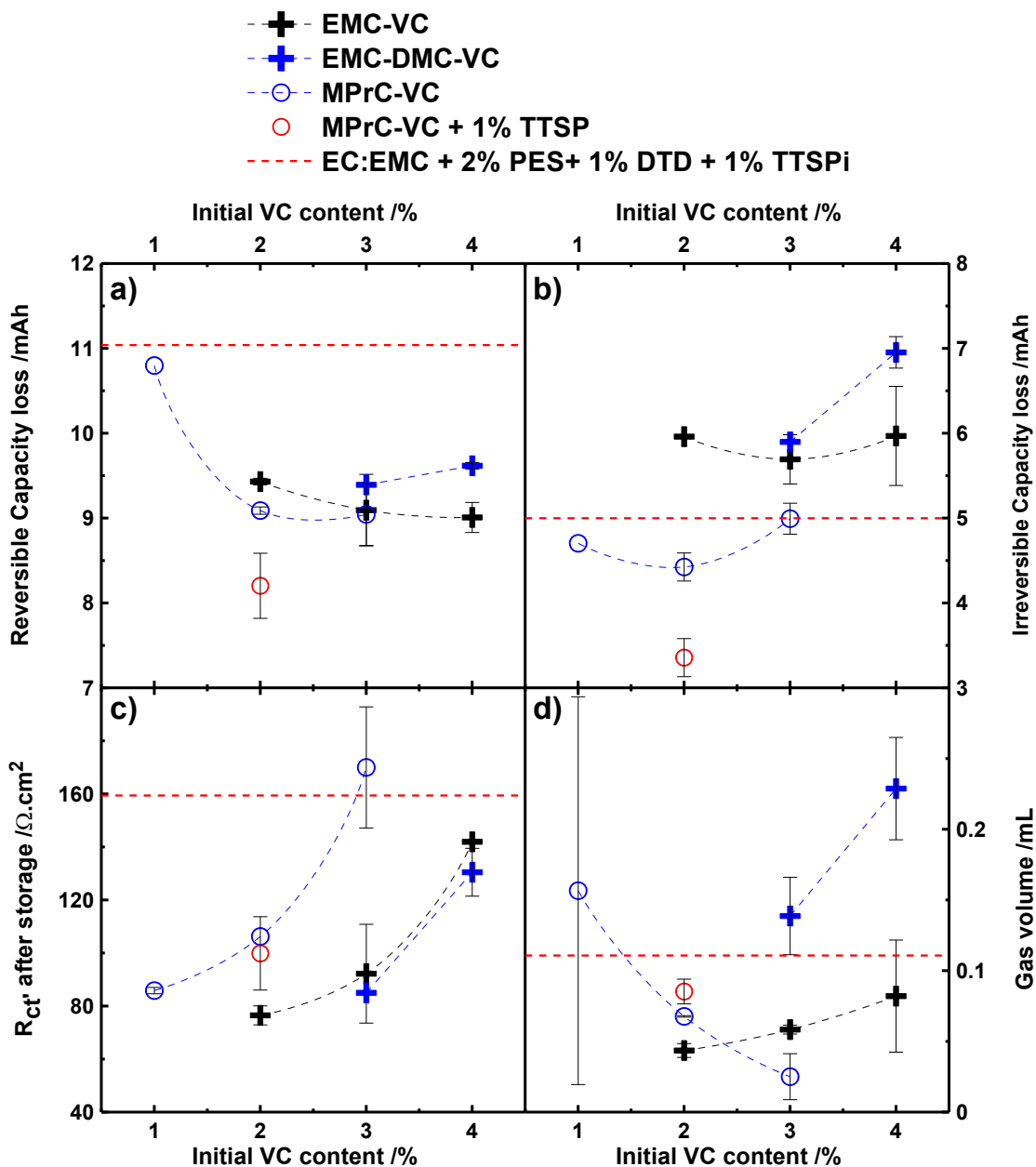


Figure 8.20. Reversible capacity loss (a), irreversible capacity loss (b), magnitude of the impedance (R_{ct}' , c) and gas volume generated (c) during 500 h 4.4 V smart storage (see Section 3.2.3) at 40°C for 180 mAh NMC(442)/graphite pouch cells filled with various electrolyte blends. All electrolytes contained 1M LiPF₆.

Section 5.1.2) thus consuming active lithium (*i.e.* irreversible lithium losses). In a similar fashion, some of the VC remaining in the electrolyte may be oxidized at the positive

electrode thus increasing the reversible lithium losses during storage, similarly to the case of VC in EC-based electrolytes (see Section 5.2 and Section 5.3).

Figure 8.20c and 8.20d also show that higher initial VC content leads to higher impedance and higher gas evolution. Section 5.2 showed that this higher impedance is caused by an increased VC consumption at the negative electrode leading to a more resistive SEI. Section 5.2 and Section 5.3 also showed that increased gas generation is caused by the oxidation of the VC remaining in the electrolyte.

Figure 8.20 shows that the optimal initial VC loading differs from one alkyl carbonate to the next. For instance, it appears that the optimal VC loading in EMC-based electrolytes is around 3% while it seems to be around 2 - 2.5% in MPrC-based electrolytes. Figure 8.20 also shows that while the choice of alkyl carbonate does not affect the reversible capacity losses much, it has a great impact on the irreversible capacity losses during storage. For instance, substituting EMC for MPrC leads to an irreversible capacity loss improvement of 20%. Figures 8.20a and 8.20b also show that the addition of co-additives such as tris(trimethylsilyl)phosphate (TTSP) greatly impacts the cell performance when linear alkyl carbonate-based electrolytes are used. For instance, the addition of only 1% TTSP to an MPrC:VC (98:2) electrolyte leads to improvements of around 10%.

Generally, Figure 8.20 shows that linear alkyl carbonate-based electrolytes yield cells with better performance than state of the art EC-based electrolytes. For instance, all EC-free blends have lower reversible capacity losses (lower electrolyte oxidation), comparable or lower irreversible capacity losses (lower electrolyte reduction), lower impedance and comparable or lower gas generation during 4.4 V operation compared to

the EC-based electrolyte containing the ternary additive blend. Readers are reminded that EC-free solvents have only one or two additives while the EC-based solvent used for comparison had a three-additive blend which was chosen based on the comparison of hundreds of cells.

8.2.5 Comparison between VC, FEC, and EC as passivating agents

Figure 8.21 shows the voltage vs. time during open circuit voltage at 4.2 V and 4.5 V and 40°C as well as coulombic efficiency (CE) vs. cycle number during cycling at 40°C between 2.8 - 4.5 V for NMC(442)/gr cells filled with various EMC-based electrolytes (all electrolytes contained 1M LiPF₆). Figures 8.21a and 8.21b show why additives are necessary in EMC-based electrolyte. For instance, Figures 8.21a and 8.21b show that adding 2% VC to EMC leads to cells with smaller voltage drops at both 4.2 V and 4.5 V and higher CE during cycling between 2.8 - 4.5 V compared to cells with an EMC-only electrolyte or EC-based electrolyte with a ternary additive blend. Figures 8.21a and 8.21b also seem to indicate that EMC-based electrolytes bring most of the improvements at high voltage. For instance, the benefits of using EMC-based electrolytes in terms of voltage drop seem to occur at 4.5 V.

Figures 8.21b, 8.21e and 8.21h show that FEC can also enable the use of EMC-based electrolytes, consistent with the data presented in Figure 8.15. For instance, Figures 8.21b, 8.21e and 8.21h show that cells with EMC and 5% or 10% FEC have lower voltage drop during storage at 4.2 V and 4.5 V as well as better CE during cycling at 4.5 V than cells filled with the EC-based electrolyte containing the ternary additive blend. Similarly to EMC:VC, the biggest improvement imparted by the EMC:FEC electrolyte

seems to be at high voltage. Figures 8.21b, 8.21e and 8.21h also indicate that there is a minimum amount of FEC needed. For instance cells with 2% FEC show mitigated improvement over cells containing EC-based electrolytes.

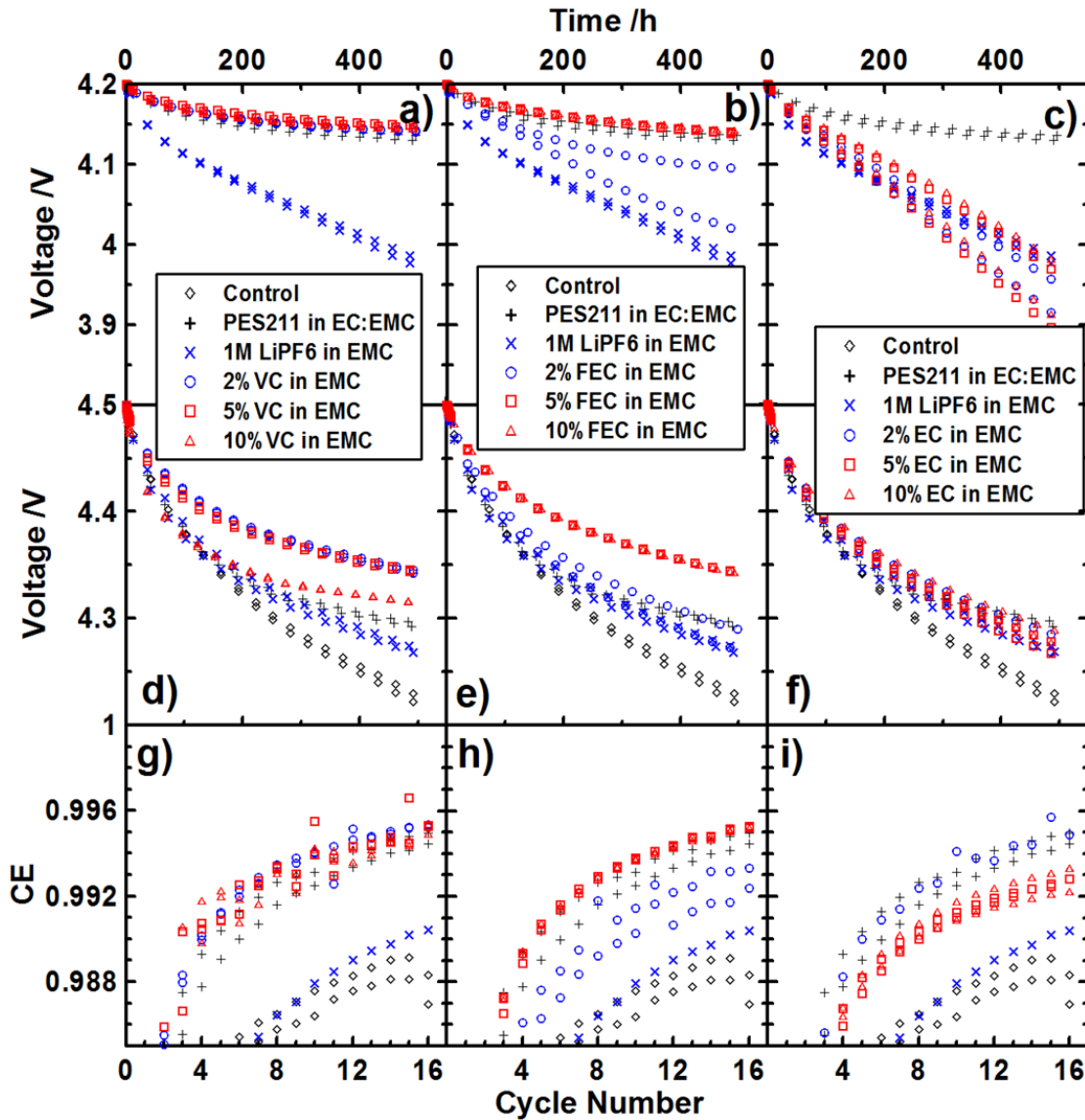


Figure 8.21. Voltage vs. time during open circuit voltage storage at 4.2 V (a-c) and 4.5 V (d-f) and coulombic efficiency during cycling between 2.8 – 4.5 V(g-i) for 180 mAh NMC(442)/graphite pouch cells filled with various electrolyte blends. All experiments were performed at 40°C and all electrolyte blends contained 1M LiPF₆. In the figure caption, PES-211 refers to 2% PES + 1% DTD + 1% TTSPi. Cells were prepared and analyzed by Jian Xia, Post-doctoral fellow, Physics & Atmospheric Science, Dalhousie University (2016).

Electrolytes consisting of EMC and FEC have been previously reported in the literature [258,293,297,298]. However these typically have high FEC loading (10 - 20%) which will ultimately lead to high cost. Here we show that only minimal amounts are necessary. Using large FEC loading (10 - 20%) also leads to higher gas evolution during cycling and storage at elevated temperature (*i.e.* > 40°C). For instance, Table F1 of Appendix F shows that increasing the FEC content from 5% to 10% leads to increased gas evolution during the first charge to 4.5 V and subsequent cycling and storage to 4.2 V or 4.5 V.

Figures 8.21c, 8.21f and 8.21i also show that lowering the EC content from 30% to 2% leads to improved high voltage performance but not low voltage (4.2 V) performance. For instance, cells filled with EMC-based electrolytes with 2% EC have voltage drop during storage at 4.5 V and CE during cycling at 4.5 V similar to cells containing the EC-based electrolyte with the ternary additive blend. However, increasing EC content to 5% or 10% lead to performance similar to cells with the EC-based blend without additive. This clearly shows that the presence of large quantities of EC is detrimental to cells cycled to high voltage. While lowering the EC content to 2% improves cell performance, cells containing an EMC:VC or EMC:FEC based electrolyte show much better performance.

Figure 8.21 clearly shows that the removal of EC leads to better cycling performance at high voltage. It also shows that the presence of small amounts of passivating agents is necessary. The exploratory work to be done in terms of EMC-based electrolyte optimization is considerable since multiple compounds can enable EMC-

based-EC-free electrolyte to function well at high voltage and multiple co-additives can help improve performance further.

8.2.6 Long term cycling of NMC(442)/graphite cells filled with EMC:VC-based electrolytes and operated to 4.4 V

Figure 8.22 shows the discharge capacity (a, c) and polarization (b, d) vs. cycle number of NMC(442)/gr pouch cells containing 1M LiPF₆ EMC:VC (98:2) electrolyte with or without pyridine pentafluorophosphate (PPF) or triallyl phosphate (TAP) and cycled up to 4.4 V at 20°C (a, b) and 55°C (c, d). These two co-additives (PPF and TAP) were chosen based on previous evaluation in EC-based electrolytes. Figures 8.22a and 8.22b show that cells containing EMC:VC had fade rate and polarization growth lower than cells filled with the EC-based electrolyte with the ternary additive blend when cycled at room temperature. It is surprising that cells containing an EC-free electrolyte with an initial VC loading of only 2% can be cycled up to 4.4 V for 3200 h with a lower fade rate than cells filled with a state of the art electrolyte. This is especially true when EC-based electrolytes containing 2% VC show such poor performance (see Figure 8.13).

Figures 8.22a and 8.22b show that adding PPF leads to lower polarization growth and better capacity retention in cells containing an EMC:VC electrolyte. Figures 8.22a and 8.22b also show that cells with the EMC:VC + TAP electrolyte have lower initial capacity and worse capacity retention which is related to a large polarization growth (see Figure 8.22b). Triallyl phosphate has been shown to yield similar cell polarization in cells with EC-based electrolytes [151].

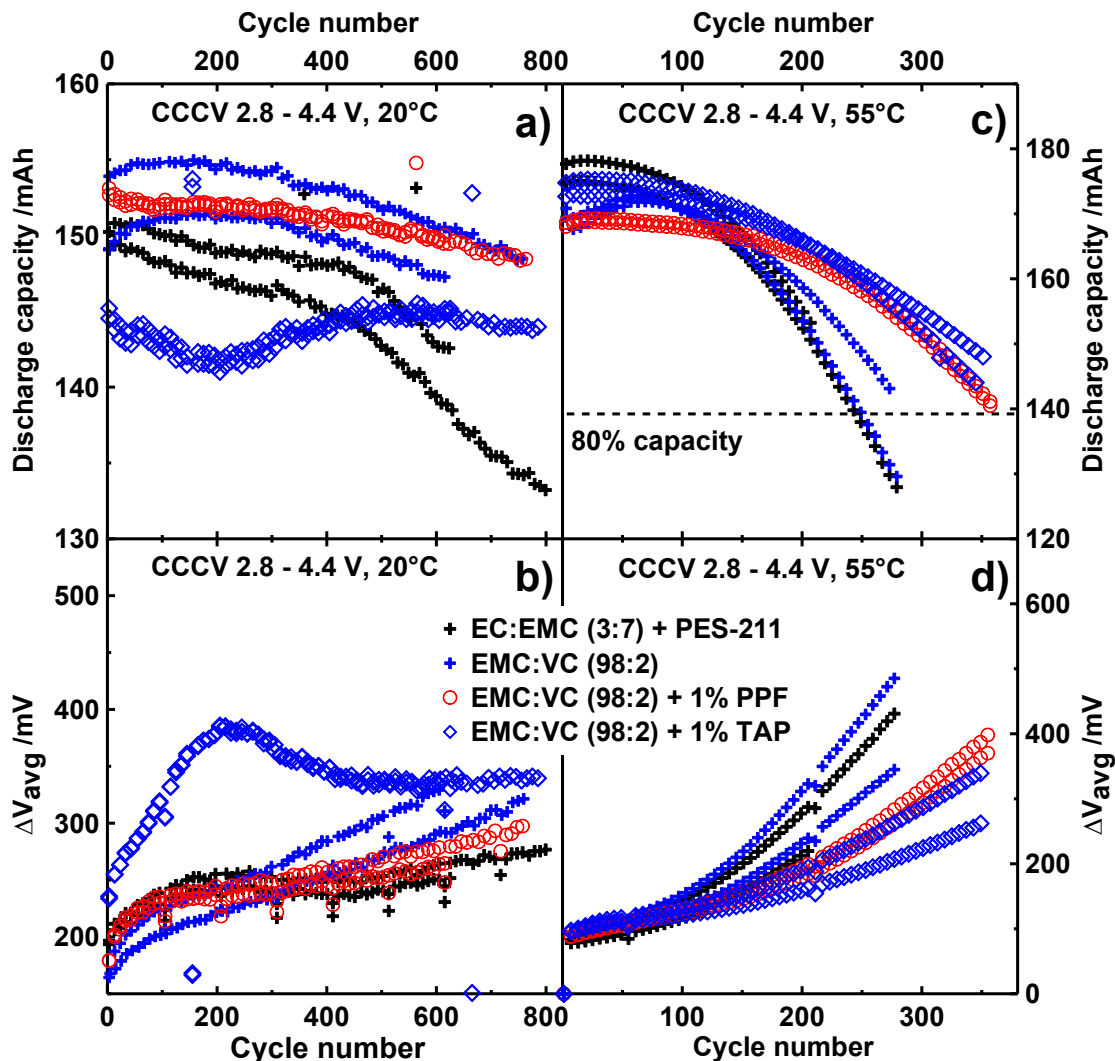


Figure 8.22. Discharge capacity vs. cycle number (a) and polarization growth (b) during cycling between 2.8 – 4.4 V and 20°C; discharge capacity vs. cycle number (c) and polarization growth (d) during cycling between 2.8 – 4.4 V and 55°C of 180 mAh NMC(442)/graphite cells filled with various electrolyte blends. Cells were cycled at C/2 with a constant voltage applied at the top of charge until the current dropped below C/20. PES-211 refers to 2% PES + 1% DTD + 1% TTSPi. All electrolyte blends contained 1M LiPF₆.

Figures 8.22c and 8.22d show that cells containing an EMC:VC electrolyte without co-additive present capacity retention and polarization growth rate similar to cells with the EC-based electrolyte when cycled at 55°C. Readers are reminded that the EC-based electrolyte containing the ternary additive blend already provides a great

improvement to NMC(442)/graphite cells cycled to high voltage compared to cells filled with other additive-containing EC-based electrolytes. This indicates that EMC:VC-based electrolyte provides comparable cycling performance to the state of the art EC-based electrolytes in NMC/graphite cells cycled to 55°C and 4.4 V.

Figures 8.22c and 8.22d also show that adding PPF or TAP to EMC:VC electrolytes improves the high voltage-high temperature cycling performance of NMC/graphite cells. For instance cells with EMC:VC + PPF or EMC:VC + TAP electrolyte reach 80% capacity retention after 350 cycles while cells with the EC-based electrolyte reach 80% capacity after 270 cycles. This represents a cycle life improvement of 30% over EC-based electrolytes.

Figure 8.22d shows that the polarization growth rate of cells cycled at 55°C and up to 4.4 V is rather large. The addition of TAP or PPF seems to improve the capacity retention of cells containing an EMC:VC-based electrolyte by slowing down cell polarization growth. Figures 8.22c and 8.22d clearly show that the removal of EC and the addition of small amounts of passivating additive and co-additives can lead to cycle life improvement of at least 30%.

8.2.7 Safety properties of charged NMC(442) and graphite electrodes in EMC-based electrolytes

Figures 8.23 shows the self-heating rate of lithiated graphite powder (a) and delithiated NMC(442) powder (b) mixed with electrolyte as a function of temperature as measured by accelerated rate calorimetry. These measurements are very useful in evaluating the impact of electrolyte composition on cell safety. Self-heating events

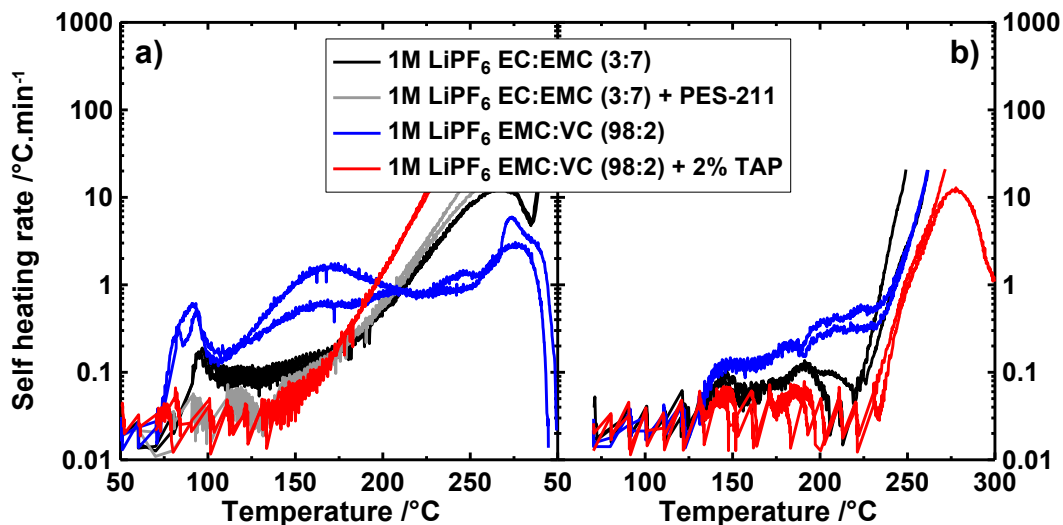


Figure 8.23. Self heating rate vs. temperature of lithiated graphite powder (a) and delithiated NMC(442) powder (b) recovered from NMC(442)/graphite pouch cells charged to 4.5 V and filled with various electrolyte blends. A description of the experimental procedure can be found in Appendix F. Samples were prepared and analyzed by Lin Ma, 1st year Ph.D. student, Chemistry Department, Dalhousie University (2016).

indicate the occurrence of exothermic reactions. It is important to have as high an onset temperature as possible and as low a self-heating rate as possible in order help ensure the safety of Li-ion cells under abuse scenarios.

Figure 8.23a shows that lithiated graphite powder soaked in 1M LiPF₆ EC:EMC (3:7) electrolyte has an exothermic event that peaks at 0.2°C.min⁻¹ with an onset around 90°C and an exothermic event around 150°C leading to thermal run-away. Figure 8.23a shows that the addition of the ternary additive blend leads to the suppression of the exotherm below 150°C thus improving the thermal stability of lithiated graphite. Figure 8.23a shows that lithiated graphite soaked in the 98% EMC + 2% VC electrolyte has an exothermic event starting at 70°C which leads to a self-heating rate of around 0.9°C.min⁻¹. This reactivity at low temperature may lead to safety issues in Li-ion cells during failure events. However, Figure 8.23a shows that the addition of 2%

TAP suppresses this exothermic event and provides similar thermal stability to EC-based electrolytes containing the ternary additive blend.

Figure 8.23b shows that delithiated NMC(442) powder goes into thermal runaway around 225°C in EC-based electrolyte blends (data for EC-based blends with ternary additive blends are not available). Figure 8.23b also shows that NMC(442) soaked in 98% EMC + 2% VC electrolyte has an exothermic event around 125°C. However Figure 8.23b shows once again that the addition of TAP leads to better safety properties. For instance, delithiated NMC(442) powder soaked in 1M LiPF₆ EMC:VC + TAP shows a higher temperature thermal run-away than NMC(442) powder soaked in an EC:EMC electrolyte.

8.2.8 Concluding remarks on linear alkyl carbonate-based electrolytes

Electrolytes consisting of LiPF₆ dissolved in linear carbonates and containing small amounts of passivating additives and other co-additives provide excellent cycling performance to NMC(442)/graphite cells during use at high voltage at both room and high temperatures. Such electrolytes provide cells with low gas evolution, low impedance (with the right co-additive choice), low rates of electrolyte oxidation, good graphite passivation, acceptable electrolyte conductivity and good safety (with the right co-additive). These blends are also expected to be low cost.

The removal of EC has been shown to enhance high voltage performance of NMC(442)/graphite cells at both room temperature and high temperature. Several compounds can enable the use of EMC-based electrolytes such as VC, FEC, MEC or EC (added at the additive level, see Figure 8.21). Adjusting the loading of these passivating

agents is key in order to get cells with good overall performance. The loading of the passivating agent needs to be high enough to passivate the graphite electrode surface and low enough to ensure low impedance (for VC) and low gassing during cell cycling (for VC and FEC). The addition of a co-additive helps lower the polarization growth during high voltage cycling as well as helps improve safety.

These results clearly show that large amounts of EC are not needed and are actually detrimental to the cycle life of NMC/graphite cells operated to high voltage. They also show that use of solvents with oxidation potential higher than organic carbonates is not mandatory in order to dramatically enhance high voltage cycling performance.

8.3 Concluding remarks on EC-free solvents

Two EC-free electrolytes were designed. These electrolytes use either esters or linear alkyl carbonates as main solvents with small amounts of passivating agents. While ester-based electrolytes provide good performance at 4.2 V and high rate at low temperature, linear alkyl carbonate-based electrolytes provide good capacity retention to cells cycled to high voltage.

The results of the GC-MS and GC-TCD studies presented in Chapter 5 also guided the optimization of these new electrolyte blends. For instance, these new solvent blends show very good performance when the amount of passivating agent is large enough to protect the graphite surface while low enough to limit the impedance and gas generation during operation resulting from the reduction and oxidation of the passivating agent left over in the electrolyte.

The results presented here also indicate that a vast variety of new EC-free electrolyte blends can be formulated. It also shows that EC is not required in order to obtain Li-ion cells with comparable cycling performance to state of the art electrolytes.

CHAPTER 9. FUTURE WORK

9.1 GC-MS experiments

9.1.1 Reactivity of additives with lithium alkoxides

When it comes to additive reactivity, most researchers focus on the possible electrochemical routes that a particular additive may undertake. However, as introduced in Chapters 5, 6 and 7, several additives display a strong reactivity with many possible reduction or oxidation by-products. This was exemplified by the suppression of trans-esterification reactions in the presence of VC, phenyl carbonates or FEC. Chapter 5 showed that lithium alkoxides can initiate the oligomerization of VC. However the exact nature of this oligomer (trimer or tetramer in the case of the experiments presented in Chapter 5) was not shown. It would be useful to analyze the structure of the product since several of the possible isomers formed may have different high temperature or high potential stability.

Most of the additives that can suppress trans-esterification reaction also lower the electrolyte oxidation rate. It would then be useful to know whether part of this electrolyte oxidation suppression is due to the prevention of the formation of compounds with poor oxidative stability. For instance, Chapter 5 showed that lithium alkoxides may react with other compounds thus forming ethers and alcohols. Testing cells with additives known to suppress trans-esterification reactions to which ethers, esters, alcohols or formates are added would help determining if the suppression of the formation of these compounds is in fact part of the reason why these additives lower electrolyte oxidation rate.

9.1.2 Exploring the reactivity of additive blends

As mentioned in Chapter 5, several researchers reported on synergetic effect of additive blends. This is highly interesting since blending additives brings new and beneficial effects to cell performance. Understanding how this comes about would be highly useful. Chapter 5 showed initial work on how multiple additives interact. For instance, adding ES to cells containing VC altered the SEI slightly as evidenced by EIS. Further adding TTSPi to VC and ES-containing cells lowered the amount of VC reacting during the first charge of NMC/gr cells. It then seems that synergetic effects of electrolyte blends occur in two different fashions. Blending additives not only alters the SEI composition, it also alters the amount by which an additive is consumed compared to a single additive blend. Systematically studying the consumption of each additive in blends compared to their consumption when individually introduced in a cell would shed light on how the synergistic behavior comes about.

9.1.3 Determination of reduction pathways of atypical solvents

In recent publication, Petibon *et al.* [299,300] reported on the use of esters in combination with very high LiFSi concentration (5 molal). In these publications, they showed that esters such as ethyl acetate and methyl propanoate do not passivate the graphite surface when used with LiPF₆ alone. However, they showed that these esters can passivate graphite and cycle quite well when used with high LiFSi concentration. It would then be useful to know the by-products of the reduction of esters in the presence of high LiFSi concentration at the graphite surface to understand how the passivation in

highly concentrated electrolytes comes about. This can be done using the gas extraction method presented in Chapter 4.

Recently, many new solvents that are more stable against high potentials have been proposed. These solvents include fluorinated carbonates [27], fluorinated esters, fluorinated ethers and sulfones [28,129,130,301]. The same experiments applied to the reduction mechanism of EMC and esters shown in Chapter 5 and Chapter 8 can be applied to evaluate the by-products of the reduction and oxidation of these new classes of solvents.

9.1.4 Evaluation of the solvent consumption in cells operated at high voltages

One of the major limitations for the use of cells operated at high voltage is the large parasitic oxidative currents. This is problematic since sustained electrolyte oxidation leads to solvent depletion which ultimately renders the cell unusable. As of yet very little is known about the oxidation mechanism of the solvents and additives in Li-ion cells. For instance, some of the oxidative parasitic current could come from shuttle mechanisms or from the irreversible oxidation of solvents. While HPC measurements can measure oxidative parasitic currents, they do not give any information as to whether the oxidative current comes from a shuttle mechanism or not. However, comparing the total capacity coming from parasitic currents at the positive electrode to the electrolyte consumption can give a rough estimate. This can easily be done with a slight modification of the extraction method presented in Chapter 4. For instance, cells cycled at high voltage over a long term on a HPC instrument can be extracted. The amount of

extracted electrolyte can then be measured and compared to both the initial solvent introduced in the cell and the charge slippage as measured by the HPC. The ratio of total charge slippage to moles of solvent consumed can indicate whether the oxidative parasitic current is from a shuttle reaction or an irreversible reaction.

9.2 LC-MS experiments

As shown in Chapters 5,6 and 7, some of the reduction or oxidation by-products are either ionic or oligomeric. While GC experiments are very useful, they cannot give any information on these types of by-products. For this reason, liquid chromatography (LC) experiments would be highly useful. There are several LC experiments described in the Li-ion battery literature, such as oligomer extraction and subsequent molecular mass assessment using gel permeation chromatography by Chen *et al.* [144] or measurements of the main liquid components of the electrolyte by Schultz *et al.* [302]. Using the different columns that a liquid chromatograph can accommodate could help detect different by-products of the decomposition of both solvents and additives at the negative and positive electrodes.

9.2.1 Using Reverse-phase chromatography to detect polar molecular by-products

Reverse-phase chromatography is used for the separation of small (*i.e.* < 300 g.mol⁻¹) polar compounds [181]. Several potential reduction and oxidation by-products fall in this category, such as short polyether or polycarbonate oligomers, aldehydes, and carboxylic acids. In order to separate these compounds from the solvent, an extraction

with pure acetonitrile can be performed. The separation of this extract could then be performed using a gradient of acetonitrile and water (mobile phase) with a C-18 (stationary phase consisting of 18 carbon long alkyl chains) reverse-phase chromatographic column, much like what Shultz *et al.* proposed in a recent publication [302] or with a hydrophilic interaction chromatography column (HILIC).

9.2.2 Using gel permeation chromatography to detect oligomers

Gel permeation chromatography is a suitable separation method for polymeric species (*i.e.* $> 500 \text{ g.mol}^{-1}$) [181]. This method separates analytes based on molecular size. Using polymer standards of different molecular mass, the retention time of analytes can be related to their molecular mass. Polymeric species could be removed from the surface of the positive and negative electrodes after cycling using solvents such as tetrahydrofuran as described by Chen *et al.* [144] in an earlier publication. The extracted polymeric species could then be analyzed using a gel permeation chromatographic column and suitable solvent blends for the elution. The LC-MS recently acquired possesses a tandem quadrupole mass spectrometer equipped with an electrospray ionization module (principal ionization technique), and an argon collision chamber between the first and second quadrupole. While the retention time will give information on the molecular mass of the polymeric species, the particular fragmentation pattern of selected molecular ions will give information as to which polymeric species are present (*e.g.* polyether *vs.* polycarbonate *vs.* polyolefin).

9.3 Linear alkyl carbonate-based electrolyte exploration

Section 8.2 showed that the choice of the linear alkyl carbonate, the passivating agent and co-additive used had a great impact on electrolyte conductivity, graphite passivation effectiveness and electrolyte oxidation rate. This indicates that a large amount of exploratory work is yet to be performed in order to fully optimize this electrolyte system. This implies comparing passivating agent consumption with different alkyl carbonates and different co-additives as well as monitoring the gas produced during formation and cycling.

Chapter 5 also showed that the amount of VC consumed during the first charge of cells with EC-based electrolytes differed substantially when cells were charged at 40°C or 50°C. It may indicate that forming cells with EC-free solvent blends using VC as passivating agent at different temperature may yield cells with different performance.

Some of the results in Section 8.2 showed that thermal stability of the electrolyte in presence of charged electrodes is an issue if the proper co-additive is not added. The addition of 2% TAP improved the situation. However, cycling data at room temperature showed that 1% TAP might already result in high impedance and poor rate capability at low temperature. This indicates that the initial loading of TAP must be tuned in order to obtain cells with good safety properties and good rate capabilities at low temperature. Much more work is also necessary in order to identify other additives and/or solvents that may provide good safety while keeping low impedance.

Other tests (tests performed by Deijun Xiong, 4th year Ph.D. student, Chemistry Department, Dalhousie University (2016)) indicated that the impedance of cells with EMC-based electrolytes have a peculiar behavior when salt molarity is changed. For

instance, the magnitude of the impedance of such cells increased strongly at low salt concentration. Similar tests performed on cells with EC-based electrolytes did not show a strong correlation between impedance and salt molarity. This behavior might indicate a Li^+ solvation shell change going from low salt concentration (*i.e.* 0.2 M) to higher concentration (*i.e.* 2 M). Further tests are necessary in order to understand this behavior.

CHAPTER 10. CONCLUSION

While GC is a widely used method in the scientific community, its application to Li-ion cell related studies has been very limited. In this thesis, GC-based methods that allow the analysis of liquid components of the electrolyte of cycled Li-ion cells and the analysis of the gas produced during cell operation have been developed. Chapter 4 gave a detailed description of these methods and presented some of the scope of their potential use.

Chapter 4 showed that a simple liquid-liquid extraction step helps separate the neutral organic components from the potentially corrosive inorganic or other ionic species in the electrolyte of cycled Li-ion cells. These extraction procedures allow the composition of the organic components such as solvents and additives to be analyzed as a function of cycling time and voltage. Chapter 4 also presented the details of a simple extraction procedure for the gas produced in Li-ion cells. This procedure relies on storing cells in a low pressure chamber for a short period of time prior to puncturing. This low pressure step is key as it allows the complete extraction of the gas from the cell headspace as well as the extraction of most of the gas that was dissolved in the electrolyte. Not only does it allow the gas composition to be determined, it also allows the small molecular weight compounds resulting from solvent reduction or solvent oxidation to be extracted and detected.

Chapter 5 put these two GC-based methods to use. The gases produced during the first charge to low (*i.e.* 3.5 V) or high voltage (*i.e.* 4.7 V) of Li-ion cells with or without additives were analyzed by GC-TCD and GC-MS. These analyses allowed the reduction

pathways of EMC and subsequent reaction pathways of the by-products to be inferred. The analysis of the gas produced in cells containing VC or PES allowed some of the reduction and oxidation pathways of these additives to be inferred and others ignored. It also showed that while PES is not oxidized in great quantities during the first charge to high voltage, VC oxidizes readily producing great quantities of CO and CO₂.

Chapter 5 also presented the results of additive quantification during the first charge of Li-ion cells or during cell operation. These quantifications showed that during the first cycle, additives react well past the differential capacity peak associated with their reduction at the graphite surface. This indicated that relying only on the differential capacity peak to assess the reactivity of an additive gives only a partial picture. The additive quantification during cell operation also showed that while VC is mainly consumed at the negative electrode during cell use at moderate voltage (*i.e.* 4.2 V and below), PES is consumed both at the positive and negative electrodes. It also showed that some VC does get oxidized at the positive electrode producing gas at cell voltage of 4.2 V. However the amount of VC reacting at the positive electrode was too low to be detected with the method used. In Chapter 5, cell impedance and VC consumption were shown to be correlated. This correlation allowed new additive blends using large amounts of VC to be designed while the impedance was kept low. These blends would be suitable for cells operated to moderated potential (*i.e.* < 4.2 V) where VC cannot oxidize.

Chapter 6 presented a UHPC and GC study of cells containing small amounts of phenyl carbonates. This class of compounds have been shown to provide cells with similar electrolyte reduction and electrolyte oxidation to VC-containing electrolytes during 4.2 V operation. Phenyl carbonates have also been shown to be superior to VC as

they provide low impedance to both the positive and the negative electrode of NMC/gr cells. Finally, MPC and DPC also have been shown to be promising additives in NMC(111)/gr and NMC(811)/gr pouch cells operated to 4.3 V and 40°C.

Chapter 7 presented the results of GC-MS analysis of the electrolyte in LCO/Si-alloy:graphite cells. These measurements showed that the sudden failure of these cells was associated with the depletion of the additive FEC. The capacity fade and FEC consumption in cells cycled at different rate was also determined. Both the fade and FEC consumption were shown to have a time dependence and a cycle number dependence. While the time dependence is associated with the ever-growing SEI at the surface of the negative electrode particles (Si-alloy and graphite), the cycle number dependence is associated with the repair of the SEI at the surface of the Si-alloy due to the repeated expansion and contraction of the particles during lithiation and delithiation. The deconvolution of the time dependence and cycle number dependence also showed that cell life-time could be greatly improved if both the surface area of the graphite and Si-alloy used was minimized. The results presented in Chapter 7 also suggest that new electrolyte systems minimizing the FEC consumption rate or utilizing a different passivating additive need to be found in order to successfully implement Si in commercial cells.

Chapter 8 presented results for two different EC-free electrolyte systems. These two systems consisted of either esters or linear alkyl carbonates with small amounts of passivating agents. The passivating agents that were shown to effectively passivate the graphite surface were VC, FEC and MEC. Many more are undoubtedly yet to be found. The results of Chapter 5 were used in order to logically optimize the passivating agent

loading. For instance, Chapter 5 showed that the impedance of cells was correlated to the amount of VC consumed at the graphite surface. Chapter 5 also showed that VC remaining in the electrolyte may oxidize at the positive electrode and produce gas. Using this knowledge, VC was added to linear alkyl carbonate-based and ester-based electrolytes in amounts sufficient to passivate the graphite surface while in low enough quantities to minimize the amount remaining in the electrolyte once the cell reached a moderately high voltage (*i.e.* > 4.1 V). Following this procedure, ester-based electrolytes showed very good rate performance at low temperature, low impedance and good capacity retention at 40°C in cells cycled to moderate voltages (*i.e.* 4.2 V and below). Linear alkyl-based electrolytes on the other hand were shown to provide low impedance, low gas generation, low electrolyte oxidization rate and very good capacity retention to cells cycled to high voltage (*i.e.* > 4.3 V). These linear alkyl carbonate-based electrolytes were also shown to out-perform state of the art EC-based electrolytes even when only two non-optimized additives (3% total additive loading) were used.

REFERENCES

- [1] T. Reddy, *Linden's Handbook of Batteries*, 4th Edition, 4 edition, McGraw-Hill Professional, New York, 2010.
- [2] M. Broussely, P. Biensan, F. Bonhomme, P. Blanchard, S. Herreyre, K. Nechev, et al., Main aging mechanisms in Li ion batteries, *J. Power Sources*. 146 (2005) 90–96. doi:10.1016/j.jpowsour.2005.03.172.
- [3] D. Aurbach, K. Gamolsky, B. Markovsky, Y. Gofer, M. Schmidt, U. Heider, On the use of vinylene carbonate (VC) as an additive to electrolyte solutions for Li-ion batteries, *Electrochimica Acta*. 47 (2002) 1423–1439. doi:10.1016/S0013-4686(01)00858-1.
- [4] G.H. Wrodnigg, J.O. Besenhard, M. Winter, Ethylene Sulfite as Electrolyte Additive for Lithium-Ion Cells with Graphitic Anodes, *J. Electrochem. Soc.* 146 (1999) 470–472. doi:10.1149/1.1391630.
- [5] J.C. Burns, A. Kassam, N.N. Sinha, L.E. Downie, L. Solnickova, B.M. Way, et al., Predicting and Extending the Lifetime of Li-Ion Batteries, *J. Electrochem. Soc.* 160 (2013) A1451–A1456. doi:10.1149/2.060309jes.
- [6] A.J. Smith, J.C. Burns, D. Xiong, J.R. Dahn, Interpreting High Precision Coulometry Results on Li-ion Cells, *J. Electrochem. Soc.* 158 (2011) A1136–A1142. doi:10.1149/1.3625232.
- [7] A.J. Smith, J.C. Burns, X. Zhao, D. Xiong, J.R. Dahn, A High Precision Coulometry Study of the SEI Growth in Li/Graphite Cells, *J. Electrochem. Soc.* 158 (2011) A447–A452. doi:10.1149/1.3557892.
- [8] J.C. Burns, G. Jain, A.J. Smith, K.W. Eberman, E. Scott, J.P. Gardner, et al., Evaluation of Effects of Additives in Wound Li-Ion Cells Through High Precision Coulometry, *J. Electrochem. Soc.* 158 (2011) A255–A261. doi:10.1149/1.3531997.
- [9] N.N. Sinha, A.J. Smith, J.C. Burns, G. Jain, K.W. Eberman, E. Scott, et al., The Use of Elevated Temperature Storage Experiments to Learn about Parasitic Reactions in Wound LiCoO₂/Graphite Cells, *J. Electrochem. Soc.* 158 (2011) A1194–A1201. doi:10.1149/2.007111jes.
- [10] O. Pashos, Private conversation, BMW, (2013).
- [11] L. Ma, J. Xia, J.R. Dahn, Improving the High Voltage Cycling of Li[Ni_{0.42}Mn_{0.42}Co_{0.16}]₂O₂ (NMC442)/Graphite Pouch Cells Using Electrolyte Additives, *J. Electrochem. Soc.* 161 (2014) A2250–A2254. doi:10.1149/2.1041414jes.
- [12] C.P. Aiken, J. Self, R. Petibon, X. Xia, J.M. Paulsen, J.R. Dahn, A Survey of In Situ Gas Evolution during High Voltage Formation in Li-Ion Pouch Cells, *J. Electrochem. Soc.* 162 (2015) A760–A767. doi:10.1149/2.0941504jes.
- [13] J. Self, C.P. Aiken, R. Petibon, J.R. Dahn, Survey of Gas Expansion in Li-Ion NMC Pouch Cells, *J. Electrochem. Soc.* (2014).
- [14] X. Lu, X. Li, Z. Wang, H. Guo, G. Yan, X. Yin, A modified co-precipitation process to coat LiNi_{1/3}Co_{1/3}Mn_{1/3}O₂ onto LiNi_{0.8}Co_{0.1}Mn_{0.1}O₂ for improving the

- electrochemical performance, *Appl. Surf. Sci.* 297 (2014) 182–187. doi:10.1016/j.apsusc.2014.01.121.
- [15] K. Abe, K. Miyoshi, T. Hattori, Y. Ushigoe, H. Yoshitake, Functional electrolytes: Synergetic effect of electrolyte additives for lithium-ion battery, *J. Power Sources*. 184 (2008) 449–455. doi:10.1016/j.jpowsour.2008.03.037.
- [16] D.Y. Wang, J. Xia, L. Ma, K.J. Nelson, J.E. Harlow, D. Xiong, et al., A Systematic Study of Electrolyte Additives in Li[Ni_{1/3}Mn_{1/3}Co_{1/3}]O₂ (NMC)/Graphite Pouch Cells, *J. Electrochem. Soc.* 161 (2014) A1818–A1827. doi:10.1149/2.0511412jes.
- [17] S. Santee, A. Xiao, L. Yang, J. Gnanaraj, B.L. Lucht, Effect of combinations of additives on the performance of lithium ion batteries, *J. Power Sources*. 194 (2009) 1053–1060. doi:10.1016/j.jpowsour.2009.06.012.
- [18] J.-S. Shin, C.-H. Han, U.-H. Jung, S.-I. Lee, H.-J. Kim, K. Kim, Effect of Li₂CO₃ additive on gas generation in lithium-ion batteries, *J. Power Sources*. 109 (2002) 47–52. doi:10.1016/S0378-7753(02)00039-3.
- [19] L. Madec, J. Xia, R. Petibon, K.J. Nelson, J.-P. Sun, I.G. Hill, et al., Effect of Sulfate Electrolyte Additives on LiNi_{1/3}Mn_{1/3}Co_{1/3}O₂/Graphite Pouch Cell Lifetime: Correlation between XPS Surface Studies and Electrochemical Test Results, *J. Phys. Chem. C*. 118 (2014) 29608–29622. doi:10.1021/jp509731y.
- [20] C. Yogi, D. Takamatsu, K. Yamanaka, H. Arai, Y. Uchimoto, K. Kojima, et al., Soft X-ray absorption spectroscopic studies with different probing depths: Effect of an electrolyte additive on electrode surfaces, *J. Power Sources*. 248 (2014) 994–999. doi:10.1016/j.jpowsour.2013.10.030.
- [21] Z.D. Li, Y.C. Zhang, H.F. Xiang, X.H. Ma, Q.F. Yuan, Q.S. Wang, et al., Trimethyl phosphite as an electrolyte additive for high-voltage lithium-ion batteries using lithium-rich layered oxide cathode, *J. Power Sources*. 240 (2013) 471–475. doi:10.1016/j.jpowsour.2013.04.038.
- [22] H.M. Jung, S.-H. Park, J. Jeon, Y. Choi, S. Yoon, J.-J. Cho, et al., Fluoropropane sultone as an SEI-forming additive that outperforms vinylene carbonate, *J. Mater. Chem. A*. 1 (2013) 11975. doi:10.1039/c3ta12580g.
- [23] S. Kaymaksiz, F. Wilhelm, M. Wachtler, M. Wohlfahrt-Mehrens, C. Hartnig, I. Tschernych, et al., Electrochemical stability of lithium salicylato-borates as electrolyte additives in Li-ion batteries, *J. Power Sources*. 239 (2013) 659–669. doi:10.1016/j.jpowsour.2012.12.105.
- [24] J.C. Burns, N.N. Sinha, G. Jain, H. Ye, C.M. VanElzen, W.M. Lamanna, et al., Impedance Reducing Additives and Their Effect on Cell Performance II. C₃H₉B₃O₆, *J. Electrochem. Soc.* 159 (2012) A1105–A1113. doi:10.1149/2.078207jes.
- [25] S. Dalavi, P. Guduru, B.L. Lucht, Performance Enhancing Electrolyte Additives for Lithium Ion Batteries with Silicon Anodes, *J. Electrochem. Soc.* 159 (2012) A642. doi:10.1149/2.076205jes.
- [26] J. Xia, M. Nie, L. Ma, J.R. Dahn, Variation of coulombic efficiency versus upper cutoff potential of Li-ion cells tested with aggressive protocols, *J. Power Sources*. 306 (2016) 233–240. doi:10.1016/j.jpowsour.2015.12.013.
- [27] Z. Zhang, L. Hu, H. Wu, W. Weng, M. Koh, P.C. Redfern, et al., Fluorinated electrolytes for 5 V lithium-ion battery chemistry, *Energy Environ. Sci.* 6 (2013) 1806–1810. doi:10.1039/C3EE24414H.

- [28] A. Abouimrane, I. Belharouak, K. Amine, Sulfone-based electrolytes for high-voltage Li-ion batteries, *Electrochem. Commun.* 11 (2009) 1073–1076. doi:10.1016/j.elecom.2009.03.020.
- [29] R. Chen, L. Zhu, F. Wu, L. Li, R. Zhang, S. Chen, Investigation of a novel ternary electrolyte based on dimethyl sulfite and lithium difluoromono(oxalato)borate for lithium ion batteries, *J. Power Sources.* 245 (2014) 730–738. doi:10.1016/j.jpowsour.2013.06.132.
- [30] M. Dahbi, F. Ghamouss, F. Tran-Van, D. Lemordant, M. Anouti, Ester based electrolyte with lithium bis(trifluoromethane sulfonyl) imide salt for electrochemical storage devices: Physicochemical and electrochemical characterization, *Electrochimica Acta.* 86 (2012) 287–293. doi:10.1016/j.electacta.2012.02.080.
- [31] Y. Yamada, M. Yaegashi, T. Abe, A. Yamada, A superconcentrated ether electrolyte for fast-charging Li-ion batteries - *Chemical Communications (RSC Publishing)*, *Chem. Commun.* 49 (2013) 11194–11196. doi:10.1039/C3CC46665E.
- [32] J. Xia, J. Self, L. Ma, J.R. Dahn, Sulfolane-Based Electrolyte for High Voltage Li(Ni_{0.42}Mn_{0.42}Co_{0.16})O₂ (NMC442)/Graphite Pouch Cells, *J. Electrochem. Soc.* 162 (2015) A1424–A1431. doi:10.1149/2.0121508jes.
- [33] L. Xing, W. Tu, J. Vatamanu, Q. Liu, W. Huang, Y. Wang, et al., On anodic stability and decomposition mechanism of sulfolane in high-voltage lithium ion battery, *Electrochimica Acta.* 133 (2014) 117–122. doi:10.1016/j.electacta.2014.03.190.
- [34] K. Xu, Nonaqueous Liquid Electrolytes for Lithium-Based Rechargeable Batteries, *Chem. Rev.* 104 (2004) 4303–4418. doi:10.1021/cr030203g.
- [35] K. Xu, Electrolytes and Interphases in Li-Ion Batteries and Beyond, *Chem. Rev.* 114 (2014) 11503–11618. doi:10.1021/cr500003w.
- [36] K. Xu, S. Zhang, T.R. Jow, W. Xu, C.A. Angell, LiBOB as Salt for Lithium-Ion Batteries: A Possible Solution for High Temperature Operation, *Electrochem. Solid-State Lett.* 5 (2002) A26–A29. doi:10.1149/1.1426042.
- [37] K. Takata, Cycling Characteristics of Secondary Li Electrode in LiBF₄/Mixed Ether Electrolytes, *J. Electrochem. Soc.* 132 (1985) 126. doi:10.1149/1.2113743.
- [38] J.T. Dudley, D.P. Wilkinson, G. Thomas, R. LeVae, S. Woo, H. Blom, et al., Conductivity of electrolytes for rechargeable lithium batteries, *J. Power Sources.* 35 (1991) 59–82. doi:10.1016/0378-7753(91)80004-H.
- [39] M. Ue, Mobility and Ionic Association of Lithium Salts in a Propylene Carbonate-Ethyl Methyl Carbonate Mixed Solvent, *J. Electrochem. Soc.* 142 (1995) 2577. doi:10.1149/1.2050056.
- [40] M. Ue, Mobility and Ionic Association of Lithium and Quaternary Ammonium Salts in Propylene Carbonate and γ -Butyrolactone, *J. Electrochem. Soc.* 141 (1994) 3336. doi:10.1149/1.2059336.
- [41] K. Matsumoto, K. Inoue, K. Nakahara, R. Yuge, T. Noguchi, K. Utsugi, Suppression of aluminum corrosion by using high concentration LiTFSI electrolyte, *J. Power Sources.* 231 (2013) 234–238. doi:10.1016/j.jpowsour.2012.12.028.
- [42] E. Krämer, T. Schedlbauer, B. Hoffmann, L. Terborg, S. Nowak, H.J. Gores, et al., Mechanism of Anodic Dissolution of the Aluminum Current Collector in 1 M

- LiTFSI EC:DEC 3:7 in Rechargeable Lithium Batteries, *J. Electrochem. Soc.* 160 (2013) A356–A360. doi:10.1149/2.081302jes.
- [43] H.-B. Han, S.-S. Zhou, D.-J. Zhang, S.-W. Feng, L.-F. Li, K. Liu, et al., Lithium bis(fluorosulfonyl)imide (LiFSI) as conducting salt for nonaqueous liquid electrolytes for lithium-ion batteries: Physicochemical and electrochemical properties, *J. Power Sources.* 196 (2011) 3623–3632. doi:10.1016/j.jpowsour.2010.12.040.
- [44] M.S. Ding, K. Xu, S.S. Zhang, K. Amine, G.L. Henriksen, T.R. Jow, Change of Conductivity with Salt Content, Solvent Composition, and Temperature for Electrolytes of LiPF₆ in Ethylene Carbonate-Ethyl Methyl Carbonate, *J. Electrochem. Soc.* 148 (2001) A1196–A1204. doi:10.1149/1.1403730.
- [45] M.C. Smart, B.V. Ratnakumar, S. Surampudi, Use of Organic Esters as Cosolvents in Electrolytes for Lithium-Ion Batteries with Improved Low Temperature Performance, *J. Electrochem. Soc.* 149 (2002) A361–A370. doi:10.1149/1.1453407.
- [46] Z. Lu, D.D. MacNeil, J.R. Dahn, Layered Cathode Materials Li[Ni_xLi_(1/3-2x/3)Mn_(2/3-x/3)]O₂ for Lithium-Ion Batteries, *Electrochem. Solid-State Lett.* 4 (2001) A191–A194. doi:10.1149/1.1407994.
- [47] S. Patoux, L. Daniel, C. Bourbon, H. Lignier, C. Pagano, F. Le Cras, et al., High voltage spinel oxides for Li-ion batteries: From the material research to the application, *J. Power Sources.* 189 (2009) 344–352. doi:10.1016/j.jpowsour.2008.08.043.
- [48] M. Xu, N. Tsiouvaras, A. Garsuch, H.A. Gasteiger, B.L. Lucht, Generation of Cathode Passivation Films via Oxidation of Lithium Bis(oxalato) Borate on High Voltage Spinel (LiNi_{0.5}Mn_{1.5}O₄), *J. Phys. Chem. C.* 118 (2014) 7363–7368. doi:10.1021/jp501970j.
- [49] L. Yang, B. Ravdel, B.L. Lucht, Electrolyte Reactions with the Surface of High Voltage LiNi_{0.5}Mn_{1.5}O₄ Cathodes for Lithium-Ion Batteries, *Electrochem. Solid-State Lett.* 13 (2010) A95–A97. doi:10.1149/1.3428515.
- [50] N.P.W. Pieczonka, Z. Liu, P. Lu, K.L. Olson, J. Moote, B.R. Powell, et al., Understanding Transition-Metal Dissolution Behavior in LiNi_{0.5}Mn_{1.5}O₄ High-Voltage Spinel for Lithium Ion Batteries, *J. Phys. Chem. C.* 117 (2013) 15947–15957. doi:10.1021/jp405158m.
- [51] D. Mohanty, S. Kalnaus, R.A. Meisner, K.J. Rhodes, J. Li, E.A. Payzant, et al., Structural transformation of a lithium-rich Li_{1.2}Co_{0.1}Mn_{0.55}Ni_{0.15}O₂ cathode during high voltage cycling resolved by in situ X-ray diffraction, *J. Power Sources.* 229 (2013) 239–248. doi:10.1016/j.jpowsour.2012.11.144.
- [52] Y.-M. Song, C.-K. Kim, K.-E. Kim, S.Y. Hong, N.-S. Choi, Exploiting chemically and electrochemically reactive phosphite derivatives for high-voltage spinel LiNi_{0.5}Mn_{1.5}O₄ cathodes, *J. Power Sources.* 302 (2016) 22–30. doi:10.1016/j.jpowsour.2015.10.043.
- [53] M. Xu, L. Zhou, Y. Dong, Y. Chen, J. Demeaux, A.D. MacIntosh, et al., Development of novel lithium borate additives for designed surface modification of high voltage LiNi_{0.5}Mn_{1.5}O₄ cathodes, *Energy Env. Sci.* (2016). doi:10.1039/C5EE03360H.

- [54] X. Yang, D. Wang, R. Yu, Y. Bai, H. Shu, L. Ge, et al., Suppressed capacity/voltage fading of high-capacity lithium-rich layered materials via the design of heterogeneous distribution in the composition, *J. Mater. Chem. A* 2 (2014) 3899. doi:10.1039/c3ta14513a.
- [55] S.K. Martha, J. Nanda, Y. Kim, R.R. Unocic, S. Pannala, N.J. Dudney, Solid electrolyte coated high voltage layered-layered lithium-rich composite cathode: $\text{Li}_{1.2}\text{Mn}_{0.525}\text{Ni}_{0.175}\text{Co}_{0.1}\text{O}_2$, *J. Mater. Chem. A* 1 (2013) 5587. doi:10.1039/c3ta10586e.
- [56] J. Li, J. Camardese, R. Shunmugasundaram, S. Glazier, Z. Lu, J.R. Dahn, Synthesis and Characterization of the Lithium-Rich Core-Shell Cathodes with Low Irreversible Capacity and Mitigated Voltage Fade, *Chem. Mater.* 27 (2015) 3366–3377. doi:10.1021/acs.chemmater.5b00617.
- [57] Samsung retail website, <http://www.samsung.com/uk/consumer/mobile-devices/accessories/battery/EB-B600BEBECWW>, visited March 16th, 2016.
- [58] T. Ohzuku, Zero-Strain Insertion Material of $\text{Li}[\text{Li}_{1/3}\text{Ti}_{5/3}]\text{O}_4$ for Rechargeable Lithium Cells, *J. Electrochem. Soc.* 142 (1995) 1431. doi:10.1149/1.2048592.
- [59] M.N. Obrovac, V.L. Chevrier, Alloy Negative Electrodes for Li-Ion Batteries, *Chem. Rev.* 114 (2014) 11444–11502. doi:10.1021/cr500207g.
- [60] M.N. Obrovac, L. Christensen, D.B. Le, J.R. Dahn, Alloy Design for Lithium-Ion Battery Anodes, *J. Electrochem. Soc.* 154 (2007) A849. doi:10.1149/1.2752985.
- [61] J.O. Besenhard, J. Yang, M. Winter, Will advanced lithium-alloy anodes have a chance in lithium-ion batteries?, *J. Power Sources.* 68 (1997) 87–90. doi:10.1016/S0378-7753(96)02547-5.
- [62] A. Esmanski, G.A. Ozin, Silicon Inverse-Opal-Based Macroporous Materials as Negative Electrodes for Lithium Ion Batteries, *Adv. Funct. Mater.* 19 (2009) 1999–2010. doi:10.1002/adfm.200900306.
- [63] H. Zhang, P.V. Braun, Three-Dimensional Metal Scaffold Supported Bicontinuous Silicon Battery Anodes, *Nano Lett.* 12 (2012) 2778–2783. doi:10.1021/nl204551m.
- [64] U. Kasavajjula, C. Wang, A.J. Appleby, Nano- and bulk-silicon-based insertion anodes for lithium-ion secondary cells, *J. Power Sources.* 163 (2007) 1003–1039. doi:10.1016/j.jpowsour.2006.09.084.
- [65] J. Wolfenstine, Critical grain size for microcracking during lithium insertion, *J. Power Sources.* 79 (1999) 111–113. doi:10.1016/S0378-7753(99)00052-X.
- [66] H. Wu, Y. Cui, Designing nanostructured Si anodes for high energy lithium ion batteries, *Nano Today.* 7 (2012) 414–429. doi:10.1016/j.nantod.2012.08.004.
- [67] C.-M. Park, J.-H. Kim, H. Kim, H.-J. Sohn, Li-alloy based anode materials for Li secondary batteries, *Chem. Soc. Rev.* 39 (2010) 3115. doi:10.1039/b919877f.
- [68] J. Graetz, C.C. Ahn, R. Yazami, B. Fultz, Highly Reversible Lithium Storage in Nanostructured Silicon, *Electrochem. Solid-State Lett.* 6 (2003) A194. doi:10.1149/1.1596917.
- [69] F. Maroni, R. Raccichini, A. Birrozzini, G. Carbonari, R. Tossici, F. Croce, et al., Graphene/silicon nanocomposite anode with enhanced electrochemical stability for lithium-ion battery applications, *J. Power Sources.* 269 (2014) 873–882. doi:10.1016/j.jpowsour.2014.07.064.

- [70] H. Zhou, J. Nanda, S.K. Martha, R.R. Unocic, H.M. Meyer, Y. Sahoo, et al., Role of Surface Functionality in the Electrochemical Performance of Silicon Nanowire Anodes for Rechargeable Lithium Batteries, *ACS Appl. Mater. Interfaces*. 6 (2014) 7607–7614. doi:10.1021/am500855a.
- [71] N. Delpuech, D. Mazouzi, N. Dupré, P. Moreau, M. Cerbelaud, J.S. Bridel, et al., Critical Role of Silicon Nanoparticles Surface on Lithium Cell Electrochemical Performance Analyzed by FTIR, Raman, EELS, XPS, NMR, and BDS Spectroscopies, *J. Phys. Chem. C*. 118 (2014) 17318–17331. doi:10.1021/jp503949y.
- [72] X. Li, M. Gu, S. Hu, R. Kennard, P. Yan, X. Chen, et al., Mesoporous silicon sponge as an anti-pulverization structure for high-performance lithium-ion battery anodes, *Nat. Commun.* 5 (2014). doi:10.1038/ncomms5105.
- [73] V.L. Chevrier, L. Liu, D.B. Le, J. Lund, B. Molla, K. Reimer, et al., Evaluating Si-Based Materials for Li-Ion Batteries in Commercially Relevant Negative Electrodes, *J. Electrochem. Soc.* 161 (2014) A783–A791. doi:10.1149/2.066405jes.
- [74] S.D. Beattie, M.J. Loveridge, M.J. Lain, S. Ferrari, B.J. Polzin, R. Bhagat, et al., Understanding capacity fade in silicon based electrodes for lithium-ion batteries using three electrode cells and upper cut-off voltage studies, *J. Power Sources*. 302 (2016) 426–430. doi:10.1016/j.jpowsour.2015.10.066.
- [75] L.Y. Beaulieu, K.W. Eberman, R.L. Turner, L.J. Krause, J.R. Dahn, Colossal Reversible Volume Changes in Lithium Alloys, *Electrochem. Solid-State Lett.* 4 (2001) A137. doi:10.1149/1.1388178.
- [76] M.T. McDowell, S.W. Lee, J.T. Harris, B.A. Korgel, C. Wang, W.D. Nix, et al., In Situ TEM of Two-Phase Lithiation of Amorphous Silicon Nanospheres, *Nano Lett.* 13 (2013) 758–764. doi:10.1021/nl3044508.
- [77] M.T. McDowell, I. Ryu, S.W. Lee, C. Wang, W.D. Nix, Y. Cui, Studying the Kinetics of Crystalline Silicon Nanoparticle Lithiation with In Situ Transmission Electron Microscopy, *Adv. Mater.* 24 (2012) 6034–6041. doi:10.1002/adma.201202744.
- [78] G. Gachot, S. Grugeon, M. Armand, S. Pilard, P. Guenot, J.-M. Tarascon, et al., Deciphering the multi-step degradation mechanisms of carbonate-based electrolyte in Li batteries, *J. Power Sources*. 178 (2008) 409–421. doi:10.1016/j.jpowsour.2007.11.110.
- [79] M.-S. Park, Y.-J. Lee, S. Rajendran, M.-S. Song, H.-S. Kim, J.-Y. Lee, Electrochemical properties of Si/Ni alloy–graphite composite as an anode material for Li-ion batteries, *Electrochimica Acta*. 50 (2005) 5561–5567. doi:10.1016/j.electacta.2005.04.042.
- [80] K. Goldshtein, K. Freedman, D. Schneier, L. Burstein, V. Ezersky, E. Peled, et al., Advanced Multiphase Silicon-Based Anodes for High-Energy-Density Li-Ion Batteries, *J. Electrochem. Soc.* 162 (2015) A1072–A1079. doi:10.1149/2.1111506jes.
- [81] I. Kim, Si/TiN Nanocomposites Novel Anode Materials for Li-Ion Batteries, *Electrochem. Solid-State Lett.* 3 (1999) 493. doi:10.1149/1.1391189.

- [82] T. Li, Y.L. Cao, X.P. Ai, H.X. Yang, Cycleable graphite/FeSi₆ alloy composite as a high capacity anode material for Li-ion batteries, *J. Power Sources*. 184 (2008) 473–476. doi:10.1016/j.jpowsour.2008.02.057.
- [83] G. Venugopal, J. Moore, J. Howard, S. Pandalwar, Characterization of microporous separators for lithium-ion batteries, *J. Power Sources*. 77 (1999) 34–41. doi:10.1016/S0378-7753(98)00168-2.
- [84] D. Linden, T.B. Reddy, *Linden's handbook of batteries*, McGraw-Hill, New York, 2001.
- [85] P.G. Balakrishnan, R. Ramesh, T. Prem Kumar, Safety mechanisms in lithium-ion batteries, *J. Power Sources*. 155 (2006) 401–414. doi:10.1016/j.jpowsour.2005.12.002.
- [86] F.C. Laman, Impedance Studies for Separators in Rechargeable Lithium Batteries, *J. Electrochem. Soc.* 140 (1993) L51. doi:10.1149/1.2056243.
- [87] J.-A. Choi, S.H. Kim, D.-W. Kim, Enhancement of thermal stability and cycling performance in lithium-ion cells through the use of ceramic-coated separators, *J. Power Sources*. 195 (2010) 6192–6196. doi:10.1016/j.jpowsour.2009.11.020.
- [88] X. Huang, Separator technologies for lithium-ion batteries, *J. Solid State Electrochem.* 15 (2011) 649–662. doi:10.1007/s10008-010-1264-9.
- [89] Y.M. Lee, J.-W. Kim, N.-S. Choi, J.A. Lee, W.-H. Seol, J.-K. Park, Novel porous separator based on PVdF and PE non-woven matrix for rechargeable lithium batteries, *J. Power Sources*. 139 (2005) 235–241. doi:10.1016/j.jpowsour.2004.06.055.
- [90] J. Hao, G. Lei, Z. Li, L. Wu, Q. Xiao, L. Wang, A novel polyethylene terephthalate nonwoven separator based on electrospinning technique for lithium ion battery, *J. Membr. Sci.* 428 (2013) 11–16. doi:10.1016/j.memsci.2012.09.058.
- [91] X. Zhang, R. Kostecki, T.J. Richardson, J.K. Pugh, P.N. Ross, Electrochemical and Infrared Studies of the Reduction of Organic Carbonates, *J. Electrochem. Soc.* 148 (2001) A1341–A1345. doi:10.1149/1.1415547.
- [92] M. Moshkovich, M. Cojocaru, H. Gottlieb, D. Aurbach, The study of the anodic stability of alkyl carbonate solutions by in situ FTIR spectroscopy, EQCM, NMR and MS, *J. Electroanal. Chem.* 497 (2001) 84–96. doi:10.1016/S0022-0728(00)00457-5.
- [93] M. Egashira, H. Takahashi, S. Okada, J. Yamaki, Measurement of the electrochemical oxidation of organic electrolytes used in lithium batteries by microelectrode, *J. Power Sources*. 92 (2001) 267–271. doi:10.1016/S0378-7753(00)00553-X.
- [94] E. Peled, The Electrochemical Behavior of Alkali and Alkaline Earth Metals in Nonaqueous Battery Systems—The Solid Electrolyte Interphase Model, *J. Electrochem. Soc.* 126 (1979) 2047–2051. doi:10.1149/1.2128859.
- [95] M. Nie, D. Chalasani, D.P. Abraham, Y. Chen, A. Bose, B.L. Lucht, Lithium Ion Battery Graphite Solid Electrolyte Interphase Revealed by Microscopy and Spectroscopy, *J. Phys. Chem. C*. 117 (2013) 1257–1267. doi:10.1021/jp3118055.
- [96] R. Yazami, Surface chemistry and lithium storage capability of the graphite–lithium electrode, *Electrochimica Acta*. 45 (1999) 87–97. doi:10.1016/S0013-4686(99)00195-4.

- [97] K. Kanamura, H. Tamura, Z. Takehara, XPS analysis of a lithium surface immersed in propylene carbonate solution containing various salts, *J. Electroanal. Chem.* 333 (1992) 127–142. doi:10.1016/0022-0728(92)80386-I.
- [98] E. Peled, D. Bar Tow, A. Merson, A. Gladkich, L. Burstein, D. Golodnitsky, Composition, depth profiles and lateral distribution of materials in the SEI built on HOPG-TOF SIMS and XPS studies, *J. Power Sources.* 97–98 (2001) 52–57. doi:10.1016/S0378-7753(01)00505-5.
- [99] A. Andersson, A. Henningson, H. Siegbahn, U. Jansson, K. Edström, Electrochemically lithiated graphite characterised by photoelectron spectroscopy, *J. Power Sources.* 119–121 (2003) 522–527. doi:10.1016/S0378-7753(03)00277-5.
- [100] S.-H. Kang, D.P. Abraham, A. Xiao, B.L. Lucht, Investigating the solid electrolyte interphase using binder-free graphite electrodes, *J. Power Sources.* 175 (2008) 526–532. doi:10.1016/j.jpowsour.2007.08.112.
- [101] D. Aurbach, M. Koltypin, H. Teller, In Situ AFM Imaging of Surface Phenomena on Composite Graphite Electrodes during Lithium Insertion, *Langmuir.* 18 (2002) 9000–9009. doi:10.1021/la020306e.
- [102] Y. Domi, M. Ochida, S. Tsubouchi, H. Nakagawa, T. Yamanaka, T. Doi, et al., In Situ AFM Study of Surface Film Formation on the Edge Plane of HOPG for Lithium-Ion Batteries, *J. Phys. Chem. C.* 115 (2011) 25484–25489. doi:10.1021/jp2064672.
- [103] S.-K. Jeong, M. Inaba, T. Abe, Z. Ogumi, Surface Film Formation on Graphite Negative Electrode in Lithium-Ion Batteries: AFM Study in an Ethylene Carbonate-Based Solution, *J. Electrochem. Soc.* 148 (2001) A989–A993. doi:10.1149/1.1387981.
- [104] S. Leroy, F. Blanchard, R. Dedryvère, H. Martinez, B. Carré, D. Lemordant, et al., Surface film formation on a graphite electrode in Li-ion batteries: AFM and XPS study, *Surf. Interface Anal.* 37 (2005) 773–781. doi:10.1002/sia.2072.
- [105] D. Aurbach, B. Markovsky, I. Weissman, E. Levi, Y. Ein-Eli, On the correlation between surface chemistry and performance of graphite negative electrodes for Li ion batteries, *Electrochimica Acta.* 45 (1999) 67–86. doi:10.1016/S0013-4686(99)00194-2.
- [106] S.S. Zhang, K. Xu, T.R. Jow, EIS study on the formation of solid electrolyte interface in Li-ion battery, *Electrochimica Acta.* 51 (2006) 1636–1640. doi:10.1016/j.electacta.2005.02.137.
- [107] R. Petibon, C.P. Aiken, N.N. Sinha, J.C. Burns, H. Ye, C.M. VanElzen, et al., Study of Electrolyte Additives Using Electrochemical Impedance Spectroscopy on Symmetric Cells, *J. Electrochem. Soc.* 160 (2013) A117–A124. doi:10.1149/2.005302jes.
- [108] R. Petibon, N.N. Sinha, J.C. Burns, C.P. Aiken, H. Ye, C.M. VanElzen, et al., Comparative study of electrolyte additives using electrochemical impedance spectroscopy on symmetric cells, *J. Power Sources.* 251 (2014) 187–194. doi:10.1016/j.jpowsour.2013.11.054.
- [109] H. Nakai, T. Kubota, A. Kita, A. Kawashima, Investigation of the Solid Electrolyte Interphase Formed by Fluoroethylene Carbonate on Si Electrodes, *J. Electrochem. Soc.* 158 (2011) A798. doi:10.1149/1.3589300.

- [110] D. Aurbach, Y. Ein-Eli, B. Markovsky, A. Zaban, S. Luski, Y. Carmeli, et al., The Study of Electrolyte Solutions Based on Ethylene and Diethyl Carbonates for Rechargeable Li Batteries II. Graphite Electrodes, *J. Electrochem. Soc.* 142 (1995) 2882–2890. doi:10.1149/1.2048659.
- [111] Y. Wang, P.B. Balbuena, Theoretical Insights into the Reductive Decompositions of Propylene Carbonate and Vinylene Carbonate: Density Functional Theory Studies, *J. Phys. Chem. B.* 106 (2002) 4486–4495. doi:10.1021/jp014371t.
- [112] K. Xu, Whether EC and PC Differ in Interphasial Chemistry on Graphitic Anode and How, *J. Electrochem. Soc.* 156 (2009) A751–A755. doi:10.1149/1.3166182.
- [113] J.M. Vollmer, L.A. Curtiss, D.R. Vissers, K. Amine, Reduction Mechanisms of Ethylene, Propylene, and Vinylethylene Carbonates A Quantum Chemical Study, *J. Electrochem. Soc.* 151 (2004) A178–A183. doi:10.1149/1.1633765.
- [114] D. Aurbach, M.D. Levi, E. Levi, A. Schechter, Failure and Stabilization Mechanisms of Graphite Electrodes, *J. Phys. Chem. B.* 101 (1997) 2195–2206. doi:10.1021/jp962815t.
- [115] M. Onuki, S. Kinoshita, Y. Sakata, M. Yanagidate, Y. Otake, M. Ue, et al., Identification of the Source of Evolved Gas in Li-Ion Batteries Using ^{13}C -labeled Solvents, *J. Electrochem. Soc.* 155 (2008) A794–A797. doi:10.1149/1.2969947.
- [116] I.A. Shkrob, Y. Zhu, T.W. Marin, D. Abraham, Reduction of Carbonate Electrolytes and the Formation of Solid-Electrolyte Interface (SEI) in Lithium-Ion Batteries. 1. Spectroscopic Observations of Radical Intermediates Generated in One-Electron Reduction of Carbonates, *J. Phys. Chem. C.* 117 (2013) 19255–19269. doi:10.1021/jp406274e.
- [117] G.V. Zhuang, P.N. Ross, Analysis of the Chemical Composition of the Passive Film on Li-Ion Battery Anodes Using Attenuated Total Reflection Infrared Spectroscopy, *Electrochem. Solid-State Lett.* 6 (2003) A136–A139. doi:10.1149/1.1575594.
- [118] S. Mori, H. Asahina, H. Suzuki, A. Yonei, K. Yokoto, Chemical properties of various organic electrolytes for lithium rechargeable batteries: 1. Characterization of passivating layer formed on graphite in alkyl carbonate solutions, *J. Power Sources.* 68 (1997) 59–64. doi:10.1016/S0378-7753(97)02619-0.
- [119] H.-L. Zhang, F. Li, C. Liu, J. Tan, H.-M. Cheng, New Insight into the Solid Electrolyte Interphase with Use of a Focused Ion Beam, *J. Phys. Chem. B.* 109 (2005) 22205–22211. doi:10.1021/jp053311a.
- [120] D. Aurbach, M. Moshkovich, A Study of Lithium Deposition-Dissolution Processes in a Few Selected Electrolyte Solutions by Electrochemical Quartz Crystal Microbalance, *J. Electrochem. Soc.* 145 (1998) 2629–2639. doi:10.1149/1.1838692.
- [121] A. Augustsson, M. Herstedt, J.-H. Guo, K. Edström, G.V. Zhuang, J. P. N. Ross, et al., Solid electrolyte interphase on graphite Li-ion battery anodes studied by soft X-ray spectroscopy, *Phys. Chem. Chem. Phys.* 6 (2004) 4185–4189. doi:10.1039/B313434B.
- [122] S.E. Sloop, J.B. Kerr, K. Kinoshita, The role of Li-ion battery electrolyte reactivity in performance decline and self-discharge, *J. Power Sources.* 119–121 (2003) 330–337. doi:10.1016/S0378-7753(03)00149-6.

- [123] M. Tochihara, H. Nara, D. Mukoyama, T. Yokoshima, T. Momma, T. Osaka, Liquid Chromatography-Quadruple Time of Flight Mass Spectrometry Analysis of Products in Degraded Lithium-Ion Batteries, *J. Electrochem. Soc.* 162 (2015) A2008–A2015. doi:10.1149/2.0231510jes.
- [124] D. Aurbach, B. Markovsky, M.D. Levi, E. Levi, A. Schechter, M. Moshkovich, et al., New insights into the interactions between electrode materials and electrolyte solutions for advanced nonaqueous batteries, *J. Power Sources.* 81–82 (1999) 95–111. doi:10.1016/S0378-7753(99)00187-1.
- [125] D. Aurbach, K. Gamolsky, B. Markovsky, G. Salitra, Y. Gofer, U. Heider, et al., The Study of Surface Phenomena Related to Electrochemical Lithium Intercalation into Li_xMO_y Host Materials (M = Ni, Mn), *J. Electrochem. Soc.* 147 (2000) 1322–1331. doi:10.1149/1.1393357.
- [126] D. Aurbach, B. Markovsky, A. Rodkin, M. Cojocaru, E. Levi, H.-J. Kim, An analysis of rechargeable lithium-ion batteries after prolonged cycling, *Electrochimica Acta.* 47 (2002) 1899–1911. doi:10.1016/S0013-4686(02)00013-0.
- [127] D. Aurbach, B. Markovsky, A. Rodkin, E. Levi, Y. Cohen, H.-J. Kim, et al., On the capacity fading of LiCoO_2 intercalation electrodes: the effect of cycling, storage, temperature, and surface film forming additives, *Electrochimica Acta.* 47 (2002) 4291–4306. doi:10.1016/S0013-4686(02)00417-6.
- [128] M. Arakawa, J. Yamaki, Anodic oxidation of propylene carbonate and ethylene carbonate on graphite electrodes, *J. Power Sources.* 54 (1995) 250–254. doi:10.1016/0378-7753(94)02078-H.
- [129] O. Borodin, W. Behl, T.R. Jow, Oxidative Stability and Initial Decomposition Reactions of Carbonate, Sulfone, and Alkyl Phosphate-Based Electrolytes, *J. Phys. Chem. C.* 117 (2013) 8661–8682. doi:10.1021/jp400527c.
- [130] O. Borodin, T.R. Jow, Quantum Chemistry Studies of the Oxidative Stability of Carbonate, Sulfone and Sulfonate-Based Electrolytes Doped with BF_4^- , PF_6^- Anions, *ECS Trans.* 33 (2011) 77–84. doi:10.1149/1.3563092.
- [131] L. Xing, O. Borodin, Oxidation induced decomposition of ethylene carbonate from DFT calculations – importance of explicitly treating surrounding solvent, *Phys. Chem. Chem. Phys.* 14 (2012) 12838–12843. doi:10.1039/C2CP41103B.
- [132] F. Lin, I.M. Markus, D. Nordlund, T.-C. Weng, M.D. Asta, H.L. Xin, et al., Surface reconstruction and chemical evolution of stoichiometric layered cathode materials for lithium-ion batteries, *Nat. Commun.* 5 (2014) 3529. doi:10.1038/ncomms4529.
- [133] S.S. Zhang, A review on electrolyte additives for lithium-ion batteries, *J. Power Sources.* 162 (2006) 1379–1394. doi:10.1016/j.jpowsour.2006.07.074.
- [134] D. Aurbach, Y. Gofer, The Behavior of Lithium Electrodes in Mixtures of Alkyl Carbonates and Ethers, *J. Electrochem. Soc.* 138 (1991) 3529–3536. doi:10.1149/1.2085454.
- [135] D.E. Irish, Z. Deng, M. Odziemkowski, Raman spectroscopic and electrochemical studies of lithium battery components, *J. Power Sources.* 54 (1995) 28–33. doi:10.1016/0378-7753(94)02035-2.
- [136] M. Dubarry, C. Truchot, B.Y. Liaw, K. Gering, S. Sazhin, D. Jamison, et al., Evaluation of commercial lithium-ion cells based on composite positive electrode for plug-in hybrid electric vehicle applications. Part II. Degradation mechanism

- under 2 C cycle aging, *J. Power Sources*. 196 (2011) 10336–10343. doi:10.1016/j.jpowsour.2011.08.078.
- [137] L.E. Downie, J.R. Dahn, Determination of the Voltage Dependence of Parasitic Heat Flow in Lithium Ion Cells Using Isothermal Microcalorimetry, *J. Electrochem. Soc.* 161 (2014) A1782–A1787. doi:10.1149/2.0301412jes.
- [138] K.J. Nelson, G.L. d'Eon, A.T.B. Wright, L. Ma, J. Xia, J.R. Dahn, Studies of the Effect of High Voltage on the Impedance and Cycling Performance of Li[Ni_{0.4}Mn_{0.4}Co_{0.2}]O₂/Graphite Lithium-Ion Pouch Cells, *J. Electrochem. Soc.* 162 (2015) A1046–A1054. doi:10.1149/2.0831506jes.
- [139] R. Kostecki, L. Norin, X. Song, F. McLarnon, Diagnostic Studies of Polyolefin Separators in High-Power Li-Ion Cells, *J. Electrochem. Soc.* 151 (2004) A522. doi:10.1149/1.1649233.
- [140] E. Wang, D. Ofer, W. Bowden, N. Iltchev, R. Moses, K. Brandt, Stability of Lithium Ion Spinel Cells. III. Improved Life of Charged Cells, *J. Electrochem. Soc.* 147 (2000) 4023–4028. doi:10.1149/1.1394013.
- [141] M. Dubarry, C. Truchot, B.Y. Liaw, K. Gering, S. Sazhin, D. Jamison, et al., Evaluation of Commercial Lithium-Ion Cells Based on Composite Positive Electrode for Plug-In Hybrid Electric Vehicle Applications III. Effect of Thermal Excursions without Prolonged Thermal Aging, *J. Electrochem. Soc.* 160 (2013) A191–A199. doi:10.1149/2.063301jes.
- [142] K.J. Nelson, Studies of the effects of electrolyte additives on the performance of lithium-ion batteries, M.Sc. thesis, Dalhousie, 2014. <http://hdl.handle.net/10222/65301>.
- [143] J.C. Burns, R. Petibon, K.J. Nelson, N.N. Sinha, A. Kassam, B.M. Way, et al., Studies of the Effect of Varying Vinylene Carbonate (VC) Content in Lithium Ion Cells on Cycling Performance and Cell Impedance, *J. Electrochem. Soc.* 160 (2013) A1668–A1674. doi:10.1149/2.031310jes.
- [144] G. Chen, G.V. Zhuang, T.J. Richardson, G. Liu, P.N. Ross, Anodic Polymerization of Vinyl Ethylene Carbonate in Li-Ion Battery Electrolyte, *Electrochem. Solid-State Lett.* 8 (2005) A344–A347. doi:10.1149/1.1921127.
- [145] Y. Hu, W. Kong, H. Li, X. Huang, L. Chen, Experimental and theoretical studies on reduction mechanism of vinyl ethylene carbonate on graphite anode for lithium ion batteries, *Electrochem. Commun.* 6 (2004) 126–131. doi:10.1016/j.elecom.2003.10.024.
- [146] N.N. Sinha, J.C. Burns, J.R. Dahn, Comparative study of tris(trimethylsilyl) phosphate and tris(trimethylsilyl) phosphite as electrolyte additives for Li-ion cells, submitted to 3M for approval to publish (Aug 1, 2013). (n.d.).
- [147] H.Y. Xu, S. Xie, Q.Y. Wang, X.L. Yao, Q.S. Wang, C.H. Chen, Electrolyte additive trimethyl phosphite for improving electrochemical performance and thermal stability of LiCoO₂ cathode, *Electrochimica Acta.* 52 (2006) 636–642. doi:10.1016/j.electacta.2006.05.043.
- [148] Y.-M. Song, J.-G. Han, S. Park, K.T. Lee, N.-S. Choi, A multifunctional phosphite-containing electrolyte for 5 V-class LiNi_{0.5}Mn_{1.5}O₄ cathodes with superior electrochemical performance, *J. Mater. Chem. A.* 2 (2014) 9506. doi:10.1039/c4ta01129e.

- [149] A. von Cresce, K. Xu, Electrolyte Additive in Support of 5 V Li Ion Chemistry, *J. Electrochem. Soc.* 158 (2011) A337. doi:10.1149/1.3532047.
- [150] K.-E. Kim, J.Y. Jang, I. Park, M.-H. Woo, M.-H. Jeong, W.C. Shin, et al., A combination of lithium difluorophosphate and vinylene carbonate as reducible additives to improve cycling performance of graphite electrodes at high rates, *Electrochem. Commun.* 61 (2015) 121–124. doi:10.1016/j.elecom.2015.10.013.
- [151] J. Xia, L. Madec, L. Ma, L.D. Ellis, W. Qiu, K.J. Nelson, et al., Study of triallyl phosphate as an electrolyte additive for high voltage lithium-ion cells, *J. Power Sources.* 295 (2015) 203–211. doi:10.1016/j.jpowsour.2015.06.151.
- [152] G. Yan, X. Li, Z. Wang, H. Guo, C. Wang, Tris(trimethylsilyl)phosphate: A film-forming additive for high voltage cathode material in lithium-ion batteries, *J. Power Sources.* 248 (2014) 1306–1311. doi:10.1016/j.jpowsour.2013.10.037.
- [153] J. Xia, N.N. Sinha, L.P. Chen, J.R. Dahn, A Comparative Study of a Family of Sulfate Electrolyte Additives, *J. Electrochem. Soc.* 161 (2014) A264–A274. doi:10.1149/2.015403jes.
- [154] J. Xia, R. Petibon, N.N. Sinha, J.R. Dahn, One Sulfonate and Three Sulfate Electrolyte Additives Studied in Graphite/LiCoO₂ Pouch Cells, *J. Electrochem. Soc.* 162 (2015) A2227–A2235. doi:10.1149/2.0151512jes.
- [155] B. Li, M. Xu, B. Li, Y. Liu, L. Yang, W. Li, et al., Properties of solid electrolyte interphase formed by prop-1-ene-1,3-sultone on graphite anode of Li-ion batteries, *Electrochimica Acta.* 105 (2013) 1–6. doi:10.1016/j.electacta.2013.04.142.
- [156] X. Zuo, M. Xu, W. Li, D. Su, J. Liu, Electrochemical Reduction of 1,3-Propane Sultone on Graphite Electrodes and Its Application in Li-Ion Batteries, *Electrochem. Solid-State Lett.* 9 (2006) A196. doi:10.1149/1.2170462.
- [157] B. Li, M. Xu, T. Li, W. Li, S. Hu, Prop-1-ene-1,3-sultone as SEI formation additive in propylene carbonate-based electrolyte for lithium ion batteries, *Electrochem. Commun.* 17 (2012) 92–95. doi:10.1016/j.elecom.2012.02.016.
- [158] B. Zhang, M. Metzger, S. Solchenbach, M. Payne, S. Meini, H.A. Gasteiger, et al., Role of 1,3-Propane Sultone and Vinylene Carbonate in Solid Electrolyte Interface (SEI) Formation and Gas Generation, *J. Phys. Chem. C.* (2015). doi:10.1021/acs.jpcc.5b00072.
- [159] L. Zhang, L. Chai, L. Zhang, M. Shen, X. Zhang, V.S. Battaglia, et al., Synergistic effect between lithium bis(fluorosulfonyl)imide (LiFSI) and lithium bis-oxalato borate (LiBOB) salts in LiPF₆-based electrolyte for high-performance Li-ion batteries, *Electrochimica Acta.* 127 (2014) 39–44. doi:10.1016/j.electacta.2014.02.008.
- [160] Z. Wang, L. Xing, J. Li, M. Xu, W. Li, Triethylborate as an electrolyte additive for high voltage layered lithium nickel cobalt manganese oxide cathode of lithium ion battery, *J. Power Sources.* 307 (2016) 587–592. doi:10.1016/j.jpowsour.2015.11.091.
- [161] L.E. Ouatani, R. Dedryvère, C. Siret, P. Biensan, D. Gonbeau, Effect of Vinylene Carbonate Additive in Li-Ion Batteries: Comparison of LiCoO₂/C, LiFePO₄/C, and LiCoO₂/Li₄Ti₅O₁₂ Systems, *J. Electrochem. Soc.* 156 (2009) A468–A477. doi:10.1149/1.3111891.
- [162] A. Koiwai, T. Shiga, K. Takechi, Nonaqueous electrolytic solution for battery and nonaqueous electrolytic solution battery, US6077628 A, 2000.

- [163] K. Takechi, T. Shiga, Nonaqueous electrolytic solution for battery and nonaqueous electrolytic solution battery using the same, US6235431 B1, 2001.
- [164] W. Li, C. Campion, B.L. Lucht, B. Ravdel, J. DiCarlo, K.M. Abraham, Additives for Stabilizing LiPF₆-Based Electrolytes Against Thermal Decomposition, *J. Electrochem. Soc.* 152 (2005) A1361–A1365. doi:10.1149/1.1926651.
- [165] K. Xu, S. Zhang, B.A. Poesse, T.R. Jow, Lithium Bis(oxalato)borate Stabilizes Graphite Anode in Propylene Carbonate, *Electrochem. Solid-State Lett.* 5 (2002) A259–A262. doi:10.1149/1.1510322.
- [166] D.Y. Wang, A. Xiao, L. Wells, J.R. Dahn, Effect of Mixtures of Lithium Hexafluorophosphate (LiPF₆) and Lithium Bis(fluorosulfonyl)imide (LiFSI) as Salts in Li[Ni_{1/3}Mn_{1/3}Co_{1/3}]O₂/Graphite Pouch Cells, *J. Electrochem. Soc.* 162 (2015) A169–A175. doi:10.1149/2.0821501jes.
- [167] Y. Ein-Eli, S.R. Thomas, V.R. Koch, The Role of SO₂ as an Additive to Organic Li-Ion Battery Electrolytes, *J. Electrochem. Soc.* 144 (1997) 1159–1165. doi:10.1149/1.1837566.
- [168] H. Mao, J.N. Reimers, U.V. Sacken, Additives for improving cycle life of non-aqueous rechargeable lithium batteries, US5891592 A, 1999.
- [169] U. Heider, M. Schmidt, A. Amann, M. Niemann, A. Kühner, Use of additives in electrolyte for electrochemical cells, US6548212 B1, 2003.
- [170] P. Murmann, B. Streipert, R. Kloepsch, N. Ignatiev, P. Sartori, M. Winter, et al., Lithium-cyclo-difluoromethane-1,1-bis(sulfonyl)imide as a stabilizing electrolyte additive for improved high voltage applications in lithium-ion batteries, *Phys Chem Chem Phys.* 17 (2015) 9352–9358. doi:10.1039/C5CP00483G.
- [171] A.J. Smith, J.C. Burns, S. Trussler, J.R. Dahn, Precision Measurements of the Coulombic Efficiency of Lithium-Ion Batteries and of Electrode Materials for Lithium-Ion Batteries, *J. Electrochem. Soc.* 157 (2010) A196–A202. doi:10.1149/1.3268129.
- [172] J.C. Burns, N.N. Sinha, D.J. Coyle, G. Jain, C.M. VanElzen, W.M. Lamanna, et al., The Impact of Varying the Concentration of Vinylene Carbonate Electrolyte Additive in Wound Li-Ion Cells, *J. Electrochem. Soc.* 159 (2011) A85–A90. doi:10.1149/2.028202jes.
- [173] M. Grützke, X. Mönnighoff, F. Horsthemke, V. Kraft, M. Winter, S. Nowak, Extraction of lithium-ion battery electrolytes with liquid and supercritical carbon dioxide and additional solvents, *RSC Adv.* 5 (2015) 43209–43217. doi:10.1039/C5RA04451K.
- [174] H. Lee, S. Choi, S. Choi, H.-J. Kim, Y. Choi, S. Yoon, et al., SEI layer-forming additives for LiNi_{0.5}Mn_{1.5}O₄/graphite 5 V Li-ion batteries, *Electrochem. Commun.* 9 (2007) 801–806. doi:10.1016/j.elecom.2006.11.008.
- [175] T. Momma, T. Yokoshima, H. Nara, Y. Gima, T. Osaka, Distinction of impedance responses of Li-ion batteries for individual electrodes using symmetric cells, *Electrochimica Acta.* 131 (2014) 195–201. doi:10.1016/j.electacta.2014.01.091.
- [176] S.E. Trask, K.Z. Pupek, J.A. Gilbert, M. Klett, B.J. Polzin, A.N. Jansen, et al., Performance of Full Cells Containing Carbonate-Based LiFSI Electrolytes and Silicon-Graphite Negative Electrodes, *J. Electrochem. Soc.* 163 (2016) A345–A350. doi:10.1149/2.0981602jes.

- [177] C.P. Aiken, J. Xia, D.Y. Wang, D.A. Stevens, S. Trussler, J.R. Dahn, An Apparatus for the Study of In Situ Gas Evolution in Li-Ion Pouch Cells, *J. Electrochem. Soc.* 161 (2014) A1548–A1554. doi:10.1149/2.0151410jes.
- [178] T.M. Bond, J.C. Burns, D.A. Stevens, H.M. Dahn, J.R. Dahn, Improving Precision and Accuracy in Coulombic Efficiency Measurements of Li-Ion Batteries, *J. Electrochem. Soc.* 160 (2013) A521–A527. doi:10.1149/2.014304jes.
- [179] M.E. Orazem, B. Tribollet, *Electrochemical impedance spectroscopy*, Wiley, Hoboken, N.J., 2008.
- [180] J.-M. Atebamba, J. Moskon, S. Pejovnik, M. Gaberscek, On the Interpretation of Measured Impedance Spectra of Insertion Cathodes for Lithium-Ion Batteries, *J. Electrochem. Soc.* 157 (2010) A1218–A1228. doi:10.1149/1.3489353.
- [181] D.C. Harris, *Quantitative chemical analysis*, 8th ed, W.H. Freeman and Co, New York, 2010.
- [182] F.W. McLafferty, *Interpretation of mass spectra*, 4th ed, University Science Books, Mill Valley, Calif, 1993.
- [183] P.E. Miller, M.B. Denton, The quadrupole mass filter: Basic operating concepts, *J. Chem. Educ.* 63 (1986) 617. doi:10.1021/ed063p617.
- [184] D.A. Skoog, F.J. Holler, S.R. Crouch, *Principles of instrumental analysis*, 6th ed, Thomson Brooks/Cole, Belmont, CA, 2007.
- [185] H. Yoshida, T. Fukunaga, T. Hazama, M. Terasaki, M. Mizutani, M. Yamachi, Degradation mechanism of alkyl carbonate solvents used in lithium-ion cells during initial charging, *J. Power Sources.* 68 (1997) 311–315. doi:10.1016/S0378-7753(97)02635-9.
- [186] T. Sasaki, T. Abe, Y. Iriyama, M. Inaba, Z. Ogumi, Formation mechanism of alkyl dicarbonates in Li-ion cells, *J. Power Sources.* 150 (2005) 208–215. doi:10.1016/j.jpowsour.2005.02.021.
- [187] L. Terborg, S. Weber, S. Passerini, M. Winter, U. Karst, S. Nowak, Development of gas chromatographic methods for the analyses of organic carbonate-based electrolytes, *J. Power Sources.* 245 (2014) 836–840. doi:10.1016/j.jpowsour.2013.07.030.
- [188] S.E. Sloop, J.K. Pugh, S. Wang, J.B. Kerr, K. Kinoshita, Chemical Reactivity of PF₅ and LiPF₆ in Ethylene Carbonate/Dimethyl Carbonate Solutions, *Electrochem. Solid-State Lett.* 4 (2001) A42–A44. doi:10.1149/1.1353158.
- [189] K. Kumai, H. Miyashiro, Y. Kobayashi, K. Takei, R. Ishikawa, Gas generation mechanism due to electrolyte decomposition in commercial lithium-ion cell, *J. Power Sources.* 81–82 (1999) 715–719. doi:10.1016/S0378-7753(98)00234-1.
- [190] H. Ota, Y. Sakata, A. Inoue, S. Yamaguchi, Analysis of Vinylene Carbonate Derived SEI Layers on Graphite Anode, *J. Electrochem. Soc.* 151 (2004) A1659–A1669. doi:10.1149/1.1785795.
- [191] J.-Y. Eom, I.-H. Jung, J.-H. Lee, Effects of vinylene carbonate on high temperature storage of high voltage Li-ion batteries, *J. Power Sources.* 196 (2011) 9810–9814. doi:10.1016/j.jpowsour.2011.06.095.
- [192] T. Sasaki, T. Abe, Y. Iriyama, M. Inaba, Z. Ogumi, Suppression of an Alkyl Dicarboxate Formation in Li-Ion Cells, *J. Electrochem. Soc.* 152 (2005) A2046–A2050. doi:10.1149/1.2034517.

- [193] H. Kim, S. Grugeon, G. Gachot, M. Armand, L. Sannier, S. Laruelle, Ethylene bis-carbonates as telltales of SEI and electrolyte health, role of carbonate type and new additives, *Electrochimica Acta*. 136 (2014) 157–165. doi:10.1016/j.electacta.2014.05.072.
- [194] R. Nozu, M. Nakamura, K. Banno, T. Maruo, T. Sato, Studying a Phenomenon during Overcharge of a Lithium-Ion Battery with Methacrylate Additives for the Gel Electrolyte, *J. Electrochem. Soc.* 153 (2006) A1031–A1037. doi:10.1149/1.2186207.
- [195] D.G. Westmoreland, G.R. Rhodes, Analytical techniques for trace organic compounds - II. Detectors for gas chromatography, *Pure Appl. Chem.* 61 (1989) 1147–1160. doi:10.1351/pac198961061147.
- [196] L. Gireaud, S. Grugeon, S. Pilard, P. Guenot, J.-M. Tarascon, S. Laruelle, Mass Spectrometry Investigations on Electrolyte Degradation Products for the Development of Nanocomposite Electrodes in Lithium Ion Batteries, *Anal. Chem.* 78 (2006) 3688–3698. doi:10.1021/ac051987w.
- [197] C.L. Campion, W. Li, B.L. Lucht, Thermal Decomposition of LiPF₆-Based Electrolytes for Lithium-Ion Batteries, *J. Electrochem. Soc.* 152 (2005) A2327–A2334. doi:10.1149/1.2083267.
- [198] B.A. Johnson, R.E. White, Characterization of commercially available lithium-ion batteries, *J. Power Sources*. 70 (1998) 48–54. doi:10.1016/S0378-7753(97)02659-1.
- [199] M. Anouti, Y.R. Dougassa, C. Tessier, L. El Ouatani, J. Jacquemin, Low pressure carbon dioxide solubility in pure electrolyte solvents for lithium-ion batteries as a function of temperature. Measurement and prediction, *J. Chem. Thermodyn.* 50 (2012) 71–79. doi:10.1016/j.jct.2012.01.027.
- [200] Y.R. Dougassa, J. Jacquemin, L. El Ouatani, C. Tessier, M. Anouti, Viscosity and Carbon Dioxide Solubility for LiPF₆, LiTFSI, and LiFAP in Alkyl Carbonates: Lithium Salt Nature and Concentration Effect, *J. Phys. Chem. B*. 118 (2014) 3973–3980. doi:10.1021/jp500063c.
- [201] Y.R. Dougassa, C. Tessier, L. El Ouatani, M. Anouti, J. Jacquemin, Low pressure carbon dioxide solubility in lithium-ion batteries based electrolytes as a function of temperature. Measurement and prediction, *J. Chem. Thermodyn.* 61 (2013) 32–44. doi:10.1016/j.jct.2012.12.025.
- [202] Y.R. Dougassa, J. Jacquemin, L. El Ouatani, C. Tessier, M. Anouti, Low pressure methane solubility in lithium-ion batteries based solvents and electrolytes as a function of temperature. Measurement and prediction, *J. Chem. Thermodyn.* 79 (2014) 49–60. doi:10.1016/j.jct.2014.07.004.
- [203] L.E. Ouatani, R. Dedryvère, C. Siret, P. Biensan, S. Reynaud, P. Iratçabal, et al., The Effect of Vinylene Carbonate Additive on Surface Film Formation on Both Electrodes in Li-Ion Batteries, *J. Electrochem. Soc.* 156 (2009) A103–A113. doi:10.1149/1.3029674.
- [204] L. Madec, R. Petibon, K. Tasaki, J. Xia, J.-P. Sun, I.G. Hill, et al., Mechanism of action of ethylene sulfite and vinylene carbonate electrolyte additives in LiNi_{1/3}Mn_{1/3}Co_{1/3}O₂/graphite pouch cells: electrochemical, GC-MS and XPS analysis, *Phys Chem Chem Phys*. 17 (2015) 27062–27076. doi:10.1039/C5CP04221F.

- [205] M. Nie, J. Demeaux, B.T. Young, D.R. Heskett, Y. Chen, A. Bose, et al., Effect of Vinylene Carbonate and Fluoroethylene Carbonate on SEI Formation on Graphitic Anodes in Li-Ion Batteries, *J. Electrochem. Soc.* 162 (2015) A7008–A7014. doi:10.1149/2.0021513jes.
- [206] H.J. Santner, C. Korepp, M. Winter, J.O. Besenhard, K.-C. Möller, In-situ FTIR investigations on the reduction of vinylene electrolyte additives suitable for use in lithium-ion batteries, *Anal. Bioanal. Chem.* 379 (2004) 266–271. doi:10.1007/s00216-004-2522-4.
- [207] J. Xia, L. Ma, C.P. Aiken, K.J. Nelson, L.P. Chen, J.R. Dahn, Comparative Study on Prop-1-ene-1,3-sultone and Vinylene Carbonate as Electrolyte Additives for Li(Ni_{1/3}Mn_{1/3}Co_{1/3})O₂/Graphite Pouch Cells, *J. Electrochem. Soc.* 161 (2014) A1634–A1641. doi:10.1149/2.0541410jes.
- [208] L. Madec, R. Petibon, J. Xia, J.-P. Sun, I.G. Hill, J.R. Dahn, Understanding the Role of Prop-1-ene-1,3-Sultone and Vinylene Carbonate in LiNi_{1/3} Mn_{1/3} Co_{1/3}O₂ /Graphite Pouch Cells: Electrochemical, GC-MS and XPS Analysis, *J. Electrochem. Soc.* 162 (2015) A2635–A2645. doi:10.1149/2.0741512jes.
- [209] J. Self, D.S. Hall, L. Madec, J.R. Dahn, The role of prop-1-ene-1,3-sultone as an additive in lithium-ion cells, *J. Power Sources.* 298 (2015) 369–378. doi:10.1016/j.jpowsour.2015.08.060.
- [210] R. Petibon, L. Rotermund, K.J. Nelson, A.S. Gozdz, J. Xia, J.R. Dahn, Study of Electrolyte Components in Li Ion Cells Using Liquid-Liquid Extraction and Gas Chromatography Coupled with Mass Spectrometry, *J. Electrochem. Soc.* 161 (2014) A1167–A1172. doi:10.1149/2.117406jes.
- [211] A.-A.G. Shaikh, S. Sivaram, Organic Carbonates, *Chem. Rev.* 96 (1996) 951–976. doi:10.1021/cr950067i.
- [212] Y. Wang, S. Nakamura, K. Tasaki, P.B. Balbuena, Theoretical Studies To Understand Surface Chemistry on Carbon Anodes for Lithium-Ion Batteries: How Does Vinylene Carbonate Play Its Role as an Electrolyte Additive?, *J. Am. Chem. Soc.* 124 (2002) 4408–4421. doi:10.1021/ja017073i.
- [213] D. Guyomard, Rechargeable Li_{1+x}Mn₂O₄/Carbon Cells with a New Electrolyte Composition, *J. Electrochem. Soc.* 140 (1993) 3071. doi:10.1149/1.2220987.
- [214] K.J. Nelson, J. Xia, J.R. Dahn, Studies of the Effect of Varying Prop-1-ene-1,3-sultone Content in Lithium Ion Pouch Cells, *J. Electrochem. Soc.* 161 (2014) A1884–A1889. doi:10.1149/2.0791412jes.
- [215] R. Petibon, E.C. Henry, J.C. Burns, N.N. Sinha, J.R. Dahn, Comparative Study of Vinyl Ethylene Carbonate (VEC) and Vinylene Carbonate (VC) in LiCoO₂/Graphite Pouch Cells Using High Precision Coulometry and Electrochemical Impedance Spectroscopy Measurements on Symmetric Cells, *J. Electrochem. Soc.* 161 (2014) A66–A74. doi:10.1149/2.030401jes.
- [216] R. Petibon, L.M. Rotermund, J.R. Dahn, Evaluation of phenyl carbonates as electrolyte additives in lithium-ion batteries, *J. Power Sources.* 287 (2015) 184–195. doi:10.1016/j.jpowsour.2015.04.012.
- [217] H.M. Dahn, A.J. Smith, J.C. Burns, D.A. Stevens, J.R. Dahn, User-Friendly Differential Voltage Analysis Freeware for the Analysis of Degradation Mechanisms in Li-Ion Batteries, *J. Electrochem. Soc.* 159 (2012) A1405–A1409. doi:10.1149/2.013209jes.

- [218] A. Jarry, S. Gottis, Y.-S. Yu, J. Roque-Rosell, C. Kim, J. Cabana, et al., The Formation Mechanism of Fluorescent Metal Complexes at the $\text{Li}_x\text{Ni}_{0.5}\text{Mn}_{1.5}\text{O}_{4-\delta}$ /Carbonate Ester Electrolyte Interface, *J. Am. Chem. Soc.* 137 (2015) 3533–3539. doi:10.1021/ja5116698.
- [219] S.R. Li, C.H. Chen, X. Xia, J.R. Dahn, The Impact of Electrolyte Oxidation Products in $\text{LiNi}_{0.5}\text{Mn}_{1.5}\text{O}_4/\text{Li}_4\text{Ti}_5\text{O}_{12}$ Cells, *J. Electrochem. Soc.* 160 (2013) A1524–A1528. doi:10.1149/2.051309jes.
- [220] D.J. Xiong, R. Petibon, M. Nie, L. Ma, J. Xia, J.R. Dahn, Interactions between Positive and Negative Electrodes in Li-Ion Cells Operated at High Temperature and High Voltage, *J. Electrochem. Soc.* 163 (2016) A546–A551. doi:10.1149/2.0951603jes.
- [221] R. Petibon, L. Madec, L.M. Rotermund, J.R. Dahn, Study of the consumption of the additive prop-1-ene-1,3-sultone in $\text{Li}[\text{Ni}_{0.33}\text{Mn}_{0.33}\text{Co}_{0.33}]\text{O}_2/\text{graphite}$ pouch cells and evidence of positive-negative electrode interaction, *J. Power Sources.* 313 (2016) 152–163. doi:10.1016/j.jpowsour.2016.02.054.
- [222] L. Ma, D.Y. Wang, L.E. Downie, J. Xia, K.J. Nelson, N.N. Sinha, et al., Ternary and Quaternary Electrolyte Additive Mixtures for Li-Ion Cells That Promote Long Lifetime, High Discharge Rate and Better Safety, *J. Electrochem. Soc.* 161 (2014) A1261–A1265. doi:10.1149/2.0541409jes.
- [223] X. Zhang, J.K. Pugh, P.N. Ross, Computation of Thermodynamic Oxidation Potentials of Organic Solvents Using Density Functional Theory, *J. Electrochem. Soc.* 148 (2001) E183. doi:10.1149/1.1362546.
- [224] R.P. Day, J. Xia, R. Petibon, J. Rucska, H. Wang, A.T.B. Wright, et al., Differential Thermal Analysis of Li-Ion Cells as an Effective Probe of Liquid Electrolyte Evolution during Aging, *J. Electrochem. Soc.* 162 (2015) A2577–A2581. doi:10.1149/2.0181514jes.
- [225] M. Metzger, B. Strehle, S. Solchenbach, H.A. Gasteiger, Origin of H_2 Evolution in LIBs: H_2O Reduction vs. Electrolyte Oxidation, *J. Electrochem. Soc.* 163 (2016) A798–A809. doi:10.1149/2.1151605jes.
- [226] C. Buhrmester, J. Chen, L. Moshurchak, J. Jiang, R.L. Wang, J.R. Dahn, Studies of Aromatic Redox Shuttle Additives for LiFePO_4 -Based Li-Ion Cells, *J. Electrochem. Soc.* 152 (2005) A2390–A2399. doi:10.1149/1.2098265.
- [227] M. Adachi, K. Tanaka, K. Sekai, Aromatic Compounds as Redox Shuttle Additives for 4 V Class Secondary Lithium Batteries, *J. Electrochem. Soc.* 146 (1999) 1256–1261. doi:10.1149/1.1391755.
- [228] H. Mao, U.V. Sacken, Aromatic monomer gassing agents for protecting non-aqueous lithium batteries against overcharge, US5776627 A, 1998. <http://www.google.ca/patents/US5776627> (accessed January 14, 2015).
- [229] L. Xiao, X. Ai, Y. Cao, H. Yang, Electrochemical behavior of biphenyl as polymerizable additive for overcharge protection of lithium ion batteries, *Electrochimica Acta.* 49 (2004) 4189–4196. doi:10.1016/j.electacta.2004.04.013.
- [230] J.N. Reimers, B.M. Way, Additives selected from the group consisting of phenyl-aliphatic hydrocarbon-phenyl compounds, fluorine substituted biphenyl compounds, and 3-thiopheneacetonitrile can provide better cycling performances; fireproofing, US6074777 A, 2000. <http://www.google.ca/patents/US6074777> (accessed January 14, 2015).

- [231] Y. Nakagawa, M. Kotato, D. Noda, S. Kinoshita, Nonaqueous electrolytic solution and nonaqueous-electrolyte battery, US20120219854 A1, 2012. <http://www.google.ca/patents/US20120219854> (accessed January 15, 2015).
- [232] E. Peled, D. Golodnitsky, C. Menachem, D. Bar-Tow, An Advanced Tool for the Selection of Electrolyte Components for Rechargeable Lithium Batteries, *J. Electrochem. Soc.* 145 (1998) 3482–3486. doi:10.1149/1.1838831.
- [233] R. Imhof, P. Novák, In Situ Investigation of the Electrochemical Reduction of Carbonate Electrolyte Solutions at Graphite Electrodes, *J. Electrochem. Soc.* 145 (1998) 1081–1087. doi:10.1149/1.1838420.
- [234] D. Xiong, R. Petibon, J.C. Burns, J. Dahn, The Effect of Intentionally Added Water on Gas Evolution in Li-Ion Pouch Cells, Meet. Abstr. MA2014-02 (2014) 441–441.
- [235] G.-Y. Kim, R. Petibon, J.R. Dahn, Effects of Succinonitrile (SN) as an Electrolyte Additive on the Impedance of LiCoO₂/Graphite Pouch Cells during Cycling, *J. Electrochem. Soc.* 161 (2014) A506–A512. doi:10.1149/2.014404jes.
- [236] J. Xia, C.P. Aiken, L. Ma, G.Y. Kim, J.C. Burns, L.P. Chen, et al., Combinations of Ethylene Sulfite (ES) and Vinylene Carbonate (VC) as Electrolyte Additives in Li(Ni_{1/3}Mn_{1/3}Co_{1/3})O₂/Graphite Pouch Cells, *J. Electrochem. Soc.* 161 (2014) A1149–A1157. doi:10.1149/2.108406jes.
- [237] M. Winter, J.O. Besenhard, Electrochemical lithiation of tin and tin-based intermetallics and composites, *Electrochimica Acta.* 45 (1999) 31–50. doi:10.1016/S0013-4686(99)00191-7.
- [238] Z. Du, R.A. Dunlap, M.N. Obrovac, High Energy Density Calendered Si Alloy/Graphite Anodes, *J. Electrochem. Soc.* 161 (2014) A1698–A1705. doi:10.1149/2.0941410jes.
- [239] C.C. Nguyen, B.L. Lucht, Comparative Study of Fluoroethylene Carbonate and Vinylene Carbonate for Silicon Anodes in Lithium Ion Batteries, *J. Electrochem. Soc.* 161 (2014) A1933–A1938. doi:10.1149/2.0731412jes.
- [240] L.-F. Cui, Y. Yang, C.-M. Hsu, Y. Cui, Carbon–Silicon Core–Shell Nanowires as High Capacity Electrode for Lithium Ion Batteries, *Nano Lett.* 9 (2009) 3370–3374. doi:10.1021/nl901670t.
- [241] N. Liu, Z. Lu, J. Zhao, M.T. McDowell, H.-W. Lee, W. Zhao, et al., A pomegranate-inspired nanoscale design for large-volume-change lithium battery anodes, *Nat. Nanotechnol.* 9 (2014) 187–192. doi:10.1038/nnano.2014.6.
- [242] H.K. Han, C. Loka, Y.M. Yang, J.H. Kim, S.W. Moon, J.S. Cho, et al., High capacity retention Si/silicide nanocomposite anode materials fabricated by high-energy mechanical milling for lithium-ion rechargeable batteries, *J. Power Sources.* 281 (2015) 293–300. doi:10.1016/j.jpowsour.2015.01.122.
- [243] L. Niedzicki, B. Brzozowski, P. Wiczorek, LiTDI and solvent mixture based electrolytes for lithium-ion cells, *Electrochimica Acta.* 174 (2015) 625–629. doi:10.1016/j.electacta.2015.06.038.
- [244] E. Markevich, K. Fridman, R. Sharabi, R. Elazari, G. Salitra, H.E. Gottlieb, et al., Amorphous Columnar Silicon Anodes for Advanced High Voltage Lithium Ion Full Cells: Dominant Factors Governing Cycling Performance, *J. Electrochem. Soc.* 160 (2013) A1824–A1833. doi:10.1149/2.085310jes.

- [245] J.-H. Cho, S.T. Picraux, Enhanced Lithium Ion Battery Cycling of Silicon Nanowire Anodes by Template Growth to Eliminate Silicon Underlayer Islands, *Nano Lett.* 13 (2013) 5740–5747. doi:10.1021/nl4036498.
- [246] H. Wu, G. Yu, L. Pan, N. Liu, M.T. McDowell, Z. Bao, et al., Stable Li-ion battery anodes by in-situ polymerization of conducting hydrogel to conformally coat silicon nanoparticles, *Nat. Commun.* 4 (2013). doi:10.1038/ncomms2941.
- [247] J. Liang, X. Li, Y. Zhu, C. Guo, Y. Qian, Hydrothermal synthesis of nano-silicon from a silica sol and its use in lithium ion batteries, *Nano Res.* 8 (2015) 1497–1504. doi:10.1007/s12274-014-0633-6.
- [248] P.P. Prosini, C. Cento, A. Rufoloni, F. Rondino, A. Santoni, A lithium-ion battery based on LiFePO_4 and silicon nanowires, *Solid State Ion.* 269 (2015) 93–97. doi:10.1016/j.ssi.2014.11.019.
- [249] K. Eom, T. Joshi, A. Bordes, I. Do, T.F. Fuller, The design of a Li-ion full cell battery using a nano silicon and nano multi-layer graphene composite anode, *J. Power Sources.* 249 (2014) 118–124. doi:10.1016/j.jpowsour.2013.10.087.
- [250] J.-K. Kim, G.-B. Cho, H.-S. Ryu, H.-J. Ahn, K.-K. Cho, K.-W. Kim, et al., Electrochemical properties of a full cell of lithium iron phosphate cathode using thin amorphous silicon anode, *Solid State Ion.* 268 (2014) 256–260. doi:10.1016/j.ssi.2014.10.010.
- [251] S.J. Lee, J.-G. Han, Y. Lee, M.-H. Jeong, W.C. Shin, M. Ue, et al., A bi-functional lithium difluoro(oxalato)borate additive for lithium cobalt oxide/lithium nickel manganese cobalt oxide cathodes and silicon/graphite anodes in lithium-ion batteries at elevated temperatures, *Electrochimica Acta.* 137 (2014) 1–8. doi:10.1016/j.electacta.2014.05.136.
- [252] I.H. Son, J. Hwan Park, S. Kwon, S. Park, M.H. Rummeli, A. Bachmatiuk, et al., Silicon carbide-free graphene growth on silicon for lithium-ion battery with high volumetric energy density, *Nat. Commun.* 6 (2015) 7393. doi:10.1038/ncomms8393.
- [253] R. Elazari, G. Salitra, G. Gershinshy, A. Garsuch, A. Panchenko, D. Aurbach, Li Ion Cells Comprising Lithiated Columnar Silicon Film Anodes, TiS_2 Cathodes and Fluoroethylene Carbonate (FEC) as a Critically Important Component, *J. Electrochem. Soc.* 159 (2012) A1440–A1445. doi:10.1149/2.029209jes.
- [254] K. Schroder, J. Alvarado, T.A. Yersak, J. Li, N. Dudney, L.J. Webb, et al., The Effect of Fluoroethylene Carbonate as an Additive on the Solid Electrolyte Interphase on Silicon Lithium-Ion Electrodes, *Chem. Mater.* 27 (2015) 5531–5542. doi:10.1021/acs.chemmater.5b01627.
- [255] C. Xu, F. Lindgren, B. Philippe, M. Gorgoi, F. Björefors, K. Edström, et al., Improved Performance of the Silicon Anode for Li-Ion Batteries: Understanding the Surface Modification Mechanism of Fluoroethylene Carbonate as an Effective Electrolyte Additive, *Chem. Mater.* 27 (2015) 2591–2599. doi:10.1021/acs.chemmater.5b00339.
- [256] H.-J. Peng, S. Urbonaitė, C. Villevieille, H. Wolf, K. Leitner, P. Novák, Consequences of Electrolyte Degradation for the Electrochemical Performance of $\text{Li}_{1+x}(\text{Ni}_a\text{Co}_b\text{Mn}_{1-a-b})_{1-x}\text{O}_2$, *J. Electrochem. Soc.* 162 (2015) A7072–A7077. doi:10.1149/2.0061513jes.

- [257] K. Leung, S.B. Rempe, M.E. Foster, Y. Ma, J.M.M. del la Hoz, N. Sai, et al., Modeling Electrochemical Decomposition of Fluoroethylene Carbonate on Silicon Anode Surfaces in Lithium Ion Batteries, *J. Electrochem. Soc.* 161 (2014) A213–A221. doi:10.1149/2.092401jes.
- [258] V. Etacheri, O. Haik, Y. Goffer, G.A. Roberts, I.C. Stefan, R. Fasching, et al., Effect of Fluoroethylene Carbonate (FEC) on the Performance and Surface Chemistry of Si-Nanowire Li-Ion Battery Anodes, *Langmuir*. 28 (2012) 965–976. doi:10.1021/la203712s.
- [259] Y. Ma, P.B. Balbuena, DFT Study of Reduction Mechanisms of Ethylene Carbonate and Fluoroethylene Carbonate on Li^+ -Adsorbed Si Clusters, *J. Electrochem. Soc.* 161 (2014) E3097–E3109. doi:10.1149/2.014408jes.
- [260] R. Bernhard, M. Metzger, H.A. Gasteiger, Gas Evolution at Graphite Anodes Depending on Electrolyte Water Content and SEI Quality Studied by On-Line Electrochemical Mass Spectrometry, *J. Electrochem. Soc.* 162 (2015) A1984–A1989. doi:10.1149/2.0191510jes.
- [261] J. Self, C.P. Aiken, R. Petibon, J.R. Dahn, Survey of Gas Expansion in Li-Ion NMC Pouch Cells, *J. Electrochem. Soc.* 162 (2015) A796–A802. doi:10.1149/2.0081506jes.
- [262] D.Y. Wang, N.N. Sinha, J.C. Burns, C.P. Aiken, R. Petibon, J.R. Dahn, A Comparative Study of Vinylene Carbonate and Fluoroethylene Carbonate Additives for LiCoO_2 /Graphite Pouch Cells, *J. Electrochem. Soc.* 161 (2014) A467–A472. doi:10.1149/2.001404jes.
- [263] A.J. Smith, H.M. Dahn, J.C. Burns, J.R. Dahn, Long-Term Low-Rate Cycling of LiCoO_2 /Graphite Li-Ion Cells at 55°C , *J. Electrochem. Soc.* 159 (2012) A705–A710. doi:10.1149/2.056206jes.
- [264] R. Fathi, J.C. Burns, D.A. Stevens, H. Ye, C. Hu, G. Jain, et al., Ultra High-Precision Studies of Degradation Mechanisms in Aged LiCoO_2 /Graphite Li-Ion Cells, *J. Electrochem. Soc.* 161 (2014) A1572–A1579. doi:10.1149/2.0321410jes.
- [265] M.B. Pinson, M.Z. Bazant, Theory of SEI Formation in Rechargeable Batteries: Capacity Fade, Accelerated Aging and Lifetime Prediction, *J. Electrochem. Soc.* 160 (2013) A243–A250. doi:10.1149/2.044302jes.
- [266] G.E. Blomgren, Electrolytes for advanced batteries, *J. Power Sources*. 81-82 (1999) 112–118. doi:10.1016/S0378-7753(99)00188-3.
- [267] T. Yoshida, M. Takahashi, S. Morikawa, C. Ihara, H. Katsukawa, T. Shiratsuchi, et al., Degradation Mechanism and Life Prediction of Lithium-Ion Batteries, *J. Electrochem. Soc.* 153 (2006) A576. doi:10.1149/1.2162467.
- [268] D.Y. Wang, N.N. Sinha, R. Petibon, J.C. Burns, J.R. Dahn, A systematic study of well-known electrolyte additives in LiCoO_2 /graphite pouch cells, *J. Power Sources*. 251 (2014) 311–318. doi:10.1016/j.jpowsour.2013.11.064.
- [269] M.C. Smart, B.V. Ratnakumar, S. Surampudi, Electrolytes for Low-Temperature Lithium Batteries Based on Ternary Mixtures of Aliphatic Carbonates, *J. Electrochem. Soc.* 146 (1999) 486–492. doi:10.1149/1.1391633.
- [270] M.C. Smart, B.V. Ratnakumar, K.B. Chin, L.D. Whitcanack, Lithium-Ion Electrolytes Containing Ester Cosolvents for Improved Low Temperature Performance, *J. Electrochem. Soc.* 157 (2010) A1361–A1374. doi:10.1149/1.3501236.

- [271] S.V. Sazhin, M.Y. Khimchenko, Y.N. Tritenichenko, H.S. Lim, Performance of Li-ion cells with new electrolytes conceived for low-temperature applications, *J. Power Sources*. 87 (2000) 112–117. doi:10.1016/S0378-7753(99)00434-6.
- [272] R.C.P.D. Weast, *CRC Handbook of Chemistry and Physics - 70th Edition*, CRC Press, 1990.
- [273] D.S. Viswanath, *Databook On The Viscosity Of Liquids*, CRC Press, New York, 1989.
- [274] Y. Ein-Eli, S.R. Thomas, V.R. Koch, New Electrolyte System for Li-Ion Battery, *J. Electrochem. Soc.* 143 (1996) L195–L197. doi:10.1149/1.1837084.
- [275] C.-C. Chang, S.-H. Hsu, Y.-F. Jung, C.-H. Yang, Vinylene carbonate and vinylene trithiocarbonate as electrolyte additives for lithium ion battery, *J. Power Sources*. 196 (2011) 9605–9611. doi:10.1016/j.jpowsour.2011.06.058.
- [276] G.V. Zhuang, K. Xu, T.R. Jow, P.N. Ross, Study of SEI Layer Formed on Graphite Anodes in PC/LiBOB Electrolyte Using IR Spectroscopy, *Electrochem. Solid-State Lett.* 7 (2004) A224–A227. doi:10.1149/1.1756855.
- [277] G.H. Wrodnigg, T.M. Wrodnigg, J.O. Besenhard, M. Winter, Propylene sulfite as film-forming electrolyte additive in lithium ion batteries, *Electrochem. Commun.* 1 (1999) 148–150. doi:10.1016/S1388-2481(99)00023-5.
- [278] S. Takeuchi, T. Fukutsuka, K. Miyazaki, T. Abe, Electrochemical lithium ion intercalation into graphite electrode in propylene carbonate-based electrolytes with dimethyl carbonate and calcium salt, *J. Power Sources*. 238 (2013) 65–68. doi:10.1016/j.jpowsour.2013.02.084.
- [279] K. Xu, S. Zhang, R. Jow, Electrochemical impedance study of graphite/electrolyte interface formed in LiBOB/PC electrolyte, *J. Power Sources*. 143 (2005) 197–202. doi:10.1016/j.jpowsour.2004.11.026.
- [280] R. Petibon, J. Xia, J.C. Burns, J.R. Dahn, Study of the Consumption of Vinylene Carbonate in Li[Ni_{0.33}Mn_{0.33}Co_{0.33}]O₂/Graphite Pouch Cells, *J. Electrochem. Soc.* 161 (2014) A1618–A1624. doi:10.1149/2.0351410jes.
- [281] L.E. Downie, K.J. Nelson, R. Petibon, V.L. Chevrier, J.R. Dahn, The Impact of Electrolyte Additives Determined Using Isothermal Microcalorimetry, *ECS Electrochem. Lett.* 2 (2013) A106–A109. doi:10.1149/2.010310eel.
- [282] N.N. Sinha, J.C. Burns, J.R. Dahn, Storage Studies on Li/Graphite Cells and the Impact of So-Called SEI-Forming Electrolyte Additives, *J. Electrochem. Soc.* 160 (2013) A709–A714. doi:10.1149/2.008306jes.
- [283] N.N. Sinha, T.H. Marks, H.M. Dahn, A.J. Smith, J.C. Burns, D.J. Coyle, et al., The Rate of Active Lithium Loss from a Soft Carbon Negative Electrode as a Function of Temperature, Time and Electrode Potential, *J. Electrochem. Soc.* 159 (2012) A1672–A1681. doi:10.1149/2.048210jes.
- [284] K. Xu, A. von Cresce, U. Lee, Differentiating Contributions to “Ion Transfer” Barrier from Interphasial Resistance and Li⁺ Desolvation at Electrolyte/Graphite Interface, *Langmuir*. 26 (2010) 11538–11543. doi:10.1021/la1009994.
- [285] M.C. Smart, B.L. Lucht, S. Dalavi, F.C. Krause, B.V. Ratnakumar, The Effect of Additives upon the Performance of MCMB/LiNi_xCo_{1-x}O₂ Li-Ion Cells Containing Methyl Butyrate-Based Wide Operating Temperature Range Electrolytes, *J. Electrochem. Soc.* 159 (2012) A739–A751. doi:10.1149/2.058206jes.

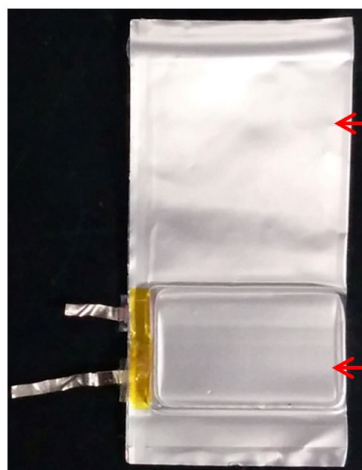
- [286] J. Li, R. Petibon, S. Glazier, N. Sharma, W.K. Pang, V.K. Peterson, et al., In-situ Neutron Diffraction Study of a High Voltage $\text{Li}(\text{Ni}_{0.42}\text{Mn}_{0.42}\text{Co}_{0.16})\text{O}_2/\text{Graphite}$ Pouch Cell, *Electrochimica Acta*. 180 (2015) 234–240. doi:10.1016/j.electacta.2015.08.122.
- [287] K.J. Nelson, D.W. Abarbanel, J. Xia, Z. Lu, J.R. Dahn, Effects of Upper Cutoff Potential on LaPO_4 -Coated and Uncoated $\text{Li}[\text{Ni}_{0.42}\text{Mn}_{0.42}\text{Co}_{0.16}]\text{O}_2/\text{Graphite}$ Pouch Cells, *J. Electrochem. Soc.* 163 (2016) A272–A280. doi:10.1149/2.0691602jes.
- [288] A.M. Wise, C. Ban, J.N. Weker, S. Misra, A.S. Cavanagh, Z. Wu, et al., Effect of Al_2O_3 Coating on Stabilizing $\text{LiNi}_{0.4}\text{Mn}_{0.4}\text{Co}_{0.2}\text{O}_2$ Cathodes, *Chem. Mater.* 27 (2015) 6146–6154. doi:10.1021/acs.chemmater.5b02952.
- [289] Y.-K. Sun, S.-W. Cho, S.-W. Lee, C.S. Yoon, K. Amine, AlF_3 -Coating to Improve High Voltage Cycling Performance of $\text{LiNi}_{1/3}\text{Co}_{1/3}\text{Mn}_{1/3}\text{O}_2$ Cathode Materials for Lithium Secondary Batteries, *J. Electrochem. Soc.* 154 (2007) A168–A172. doi:10.1149/1.2422890.
- [290] S.-K. Hu, G.-H. Cheng, M.-Y. Cheng, B.-J. Hwang, R. Santhanam, Cycle life improvement of ZrO_2 -coated spherical $\text{LiNi}_{1/3}\text{Co}_{1/3}\text{Mn}_{1/3}\text{O}_2$ cathode material for lithium ion batteries, *J. Power Sources*. 188 (2009) 564–569. doi:10.1016/j.jpowsour.2008.11.113.
- [291] J. Xia, M. Nie, J.C. Burns, A. Xiao, W.M. Lamanna, J.R. Dahn, Fluorinated electrolyte for 4.5 V $\text{Li}(\text{Ni}_{0.4}\text{Mn}_{0.4}\text{Co}_{0.2})\text{O}_2/\text{graphite}$ Li-ion cells, *J. Power Sources*. 307 (2016) 340–350. doi:10.1016/j.jpowsour.2015.12.132.
- [292] H. Duncan, N. Salem, Y. Abu-Lebdeh, Electrolyte Formulations Based on Dinitrile Solvents for High Voltage Li-Ion Batteries, *J. Electrochem. Soc.* 160 (2013) A838–A848. doi:10.1149/2.088306jes.
- [293] E. Markevich, G. Salitra, K. Fridman, R. Sharabi, G. Gershinsky, A. Garsuch, et al., Fluoroethylene Carbonate as an Important Component in Electrolyte Solutions for High-Voltage Lithium Batteries: Role of Surface Chemistry on the Cathode, *Langmuir*. 30 (2014) 7414–7424. doi:10.1021/la501368y.
- [294] E.M. Erickson, E. Markevich, G. Salitra, D. Sharon, D. Hirshberg, E. de la Llave, et al., Review—Development of Advanced Rechargeable Batteries: A Continuous Challenge in the Choice of Suitable Electrolyte Solutions, *J. Electrochem. Soc.* 162 (2015) A2424–A2438. doi:10.1149/2.0051514jes.
- [295] L. Ma, J. Xia, J.R. Dahn, Ternary Electrolyte Additive Mixtures for Li-Ion Cells that Promote Long Lifetime and Less Reactivity with Charged Electrodes at Elevated Temperatures, *J. Electrochem. Soc.* 162 (2015) A1170–A1174. doi:10.1149/2.0181507jes.
- [296] J. Xia, J.E. Harlow, R. Petibon, J.C. Burns, L.P. Chen, J.R. Dahn, Comparative Study on Methylene Methyl Disulfonate (MMDS) and 1,3-Propane Sultone (PS) as Electrolyte Additives for Li-Ion Batteries, *J. Electrochem. Soc.* 161 (2014) A547–A553. doi:10.1149/2.049404jes.
- [297] K. Fridman, R. Sharabi, R. Elazari, G. Gershinsky, E. Markevich, G. Salitra, et al., A new advanced lithium ion battery: Combination of high performance amorphous columnar silicon thin film anode, 5V $\text{LiNi}_{0.5}\text{Mn}_{1.5}\text{O}_4$ spinel cathode and fluoroethylene carbonate-based electrolyte solution, *Electrochem. Commun.* 33 (2013) 31–34. doi:10.1016/j.elecom.2013.04.010.

- [298] L. Wang, Y. Ma, Y. Qu, X. Cheng, P. Zuo, C. Du, et al., Influence of fluoroethylene carbonate as co-solvent on the high-voltage performance of $\text{LiNi}_{1/3}\text{Co}_{1/3}\text{Mn}_{1/3}\text{O}_2$ cathode for lithium-ion batteries, *Electrochimica Acta*. 191 (2016) 8–15. doi:10.1016/j.electacta.2016.01.032.
- [299] R. Petibon, C.P. Aiken, L. Ma, D. Xiong, J.R. Dahn, The use of ethyl acetate as a sole solvent in highly concentrated electrolyte for Li-ion batteries, *Electrochimica Acta*. 154 (2015) 287–293. doi:10.1016/j.electacta.2014.12.093.
- [300] R. Petibon, J. Li, N. Sharma, W.K. Pang, V.K. Peterson, J.R. Dahn, The use of deuterated ethyl acetate in highly concentrated electrolyte as a low-cost solvent for in situ neutron diffraction measurements of Li-ion battery electrodes, *Electrochimica Acta*. 174 (2015) 417–423. doi:10.1016/j.electacta.2015.05.169.
- [301] K. Chiba, T. Ueda, Y. Yamaguchi, Y. Oki, F. Shimodate, K. Naoi, Electrolyte Systems for High Withstand Voltage and Durability I. Linear Sulfones for Electric Double-Layer Capacitors, *J. Electrochem. Soc.* 158 (2011) A872–A882. doi:10.1149/1.3593001.
- [302] C. Schultz, V. Kraft, M. Pyschik, S. Weber, F. Schappacher, M. Winter, et al., Separation and Quantification of Organic Electrolyte Components in Lithium-Ion Batteries via a Developed HPLC Method, *J. Electrochem. Soc.* 162 (2015) A629–A634. doi:10.1149/2.0401504jes.
- [303] M.J. Frisch, Gaussian, Gaussian, Inc., Wallingford, CT, USA, 2009.
- [304] A.D. Becke, Density-functional exchange-energy approximation with correct asymptotic behavior, *Phys. Rev. A*. 38 (1988) 3098–3100. doi:10.1103/PhysRevA.38.3098.
- [305] E. Jónsson, P. Johansson, Electrochemical oxidation stability of anions for modern battery electrolytes: a CBS and DFT study, *Phys Chem Chem Phys*. 17 (2015) 3697–3703. doi:10.1039/C4CP04592K.
- [306] M. Walker, A.J.A. Harvey, A. Sen, C.E.H. Dessent, Performance of M06, M06-2X, and M06-HF Density Functionals for Conformationally Flexible Anionic Clusters: M06 Functionals Perform Better than B3LYP for a Model System with Dispersion and Ionic Hydrogen-Bonding Interactions, *J. Phys. Chem. A*. 117 (2013) 12590–12600. doi:10.1021/jp408166m.
- [307] M.D. Wodrich, C. Corminboeuf, P.R. Schreiner, A.A. Fokin, P. von R. Schleyer, How Accurate Are DFT Treatments of Organic Energies?, *Org. Lett.* 9 (2007) 1851–1854. doi:10.1021/ol070354w.
- [308] Y. Zhao, D.G. Truhlar, The M06 suite of density functionals for main group thermochemistry, thermochemical kinetics, noncovalent interactions, excited states, and transition elements: two new functionals and systematic testing of four M06-class functionals and 12 other functionals, *Theor. Chem. Acc.* 120 (2008) 215–241. doi:10.1007/s00214-007-0310-x.
- [309] T. Clark, J. Chandrasekhar, G.W. Spitznagel, P.V.R. Schleyer, Efficient diffuse function-augmented basis sets for anion calculations. III. The 3-21+G basis set for first-row elements, Li-F, *J. Comput. Chem.* 4 (1983) 294–301. doi:10.1002/jcc.540040303.
- [310] M.J. Frisch, J.A. Pople, J.S. Binkley, Self-consistent molecular orbital methods 25. Supplementary functions for Gaussian basis sets, *J. Chem. Phys.* 80 (1984) 3265. doi:10.1063/1.447079.

- [311] R. Krishnan, J.S. Binkley, R. Seeger, J.A. Pople, Self-consistent molecular orbital methods. XX. A basis set for correlated wave functions, *J. Chem. Phys.* 72 (1980) 650. doi:10.1063/1.438955.
- [312] A.D. McLean, G.S. Chandler, Contracted Gaussian basis sets for molecular calculations. I. Second row atoms, $Z=11-18$, *J. Chem. Phys.* 72 (1980) 5639. doi:10.1063/1.438980.
- [313] J. Tomasi, B. Mennucci, R. Cammi, Quantum Mechanical Continuum Solvation Models, *Chem. Rev.* 105 (2005) 2999–3094. doi:10.1021/cr9904009.
- [314] J. Tomasi, B. Mennucci, E. Cancès, The IEF version of the PCM solvation method: an overview of a new method addressed to study molecular solutes at the QM ab initio level, *J. Mol. Struct. THEOCHEM.* 464 (1999) 211–226. doi:10.1016/S0166-1280(98)00553-3.
- [315] D.S. Hall, J. Self, J.R. Dahn, Dielectric Constants for Quantum Chemistry and Li-Ion Batteries: Solvent Blends of Ethylene Carbonate and Ethyl Methyl Carbonate, *J. Phys. Chem. C.* 119 (2015) 22322–22330. doi:10.1021/acs.jpcc.5b06022.
- [316] J. Jiang, J.R. Dahn, Effects of solvents and salts on the thermal stability of LiC₆, *Electrochimica Acta.* 49 (2004) 4599–4604. doi:10.1016/j.electacta.2004.05.014.

APPENDIX A

NMC/graphite pouch cell



LCO/graphite pouch cell



← Gas bag →

← Jelly roll
(wound electrodes) →

Figure A1. Picture of NMC/graphite and LCO/graphite pouch cells used throughout the work presented in this thesis. NMC(442)/graphite, NMC(111)/graphite and LCO/Si:graphite pouch cells have the same format.

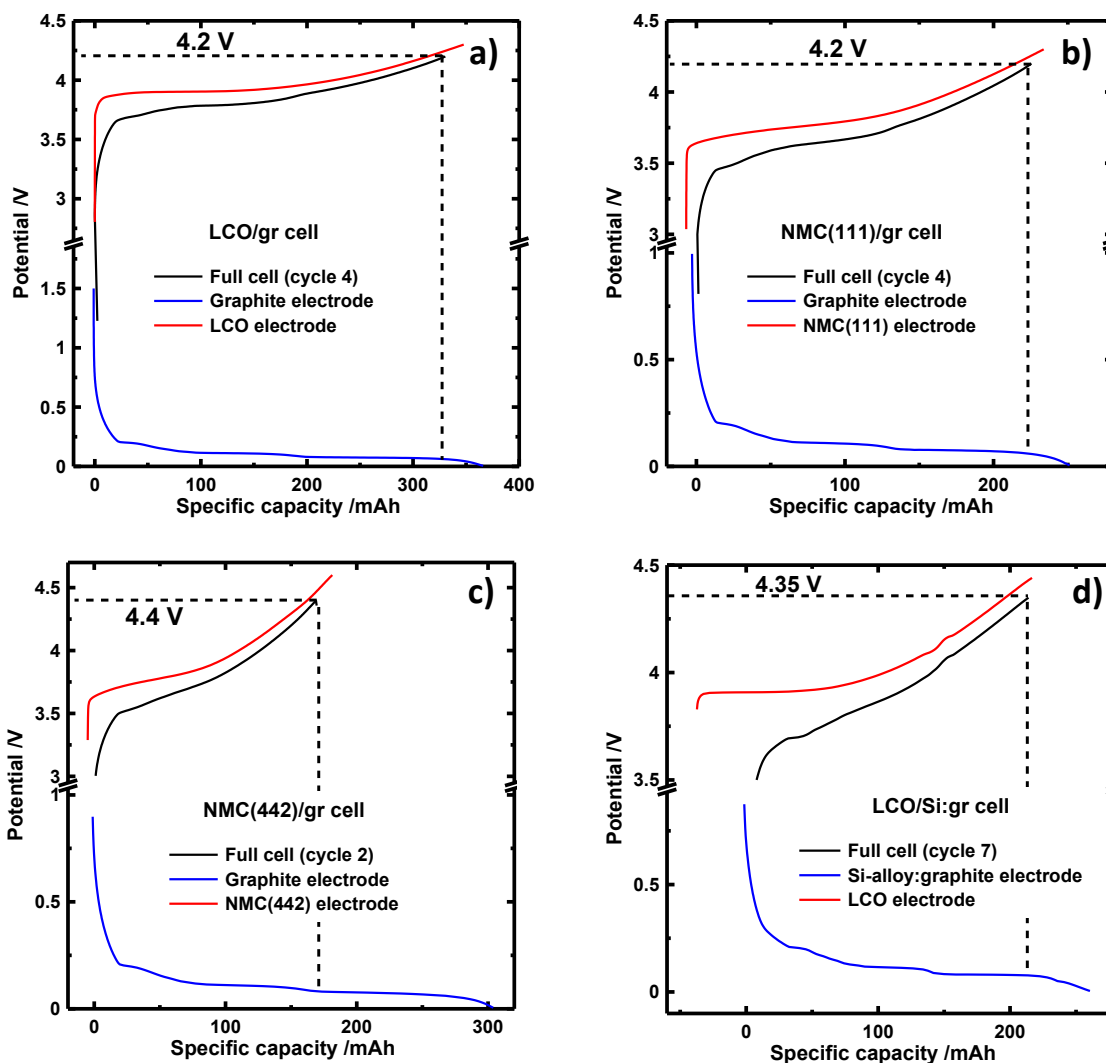


Figure A2. Voltage vs. capacity of LCO/gr (a), NMC(111)/gr (b), NMC(442)/gr (c) and LCO/Si:gr (d) pouch cells measured at 40°C along with the potential vs. capacity of the negative electrode and positive electrode as fitted by differential voltage analysis. Fitting for panel d) was performed by Jeremy Peters, 1st year B.Sc. student, Physics & Atmospheric Science, Dalhousie University (2016).

Table A1. Supplier and purity of chemicals used

Chemical	Common name	Company	Purity /%	Water content /ppm
CH ₂ Cl ₂	dichloromethane	Fisher	99.9	NA
DEC	diethyl carbonate	BASF	99.95	< 20
DMC	dimethyl carbonate	BASF	99.95	< 20
DTD	1,3,2-dioxathiolane-2,2-dioxide or ethylene sulfite	Sigma Aldrich	98	NA
EA	ethyl acetate	BASF	99.99	< 20
EC	ethylene carbonate	BASF	99.95	< 10
EMC	ethyl methyl carbonate	BASF	99.92	< 6
ES	ethylene sulfite	Sigma Aldrich	99	NA
FEC	fluoroethylene carbonate	BASF	99.94	< 20
LiPF ₆	lithium hexafluorophosphate	BASF	99.94	< 20
LiTFSi	lithium bis(fluorosulfonyl)imide	3M	NA	NA
MA	methyl acetate	BASF	99.95	< 20
MB	methyl butyrate	BASF	99.99	< 19
MEC	methylene ethylene carbonate	BASF	NA	NA
MMDS	methylene methanedisulfonate	Guangzhou Tinci Co. Ltd	98.7	NA
MP	methyl propanoate	BASF	99.99	< 18
MPrC	methyl propyl carbonate	BOC science	99.95	NA
PBF	pyridine trifluoroborate	3M	95.2	NA
PES	prop-1-ene-1,3-sultone	Lianchuang Medicinal Chemistry Co., Ltd.	98.2	NA
PLS	propylene sulfite	Sigma Aldrich	99	NA
PPF	pyridine pentafluorophosphate	3M	98.9	NA
PS	1,3-propane sultone	Sigma Aldrich	98	NA
TAP	triallyl phosphate	TCI America	> 94	NA
TMS	1,3,2-dioxathiane 2,2-dioxide or trimethylene sulfite	Sigma Aldrich	98	NA
TTSPi	tris(trimethylsilyl) phosphite	TCI America	> 95	NA
VC	vinylene carbonate	BASF	99.5	< 100

Table A3. Oven temperature program during GC-MS measurements of liquid components of Li-ion cells.

Time /min	Starting Temperature /°C	Ramp /°C.min ⁻¹	Hold time
0	45	0	2.5
2.5	45	40	
8.63	290	0	5.0

Table A2. Oven temperature program during GC-MS measurements of gaseous and liquid components formed during Li-ion cell use.

Time /min	Starting Temperature /°C	Ramp /°C.min ⁻¹	Hold time
0	35	0	3.0
3.0	35	10	
19.5	200	0	9.0
28.5	200	100	
29.0	250	0	

Table A4. Oven temperature program during GC-TCD measurements of gaseous compounds produced during Li-ion cell use.

Time /min	Starting Temperature /°C	Ramp /°C.min ⁻¹	Hold time
0	33	0	8.5
8.5	33	15	
10.97	160	0	6.05
17.02	160	120	
18.85	260	0	8

APPENDIX B

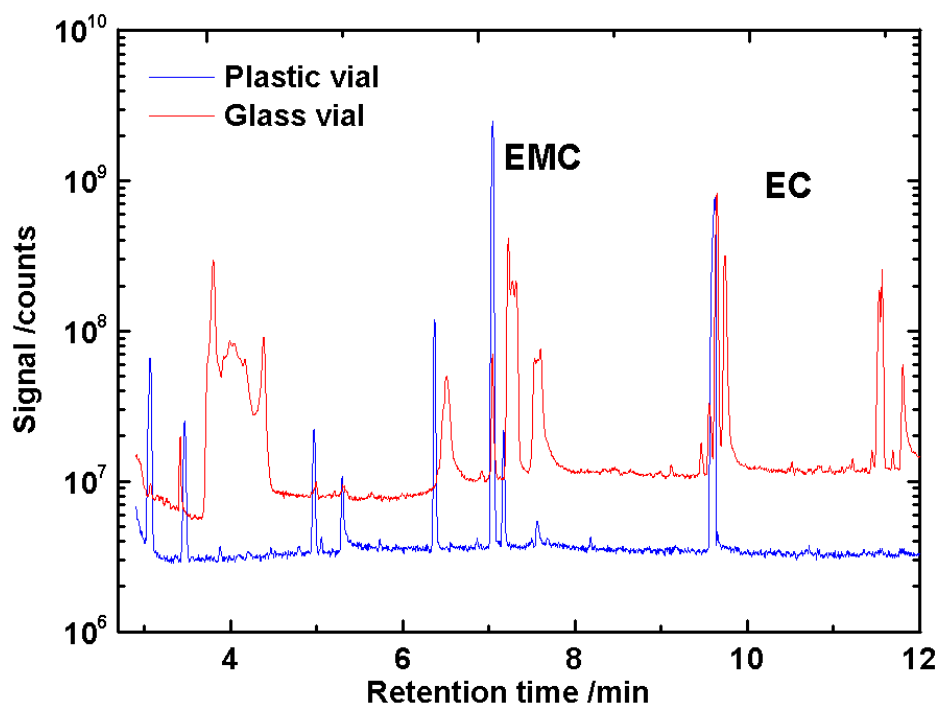


Figure B1. Chromatogram of the electrolyte extracted from a cyclized LCO/graphite pouch cell filled with a 1M LiPF_6 EC:EMC (3:7) + 2% VC electrolyte. The blue line presents the chromatogram of the electrolyte extracted using polymer vials (PFA) and the red line using glass vials. The additional peaks in the chromatogram of the extraction using glass vials are silicon containing compounds.

APPENDIX C

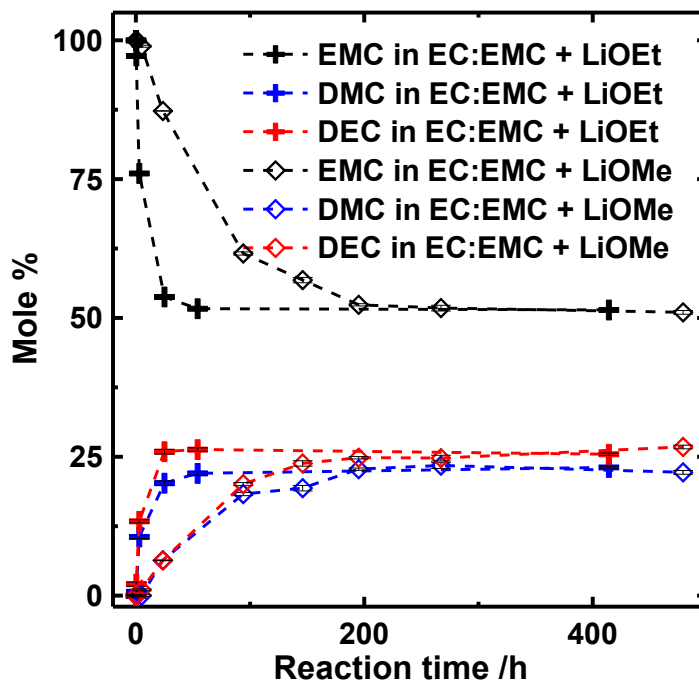
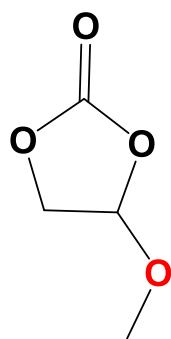
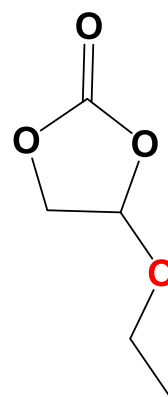


Figure C1. EMC, DMC and DEC mole ratio as a function of time after adding lithium methoxide (LiOMe), or lithium ethoxide LiOEt to an EC:EMC (3:7) solution. The amount of LiOMe and LiOEt added was around 1 wt%. Reactions were carried out in closed high density polyethylene vial under mild agitation in an Ar-filled glovebox at a temperature of $25^{\circ}\text{C} \pm 5^{\circ}\text{C}$.



EC-OMe
(molar mass =118)



EC-OEt
(molar mass =132)

Figure C2. Structure and molar mass of the compounds listed as EC-OMe and EC-OEt resulting from the addition-neutralization reaction between VC and LiOMe or LiOEt shown in Equation 5.6.

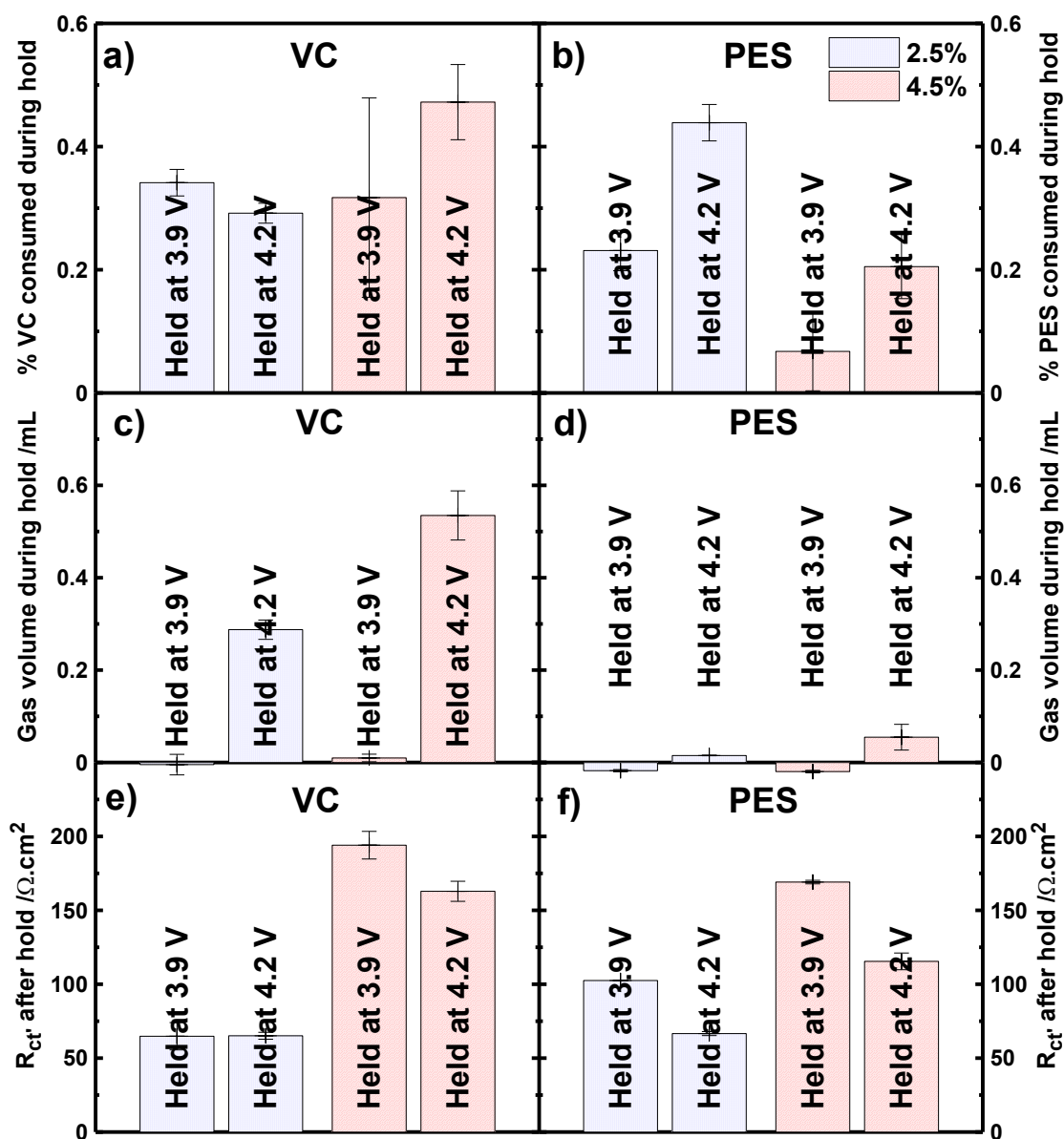


Figure C3. Amount of VC (a) and PES consumed (b), volume of gas produced in cells containing VC (c) and PES (d), and magnitude of the impedance of cells containing VC (e) and PES (f) for NMC(111)/graphite pouch cells held for 250 h and 50°C at either 3.9 V or 4.2 V. Some of the PES-containing cells were prepared and analyzed by Lina Rotermund, 2nd year B.Sc. student, Physics & Atmospheric Science, Dalhousie University (2014).

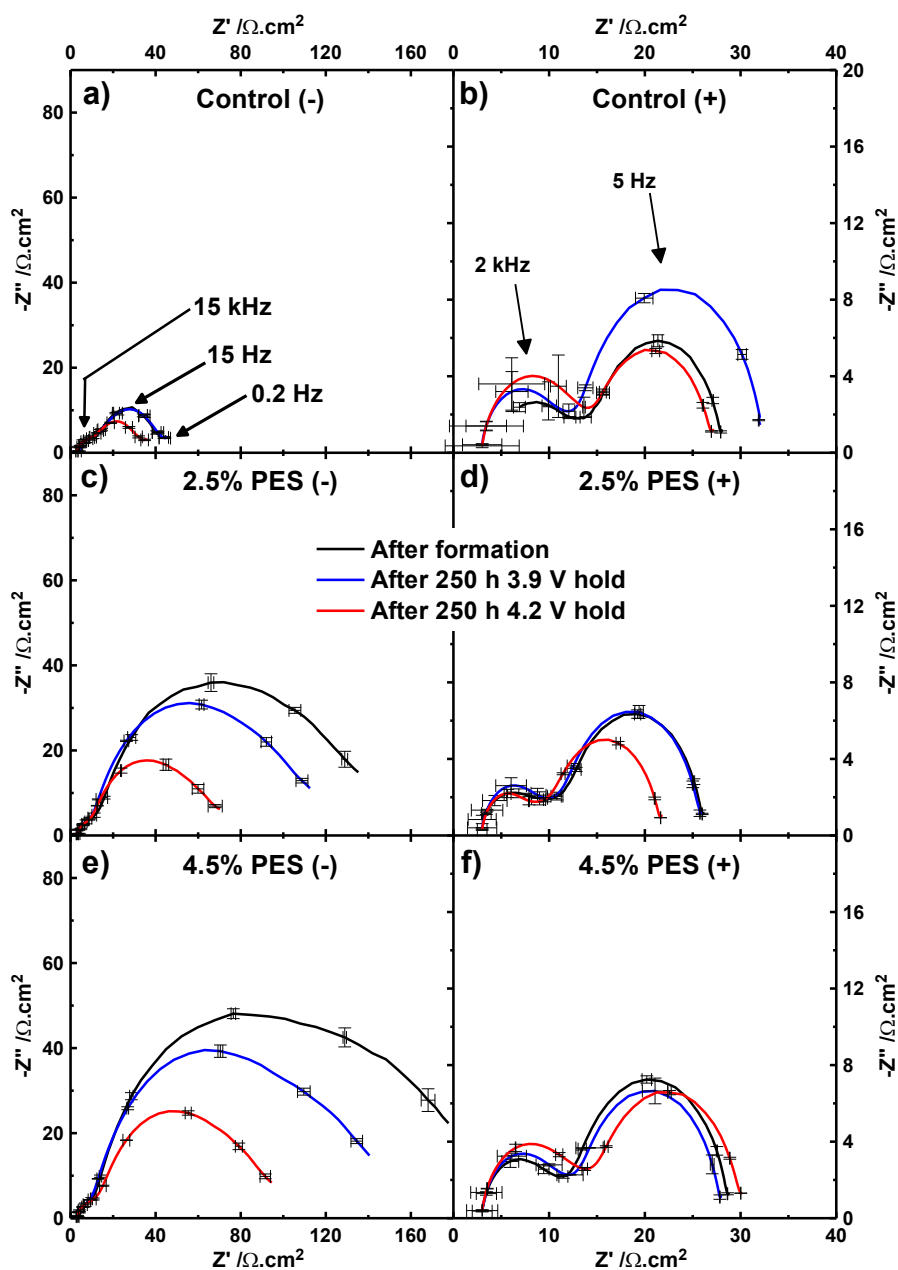


Figure C4. Impedance spectra of negative electrode symmetric cells (a,c,e) and positive electrode symmetric cells (b,d,f) reconstructed from NMC(111)/graphite pouch cells filled with electrolytes containing various amounts of PES after formation, after a 250 h hold at 3.9 V and 40°C or after a 250 h hold at 4.2 V and 40°C. All impedance spectra were measured at 10°C and were divided by two in order to present the impedance of a single electrode. Pouch cells were equilibrated at 3.80 V prior to symmetric cell reconstruction.

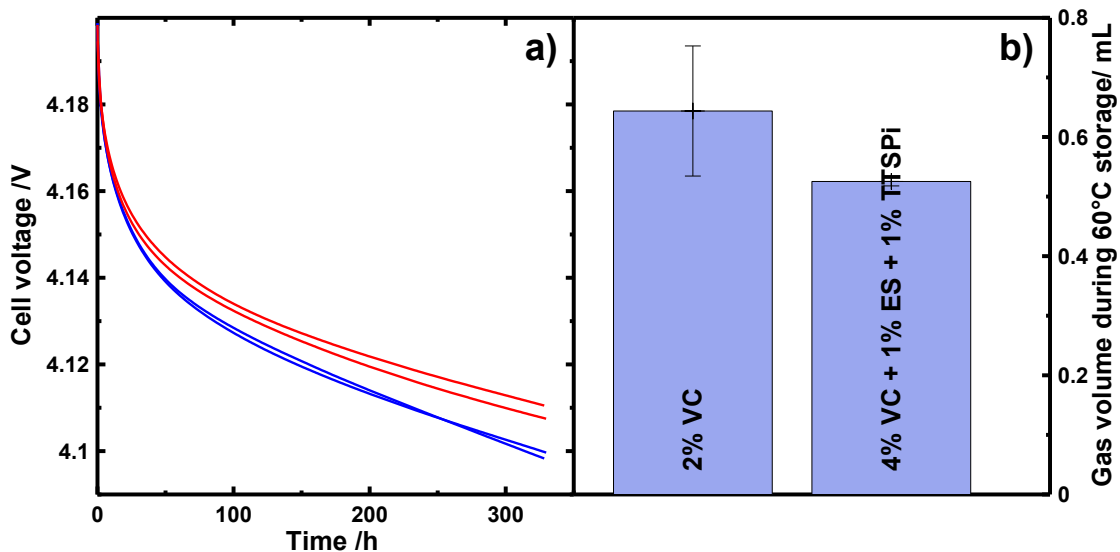


Figure C5. Cell voltage vs. storage time (a) and gas volume production (b) during open circuit voltage storage at 4.2 V and 60°C for NMC(111)/graphite pouch cells filled with a 1M LiPF₆ EC:EMC (3:7) base electrolyte containing 2% VC or 4% VC + 1% ES + 1% TTSPi.

APPENDIX D

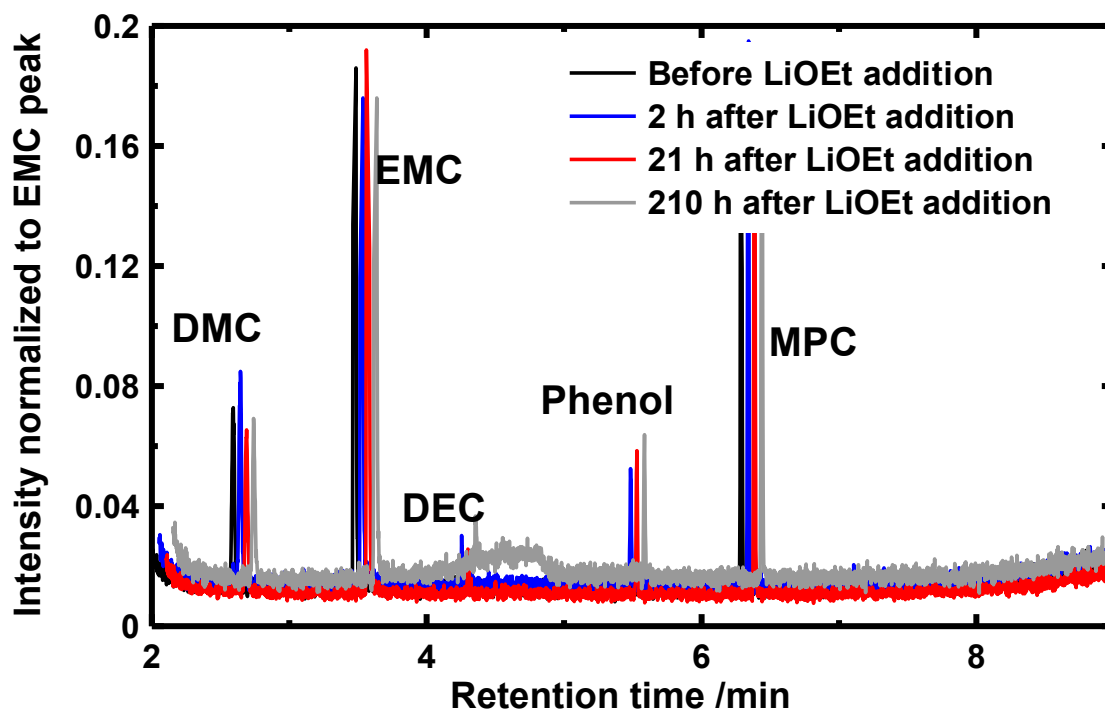


Figure D1. Chromatogram of an EMC:MPC (90:10) solution before and after the addition of 1% lithium methoxide. Reaction was carried out in closed high density polyethylene vial under mild agitation in an Ar-filled glovebox at a temperature of $25^{\circ}\text{C} \pm 5^{\circ}\text{C}$. The y-axis scale was adjusted to emphasize the apparition of phenol after the addition of lithium ethoxide. Each chromatogram was shifted by 0.05 min for clarity.

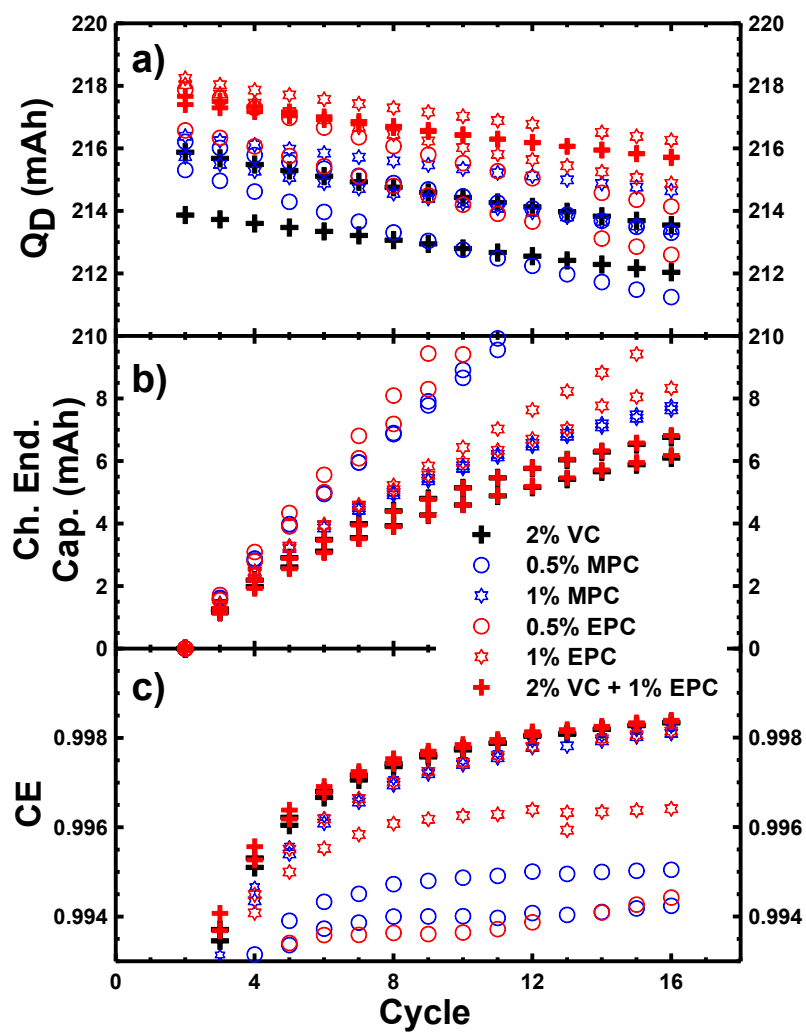


Figure D2. Discharge capacity (Q_D) (a), charge-end-point capacity (b) and coulombic efficiency (c) of 220 mAh NMC(111)/graphite pouch cells filled with control electrolyte in combination with various additive blends, cycled between 2.8 V and 4.2 V at C/20 and $40 \pm 0.1^\circ\text{C}$ on a UHPC.

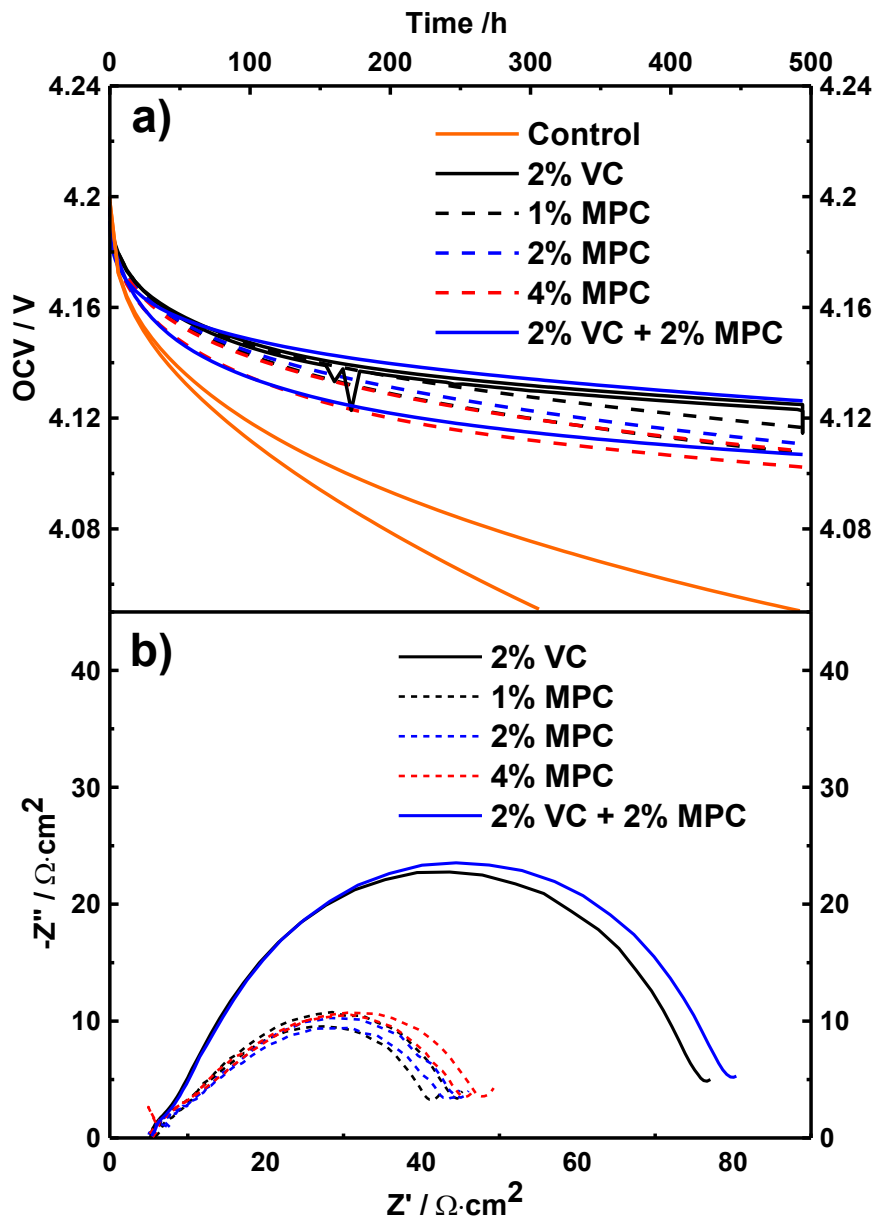


Figure D3. OCV vs. time (a) of 220 mAh NMC(111)/graphite pouch cells filled with control electrolyte in combination with various additive blends stored at 40°C at 4.2 V and cell impedance after storage (b). Cells underwent two full cycles between 4.2 V and 2.8 V at C/20, before being charged to 4.2 V (no constant voltage step) and left at open circuit for 500 h. Impedance measurements were done at a cell voltage of 3.80 V and 10°C.

APPENDIX E

Density functional theory calculations

All calculations were performed using the Gaussian software package (G09.d01) [303]. Density functional theory (DFT) geometry optimization and free energy calculations were performed using the M06-2X double hybrid functional. This functional is known to offer good accuracy for molecules with charge separation [304–308], which may be the case for the lithium salts studied in this work. The 6-311++(2df,2pd) basis set was used for all calculations [309–312]. Diffuse Kohn-Sham functions were included on all atoms (denoted by the double plus, ‘++’) to accurately model anionic species and to allow for the possibility of the accumulation of negative charge on hydrogen atoms (*i.e.*, to allow hydridic species). Several polarization functions were included to accurately represent any hypervalency effects. Solvation effects were modeled by the IEFPCM-UFF model [313,314] with the dielectric constant (ϵ) of 3:7 EC/EMC set to 20, as discussed previously [209,315]. All geometries were tested by normal mode analysis and have only positive (real) vibrational modes. Thermal contributions to the Gibbs free energy were calculated at room temperature (25°C).

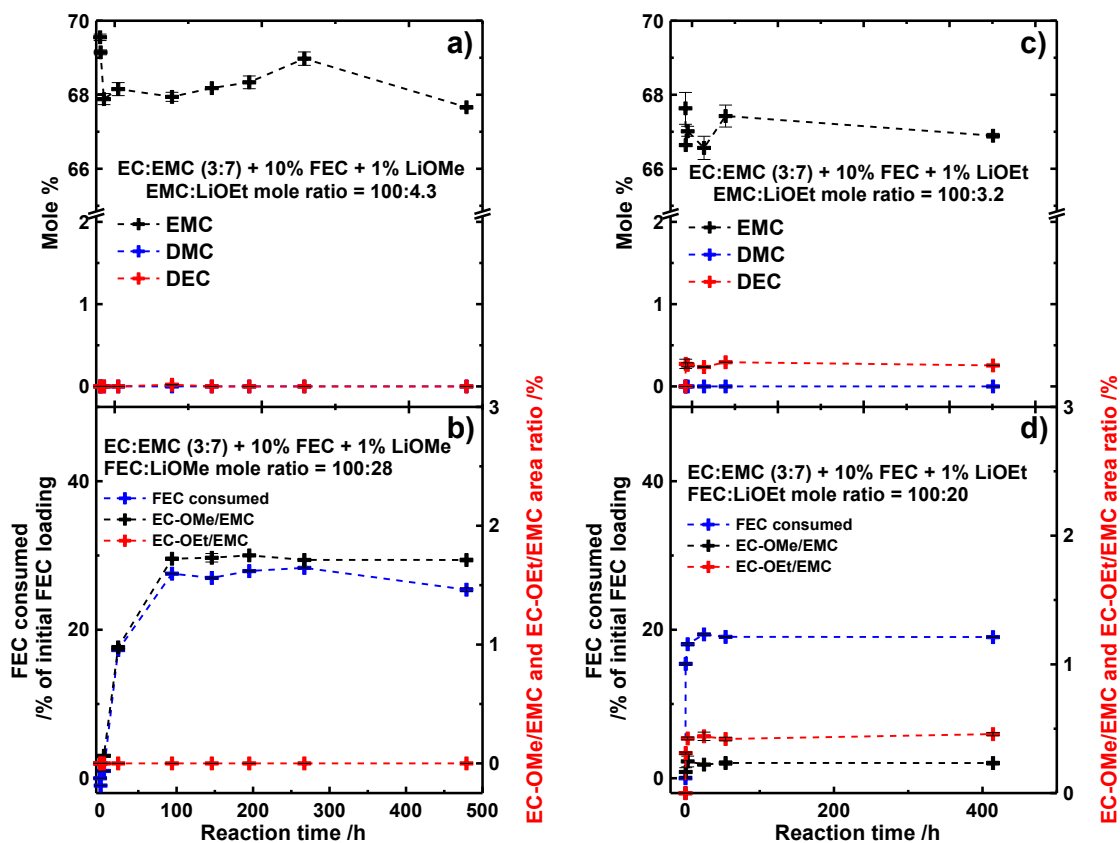


Figure E1. EMC, DMC, and DEC mole ratio (a, c) and amount of FEC left (normalized to the starting content) (b, d) as a function of time after adding lithium methoxide (a, b) or lithium ethoxide (c, d) to EC:EMC + 10% FEC mixtures. Reactions were carried in closed high density polyethylene vial under mild agitation in an Ar-filled glovebox at a temperature of $25^{\circ}\text{C} \pm 5^{\circ}\text{C}$.

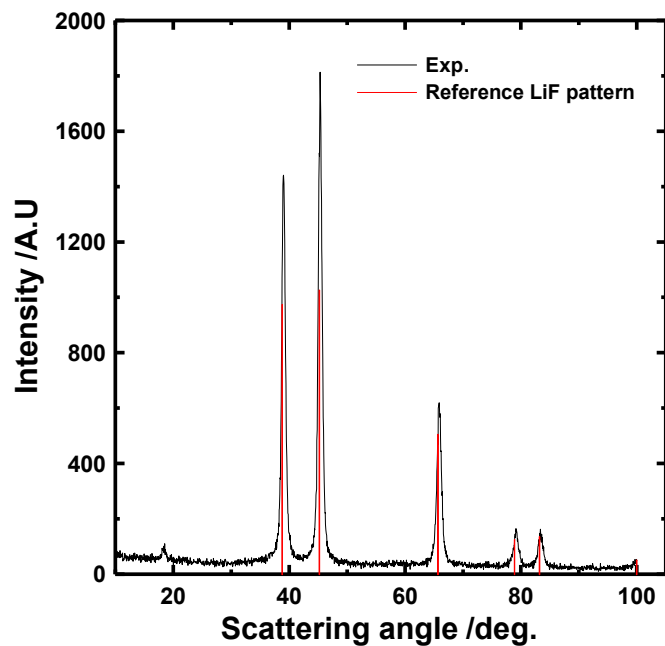


Figure E2. XRD pattern of the solid product of the reaction resulting from the addition of 1% lithium ethoxide to a EMC:FEC (90:10) mixture and a reference pattern for LiF. Measurements performed by Ramesh Shunmugasundaram, 5th year Ph.D. student, Chemistry department, Dalhousie University (2016).

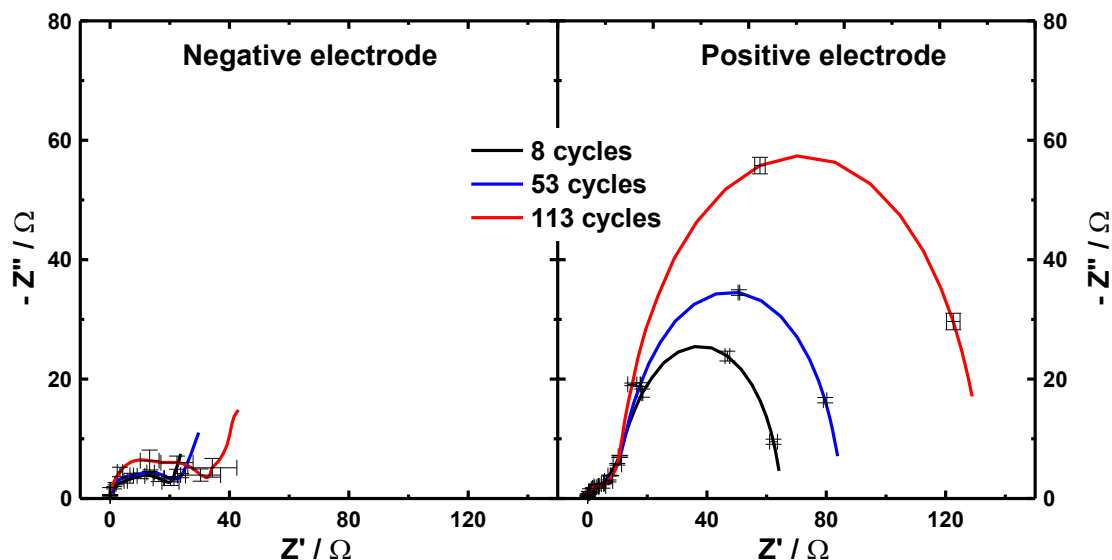


Figure E3. Impedance spectra of negative electrode symmetric cells (a) and positive electrode symmetric cells (b) reconstructed from the electrodes of 200 mAh LCO/Si-alloy:graphite pouch cells filled with a 1 M LiPF_6 EC:EMC:FEC (27:63:10) electrolyte cycled at 40°C between 3.0 V and 4.35V and a current of $C/2$. A constant voltage step at the top of charge was applied until the current dropped below $C/20$. Symmetric cells were reconstructed from the pouch cells after 8 cycles (black), 53 cycles (blue) and 113 cycles (red). The impedance spectra were divided by two to represent the impedance of individual electrodes.

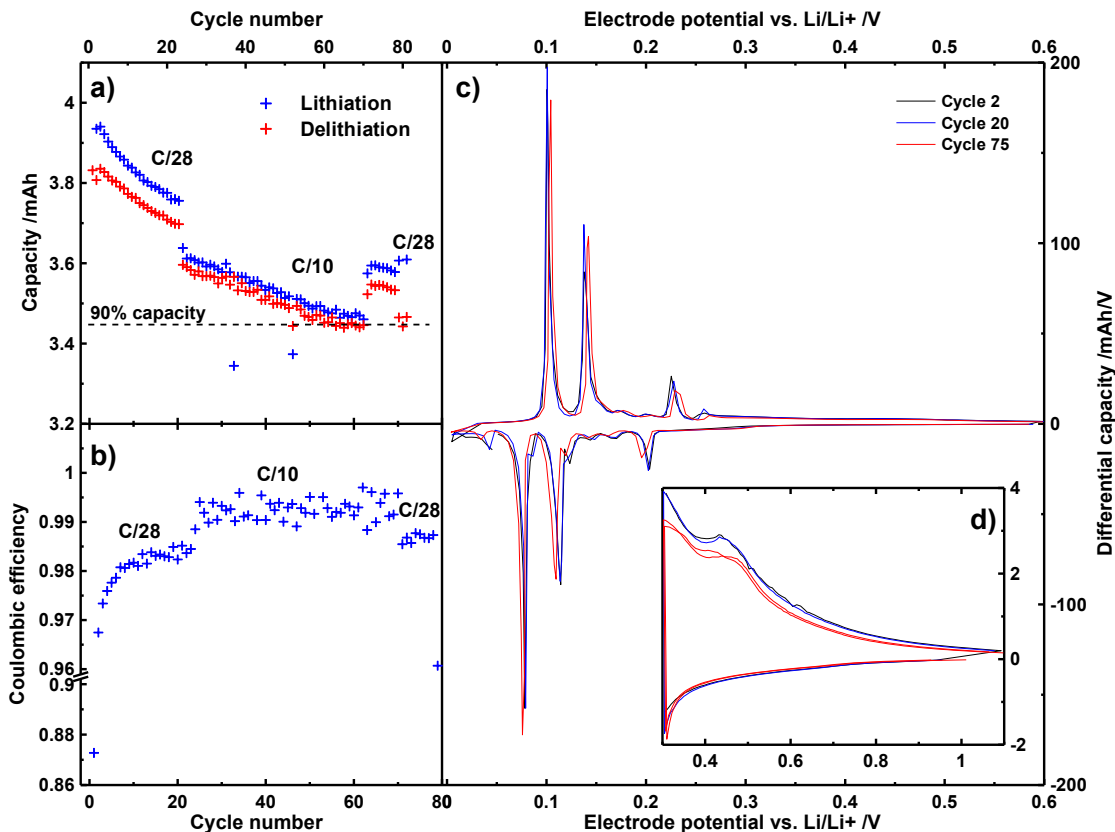


Figure E4. Charge and discharge capacity (a) and coulombic efficiency (b) vs. cycle number as well as differential capacity vs. potential of Si-alloy:graphite/Li half cells filled with a 1 M LiPF₆ EC:EMC:FEC (27:63:10) electrolyte cycled at 40°C with currents corresponding to C/28 and C/10. The inset (d) shows an expanded view of the differential capacity in the 0.3 - 1.1 V vs. Li/Li⁺ region. The Si-alloy electrodes were cut from the negative electrode of the 200 mAh LCO/Si-alloy:graphite pouch cells used throughout this study.

APPENDIX F

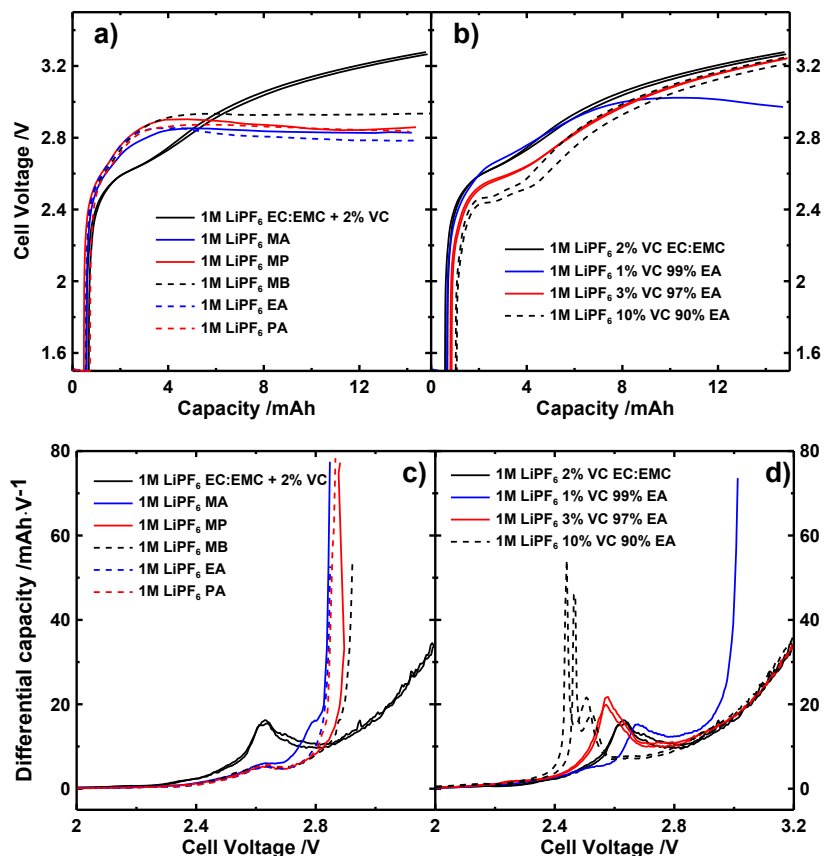


Figure F1. Cell voltage vs. capacity (a,b) and differential capacity vs. cell voltage (c,d) during the first charge of NMC(111)/graphite pouch cells filled with ester-based electrolytes with or without VC. Cells containing 1M LiPF₆ EC:EMC (3:7) + 2% VC are shown in each panel for comparison. Cells were charged at a current of C/20 and 40°C. Some of the ester-containing cells were prepared by Lina Rotermund, 2nd year B.Sc. student, Physics & Atmospheric Science, Dalhousie University (2014).

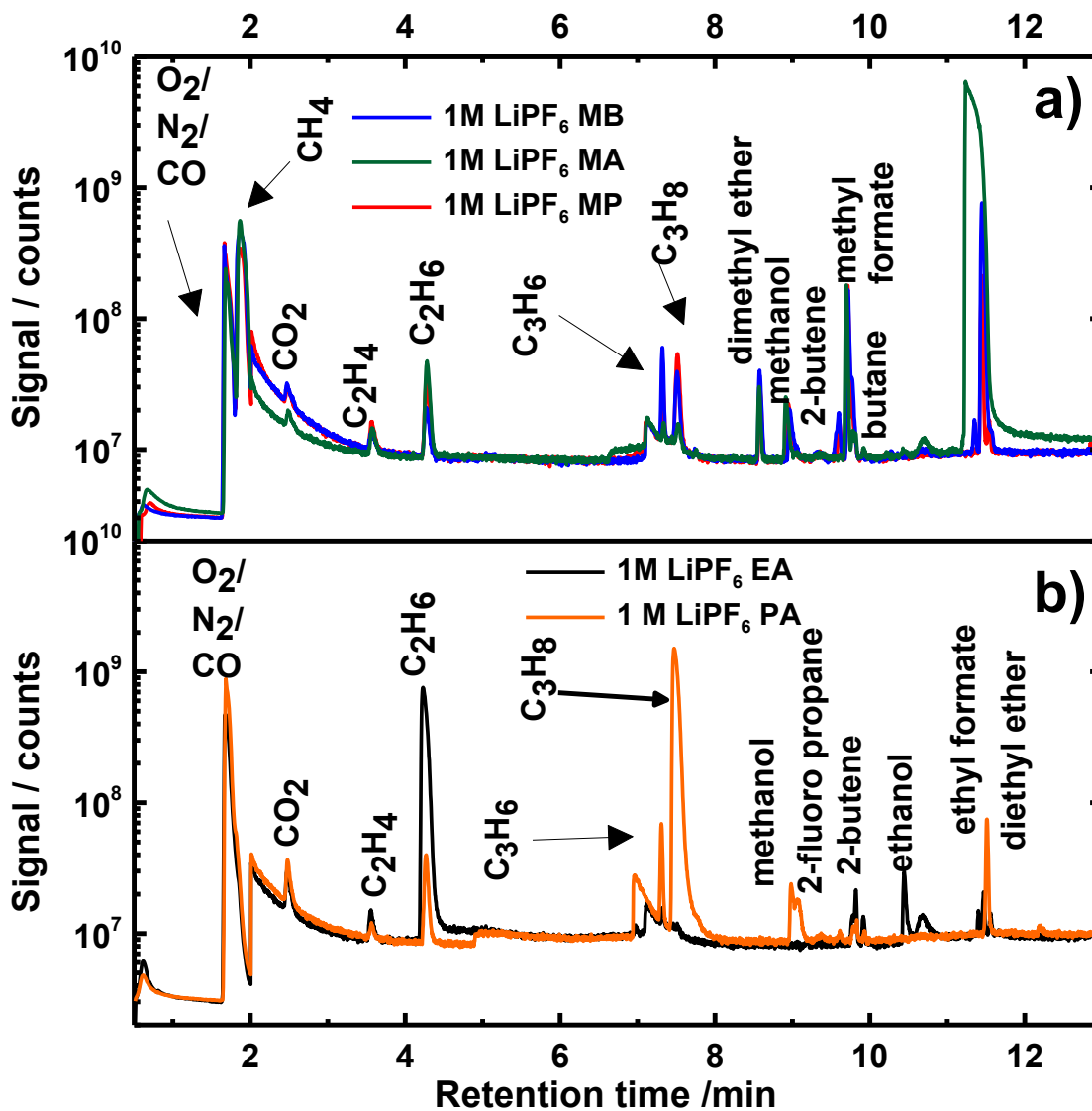


Figure F2. Chromatogram (total ion count) of the gas extracted from 220 mAh NMC(111)/graphite pouch cells containing various MB, MA or MP-based (a) and EA or PA-based (b) electrolytes and charged to 20 mAh at C/20 and 40°C. Cells were prepared and the gas analyzed by Lina Rotermund, 2nd year B.Sc. student, Physics & Atmospheric Science, Dalhousie University (2014).

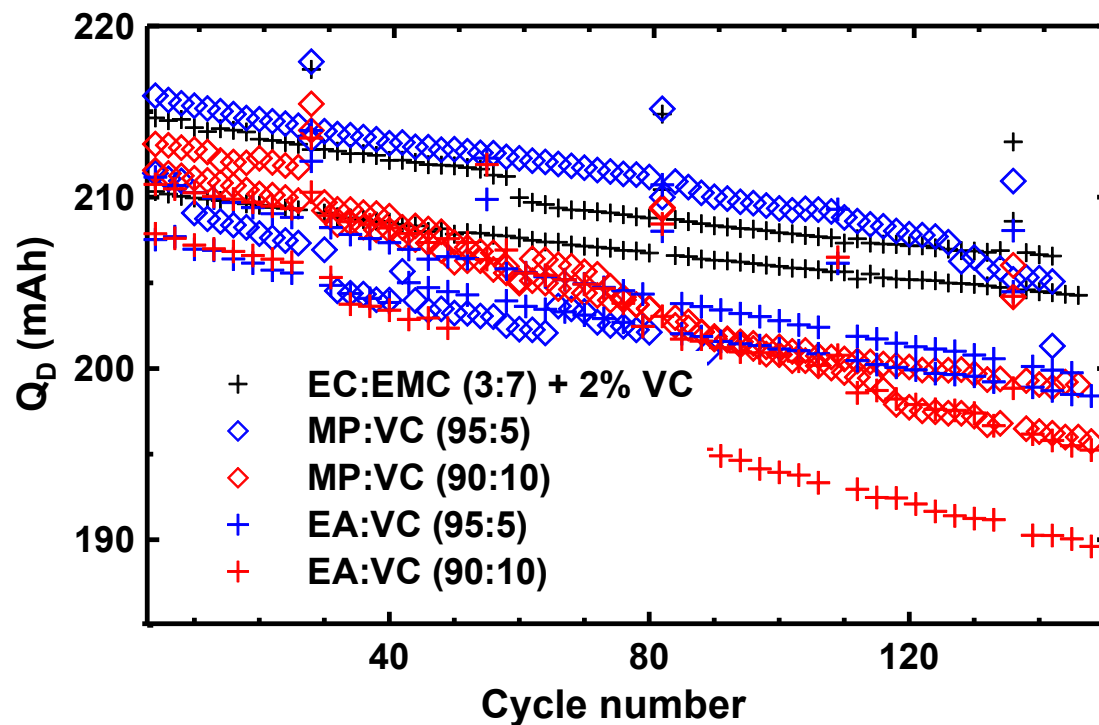


Figure F3. Discharge capacity vs. cycle number of 240 mAh NMC(111)/graphite pouch cells filled with 1M LiPF₆ x% MP + 100-x% VC or 1M LiPF₆ x% EA + 100-x% VC electrolytes, cycled at C/5 between 2.8 V and 4.2 V at 40°C. Only every second cycle is shown for clarity. A cycle at C/20 was performed every 20 cycles.

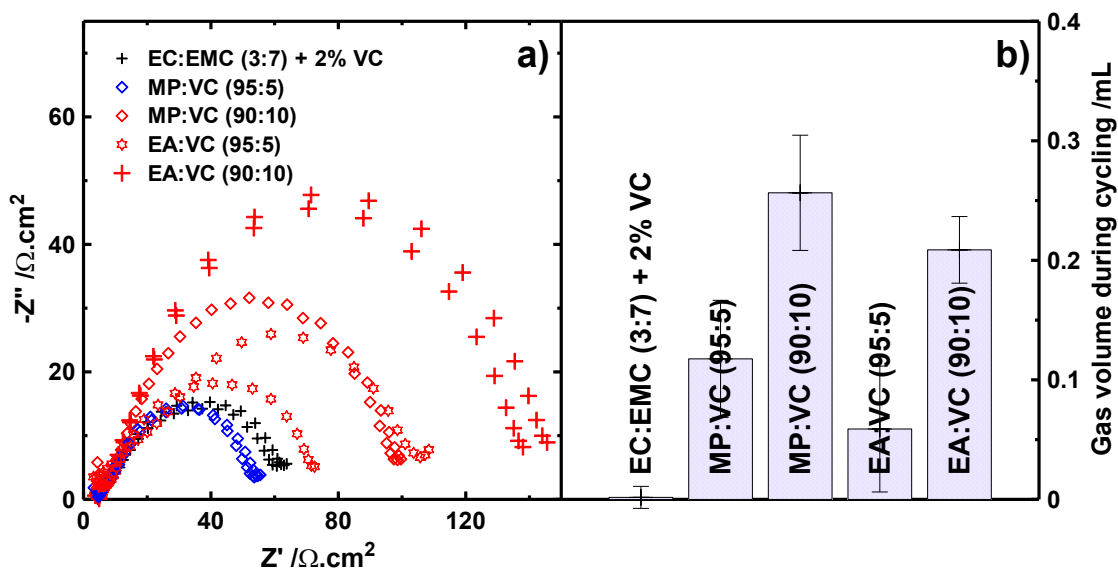


Figure F4. Impedance spectra (a) and gas volume formed (b) for 240 mAh NMC(111)/graphite pouch cells filled with 1M LiPF_6 x% MP + 100-x% VC or 1M LiPF_6 x% EA + 100-x% VC electrolytes, cycled at C/5 between 2.8 V and 4.2 V at 40°C for 1700 h. Data for cells filled with 1M LiPF_6 EC:EMC + 2% VC is shown in each panel for comparison. Impedance spectra were measured at a cell voltage of 3.80 V and at 10°C.

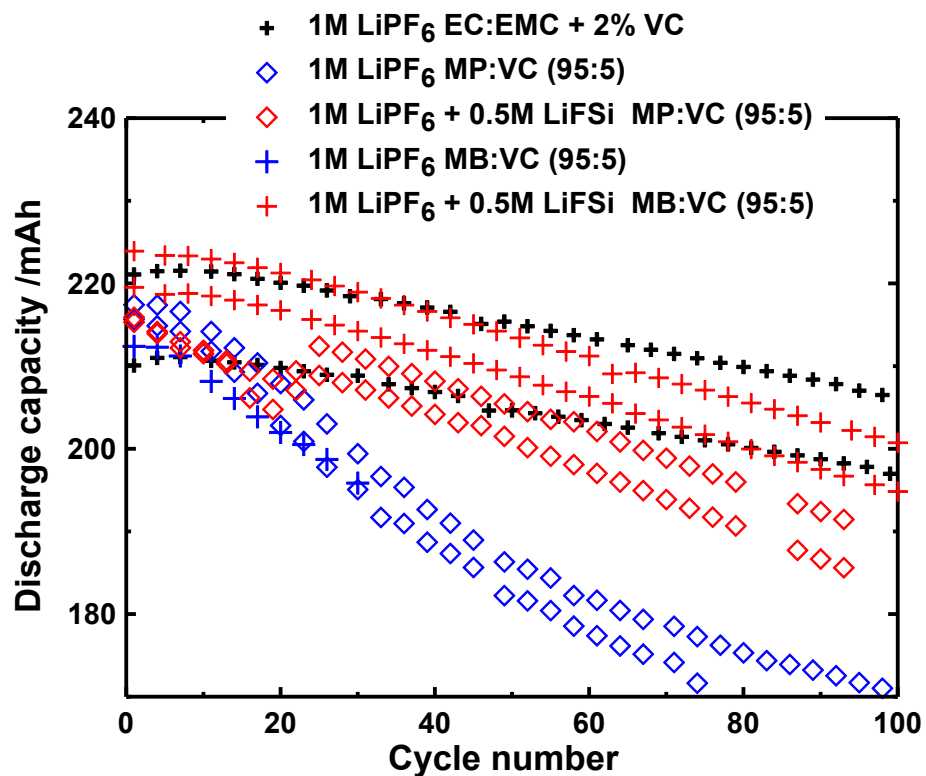


Figure F5. Discharge capacity of NMC(111)/graphite pouch cells filled with various electrolyte blends and cycled between 2.8 – 4.2 V at 55°C and C/10. Cells underwent an 800 h open circuit voltage period at 40°C and 4.2 V prior to cycling at 55°C.

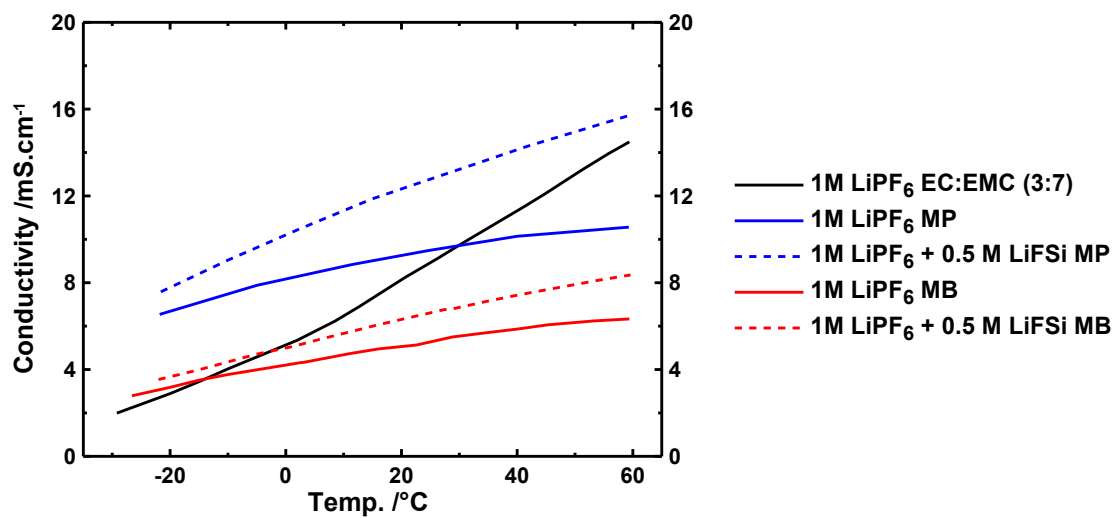


Figure F6. Conductivity vs. temperature for MP or MB-based electrolytes with or without LiFSi.

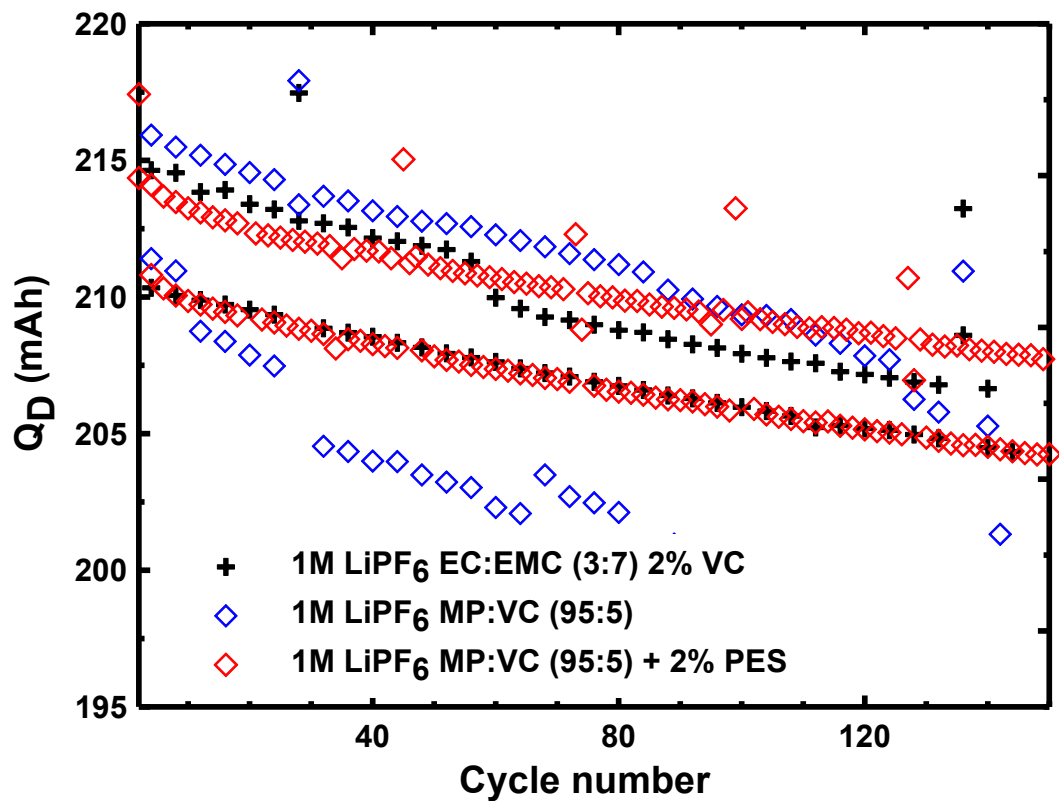
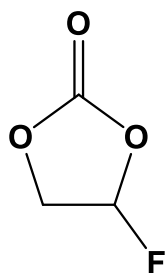
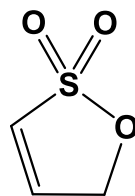


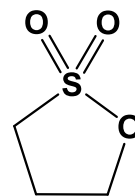
Figure F7. Discharge capacity of NMC(111)/graphite pouch cells filled with various electrolyte blends and cycled between 2.8 – 4.2 V at 40°C and C/5.



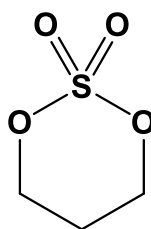
fluoroethylene carbonate
(FEC)



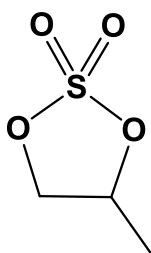
propene sultone
(PES)



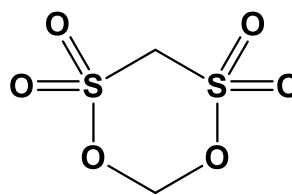
1,3-propane sultone
(PS)



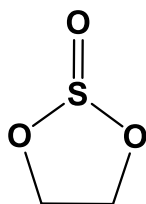
1,3,2-dioxathiane 2,2-
dioxide
(TMS)



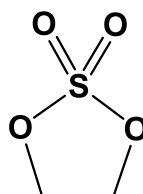
propylene sulfate
(PLS)



methylene
methanedisulfonate
(MMDS)



ethylene sulfite
(ES)



ethylene sulfate
(DTD)

Figure F8. Structure and common names of the additives tested in Section 8.1.7

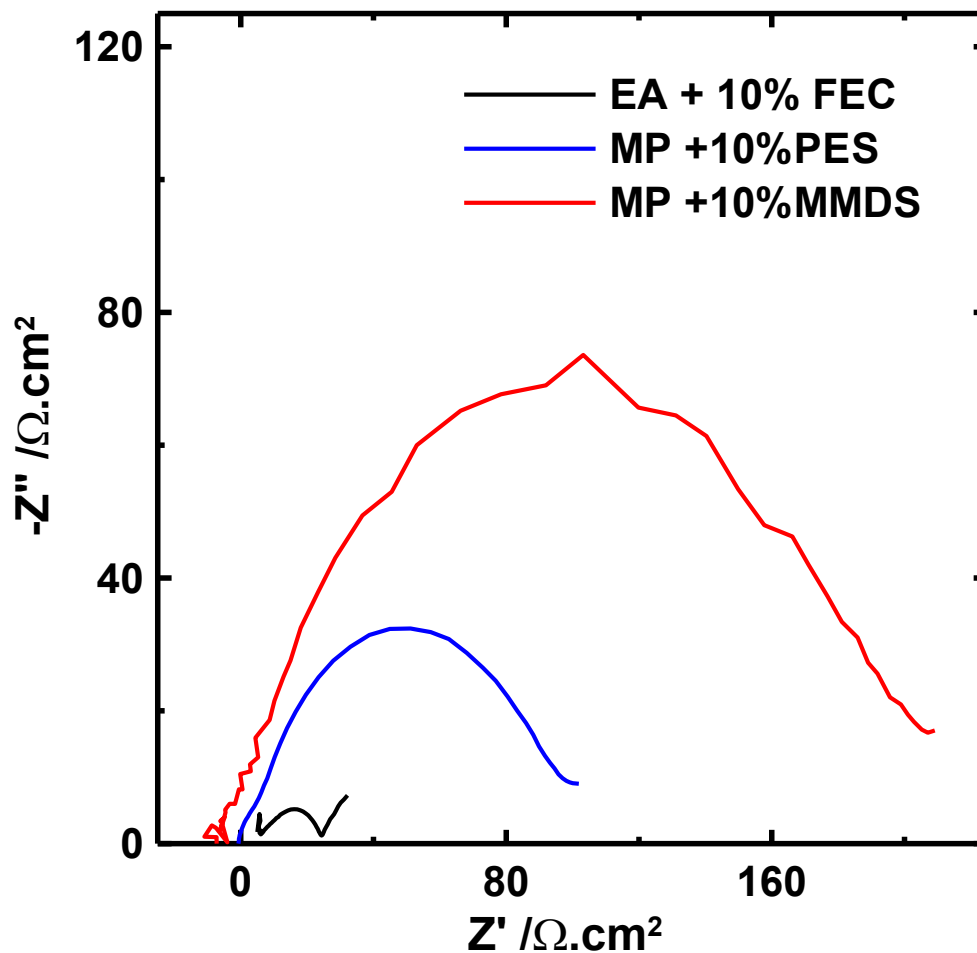


Figure F9. Impedance spectra after the first cycle between 2.8 – 4.2 V at 40°C of 240 mAh NMC(111)/graphite pouch cells filled with various ester-based electrolytes. Impedance spectra were measured at a cell voltage of 3.80 V and at 10°C. Cells were prepared by Lina Rotermund, 2nd year B.Sc. student, Physics & Atmospheric Science, Dalhousie University (2014).

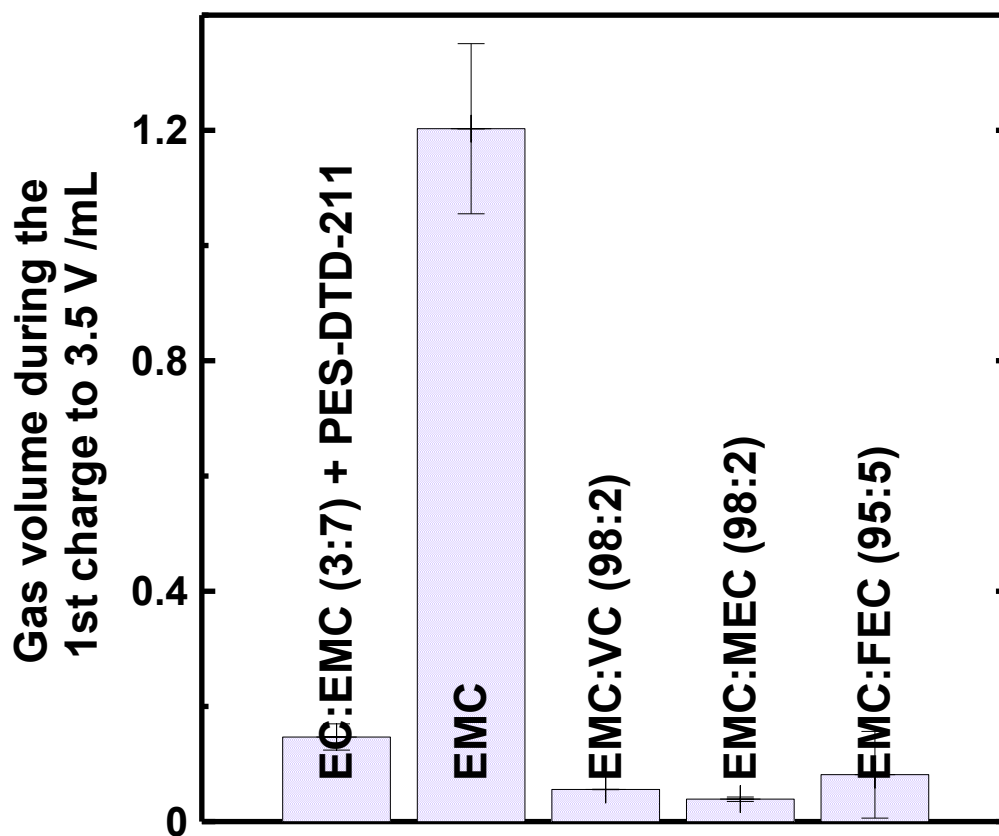


Figure F10. Gas volume produced during the first charge to 3.5 V at 40°C and C/20 of 180 mAh NMC(442)/graphite pouch cells filled with various EMC-based blends. For comparison the cell volume before cycling is about 2 mL. All electrolytes contained 1M LiPF₆. PES-DTD-211 refers to 2% PES + 1% DTD + 1% TTSPi. Cells filled with the EMC:FEC electrolyte were prepared by Jian Xia, Post-doctoral fellow, Physics & Atmospheric Science, Dalhousie University (2015).

Table F1. Volume change of 180 mAh NMC(442)/graphite pouch cells during the first charge, cycling or storage at various voltages and temperatures. For comparison the cell volume before cycling is about 2 mL. PES-211 refers to 2% PES + 1% DTD + 1% TTSPi. Cells were prepared and analyzed by Jian Xia, Post-doctoral fellow, Physics & Atmospheric Science, Dalhousie University (2015).

Solvent blend	Gas volume during 1st charge to 3.5 V /mL	Gas volume during 1st charge between 3.5 and 4.5 V /mL	Gas volume during 500 h of storage at 4.5 V and 40°C /mL	Gas volume during 500 h of cycling up to 4.2 V and 40°C /mL	Gas volume during 500 h of cycling up to 4.4 V and 40°C /mL
EC:EMC (3:7) + PES-211	0.13	0.06	0.08	0.00	-0.08
EMC:VC (98:2)	0.04	0.22	0.03	-0.03	-0.03
EMC:FEC (95:5)	0.08	0.14	0.01	NA	NA
EMC:FEC (90:10)	0.04	0.20	0.12	NA	NA

Experimental description of the Accelerated rate calorimetry measurements

The delithiated NMC(442) powder and lithiated graphite powder were obtained from NMC(442)/graphite pouch cells formed to 4.5V [46]. The single-point BET surface areas of the graphite and NMC powders were $1.5 \text{ m}^2\cdot\text{g}^{-1}$ and $0.38 \pm 0.01 \text{ m}^2\cdot\text{g}^{-1}$, respectively. ARC sample preparation followed the procedure shown in Jiang's earlier work [316]. The electrode:electrolyte mass ratios were 72 mg delithiated NMC with 23 mg electrolyte and 100 mg lithiated graphite with 100 mg electrolyte, respectively. The ARC starting temperature was set at 70°C and 50°C for NMC and graphite, respectively. ARC tests were tracked under adiabatic conditions when the sample self-heating rate (SHR) exceeded 0.03°C/min. Experiments were stopped at 350°C or when the SHR exceeded 20°C/min. To test the reproducibility of the ARC sample construction and measurements, two identical ARC samples were made and tested for every condition.

APPENDIX G

Request for Permission to Reproduce or Re-Publish ECS Material

Please fax this form to: The Electrochemical Society (ECS), Attn: Permissions Requests, 1.609.730.0629.
You may also e-mail your request to: copyright@electrochem.org. Include all the information as required on this form. Please allow 3-7 days for your request to be processed.

I am preparing a (choose one): paper chapter book thesis

entitled: Study of the reactivity of electrolyte solvents and additives in Li-ion cells using gas chromatography and ...

to be published by: Remi Petibon

in an upcoming publication entitled: Study of the reactivity of electrolyte solvents and additives in Li-ion cells using ...

I request permission to use the following material in the publication noted above, and request nonexclusive rights for all subsequent editions and in all foreign language translations for distribution throughout the world.

Description of material to be used—Indicate what material you wish to use (figures, tables, text, etc.) and give the full bibliographic reference for the source publication. You may attach a separate list, organized by ECS title.

R. Petibon, L. Rotermund, K.J. Nelson, A.S. Gozdz, J. Xia, J.R. Dahn, Study of Electrolyte components in Li Ion Cells Using Liquid-Liquid Extraction and Gas Chromatography Coupled with Mass Spectrometry, *J. Electrochem. Soc.* 161 (2014) A1167 - A1172. doi:10.1149/2.117406jes.

R. Petibon, J. Xia, J.C. Burns, J.R. Dahn, Study of the Consumption of Vinylene Carbonate in Li [Ni_{0.33}Mn_{0.33}Co_{0.33}]O₂/Graphite Pouch Cells, *J. Electrochem. Soc.* 161 (2014) A1618 - A1624. doi:10.1149/2.0351410jes.

Signature:  Date: March 11, 2016

Name: Remi Petibon

Address: 87-19 Irishton road, Dartmouth, Nova Scotia, Canada, B2Y 0B7

Telephone: 902-877-2226 Fax: _____

E-mail: remi.petibon@dal.ca

Permission is granted to include the above-referenced paper in your thesis, provided that you obtain permission of the other individual authors. In the thesis, please acknowledge the authors and the citation given above, and include the words: "Reproduced by permission of ECS — The Electrochemical Society."

3/11/16

Date


James Ryan, Director of Publications

**ELSEVIER LICENSE
TERMS AND CONDITIONS**

Mar 11, 2016

This is a License Agreement between Remi Petibon ("You") and Elsevier ("Elsevier") provided by Copyright Clearance Center ("CCC"). The license consists of your order details, the terms and conditions provided by Elsevier, and the payment terms and conditions.

All payments must be made in full to CCC. For payment instructions, please see information listed at the bottom of this form.

Supplier	Elsevier Limited The Boulevard, Langford Lane Kidlington, Oxford, OX5 1GB, UK
Registered Company Number	1982084
Customer name	Remi Petibon
Customer address	B7-19 Irishtown road Dartmouth, NS B2Y0B7
License number	3825870536995
License date	Mar 11, 2016
Licensed content publisher	Elsevier
Licensed content publication	Journal of Power Sources
Licensed content title	Evaluation of phenyl carbonates as electrolyte additives in lithium-ion batteries
Licensed content author	R. Petibon, L.M. Rotermond, J.R. Dahn
Licensed content date	1 August 2015
Licensed content volume number	287
Licensed content issue number	n/a
Number of pages	12
Start Page	184
End Page	195
Type of Use	reuse in a thesis/dissertation
Intended publisher of new work	other
Portion	full article
Format	electronic
Are you the author of this Elsevier article?	Yes
Will you be translating?	No

Expected completion date	Jun 2016
Estimated size (number of pages)	200
Elsevier VAT number	GB 494 6272 12
Permissions price	0.00 USD
VAT/Local Sales Tax	0.00 USD / 0.00 GBP
Total	0.00 USD

**ELSEVIER LICENSE
TERMS AND CONDITIONS**

Mar 11, 2016

This is a License Agreement between Remi Petibon ("You") and Elsevier ("Elsevier") provided by Copyright Clearance Center ("CCC"). The license consists of your order details, the terms and conditions provided by Elsevier, and the payment terms and conditions.

All payments must be made in full to CCC. For payment instructions, please see information listed at the bottom of this form.

Supplier	Elsevier Limited The Boulevard, Langford Lane Kidlington, Oxford, OX5 1GB, UK
Registered Company Number	1982084
Customer name	Remi Petibon
Customer address	B7-19 Irishtown road Dartmouth, NS B2Y0B7
License number	3825870617392
License date	Mar 11, 2016
Licensed content publisher	Elsevier
Licensed content publication	Electrochimica Acta
Licensed content title	The use of ethyl acetate and methyl propanoate in combination with vinylene carbonate as ethylene carbonate-free solvent blends for electrolytes in Li-ion batteries
Licensed content author	R. Petibon, J. Harlow, D.B. Le, J.R. Dahn
Licensed content date	1 February 2015
Licensed content volume number	154
Licensed content issue number	n/a
Number of pages	8
Start Page	227
End Page	234
Type of Use	reuse in a thesis/dissertation
Intended publisher of new work	other
Portion	full article
Format	electronic
Are you the author of this Elsevier article?	Yes
Will you be translating?	No

Title of your thesis/dissertation	STUDY OF THE REACTIVITY OF ELECTROLYTE SOLVENTS AND ADDITIVES IN LI-ION CELLS USING GAS CHROMATOGRAPHY AND DESIGN OF NEW ELECTROLYTE BLENDS
Expected completion date	Jun 2016
Estimated size (number of pages)	200
Elsevier VAT number	GB 494 6272 12
Permissions price	0.00 USD
VAT/Local Sales Tax	0.00 USD / 0.00 GBP
Total	0.00 USD

ELSEVIER LICENSE
TERMS AND CONDITIONS

Mar 22, 2016

This is a License Agreement between Remi Petibon ("You") and Elsevier ("Elsevier") provided by Copyright Clearance Center ("CCC"). The license consists of your order details, the terms and conditions provided by Elsevier, and the payment terms and conditions.

All payments must be made in full to CCC. For payment instructions, please see information listed at the bottom of this form.

Supplier	Elsevier Limited The Boulevard, Langford Lane Kidlington, Oxford, OX5 1GB, UK
Registered Company Number	1982084
Customer name	Remi Petibon
Customer address	B7-19 Irishtown road Dartmouth, NS B2Y0B7
License number	3834261197790
License date	Mar 22, 2016
Licensed content publisher	Elsevier
Licensed content publication	Journal of Power Sources
Licensed content title	Study of the consumption of the additive prop-1-ene-1,3-sultone in Li[Ni _{0.33} Mn _{0.33} Co _{0.33}]O ₂ /graphite pouch cells and evidence of positive-negative electrode interaction
Licensed content author	R. Petibon, L. Madec, L.M. Rotermond, J.R. Dahn
Licensed content date	1 May 2016
Licensed content volume number	313
Licensed content issue number	n/a
Number of pages	12
Start Page	152
End Page	163
Type of Use	reuse in a thesis/dissertation
Portion	full article
Format	electronic
Are you the author of this Elsevier article?	Yes
Will you be translating?	No
Title of your thesis/dissertation	STUDY OF THE REACTIVITY OF ELECTROLYTE SOLVENTS AND ADDITIVES IN LI-ION CELLS USING GAS CHROMATOGRAPHY AND DESIGN OF NEW ELECTROLYTE BLENDS

Expected completion date	Jun 2016
Estimated size (number of pages)	200
Elsevier VAT number	GB 494 6272 12
Permissions price	0.00 USD
VAT/Local Sales Tax	0.00 USD / 0.00 GBP
Total	0.00 USD